Nuclear Magnetic Resonance of Paramagnetic Metalloproteins

Ivano Bertini,* Paola Turano, and Alejandro J. Vila

Department of Chemistry, University of Florence, 50121 Florence, Italy

Received December 16, 1992 (Revised Manuscript Received September 7, 1993)

Contents

Ivano Bertini (center) was born in Pisa, Italy, in 1940. He obtained the degree in Chemistry in 1964 with Luigi Sacconi at the University of Florence, where he was first research associate, then lecturer, free docent, and finally full professor (1975). He started characterizing by infrared spectroscopy coordination compounds. Then he moved toward the understanding of the electronic structure of metal ions in different environments. Since 1965 he has given preference to NMR of paramagnetic molecules. He visited ETH (Zürich, Switzerland) in 1965 to measure NMR spectra with an NMR instrument operating at 60 MHz without lock, then in 1968–1969 he spent a year at Princeton University (New Jersey) still working on NMR with W. D. Horrocks, Jr. He moved then to the field of paramagnetic metalloproteins after a stage at Caltech with Harry B. Gray. His interests span from metal-substituted zinc enzymes to copper–zinc superoxide dismutase and Fe–S proteins and peroxidases.

Paola Turano (right) was born in Florence, Italy, in 1964. She graduated in Chemistry in 1989 at the University of Florence with Professor Ivano Bertini working on the NMR characterization of superoxide dismutase. She has now completed her Ph.D. at the University of Florence in the field of NMR of paramagnetic metalloproteins applied to heme proteins.

Alejandro J. Vila (left) was born in Rosario, Argentina, in 1962. He graduated in Chemistry in 1986, and in 1990 he received his Ph.D. degree from the University of Rosario under the direction of Professor Manuel Gonzalez Sierra in organic chemistry. He then collaborated with Professor Alejandro Olivieri working in solid-state NMR spectroscopy. Since 1991 he has been a postdoctoral fellow under the direction of Professor Ivano Bertini at the University of Florence working in NMR of paramagnetic metalloproteins.

I. Introduction

Paramagnetic compounds are characterized by the presence of unpaired electrons. Compounds with unpaired electrons usually contain one or more transition metal ions. Radicals are also paramagnetic but they are not suitable for high-resolution NMR experiments (as it happens also with some metal ions) for reasons which will be discussed later. Here we deal with NMR spectroscopy applied to metalloproteins containing one or more transition metal ions bearing unpaired electrons. We limit the interest to the high-resolution experiments, i.e., to studies aimed at the assignment of the protein signals, sometimes in the presence of cofactors, substrates, and inhibitors. We will not discuss here the NMR investigation of nuclei belonging to substrates and inhibitors in rapid exchange between free and protein-bound forms, which is aimed at obtaining exchange parameters or at the mapping of such molecules within the enzymatic cavities. Analogously, we will not discuss the investigation of water molecules interacting with the metal ion in rapid exchange with the bulk water. Reviews dealing with

0009-2665/93/0793-2833$12.00/0

water and other exogenous ligands interacting with paramagnetic proteins are available.[1-4]

The choice of discussing only the protein as a whole is due to a flourish of results in this area since the progress in NMR technology is forever yielding more refined methods for investigation. Nowadays a few research groups interested in this field attempt to do with paramagnetic macromolecules what has been done with the diamagnetic ones, i.e. solving the three-dimensional (3D) structure in solution.

One of the most relevant effects of the presence of unpaired electrons is a considerable line broadening of the NMR signals corresponding to nuclei in the neighborhood of the paramagnetic center.[5-8] This is a very severe limitation for high-resolution NMR. However, other effects of the paramagnetism may be exploited in order to overcome this problem. Since the broadened signals are often outside the diamagnetic region of the spectrum and well spread among them, with especially adapted pulse sequences it is possible to detect their connectivities with other signals. If a broadened signal is under the diamagnetic envelope, it can still be located because its cross peaks in 2D experiments can be observed under particular experimental conditions.[9-12] Under these conditions the cross peaks between the signals of slow relaxing nuclei have not developed to a level to be detected. With regard to the 1D NOE experiments, as they are carried out as difference spectra,[13,14] only signals which give NOEs with the irradiated one are detected. This is another way to locate a broad signal under a complex envelope if it responds through NOE.

The fast relaxing nature of nuclei sensing a paramagnetic center prevents us from performing all the experiments designed for slow relaxing nuclei but they are a challenge for NMR investigations in order to develop strategies aimed at the detection of either dipolar or scalar connectivities.

A final point to be discussed here is related to the magnitude of the external magnetic field. At high magnetic fields, the separation between the electron Zeeman levels increases, and this induces a large electron magnetic moment. Upon molecular tumbling nuclear relaxation occurs. This effect is dramatic on the line width for large S and large magnetic fields (i.e. large electron magnetic moment) and for macromolecules with molecular weight larger than 30 000 (which experience large rotational correlation times). Therefore, whereas in general larger and larger magnetic fields are needed to increase resolution and sensitivity, in paramagnetic systems, eventually the intensity of the magnetic field can be a negative factor. The magnetic field that falls between 100 and 600 MHz can be the best compromise.

II. NMR of Paramagnetic Compounds

A. The Hyperfine Coupling: The Pseudocontact and Contact Shifts

The chemical shifts in diamagnetic compounds are given by the shielding and deshielding effects caused by the motion of the electrons in the molecule in the presence of an external magnetic field.

In the case of paramagnetic compounds, one should be reminded that unpaired electrons have a magnetic moment μ_S given by

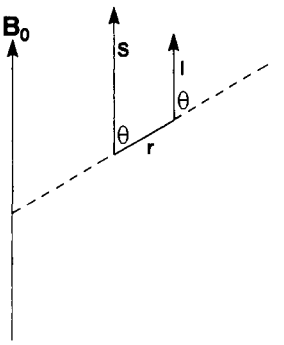

Figure 1. Schematic representation of the dipolar interaction between the electron and nuclear magnetic dipoles in an external magnetic field B_0. **r** is the electron–nucleus vector and θ is the angle between **r** and the external magnetic field.

$$\mu_S = g\mu_B\sqrt{S(S+1)} \tag{1}$$

where g is a proportionality parameter between the angular and magnetic moments (in the free-electron case it is indicated as g_e, which is 2.0023), S is half the number of unpaired electrons (i.e., the electron spin quantum number), and μ_B is the electron Bohr magneton. Such a magnetic moment may be the main contributor to the screening constant of nuclei sensing the paramagnetic center. Then it will be a dominant factor in determining the chemical shift value in a paramagnetic substance. Such contribution is called hyperfine shift because it is due to the hyperfine coupling between the unpaired electrons and the resonating nucleus. We can describe such an effect either as a magnetic field generated by the unpaired electrons or as an energy contribution to the nuclear Zeeman energy levels. If we choose to describe the effects in energy units then we can use the usual Hamiltonians. The hyperfine coupling is described as

$$\mathcal{H} = \mathbf{I}\cdot\hat{\mathbf{A}}\cdot\mathbf{S} \tag{2}$$

where **I** is the nuclear spin operator (or vector), **S** the electron spin operator (or vector), and $\hat{\mathbf{A}}$ the coupling tensor. Thus, the coupling depends on the orientation of **I** and **S**. If, as in accordance with the so called spin Hamiltonian formalism, we take I and S to be aligned along the external magnetic field anchored at their positions in the molecular frame (Figure 1), the interaction energy depends on the angle θ according to the following equation:

$$E = \frac{\mu_I\mu_S}{\mathbf{r}^3}(3\cos^2\theta - 1) \tag{3}$$

where μ_S and μ_I are the electron and the nuclear magnetic moments, respectively and θ and **r** are as indicated in Figure 1.

If the interaction energy as expressed in eq 3 is averaged for an isotropic molecular tumbling, it becomes zero since the angular term cancels out when integrated over all space. However, if g (eq 1) changes upon molecular rotation, the magnetic moment associated with S (μ_S) changes with the orientation of the molecule and it can now be shown that the average interaction energy is different from zero. The shift due to this interaction, which is dipolar in origin is given by[15,16]

$$\left(\frac{\Delta\nu}{\nu_o}\right) = \frac{1}{4\pi}\frac{1}{3N_A}\left[\chi_{zz} - \frac{1}{2}(\chi_{xx} + \chi_{yy})\frac{3\cos^2\theta - 1}{\mathbf{r}^3}\right] - \frac{1}{4\pi}\frac{1}{2N_A}(\chi_{xx} - \chi_{yy})\frac{\sin^2\theta\cos 2\varphi}{\mathbf{r}^3} \quad (4)$$

where $\Delta\nu$ is the averaged hyperfine shift, ν_o is the resonance frequency of a reference nucleus at the magnetic field of the experiment, N_A is Avogadro's constant, and χ_{xx}, χ_{yy}, and χ_{zz} are the three principal components of the magnetic susceptibility tensor. The existence of an anisotropic magnetic susceptibility tensor is somewhat related to the existence of anisotropy in the **g** values (the relationship between **g** and χ will be discussed in detail in section V.B). The polar coordinates **r**, θ, and φ are related to the position of the resonating nucleus within the axis frame determined by the main directions of the χ tensor.

Equation 4 is of fundamental importance because it relates a structural property defined by the polar coordinates with an observable, $\Delta\nu/\nu_o$. This shift is often called dipolar shift because it is the result of a through-space coupling between **I** and **S**. However, since it is an averaged value and as such is isotropic, it is more properly called pseudocontact shift for the reasons which will be discussed later.

The derivation of eq 4 is based on the assumption that the unpaired electron is anchored in a single position within the molecular framework. In a metalloprotein such a position is identified with the metal ion. Equation 4 is correct within the metal-centered point–dipole approximation. We know, however, that the unpaired electron is not simply localized on the metal ion. It is, in principle, delocalized all over the molecule through the molecular orbitals (MO) which contain the unpaired electrons. Furthermore, an unpaired electron in a given MO (MO_1) polarizes the paired electrons in another MO (MO_2). This means that although the two electrons in the MO_2 will have total $S = 0$, they may have $S \neq 0$ in each point where MO_2 extends. This is because where the unpaired electron density is larger in MO_1, there one electron of MO_2 with the same spin will have a larger probability. This effect is called spin polarization. It is obvious that the **I**·**S** interaction should be evaluated as an integral over all space provided the distribution of S is known. This is seldom possible and it is sometimes taken into account parametrically.[7,17-24]

We know therefore that eq 4 is approximated and that this approximation may be severe in the presence of unpaired spin delocalization. We should also consider the possibility that a small fraction of the unpaired electron may be associated with the resonating nucleus itself. We should remember though that s-type orbitals have a finite, different from zero, electron density at the nucleus. Therefore, if s-type orbitals participate in the MO containing the unpaired electrons, the latter have some probability of being located on the resonating nucleus. If this is not the case, unpaired electrons in given MO's can spin polarize the two electrons of an s orbital, thus introducing some unpaired spin at the nucleus. The algebraic sum of the various contributions define the amount of unpaired spin at the resonating nucleus. This amount of unpaired spin is called spin density, although in principle spin density can be defined in any point of the space.

This spin density, even if small, is precisely located on the nucleus and its effects can be quite large. In terms of Hamiltonians, it is indicated as

$$\mathcal{H} = A\mathbf{I}\cdot\mathbf{S} \quad (5)$$

where A is now a constant which does not depend on the molecular orientation and is related to the spin density ρ at the nucleus by

$$A = K(\rho/2S) \quad (6)$$

where K is the experimental hyperfine splitting, and $\rho/2S$ is the unpaired electron spin density, normalized to one electron. The constant A is called contact or Fermi contact hyperfine coupling constant. This denomination comes from certain features of the spectrum of the hydrogen atom: the hyperfine splitting of some lines were explained by Fermi by assuming that the 1s electron has a finite density at the nucleus.[25]

The magnetic field generated by such spin density on the nucleus itself depends on another feature. The unpaired electron has more than one orientation in a magnetic field, according to the allowed M_S values. The transitions among the various orientations or energy levels depend on the electron relaxation times which are always fast with respect to the nuclear relaxation times. The nucleus therefore senses an average of the various orientations of the electron. This average provides a magnetic moment different from zero because some spin orientations have more probability or smaller energy. The residual magnetic moment due to an average of the various orientations having different probabilities according to Boltzmann's statistics is

$$\langle\mu\rangle = \mathbf{g}\mu_B\langle\mathbf{S}_z\rangle \quad (7)$$

where $\langle\mathbf{S}_z\rangle$ is the so called expectation value of S_z, which is given by

$$\langle\mathbf{S}_z\rangle = -S(S+1)\frac{\mathbf{g}\mu_B B_0}{3kT} \quad (8)$$

with B_0 being the external magnetic field, k Boltzmann's constant, and T is the absolute temperature.[26]

The different orientations of the electron magnetic moment have also been taken into consideration when dealing with the dipolar coupling because the magnetic susceptibility is also the result of the different probabilities of the various orientations of an electron spin in a magnetic field.

The resulting shift is then[27,28]

$$\left(\frac{\Delta\nu}{\nu_o}\right) = \frac{A}{\hbar\gamma_N B_0}\langle\hat{\mathbf{S}}_z\rangle = \frac{A}{\hbar}S(S+1)\frac{\mathbf{g}\mu_B}{3\gamma_N kT} \quad (9)$$

This is the contact shift. A more general expression which takes into account the **g** anisotropy and zero field splitting of an orbitally nondegenerated spin multiplet may be formulated as

$$\left(\frac{\Delta\nu}{\nu_o}\right) = \frac{1}{\mu_0}\frac{A}{3\hbar\gamma_N\mu_B}\left[\frac{\chi_{xx}}{\mathbf{g}_{xx}} + \frac{\chi_{yy}}{\mathbf{g}_{yy}} + \frac{\chi_{zz}}{\mathbf{g}_{zz}}\right] \quad (10)$$

where $\mathbf{g}_{ii}$ are the principal components of the **g** tensor.

When recording a spectrum we measure a chemical shift which includes a diamagnetic contribution and the paramagnetic ones outlined here. The diamagnetic chemical shift for a certain nucleus in a particular compound can be predicted or even measured in an

analogous diamagnetic derivative. The difference in chemical shift between the paramagnetic and the diamagnetic species is called *hyperfine shift*. It contains two contributions: one contact in origin and the other dipolar in origin.[15,16,27,28] If the spectrum is recorded in solution, the latter contribution should be indicated as pseudocontact shift, since under these conditions it is isotropic, like the contact contribution.

It is difficult to factorize out the two contributions to the hyperfine shift. Several procedures, some extremely effective, some less so, are available in the literature.[29-34] Some of them will be discussed here. In any case, when it can be reasonably assumed that the magnetic anisotropy is small, the pseudocontact contribution may be neglected.

B. The Nuclear Relaxation Due to the Hyperfine Coupling

Unpaired electrons provide fluctuating magnetic fields which allow nuclei to relax through nonradiative pathways. Such fluctuating magnetic fields arise essentially from three contributions.

1. Electron Relaxation

Electrons relax in metal ions with time constants of the order of 10^{-8} to 10^{-13} s.[8,35,36] In radicals they can increase up to 10^{-5} s.[37,38] These are random and unpredictable magnetic field variations efficient for nuclear relaxation. Note that all the electron magnetic moment is efficient for the nuclear relaxation. It is not considered that there is a small preference among the various orientations of the electron in the magnetic field. Consideration of this effect introduces a negligible correction.

2. Molecular Tumbling in Solution

The molecular tumbling causes the θ value of Figure 1 to change. As a result, the nucleus senses a fluctuating magnetic field caused by the rotation of the electron magnetic moment. This random motion may be quite effective in providing pathways for nuclear relaxation. Again, the full electron magnetic moment must be considered. There is another relaxation mechanism modulated by the molecular tumbling. The Boltzmann distribution on the different Zeeman levels gives a resultant nonzero $\langle \mathbf{S}_z \rangle$, as defined by eq 8 and an induced magnetic moment. Upon molecular rotation, this magnetic moment causes relaxation. This mechanism is called Curie relaxation, since the well-known Curie law depends also on the averaged $\langle \mathbf{S}_z \rangle$ value.[39,40]

3. Chemical Exchange

When a nucleus approaches an electron and then goes away as in the case of a ligand bound to a metal in chemical exchange with excess ligand, the nucleus senses a fluctuating magnetic field.

Nuclear relaxation depends on the square of the hyperfine coupling energy and on the availability of the right frequency for the nuclear transition. The latter is expressed by the so-called spectral density function. It represents the intensity of the frequencies available in the environment of the nucleus or in the lattice. The general equation for nuclear relaxation is[8,41]

$$T_{1,2}^{-1} = (E^2)_{av}\, f(\omega,\tau_c) \tag{11}$$

where $f(\omega,\tau_c)$ is a function containing the frequency of the nuclear transition which of course depends on B_0. τ_c is the correlation time. The latter is a time constant of an exponential process according to which the electron spin and the nuclear spin change their interaction energy due for example to changes in their reciprocal orientation. It is expected that for times shorter than τ_c the two particles will keep their original energy (or orientation as an example), whereas for times longer than τ_c the energy (or orientation) of the two spins will be varied and will not have any memory of the starting situation.

As in the case of the shift, a dipolar and a contact contribution are operative for relaxation. For a simpler description, the dipolar coupling will be treated by using the metal-centered approximation. When it is appropriate, the effect of the spin density in any generic position far from the metal center will be mentioned.

For the dipolar relaxation, the equations are[30,40,42-47]

$$T_1^{-1} = \frac{2}{15}\left(\frac{\mu_o}{4\pi}\right)^2 \frac{\gamma_N^2 g_e^2 \mu_B^2 S(S+1)}{r^6}\left[\frac{\tau_c}{1+(\omega_I-\omega_S)^2\tau_c^2} + \frac{3\tau_c}{1+\omega_I^2\tau_c^2} + \frac{6\tau_c}{1+(\omega_I+\omega_S)^2\tau_c^2}\right] \tag{12}$$

$$T_2^{-1} = \frac{1}{15}\left(\frac{\mu_o}{4\pi}\right)^2 \frac{\gamma_N^2 g_e^2 \mu_B^2 S(S+1)}{r^6}\left[4\tau_c + \frac{\tau_c}{1+(\omega_I-\omega_S)^2\tau_c^2} + \frac{3\tau_c}{1+\omega_I^2\tau_c^2} + \frac{6\tau_c}{1+(\omega_I+\omega_S)^2\tau_c^2} + \frac{6\tau_c}{1+\omega_S^2\tau_c^2}\right] \tag{13}$$

$$T_2^{-1}\,(\text{Curie}) = \frac{1}{5}\left(\frac{\mu_o}{4\pi}\right)^2 \frac{\omega_I^2 g_e^4 \mu_B^4 S^2(S+1)^2}{(3kT)^2 r^6}\left[4\tau_c + \frac{3\tau_c}{1+\omega_I^2\tau_c^2}\right] \tag{14}$$

$$T_{1\rho}^{-1} = \frac{1}{15}\left(\frac{\mu_o}{4\pi}\right)^2 \frac{\gamma_N^2 g_e^2 \mu_B^2 S(S+1)}{r^6}\left[\frac{4\tau_c}{1+\omega_1^2\tau_c^2} + \frac{\tau_c}{1+(\omega_I-\omega_S)^2\tau_c^2} + \frac{3\tau_c}{1+\omega_I^2\tau_c^2} + \frac{6\tau_c}{1+(\omega_I+\omega_S)^2\tau_c^2} + \frac{6\tau_c}{1+\omega_S^2\tau_c^2}\right] \tag{15}$$

It is clear that the term before the parentheses is proportional to the square of the dipolar interaction energy. In eqs 12, 13, and 15 the term contains the square of the electron magnetic moment, a factor proportional to the square of the nuclear magnetic moment, and the sixth power of the electron-nucleus distance. In general (see later for eq 14), the correlation time is given by

$$\tau_c^{-1} = \tau_s^{-1} + \tau_r^{-1} + \tau_M^{-1} \tag{16}$$

where τ_s is the electron relaxation time, τ_r is the rotation correlation time and τ_M is the exchange time. Usually, one of these contributions, i.e. the faster process, will be dominant.

The necessary frequencies for nuclear relaxation are $\omega_S + \omega_I$ (double quantum), $\omega_S - \omega_I$ (zero quantum), and ω_I, where ω_I is the nuclear Larmor frequency and ω_S is the electron Larmor frequency. The terms $\omega_S + \omega_I$ and $\omega_S - \omega_I$ are usually approximated to ω_S. The coefficients inside the $f(\omega,\tau_c)$ function express the probability of the ω_S or ω_I transitions. In eq 13 and 14 there is a frequency-independent term, known as a nondispersive term. It is related to near zero frequencies which affect T_2 and not T_1.

Equation 14 describes the effects of the so called Curie spin relaxation, which introduce the external magnetic field contribution to line widths.[39,49] Here the interaction energy is given by the dipolar coupling between the induced magnetic moment (eq 7) and the nuclear magnetic moment. The correlation time can only be τ_r or τ_M since the induced electron magnetic moment is already an average of the population of the Zeeman levels and hence does not depend on τ_s. Curie relaxation does not appreciably affect nuclear T_1.

We have reported also the equation for $T_{1\rho}$, i.e. the relaxation time in the xy plane under spin-locking conditions, and along the spin-locked axis.[46,47] Here ω_1 is the nuclear Larmor frequency in the oscillating B_1 field, and ω_1 has been neglected with respect to ω_S. Since $\omega_1\tau_c \ll 1$, $T_{1\rho}$ is equal to T_2.

In the case of contact relaxation, the square of the coupling energy is A^2. The equations are[47,48]

$$T_1^{-1} = \frac{2}{3}\left(\frac{A}{\hbar}\right)^2 S(S+1)\frac{\tau_e}{1+(\omega_I-\omega_S)^2\tau_e^2} \quad (17)$$

$$T_2^{-1} = \frac{1}{3}\left(\frac{A}{\hbar}\right)^2 S(S+1)\left(\frac{\tau_e}{1+(\omega_I-\omega_S)^2\tau_e^2} + \tau_e\right) \quad (18)$$

$$T_{1\rho}^{-1} = \frac{1}{3}\left(\frac{A}{\hbar}\right)^2 S(S+1)\left(\frac{\tau_e}{1+(\omega_I-\omega_S)^2\tau_e^2} + \frac{\tau_e}{1+\omega_1^2\tau_e^2}\right) \quad (19)$$

Note that τ_c cannot include τ_r for the nature of the contact coupling, which is independent of the molecular tumbling. Hence,

$$\tau_c^{-1} = \tau_M^{-1} + \tau_S^{-1} \quad (20)$$

As will be discussed later, T_1 and T_2 values may provide valuable information in performing signal assignments or in evaluating the electronic properties of the paramagnetic center. It is difficult to quantify the different contributions to the observed relaxation times. However, relaxation times are often dominated by one of the possible contributions. In the case of metal-bound residues, for nuclei belonging to atoms directly bound to the metal ion the contact contribution may be dominant. For nuclei of the other atoms in the bound residues the dipolar contribution is dominant, although ligand-centered effects may break the rule that states that the broader the line the closer the nucleus to the metal ion. For atoms belonging to nonbound residues it is obvious that the relaxation is due only to dipolar mechanisms. This is a common case for metalloproteins since the density of nuclei is rather high in a sphere centered at the metal ion in which dipolar relaxation mechanisms are operative. The contact relaxation has little effect in the cases which will be discussed here since they are limited to situations in which τ_s is very short and small contact hyperfine coupling occurs. In the case of large proteins, the Curie relaxation mechanism could be dominant on determining T_2.

C. The Systems Suitable for High-Resolution NMR

In Table I a list of transition metal ions in the most common oxidation states is reported together with their estimated τ_s and with the line broadening effect on a proton at a 5-Å distance and at 100 MHz.[7] For our purposes the correlation time τ_s is the crucial parameter which determines the line width of an NMR signal.[7,8] In proteins τ_r is always very large (for example, a protein of molecular weight 30 000 has a τ_r of 1.5×10^{-8} s). If τ_r is shorter than τ_s, it is not possible to observe enough narrow NMR signals of nuclei sensing the paramagnetic center. The exchange time can in principle approach the diffusion limit but in general is too long to determine the correlation time. Therefore τ_s has to be short in order to attempt a fruitful NMR analysis.

The metal ions which are most suitable for performing NMR spectra are high-spin tetrahedral nickel(II), penta- or hexacoordinate high-spin cobalt(II), low-spin iron(III), the lanthanides(III) except gadolinium(III), and high-spin iron(II). All these yield proton NMR spectra with relatively narrow signals. Copper(II), manganese(II), and gadolinium(III) are on the other extreme: the line broadening is so severe that generally the hyperfine-coupled nuclei escape detection. Hexacoordinate nickel(II), tetrahedral cobalt(II), and high-spin iron(III) are borderline cases. There are some instances in which τ_s is a little shorter than usual and the systems can be investigated with success. In the less favorable cases, 2D spectra involving hyperfine-coupled systems cannot be attempted. One-dimensional spectra may be obtained on small molecules if they are deuterated and the resonating nuclei is ^2H.[49,50] This is because the magnetic moment of ^2H is 6.51 times smaller than that of ^1H and T_2^{-1} is consequently reduced. However, ^2H nuclei have a quadrupole moment, and if the rotation is slow as in the case of macromolecules, the lines may again be too broad.[51,52]

Another severe limitation is the size of the protein. For a proton 5 Å away from an $S = 5/2$ in a protein of molecular weight 100 000 the line width due to Curie relaxation (eq 14)[39,40] is 700 Hz at 200 MHz and 6400 Hz at 600 MHz. It follows that there is an intrinsic limit in the size of the proteins which may be studied and that for large proteins smaller magnetic fields may be more appropriate. In diamagnetic proteins the size determines overcrowding of the signals and a slight line broadening. In paramagnetic proteins, the hyperfine-shifted signals are far away but the size of the protein may make them undetectable.

Table I. Electron-Relaxation Times of Some Metal Ions[a] and Nuclear Line Broadenings Induced on a Proton at 5 Å from the Metal at 100 MHz Due to Metal-Centered Dipolar Relaxation

metal ion	τ_s (s)	$\Delta\nu$ (Hz)[b]
Ti^{3+}	10^{-9}–10^{-10}	1 000–100
V^{2+}	5×10^{-10}	2 500
V^{3+}	5×10^{-12}	5
VO^{2+}	10^{-8}–10^{-9}	10 000–1 000
Cr^{3+}	5×10^{-10}	2 500
Cr^{2+}	10^{-11}	80
Mn^{3+}	10^{-10}–10^{-11}	800–80
Mn^{2+}	10^{-9}–10^{-10}	12 000–1 200
Fe^{3+} (HS)	10^{-10}–10^{-11}	1 200–120
Fe^{3+} (LS)	10^{-11}–10^{-12}	10–1
Fe^{2+} (HS)	10^{-11}–10^{-12}	80–10
Co^{2+} (HS)	10^{-11}–10^{-12}	50–5
Co^{2+} (LS)	10^{-9}–10^{-10}	1 000–100
Ni^{2+}	10^{-10}–10^{-12}	300–3
Cu^{2+}	$(1–3) \times 10^{-9}$	3 000–1 000
Ru^{3+}	10^{-11}–10^{-12}	10–1
Re^{3+}	10^{-11}	30
Gd^{3+}	10^{-8}–10^{-9}	400 000–60 000
Dy^{3+}	8×10^{-13}	100
Ho^{3+}	8×10^{-13}	100
Tb^{3+}	8×10^{-13}	100
Tm^{3+}	8×10^{-13}	70
Yb^{3+}	1×10^{-12}	30

[a] These values are generally referred to low magnetic fields, i.e. before any magnetic field effect on τ_s becomes operative. [b] As calculated from eq 13.

Inspection of Table I would restrict the applicability of NMR to low-spin iron(III) proteins, cobalt(II) proteins where cobalt substitutes a native metal like zinc, nickel(II) which substitutes zinc, iron, or copper in tetrahedral sites, and lanthanides(III) as probes for calcium.

As will be discussed soon, when two or more metal ions are magnetically coupled, new electron energy levels are available which may cause a shortening of the electron relaxation times. In other words, polymetallic systems in which magnetic coupling occurs are generally suitable for NMR investigation. These systems include all Fe–S proteins[8,53,54] and, in principle, the Fe–S–Mo systems.

In dimetallic systems where magnetic coupling is operative we may have interesting features.[55] If the metal ions are different and one of them has short electron relaxation times, the other can take advantage of the electron relaxation mechanism of the former through the magnetic coupling. The τ_S of the slow relaxing metal ion decreases as a function of the extent and nature of the magnetic coupling constant. For example, when copper(II) is magnetically coupled to cobalt(II) or nickel(II), its electron relaxation time shortens until well-resolved proton NMR spectra can be obtained. This is the case for the enzyme copper–zinc superoxide dismutase (SOD) in which zinc(II) is substituted by cobalt(II)[56] or nickel(II).[57] Something similar happens in the alkaline phosphatase where copper(II) and cobalt(II) interact in the polymetallic system.[58] Other interesting dimers are hemerythrin, acid phosphatase, and ribonucleotide reductase.[59,60] When dimers are formed by the same metal ions, nonappreciable variations in the electron relaxation times are expected.[61] This limitation does not hold for polymetallic systems. In these cases the new energy levels arising from magnetic coupling may allow electron transitions responsible for electron relaxation. It is therefore quite common to observe short electron correlation time and therefore sharp NMR signals.

D. The Contact Shift in Magnetically Coupled Polymetallic Systems

For the title compounds a theoretical treatment is available which relates the hyperfine coupling of a nucleus with a paramagnetic center and the hyperfine coupling with a metal ion in a polymetallic system.[53,62] This treatment is straightforward for the contact contribution but the concepts hold also for the pseudo-contact term.

We are going to consider a dimetallic system. The magnetic coupling is described in a simple way by the Hamiltonian

$$\mathcal{H} = J\mathbf{S}_1\cdot\mathbf{S}_2 \tag{21}$$

where J is the isotropic magnetic coupling constant and $\mathbf{S}_1$ and $\mathbf{S}_2$ are the spin vectors of the two metal ions. The limits of validity of the above expression are discussed elsewhere.[53,63] As a result of this Hamiltonian, new energy levels arise characterized by spin vectors $\mathbf{S}'$ which vary from $S_1 - S_2$ to $S_1 + S_2$ (S_1 being larger than S_2). The energy separation between two adjacent levels $\mathbf{S}'$ and $\mathbf{S}' + 1$ is $J\mathbf{S}'$. If the coupling is antiferromagnetic, J is positive and the ground state is $S_1 - S_2$, otherwise the coupling is ferromagnetic and the ground state is $S_1 + S_2$.

Since excited states are available for the paramagnetic ion, the contact shift should be evaluated over all the $\mathbf{S}'$ states. For the case of a nucleus sensing one of the two metal ions (M_1) the contact shift is given by[53,54,62]

$$\left(\frac{\Delta\nu}{\nu_o}\right) = \frac{1}{\hbar\gamma_N B_0}\sum_i A_i\langle\mathbf{S}'_z\rangle_i \frac{(2\mathbf{S}'_i + 1)\exp(-E_i/kT)}{\sum_i(2\mathbf{S}'_i + 1)\exp(-E_i/kT)} \tag{22}$$

where A_i is the hyperfine coupling constant of each $\mathbf{S}'_i$ multiplet with the resonating nucleus, and $\langle\mathbf{S}'_z\rangle_i$ is the expectation value of the $\mathbf{S}'_i$ level. The exponential part is the Boltzmann partition function which averages the expectation values over the populated $\mathbf{S}'_i$ states. If the nucleus senses also the other metal ion (M_2), the sum should be repeated also for the other metal ion with a different hyperfine coupling constant. The latter contribution will be neglected for the sake of simplicity. Under these circumstances, it is intuitive that[53]

$$A_{M_1}\langle\mathbf{S}_{1z}\rangle_i = A_i\langle\mathbf{S}'_z\rangle_i \tag{23}$$

where A_{M_1} is the hyperfine coupling with the metal M_1 when $J = 0$ and $\langle\mathbf{S}_{1z}\rangle_i$ is the contribution of metal M_1 to the total expectation value in each ith level. Equation 23 can be rearranged as

$$A_i = A_{M_1}\frac{\langle\mathbf{S}_{1z}\rangle_i}{\langle\mathbf{S}'_z\rangle_i} = A_{M_1}C_{i1} \tag{24}$$

where the C_{iM} coefficients may be calculated once only, for each $i$level of the most common dimetallic spin system.[8,53–55,64] Equation 22 takes then the general form

$$\left(\frac{\Delta\nu}{\nu_o}\right) = \frac{g_e\mu_B}{\hbar\gamma_N{}^3kT} \times \frac{A_{M_1}\sum_i C_{i1}\mathbf{S'}_i(\mathbf{S'}_i + 1)(2\mathbf{S'}_i + 1)\exp(-E_i/kT)}{\sum_i (2\mathbf{S'}_i + 1)\exp(-E_i/kT)} \quad (25)$$

In this way, by knowing (or assuming) the hyperfine coupling constants for mononuclear isolated systems, the contact shifts for the coupled situation may be predicted. Equation 25 allows also the prediction of the temperature dependence of the shifts which, as will be discussed later, is of great importance in the characterization of exchange coupled systems.

The T_1 and T_2 equations should also have coefficients of the type $C_{iM}{}^2$ for each $\mathbf{S'}_i$ level but here the largest effect is the change in τ_s upon establishment of the magnetic coupling when the ions are different.[8,64,65]

Equations analogous to eqs 22 and 25 are available for polymetallic Fe–S proteins.[53–55,64,66–69] In principle, one should solve for any polymetallic system the Hamiltonian:

$$\mathcal{H} = \sum_{i \neq j} J_{ij}\mathbf{S}_i\cdot\mathbf{S}_j \quad (26)$$

where i and j refer to pair of metal ions. The S'_k wave functions can be obtained as linear combinations of S_i and S_j. Equation 24 provides the C_{ik} coefficients, eqs 25 can then be used to predict the contact shift. Equation 26 may be solved only numerically, but Hamiltonians which provide analytical solutions may be obtained when symmetry is present in the cluster.[66–69]

III. Spectral Assignment in Paramagnetic Metalloproteins

Until 1970 researchers used to record NMR spectra (both for diamagnetic and for paramagnetic compounds) in the continuous wave mode. The classical assignment procedure for NMR spectra of diamagnetic systems essentially relied on chemical shift and J coupling information.[70] In the presence of unpaired electrons, a different approach is needed. First, chemical shift values are mainly due to the contact and pseudocontact shifts, as outlined in section II. Hence, it is not easy to assess the diamagnetic contribution, which can be directly correlated to structurally defined functional groups. On the other hand, the line widths present in NMR spectra of paramagnetic substances often wipe out the scalar couplings. Due to these limitations, the signal assignment of paramagnetic substances was initially based on signal intensity and line widths.[29,71–74] The former criterion could distinguish between a methyl and a methine group, while the latter could allow the establishment of which proton is closer to the paramagnetic center. The most powerful technique, however, was the comparison of spectra of related compounds in which the different chemical groups were selectively modified or substituted.[24,71,75–83] With regard to paramagnetic metalloproteins, this approach could only be used in the cases where it was possible to perform some chemical modifications on residues near the paramagnetic center. This is the case with some hemeproteins containing a noncovalently bound heme prosthetic group.[84–87]

Since 1970, the advent of FT instruments having capabilities of performing multipulse sequences has made routinely available the measurement of T_1 values.[88] Nuclei in paramagnetic compounds often relax by direct coupling with unpaired electrons making cross relaxation to other nuclei small and sometimes negligible.[89] Therefore, in paramagnetic compounds T_1 values become as close as possible to the ideal case of an exponential process. This allows in principle the use of T_1 values as a means of obtaining structural information. In fact, since the spin nuclear relaxation depends on the square of the interaction energy which causes the relaxation, it will finally depend on the sixth power of the electron–nucleus distance.[43] A drawback in this strategy is that the unpaired electron is often delocalized onto the ligand. In such cases the fractional amount of unpaired spin present on nuclei different from the metal provides a new dipolar relaxation mechanism for the nucleus (ligand-centered contribution), which is difficult to account for. This has been proved to be the case for some low-spin ferric porphyrins[90] and for cobalt(II)-substituted SOD.[91,92] This fact means that the equations derived in the frame of a point–dipolar model become approximations. The analysis of T_1 and T_2 values (including the Curie relaxation contribution to the line width) is quite informative, although the results are not conclusive. Even a small amount of electron delocalization can produce a sizable enhancement of nuclear relaxation rates, simulating shorter metal–nucleus distances.

In the late 1980s the nuclear Overhauser effect allowed the determination of distances between nuclei. Later, 2D NOESY have become a routine investigation and finally the possibility of detecting scalar coupling in fast relaxing systems is being investigated. These techniques, coupled with the use of the theory of pseudocontact shifts and with the analysis of nuclear relaxation times, represent powerful tools for the assignment and for providing structural information around the metal ion.

A. Nuclear Overhauser Effect

Before the availability of instruments operating at high magnetic fields and at the same time providing adequate acquisition conditions (i.e. field and temperature stabilities for long periods of time), it was not possible to measure nuclear Overhauser effect (NOEs) in fast relaxing systems. The first reported NOE experiment on a paramagnetic metalloprotein is dated 1983.[93] Of course we deal only with proton–proton NOEs.

The NOE η_{ij} is the fractional variation of the intensity I of signal i upon saturation of another signal j dipolarly coupled to it and is given by[13,14]

$$\eta_{ij} = (I - I^o)/I^o \quad (27)$$

where I^o is the equilibrium intensity of i. It may be

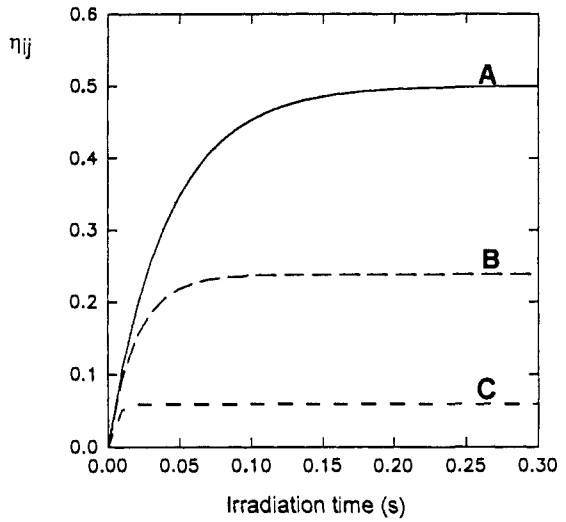

Figure 2. Calculated NOE values as a function of the irradiation time according to eq 30 at 300 MHz, for a τ_r value of 10 ns, for two protons 1.8 Å apart. ρ_i was set to values of (A) 20, (B) 50, and (C) 200 s^{-1}.

demonstrated that the rate of change of I upon saturation of signal j in a multispin system is[14]

$$dI/dt = -\rho_i(I - I^0) - \sigma_{ij}(J - J^0) - \sum_k \sigma_{ik}\eta_{kj}(K - K^0) \quad (28)$$

where σ_{ij} is the cross relaxation rate between the saturated (j) and the observed (i) signals, σ_{ik} is the cross relaxation rate between i and the other nuclei k to which i is dipolarly coupled, η_{kj} is the NOE on signal k upon irradiation of signal j and ρ_i is the reciprocal of the selective T_1 value of nucleus i. In paramagnetic systems, selective and nonselective T_1 values are often equal.[8,94]

In fast relaxing systems, some approximations which simplify the treatment of NOE data may be made. If nucleus i relaxes quickly by coupling with the unpaired electrons, cross relaxation rates between i and other nuclei (i.e., σ_{ij} and σ_{ik}) are small respect to ρ_i. Due to the factor η_{kj} which multiplies the cross relaxation σ_{ik}, the third term of eq 28 may be neglected. This means that spin diffusion effects are negligible under certain experimental conditions in paramagnetic systems.[10,95-97] This allows one to use the two-spin approximation for describing the evolution of I with time:

$$dI/dt = -\rho_i(I - I^0) - \sigma_{ij}(J - J^0) \quad (29)$$

Integration of eq 29 shows that the response, as defined in eq 27, is time dependent:

$$\eta_{ij}(t) = \frac{\sigma_{ij}}{\rho_i}(1 - e^{-\rho_i t}) \quad (30)$$

The plot of $\eta_{ij}(t)$ according to eq 30 is reported in Figure 2. Fast relaxation rates make NOE detection difficult. By inspecting both eq 30 and Figure 2 it is obvious that large ρ_i values will be reflected in small measured η_{ij}. In addition, broad signals are difficult to detect in difference spectra.

If the irradiation time t is long with respect to ρ_i^{-1} eq 30 becomes

$$\eta_{ij} = \sigma_{ij}/\rho_i \quad (31)$$

The NOE becomes time independent. This is the so-called steady-state NOE experiment.[13,14]

On the other hand, if saturation times $t \ll \rho_i^{-1}$ (but long enough to saturate I) are applied, eq 30 adopts the form

$$\eta_{ij} = \sigma_{ij}t \quad (32)$$

which represents the truncated NOE experiment (TOE).[98] Equation 32 shows that the observed NOE in this case is independent of the relaxation rate of nucleus i. On the other hand, it is clear that by using different irradiation times it is possible to measure the cross relaxation rate σ_{ij} from the NOE buildup. In any case, the acquisition of the complete buildup curve allows the estimation of the selective T_1 value by fitting the experimental data with eq 30.[96]

In principle, the TOE experiment is superior for diamagnetic proteins since it avoids spin diffusion problems.[98] In the case of paramagnetic compounds, ρ_i^{-1} values are short and hence the steady-state condition is reached using short irradiation times during which secondary NOEs cannot build up to an observable extent.

With the demanding need of NMR applications, the transient NOE technique was developed in order to reduce spin diffusion effects.[99] In this case, a selective 180° pulse is applied on j and the system is allowed to return to equilibrium during a certain delay, and then an observation pulse is applied. Transient NOE is hardly ever superior to steady state NOE in paramagnetic proteins, since in order to achieve inversion of the magnetization of a broad signal, some selectivity must be sacrificed.[10,97,100] Steady-state NOE experiments are then quite adequate in paramagnetic systems.

The cross relaxation rate σ_{ij} is given by

$$\sigma_{ij} = \left(\frac{\mu_0}{4\pi}\right)^2 \frac{\hbar^2\gamma_i^2\gamma_j^2}{10r_{ij}^6}\left(\frac{6\tau_c}{1 + (\omega_i + \omega_j)^2\tau_c^2} - \frac{\tau_c}{1 + (\omega_i - \omega_j)^2\tau_c^2}\right) \quad (33)$$

It depends on the square of the dipolar coupling between nuclei i and j, on the Larmor frequency of nuclei i and j and on the reorientation correlation time τ_c. The relaxation rate ρ_i in eq 31 is the sum of the dipolar proton–proton contribution and a paramagnetic contribution ρ_{par}:

$$\rho_i = \left(\frac{\mu_0}{4\pi}\right)^2 \frac{\hbar^2\gamma_i^2\gamma_j^2}{10r_{ij}^6}\left(\frac{6\tau_c}{1 + (\omega_i + \omega_j)^2\tau_c^2} + \frac{\tau_c}{1 + (\omega_i - \omega_j)^2\tau_c^2} + \frac{3\tau_c}{1 + \omega_i^2\tau_c^2}\right) + \rho_{par} \quad (34)$$

In diamagnetic proteins, the main relaxation pathway is the proton–proton dipolar interaction ($\rho_{par} = 0$) and the distance dependence of the NOE cancels out in eq 31. This is not the case for paramagnetic systems, since ρ_i is given almost exclusively by the term ρ_{par} which does not depend on r_{ij}^{-6}. In fact, if ρ_i is dominated by ρ_{par}, the NOE amount for a signal sensing the influence of the paramagnetic center in the slow-motion limit

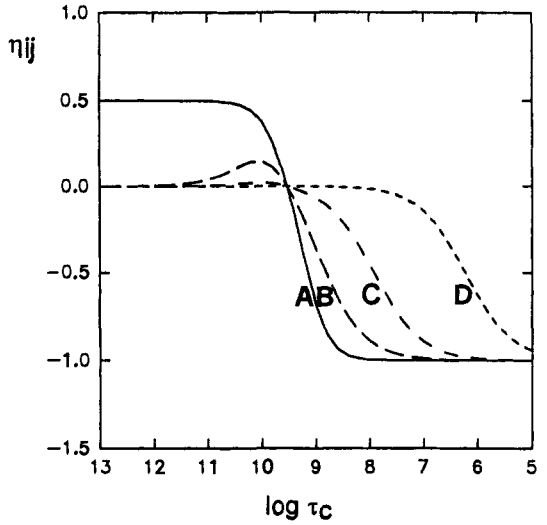

Figure 3. Motional dependence of the NOE values for a pair of protons 1.8 Å apart as calculated from eq 31 for a magnetic field of 500 MHz. σ_{ij} and ρ_k are calculated from eqs 33 and 34, respectively. ρ_{par} was set to values of (A) 0, (B) 2, (C) 20, and (D) 1000 s^{-1}.

($\omega_i\tau_c \gg 1$) may be expressed by the following equation:

$$\eta_{ij} = -\left(\frac{\mu_o}{4\pi}\right)^2 \frac{\hbar^2\gamma^4\tau_c}{10r_{ij}^6\rho_i} \qquad (35)$$

which shows that the measurement of NOE between paramagnetic signals allows the direct determination of interproton distances provided ρ_i is known.

The NOE dependence of τ_c for different ρ_{par} values as calculated from the full form of eq 31 is shown in Figure 3. In very large diamagnetic proteins, in the slow motion limit, τ_c is long and $\eta_{ij} = -1$ since $6\tau_c/[1 + (\omega_i + \omega_j)^2\tau_c^2]$ in eqs 33 and 34 as well as $3\tau_c/(1 + \omega_i^2\tau_c^2)$ in eq 34 vanish. It is then not possible to distinguish between different protons since most of them yield NOE values of −1 (line A, Figure 3).[95,101] As shown in Figure 3, paramagnetically induced relaxation modulates the τ_c dependence in the sense that a much longer τ_c is required for the spins to yield sizable NOEs (lines B–D, Figure 3).[95] Paramagnetic metalloproteins are therefore particularly suitable for NOE studies as τ_c is large.

In the fast-motion limit, η_{ij} approaches the maximum value of 0.5 in diamagnetic compounds. Again, the electron–nucleus relaxation diminishes the observable NOEs, which may be unobservably small (lines C and D, Figure 3). Hence, in the cases where the protein is not large enough, the use of viscous solvents (like ethylene glycol/water mixtures) may help in increasing the expected NOEs.[102,103]

When ρ_i^{-1} becomes long, then all the problems encountered in NOE of diamagnetic molecules become increasingly more relevant and cross relaxation with other nuclei (i.e., spin-diffusion effects) cannot be neglected with respect to ρ_{par}.[101]

When performing NOE experiments on paramagnetic macromolecules, strong rf fields should be used in order to saturate signals displaying short T_1 and T_2 values. Hence, it is highly probable that off-resonance saturation effects will be produced on nearby signals. This problem may be avoided by selecting appropriate off-resonance frequencies which, upon FID subtraction, provide cancellation of the off-resonance signals in the difference spectrum.[89,104] Off-resonance effects may become considerably large in transient NOE experiments.[97]

With regard to dynamic range problems, several methods for suppressing more intense signals may be appropriate.[105–107]

Detection of NOEs has provided a very important tool for the assignment of paramagnetic NMR signals. Nuclear relaxation measurements yield information regarding the nucleus–metal distance, while NOE experiments provide nucleus–nucleus distances. The development of NOE in paramagnetic proteins constituted the first step aimed at the determination of the three-dimensional structure around the paramagnetic ion.

B. Two-Dimensional Techniques

Once researchers had become more and more confident of the capability of measuring NOEs, efforts were channeled into the detection of cross peaks in 2D NOESY spectra between nuclei sensing the paramagnetic center. The first attempts to use NOESY were made on cytochrome b_5[108] and metcyanomyoglobin,[109] which are both highly soluble and whose signals have relatively long T_1 values (i.e. 150 ms for proton–metal distances of about 6 Å). 2D spectra[110–115] allow the detection of all the connectivities in a single experiment, thus considerably reducing the total experimental time. Moreover, off-resonance and selectivity problems arising from the use of saturation pulses in 1D NOE experiments are no longer an issue.

On passing from one-dimensional to two-dimensional experiments, there is a loss in sensitivity of a factor 2–3.[116] Besides, in paramagnetic compounds the system returns to equilibrium before sizable magnetization or coherence transfer occurs.[8,11,12] Therefore, a careful adaptation of the classical 2D NMR experiments to fast relaxing systems is necessary. Due to their short T_1 and T_2 values, substantial relaxation is operative during the evolution time t_1, the mixing time τ_m and the detection time t_2. Long acquisition times are never necessary as the x and y components of the magnetization disappear with time constant T_2. Also during t_1 transverse magnetization decays with time constant T_2. That means that for t_1 values longer than T_2, the interferogram in the F1 dimension contains no useful information and only noise is acquired. Therefore, too many data points in both dimensions results in longer experimental time without any signal-to-noise improvement. On the other hand, as far as connectivities between hyperfine shifted resonances are concerned, the large shift spreading makes unnecessary high resolution as in the diamagnetic cases.

It is important to take into account the time evolution of the magnetization or the coherence in each 2D experiment. Thus, the application prior to Fourier transform of a window function with the same time dependence magnifies the FID components responsible for the cross peak.

The "mixing" part of the 2D experiment is different for each 2D pulse sequence (see Figure 4).[110–115] In the NOESY case (Figure 4A),[117] it consists of a time period (τ_m) during which magnetization transfer between the z components of the dipolarly coupled nuclei occurs. At the same time (during τ_m) longitudinal relaxation is

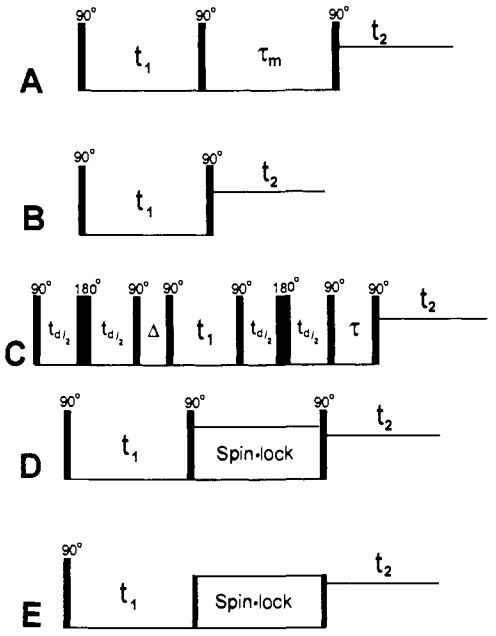

Figure 4. Schematic drawings of pulse sequences for (A) NOESY, (B) COSY, (C) ISECR-COSY, (D) HOHAHA, and (E) ROESY experiments.

operative. The time dependence of the intensity of the cross peak between two dipolarly coupled nuclei i and j is as follows:[14]

$$I_{ij} = \frac{I(0)}{2}\frac{\sigma_{ij}}{D}(e^{-(R'-D)\tau_m} - e^{-(R'+D)\tau_m})\, e^{-t_{1,2}/T_2} \quad (36)$$

where

$$R' = {}^1/_2(T_{1sel(i)}{}^{-1} + T_{1sel(j)}{}^{-1}) \quad (37)$$

and

$$D = ({}^1/_4(T_{1sel(i)}{}^{-1} - T_{1sel(j)}{}^{-1})^2 + \sigma_{ij}{}^2)^{1/2} \quad (38)$$

It can be demonstrated that the best results are obtained for τ_m values of the order of the T_{1sel} values of the two dipolarly coupled signals. When T_{1sel} is short, the magnetization transfer is small and the cross-peak intensities are reduced accordingly. However, if suitable signal-to-noise ratios are achieved, cross peaks may still be observed and used to obtain structural information. Interproton distances of about 3 Å or less can be sampled by this approach. With the mixing times used, spin-diffusion effects are usually negligible.[10,95] When the T_{1sel} are different, appropriate values of τ_m intermediate between them should be used.[118]

If the NOESY pulse sequence follows the selective saturation of a hyperfine-shifted signal we have the so-called NOE–NOESY experiment:[119] upon saturation of a resonance the intensity of all the other proton signals dipolarly coupled with it, as well as that of the dipolar connectivities involving these signals, results reduced by the relative NOE. Analogously to the 1D NOE case, difference spectra are obtained alternating off- and on-resonance experiments: the resulting NOESY–difference map contains only the dipolar connectivities involving the signals that experience NOE from the irradiated resonance. The NOE–NOESY method thus allows the clear detection of NOESY cross peaks among all the resonances due to protons close to the saturated one and coupled to it directly or through spin-diffusion effect.

The unique ability to resolve signals due to nuclei in different chemical environments makes NMR especially powerful for the study of dynamic processes. Whenever the interconversion rate between two species is shorter than the chemical shift difference (in hertz) of the corresponding NMR resonances, two distinct sets of signals are detectable. The use of 2D NMR for chemical kinetics was first proposed by Jeener, Meier, Bachmann, and Ernst.[120] 2D saturation transfer experiments (EXchange SpectroscopY or EXSY) are based on the NOESY pulse sequence.[121] They have been extensively employed for the assignment of the NMR spectra of systems obtainable in the diamagnetic form. The extensive assignments on the latter species could then be transferred to the paramagnetic homologue by saturation transfer modulated by facile electron exchange.[122–124] On this subject, it should be mentioned that the first 2D NMR experiment on a paramagnetic protein was an EXSY spectrum, performed by Xavier's group.[122] More recently other EXSY experiments between two or more paramagnetic species have been successfully performed.[125–127] In this case the optimum τ_m should be longer than the exchange time of the two species and shorter than the T_1 values of the corresponding signals. When the exchange time is longer than T_1, best results are obtained with mixing times of the order of T_1. Whenever it is necessary to quantitatively measure the extent of the saturation transfer effect, 1D saturation transfer experiments are more readily useful than the 2D EXSY maps. Indeed, they have been applied to evaluate the electron self-exchange rate constants in samples containing a mixture of oxidized and reduced proteins.[128–130] As the difference in shift between the oxidized and the reduced forms of a protein usually do not exceed 100 ppm, at 600 MHz an upper limit of about 2×10^5 s^{-1} for the self exchange rates measurable by NMR can be predicted. The lower limit results from the observation that a too low self-exchange rate will not allow significant magnetization transfer before relaxation occurs. That means that self-exchange rates higher than 0.01 times the T_1^{-1} value of the resonance on which the saturation transfer effect is observed are needed.

In the COSY experiment (Figure 4B) the "mixing" is represented by the second 90° pulse.[131,132] The scalar connectivities build up during the t_1 and t_2 times. During both these times relaxation is operative with time constant T_2, leading to a drastic decrease of cross-peak intensities in paramagnetic compounds. Therefore, in COSY experiments, optimum coherence transfer from one nucleus A to another nucleus X occurs when $\sin(\pi J_{AX} t_1) \exp(-t_1/T_{2A})$ is maximum.[132] On the other hand optimum detection of the transferred magnetization occurs when $\sin(\pi J_{AX} t_2) \exp(-t_2/T_{2X})$ is maximum.[132] In fast relaxing systems the decay of these functions is faster than the coherence transfer build up, and the position of the maxima corresponds to t_1 and t_2 values of the order of the T_2 of the signals between which scalar connectivity is expected. Therefore, an appropriate choice of the t_2 value, of the number of t_1 increments, and of the shape of the weighting functions is required. Moreover, in COSY experiments the J-split components of the cross peaks are in antiphase. In

paramagnetic compounds, where the line widths are usually much broader than the J values, this leads to partial or total cancellation of the cross peaks themselves. It has been found that this problem is less dramatic if acquisition and Fourier transform in the so-called magnitude mode are employed.[133,134] However, magnitude-type COSY experiments (MCOSY) are characterized by an intrinsically lower resolution when compared with the phase-sensitive ones. Recently, Xavier et al. illustrated the advantages to phase cross peaks in a pure dispersive mode.[135] However, as far as scalar connectivities between well-resolved hyperfine-shifted signals are concerned, the best results have been reported by employing MCOSY experiments with t_1 and t_2 values of the order of $2T_2$ of the signals between which cross peaks are expected. If sine bell or sine-squared bell window functions are used prior to Fourier transform, the maximum of the window function corresponds to the T_2 value. When higher resolution is necessary, the problem of the low quality of the simple phase-sensitive COSY spectrum can be overcome by employing the ISECR COSY pulse sequence (Figure 4C),[136] which provides in-phase cross peaks. In this sequence the time t_d can be adjusted in such a way that the coherence transfer is maximum at the beginning of the t_1 and t_2 times, i.e. a t_d time of the order of T_2 should be used.[134] Analogous to the NOESY sequence, in this kind of experiment cosine bell or cosine-squared bell window functions are employed before Fourier transform. Indeed, the maximum information is contained at the beginning of the FID and of the interferogram along the t_1 axis.

A warning regarding COSY experiments on paramagnetic metalloproteins should be made. Recent theoretical calculations[137] have demonstrated that cross peaks due to relaxation-allowed coherence transfer may be detected in COSY maps and mistaken as scalar connectivities. They are due to cross correlation between dipolar coupling and Curie relaxation. Therefore, the more T_2 is affected by Curie relaxation (i.e. in large macromolecules and with large S values), the more dramatic this effect becomes (see also section V). For this reason, the development of pulse sequences allowing spectroscopists to separate true scalar connectivities from dipolar relaxation-allowed cross peaks is an issue. It should be noted that the ISECR COSY pulse sequence allows the selection of the true scalar connectivities (Luchinat, personal communication).

2D correlated spectroscopy has been used also in the heteronuclear case. The lower giromagnetic constant and the lower natural abundance of ^{13}C and ^{15}N, which are the two heteronuclei found in proteins, cause a loss in sensitivity. However, when considering ^{15}N NMR experiments in paramagnetic proteins, it is important to remember that $\gamma(^{15}N)/\gamma(^{1}H) = -0.101$. Hence, the relaxation rate enhancement for nonbound residues (experiencing pseudocontact contribution) according to eqs 12 and 13 in a ^{15}N nucleus will be one-hundredth of that experienced by a proton at the same distance from the paramagnetic center. In this way, hyperfine-shifted ^{15}N signals will be much sharper that hyperfine-shifted proton signals. This effect is also important for the ^{13}C nucleus, even if less markedly so [$\gamma(^{13}C)/\gamma(^{1}H) = 0.25$]. The recording of 1D experiments on ^{13}C and ^{15}N nuclei are thus favored by their slower relaxing

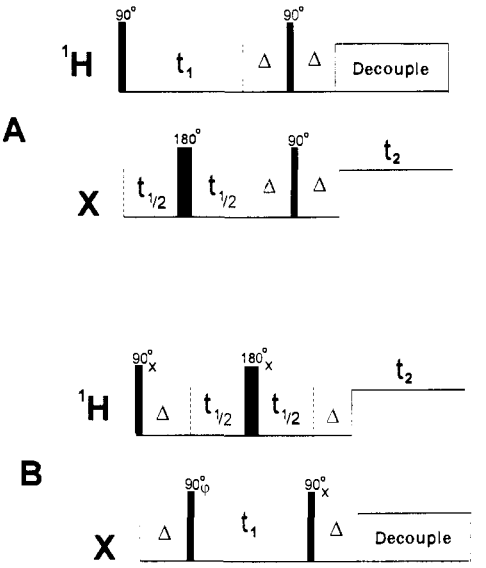

Figure 5. Schematic drawings of pulse sequences for (A) heteronuclear ^{1}H–X COSY and (B) inverse detection ^{1}H–X HMQC experiments.

nature. Figure 5 shows the two most common pulse sequences to record 2D heteronuclear spectra. In the normal HETCOR experiment (Figure 5A), the X nucleus is detected, so that the sensitivity problem found in 1D experiments is also present. The Δ delay is usually set equal to $1/(2J)$, and it is necessary when proton-decoupled spectra are desired. Inverse detection experiments allow the acquisition of heteronuclear correlation spectra taking advantage of the higher sensitivity of proton nuclei. The spectrum of the X heteronucleus is indirectly measured as the F_1 dimension of a 2D spectrum, either in multiple or single quantum coherence experiments. The X chemical shift information can be encoded by allowing the ^{1}H–X multiple quantum coherences to evolve during the evolution time t_1[138,139] in the heteronuclear multiple quantum coherence experiments (HMQC) (Figure 5B). HSQC (heteronuclear single quantum coherence) experiments transfer magnetization from the proton to the low γ nucleus and back to the protons by means of two INEPT-like sequences.[140] One should be reminded that in the latter case the detected nucleus is the proton, so that in paramagnetic substances the same fast relaxing features already discussed in homonuclear 2D experiments will be met here. Since the coherence transfer during Δ is proportional to $\sin(\pi J\Delta)$, it will reach its maximum for $\Delta = 1/(2J)$. There is, however, one important advantage: heteronuclear one-bond coupling constants are much larger ($^1J_{CH}$ = 120–160 Hz, $^1J_{NH}$ = 90 Hz) than homonuclear proton–proton coupling constants. Thus, the magnetization coherence transfer occurs in a shorter period of time and it is unnecessary to use long delays. Nevertheless, the proton line widths may be larger than the heteronuclear $^1J_{XH}$ couplings. In this case, the Δ delay should be adjusted according to the T_2 values, as in the case of the ISECR-COSY spectrum.[134]

The HOHAHA pulse sequence, widely used to reveal scalar connectivities in diamagnetic systems, is reported in Figure 4D.[141,142] One of the advantages of this experiment with respect to COSY is that it has in-phase coherence transfer. The mixing part consists of a spin-lock pulse sequence. $T_{1\rho}$ is the time constant for the

exponential decay of the transverse magnetization when this is kept locked by a radiofrequency field in the xy plane along the direction of the radio frequency itself. $T_{1\rho}$ is very close to T_2. Therefore, for paramagnetic compounds, it is appropriate to use mixing times of the order of T_2. Additional problems arise from the difficulties of obtaining a regular spin-lock field profile over a large chemical-shift range. At the high magnetic field required for studying macromolecular systems the problem becomes more serious due to the larger chemical shift spreading (in hertz) and to the lengthening of the 90° and 180° pulse durations.[134]

When considering rotating-frame 2D experiments, the ROESY experiment should be mentioned. The pulse sequence is reported in Figure 4E.[143] As in NOESY experiments, magnetization transfer occurs through dipolar coupling. Besides the common spin-locking problems, the interest of ROESY experiments arises from the possibility of distinguishing NOE-type connectivities from saturation transfer-type ones. As the sequence for EXSY and NOESY experiments is exactly the same, and in macromolecules also the sign of the two different type of connectivities is the same,[121] NOESY and EXSY cross peaks cannot be distinguished. In ROESY experiments the former are negative and the latter are positive. An experiment which distinguishes between dipolar coupling and chemical exchange in a paramagnetic protein has been performed.[144]

C. Genetics and NMR

A great aid to NMR spectroscopy comes from isotopic labeling. The simplest idea is that of investigating a system in which one or all the protons in a residue have been selectively substituted by deuterium. Selective deuteration in proteins has been used since the late 1960s with the aim of simplifying the ^{1}H NMR spectra.[145,146] This procedure has been also used in paramagnetic proteins.[84,65,147] With the advent of 2D NMR techniques, selective deuteration has been useful in obtaining residuetype and stereoselective assignments. Selectively deuterated amino acids can be chemically synthesized in the laboratory, or even purchased.

Nowadays the overproduction of wild-type, mutated, or labeled proteins in quantities as required for NMR experiments can be achieved. For this a bacterial host is often chosen for which the metabolic pathways for amino acid synthesis and degradation are known. Then a controlled, high-level expression system for the synthesis of the desired protein should be developed in the bacterial host. The selective labeling is performed by growing the bacteria on defined media supplemented with the deuterated amino acid. The use of bacteria with amino acid auxothropies and aminotransferase deficiencies ensures an efficient and controlled incorporation of the labeled amino acid(s) in the protein.

The spectrum of the deuterated protein will be simplified, and the missing signals can be identified as those belonging to the deuterated amino acid. Unfortunately, in general it is not possible to record the ^{2}H spectrum because the slow rotation of the protein induces a severe line broadening of the deuterium resonances. However, if the deuterated moiety is a methyl group, which may display an internal rotation rate larger than that of the protein, the signals may be observed.[51]

Another possibility is to produce ^{13}C- or ^{15}N-enriched proteins.[148-150] In these cases the protein should be grown in a media supplemented with the desired isotope. ^{13}C enrichment generally is performed up to an extent of 20–25%, since ^{13}C is a $^1/_2$ nucleus and direct ^{13}C–^{13}C scalar couplings could complicate the spectra. Isotope enrichment may be performed by supplying $^{13}CO_2$ as carbon source diluted with natural abundance CO_2 to 20–25% isotopic purity. For the ^{15}N case, since there are no direct nitrogen–nitrogen bonds in proteins, this problem is not encountered and large enrichment levels may be attempted.

The general advantages and the utility of obtaining ^{13}C- and ^{15}N-enriched proteins, as well as the application to paramagnetic metalloproteins, will be discussed in section IX.

IV. Iron–Sulfur Proteins

Iron–sulfur proteins are a wide group of non-heme iron proteins containing polymetallic centers in which the iron ions are tetrahedrally coordinated, generally with bridging sulfide ions and cysteinyl residues as ligands (see Figure 6, parts B–D).[151-154] In addition, proteins containing a single ion coordinated to four cysteines (Figure 6A) are included in this class because they represent a reference point for the polymetallic center. They have always been considered electron-transfer proteins, but some iron–sulfur proteins display catalytic properties, like aconitases (aconitate hydratases).[155] Much effort has been devoted to the synthesis and analysis of model complexes in order to understand the properties of these polymetallic centers.[156-161]

Being in a tetrahedral or pseudotetrahedral environment, both iron(II) and iron(III) ions are always high spin ($S = 2$ and $^5/_2$, respectively). Figure 6 displays the structurally characterized iron–sulfur centers present in proteins, and Table II describes the oxidation states in naturally occurring polymetallic systems. The existence of these clusters has been established by X-ray crystallography.[162-180] In some proteins more than one iron–sulfur cluster may be found, as well as other structurally different redox centers. Recently, the existence of a Fe_6S_6 cluster in a six-iron protein isolated from *Desulfovibrio vulgaris* has been suggested on the basis of its Mossbauer and EPR spectra.[181,182]

Although the most common ligands in iron–sulfur clusters in proteins are cysteine sulfurs, some exceptions have been reported. For example, ENDOR spectroscopy has indicated the existence of histidine nitrogen ligands in Rieske-type proteins[183,184] or oxygen ligands in aconitase,[155,165] in ferredoxin III from *Desulfovibrio africanus*[186] and in a ferredoxin from *Pyrococcus furiosus*.[187]

Iron–sulfur proteins have attracted the interest of NMR investigators from the very beginning of NMR studies of paramagnetic systems[188-191] and since then many biochemists have used NMR in an attempt to characterize them.[192-196] As outlined in section II.C of this review, polymetallic systems have short electronic relaxation times, especially if they are constituted by different ions.[55] This accounts for the numerous spectra reported in the early literature which were used as fingerprints to recognize the different types of clusters

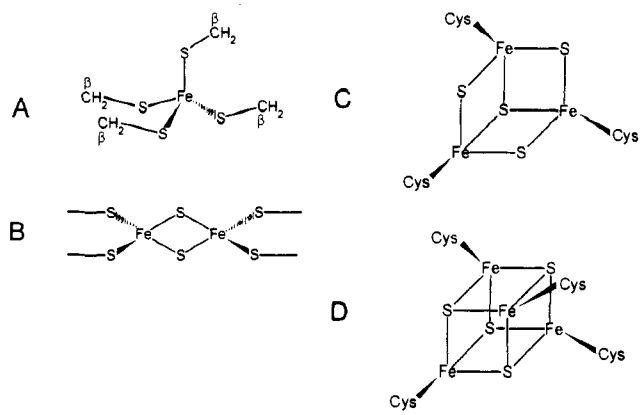

Figure 6. Schematic representation of the structurally characterized iron–sulfur centers in proteins: (A) monoiron center, as present in rubredoxin, (B) Fe_2S_2 cluster, (C) Fe_3S_4 cluster, and (D) Fe_4S_4 cluster.

Table II. Oxidation States of the Most Typical Iron–Sulfur Clusters in Proteins

cluster	oxidized	reduced
(Fe_2S_2) Fds[a]	2 Fe(III)	Fe(III), Fe(II)
(Fe_3S_4) Fds	3 Fe(III)	2 Fe(III), Fe(II)
(Fe_4S_4)Fds	2 Fe(III), 2 Fe(II)	1 Fe(III), 3 Fe(II)
(Fe_4S_4)HiPIPs[a]	3 Fe(III), 1 Fe(II)	2 Fe(III), 2 Fe(II)

[a] Abbreviations: Fd, ferredoxin; HiPIP, high potential iron–sulfur protein.

upon the temperature dependence of the paramagnetic shifts.[192,197]

All the iron–sulfur proteins studied up to date by means of NMR spectroscopy possess cysteine residues as iron ligands. The β-CH_2 and the α-CH protons of these Cys experience hyperfine shifts which are mainly contact in origin, as was shown for model compounds.[160,161]

We would like to review here the systems represented in Figure 6 by mentioning first rubredoxin, which has only one iron ion, and by discussing then Fe_2S_2 and Fe_3S_4 ferredoxins, high-potential iron–sulfur proteins, and Fe_4S_4 ferredoxins. Finally, some systems of greater complexity will be considered.

A. Single Iron Containing Proteins

Rubredoxin,[198,199] desulforedoxin,[200] desulfoferrodoxin,[201] and rubrerythrin[202] are examples of iron–sulfur proteins containing a mononuclear iron center tetrahedrically coordinated to four cysteines (see Figure 6A).[198] Rubredoxin (MW 6 000) was the first non-heme iron protein studied by ^1H NMR spectroscopy.[188] In the case of oxidized rubredoxin (Rd), the long τ_e of the iron(III) ion ($\simeq 10^{-9}$ s) induces such a large broadening of the β-CH_2 cysteine proton signal that they are rendered undetectable.[203,204]

In reduced Rd, the shorter τ_e of iron(II) allows the detection of four very broad signals in the 260–150-ppm range (cf. signals A–D in Figure 7A), and four broad signals in the 17–11-ppm region (signals E–H, Figure 7B).[204] The four more shifted resonances have roughly the same area, being double that of signals E–H. Signals A–D have been assigned to the β-CH_2 protons of the bound cysteines by comparison with the shifts observed in model iron(II)–alkylthiolate complexes.[204-206]

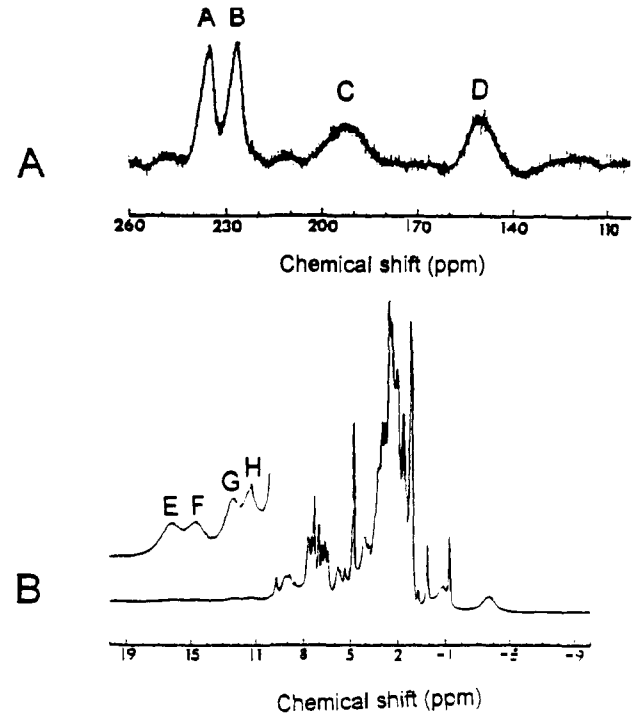

Figure 7. ^1H NMR spectrum (300 MHz) of reduced *Desulfovibrio gigas* rubredoxin at 328 K: (A) 260–100 ppm region, (B) 20 to −10 ppm region. (Reprinted from ref 204. Copyright 1987 American Chemical Society.)

The possible origin of the four resonances E–H from the cysteine α-CH protons was also mentioned.[204]

One would expect to observe eight resonances for the cysteine β-CH_2 protons. The fact that four signals are observed instead of eight has been attributed[204] to the quasi-D_{2d} symmetry of the metal center observed in crystallographic studies.[199] The observation of two signals (C,D) broader than the other two (A,B) is consistent with a ligand conformation placing one β proton closer to the iron ion for each geminal pair. Each signal would then correspond to two protons of different cysteine residues symmetrical to one another.

Owing to the large line widths of these signals (up to 4500 Hz) it is very difficult to carry out NOE or 2D experiments on them in order to perform a sequence specific assignment of the ligands. A recent work[207] reports the inability to detect 2D connectivities near the paramagnetic center both in the oxidized and reduced forms of the Rd from *P. furiosus*. Interesting perspectives arise upon metal substitution by introducing metal ions more suitable for NMR investigations, such as nickel(II) or cobalt(II) (see sections VII and VIII).[208]

B. Fe_2S_2 Proteins

Fe_2S_2 ferredoxins (Fds) are found in chloroplasts, bacteria, vertebrate mitochondria, and oxygenase systems.[170] Fe_2S_2 Fds contain two iron ions, each coordinated to two cysteines and bridged by two inorganic sulfur atoms (see Figure 6B). They have molecular weights around 11 000.[209] X-ray structures are available for several Fe_2S_2 proteins.[162-164,170] The oxidized protein contains two iron(III) ions and the reduced protein an iron(III) and an iron(II).

In the case of oxidized Fe_2S_2 Fds, the two iron(III) ions display a strong antiferromagnetic coupling.[62,210,211]

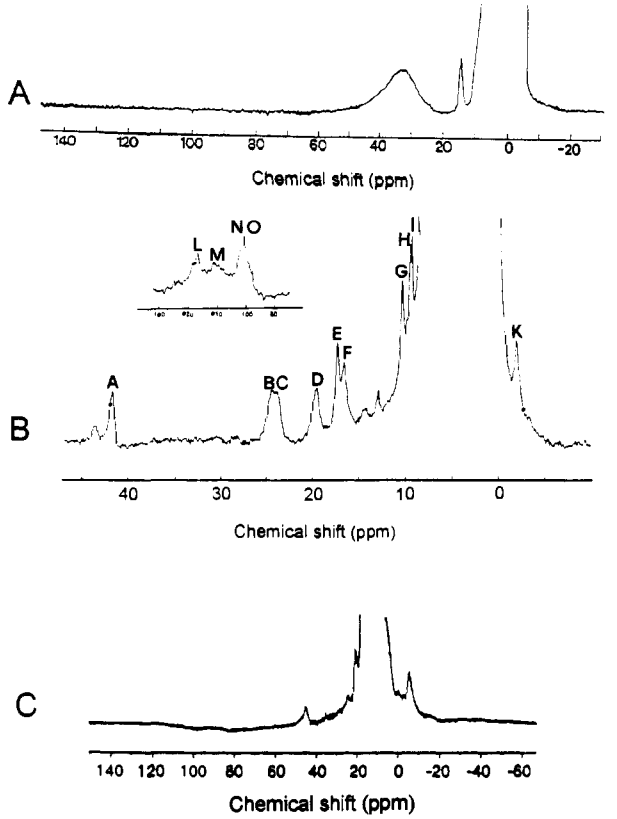

Figure 8. ^{1}H NMR spectra of Fe_2S_2 ferredoxins: (A) oxidized ferredoxin from *P. umbilicalis*, recorded at 303 K and 200 MHz (B) 300-MHz ^{1}H NMR spectrum of reduced Fe_2S_2 spinach ferredoxin (signals L, M, N, O, A and E follow a Curie behavior, whereas signals B, C, D and F display an anti-Curie behavior), and (C) 600-MHz ^{1}H NMR spectra of bovine reduced Fe_2S_2 ferredoxins at 300 K. (Part A, reprinted from ref 53. Copyright 1990 Springer-Verlag. Part B, reprinted from ref 223. Copyright 1984 American Chemical Society. Part C, reprinted from ref 220. Copyright 1991 American Chemical Society.)

However, the magnetic coupling between two identical metal ions is not so effective on reducing their electronic relaxation times[212] so that a broad resonance (ca. 2000 Hz at 200 MHz) is seen in the NMR spectrum at about 34–37 ppm corresponding to eight protons, (see Figure 8A) displaying a strong anti-Curie dependence. Nevertheless, the large magnetic coupling renders the system less paramagnetic and therefore the proton signals display line widths and chemical shifts smaller than the corresponding values that would be observed in absence of magnetic coupling.[53,190,213–215] Similar spectra have been found for algae,[53,216] plant,[190,217,218] bacterial,[215,219] and vertebrate Fds.[220,221] A study reports the spectra of the oxidized *Anabaena* 7120 Fd at different fields showing that at 600 MHz a better resolution is obtained.[215] Nevertheless, it is difficult to resolve these signals and even to determine their T_1 values.

With regard to the reduced Fe_2S_2 Fds, it is interesting to note that a set of sharp signals was found in the 45–15-ppm region[190,210] (see Figure 8B) in early experiments. Four of these signals were tentatively assigned to the β-CH_2 protons of cysteines bound to iron(II). The theoretical approach proposed by Dunham et al.[62] accounted for the anti-Curie temperature dependence of these signals, and predicted a Curie behavior and considerably larger shifts for the proton signals of the

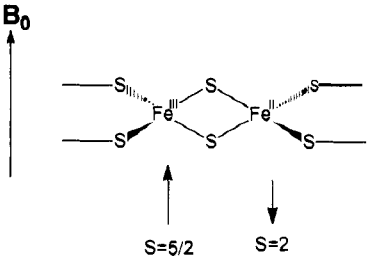

Figure 9. Schematic picture of a Fe_2S_2 cluster indicating the alignment of the individual spins with the external magnetic field B_0.

cysteines bound to iron(III). The latter were not detected for over a decade[192,194,217,222] until 1984, when Bertini et al.[223] reported an experiment using a larger spectral window, which allowed the observation of a group of broad and very far-shifted signals (over 100 ppm) corresponding to four protons with a Curie temperature dependence (note signals L, M, and N in Figure 8B). In this way, the initial predictions of Dunham et al.[62] were confirmed, providing a useful method for identifying protons sensing iron(II) and those sensing iron(III).

This former theoretical treatment[62] has been recently generalized.[53] Its predictions may be summarized as follows: iron(III) has $S = {}^5/_2$ and it is antiferromagnetically coupled with iron(II) (possessing $S = 2$). In the ground state the $S = {}^5/_2$ spin will be oriented along the external magnetic field because it is the larger spin, while the $S = 2$ spin (the smaller one) will be oriented the other way around because of the antiferromagnetic coupling (see Figure 9). If this were the only populated state, the nuclei sensing iron(III) would feel a negative $\langle \mathbf{S}_z \rangle$ (in the same direction of the external magnetic field), and the contact hyperfine shift would be downfield, whereas the opposite situation would hold for the nuclei sensing iron(II), which should show upfield shifts. In the infinite temperature limit ($J \ll kT$), all the levels are populated, and the $\langle \mathbf{S}_z \rangle$ values for each metal ion would be as in the uncoupled systems. Therefore, the nuclei would experience downfield hyperfine shifts from both metal sites.

The actual case in iron–sulfur proteins is intermediate ($J \simeq kT$): several excited levels are occupied, and therefore protons sensing the iron(II) ion are slightly downfield. At higher temperatures, the population of the excited levels increases and the shifts of the latter protons increase. Figure 10 shows the calculated temperature dependence of the shifts of the β-CH_2 cysteine protons bound to the iron(II) and the iron(III) centers compared with the expected ones in the absence of magnetic coupling.[53]

The theory applied to magnetically coupled systems is based on the perturbational Hamiltonian as described in eq 21 as a simplified treatment. It is important to note that this theoretical approach does not take into account the zero-field splitting in the iron ions nor the fact that iron(II) has two spin systems orbitally degenerate in tetrahedral symmetry. The two spins belonging to different orbitals split by low symmetry components will then present different J coupling constants. This fact was already considered in the original treatment by Dunham et al.[62] MO calculations could in principle provide relative J values. However, the introduction of a new parameter in the description,

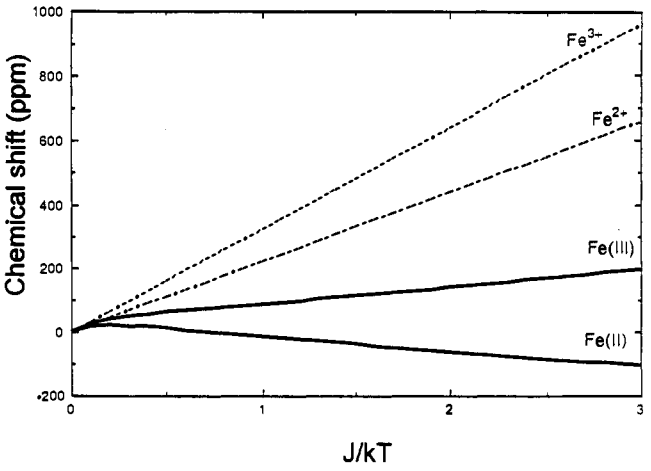

Figure 10. Temperature dependence of the hyperfine-shifted signals calculated for an iron(III)–iron(II) system antiferromagnetically coupled (solid lines) and for the noncoupled ions (dashed lines). (Reprinted from ref 55.)

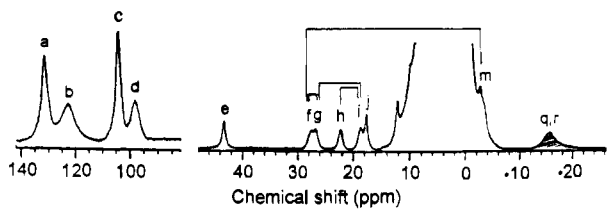

Figure 11. ^{1}H NMR spectrum (360 MHz) at 303 K of reduced Fe_2S_2 ferredoxin from *P. umbilicalis* in H_2O. The shaded signals correspond to exchangeable protons in D_2O solution. The 140–80 ppm region is expanded 5 times vertically. The solid lines indicate NOE connectivities. Signals a–e and j follow a Curie behavior, whereas signals f–i display an anti-Curie behavior (from ref 216).

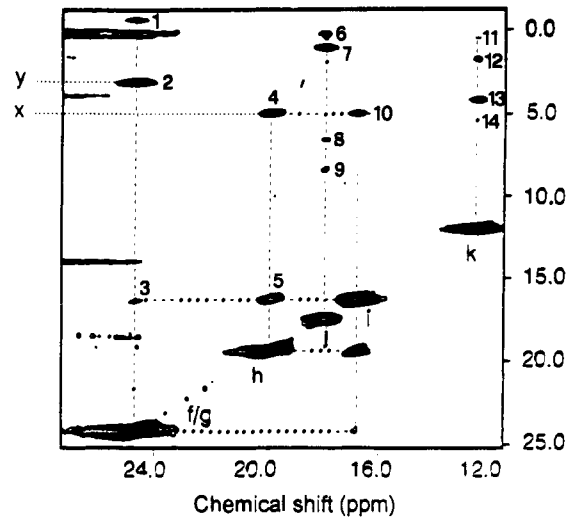

Figure 12. ^{1}H NMR NOESY spectrum (600 MHz) of reduced Fe_2S_2 *Anabaena* 7120 ferredoxin at 300 K performed with a mixing time of 10 ms. (Reprinted from ref 214. Copyright 1991 American Chemical Society.) The signal labeling is the same as in Figure 11. Cross-peak assignments are as follows: (1) Hβ1 Cys 41, β-CH_3 Ala 43; (2) Hβ2–Hβ1 Cys 41, Hα Cys 41; (3) Hβ2 Cys 41, Hβ2 Cys 46; (4) Hβ1, Hα Cys 46; (5) Hβ1, Hβ2 Cys 46; (6) Hα Cys 79, δ_1-CH_3 Leu 27; (7) Hα Cys 79, δ_2-CH_3 Leu 27; (8) Hα Cys 79, Hβ1 Leu 27; (9) Hα Cys 79, Hβ2 Leu 27; (10) Hβ2, Hα Cys 46; (11) Hα Arg 42, Hβ1 Arg 42; (12) Hα Arg 42, Hβ2 Arg 42; (13) Hα Arg 42, Hγ1 Arg 42; (14) Hα Arg 42, Hγ2 Arg 42. A cross peak between signals f and j was detected at a temperature in which these signals do not overlap.

while providing a more correct approach to the understanding of the experimental data, makes the obtained parameters less reliable.

The NMR investigation of these systems at this point shows that there is one iron(III) and one iron(II) ion in the active site with the electron localized on a single iron ion.[53,223] If there were two species with two different localizations of the electron in slow exchange, two sets of signals would be detected. In the case of a fast exchange, only an average set would be observed, but the Curie and anti-Curie characteristics would be lost.

The following question which was answered by NMR is: which are the cysteines bound to iron(III) and which are those bound to iron(II)? NOE investigations on algae Fds allowed the pairwise assignment of the β-CH_2 protons bound to iron(II), i.e., NOE experiments were successful on the sharp proton signals of the protons sensing iron(II).[216] Figure 11 shows the spectra of the Fd from *P. umbilicalis*, indicating the dipolar connectivities found through NOE experiments. Signals f,g and h,i were assigned pairwise to β-CH_2 geminal protons of Cys residues coordinated to iron(II), and signals e and j to α-CH protons of the iron(III)-bound cysteines. Besides, an interresidue NOE between signals g and i was also observed, as well as a NOE between resonances f and m (the latter attributable to a methyl group).[216] These interresidue connectivities allowed the authors to recognize that iron(II) was bound to Cys 41 and to Cys 46, which have a very close intercysteine distance. The methyl signal, according to the X-ray structure of the protein,[163] has been ascribed to Thr 48. In this way, the reduced iron has been identified as the one closer to the protein surface.

The Fe_2S_2 ferredoxin from *Anabaena* 7120 yields similar spectra both in the oxidized and in the reduced forms, with the same Curie and anti-Curie features.[214,215] This protein, whose X-ray structure is available,[162] has been studied thoroughly by Markley. In the first studies, aimed at the assignment of the diamagnetic signals of the oxidized protein, it was noted that the nuclear spin patterns of several residues were not complete: only 78 out of 98 residues were then assigned by the combined use of ^{1}H, ^{13}C, and ^{15}N 2D NMR spectra.[150,224,225] The finding of incomplete nuclear spin patterns was attributed to the broadening effect of the paramagnetic center. It is interesting to note that the 2D spectra of the diamagnetic region are similar in both oxidation states. From this it can be inferred that no significant conformational changes arise upon reduction of the iron ion, and hence only the analysis of the hyperfine-shifted signals is of help for the understanding of the properties of the metal site. NOESY spectra performed on the reduced protein using shorter mixing times[214] (Figure 12) enabled the authors to detect cross peaks accounting for the same dipolar connectivities found by means of 1D NOE experiments in the algae Fds.[216] In addition, the α-CH resonances of the ferrous-bound Cys were located in the diamagnetic envelope (cf. signals x and y in Figure 12). Further connectivities were detected with some signals whose cross peaks were missing in the diamagnetic 2D maps. From this information, and by comparison with the X-ray structure, a definite assignment for the ferrous-bound cysteines has been proposed. The results for algae and *Anabaena* Fds are quite similar. EXSY cross peaks

were also found for the α-CH protons of the cysteines which remain bound to iron(III) upon reduction in a sample containing both the oxidized and reduced protein.

It now remains to explain why that particular iron has a higher reduction potential. By observing the structure both of the *Spirulina platensis*[163] and of the *Anabaena* Fds,[162] it is seen that the reducible iron is bound to three sulfur atoms which, in turn, are hydrogen bonded to three peptidic NH groups. This is a contribution to a higher reduction potential. At this point, it should be noted that two broad exchangeable signals found at −15 ppm (see signals q and r in Figure 11) were tentatively attributed to amino acids which may establish hydrogen bonds with the sulfur atoms.[216] Recently, Carloni and Corongiu[226] have attempted to account for a higher reduction potential of this iron ion on the basis of the electrostatic field caused by the charges of each individual atom in the protein.

Reduced vertebrate Fe_2S_2 Fds (which have a more positive redox potential than plant Fds) show spectra with different features:[220,221] signals in the upfield as well as in the downfield region are observed, all of them displaying a Curie behavior (see Figure 8C). By inspecting Figure 10 it may be noted that for large values of J, the shifts induced by the iron(II) ion become upfield and the signals are expected to shift even more upfield with decreasing temperature. This behavior has been termed "pseudo-Curie" behavior.[227] The extrapolation at infinite temperatures provides enormously large diamagnetic shift values. Therefore, the four upfield signals could correspond to the β-CH_2 protons of the cysteines bound to the ferrous ion.[220] The β-CH_2 protons of the ferric-bound cysteines, which are expected to be found beyond 100 ppm, have not been detected, probably due to their large line widths. This shows that also in vertebrate Fds localized oxidation states occur in the reduced protein. Two broad signals at 40 and 13 ppm were detected in the downfield region, probably arising from the α-CH protons of the cysteines bound to the ferric ion. The signals are considerably broader than in reduced plant or bacterial Fds. This may be attributed to the larger J measured for these proteins with respect those observed in plant and bacterial Fds.

C. Fe_3S_4 Proteins

These clusters possess a voided-cubane structure (Figure 6C) and have been found in bacterial ferredoxins,[186,228,229] aconitase,[155,230] *Escherichia coli* fumarate reductase, and succinate dehydrogenase.[170] The X-ray structure of Fd II from *Desulfovibrio gigas*, one of the most studied Fe_3S_4 systems, is available.[168,169,174]

In the oxidized case, the iron(III) ions are antiferromagnetically coupled, providing a $S = {}^1/_2$ ground state.[231-233] Figure 13A shows the spectrum of native Fd II from *D. gigas*, with four downfield hyperfine-shifted signals below 30 ppm.[196] Two signals (a and b) show a Curie temperature dependence. Mössbauer data on Fd II from *D. gigas*[231] suggested that a J inequivalence could be present. By incorporating it in a Hamiltonian of the type of eq 25 applied to a three-center system, the β-CH_2 Cys protons bound to the Fe_1 and Fe_2 ions are expected to display an anti-Curie behavior, while those sensing Fe_3 are predicted to show

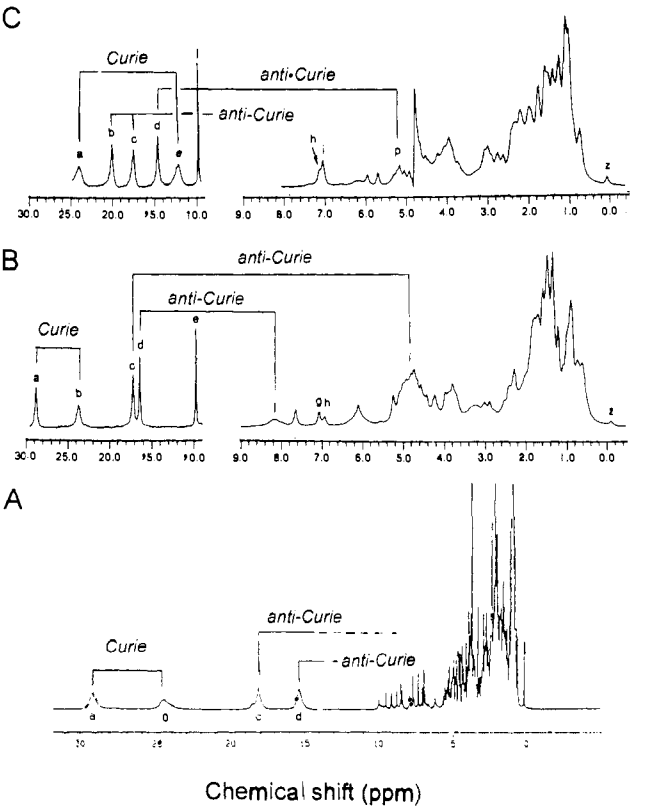

Figure 13. ^1H NMR spectra (500 MHz) in D_2O solution at 303 K of (A) native *D. gigas* Fd II (the 35–14 ppm region expanded 6 times vertically), (B) *T. litoralis* Fd, and (C) *P. furiosus* Fd. The solid lines indicate the β-CH_2 Cys pairs. (Part A, reprinted from ref 234. Copyright 1993 American Chemical Society. Parts B and C, reprinted from ref 235. Copyright 1992 American Chemical Society.)

a Curie behavior.[234] A similar situation has been found in the Fe_3S_4 Fds from archaebacteria *Thermococcus litoralis* and *Pyrococcus furiosus* (Figure 13, parts B and C).[235] Recent NOE and 2D experiments on these proteins have shown that the signals displaying a Curie behavior (a and b) belong always to the same β-CH_2 pair, confirming the above hypothesis.[234,235] Variable-temperature experiments have revealed the existence of a conformational equilibrium in the environment of some cysteines in the *P. furiosus* Fd.

The ^1H NMR shift pattern of the *T. litoralis* and the *D. gigas* Fds are similar each other (cf. Figure 13), both being somewhat different to that of the *P. furiosus* Fd. In the former case, the two β-CH_2 proton signals showing Curie behavior are well shifted downfield (over 20 ppm, cf. signals a and b in Figure 13, parts A and B), whereas in the latter only one of them is experiencing a sizeable downfield shift. Although the sequence-specific assignment of the three bound cysteines is not available for these proteins, this suggests that cysteine bound to the Fe_3 ion does not have the same sequence origin in the three cases. The situation found in the cases of the *T. litoralis* and *D. gigas* Fds is similar to that observed in the seven-iron Fds, which contain a similar Fe_3S_4 cluster (see later).

With regard to the reduced form, Mössbauer data have been accounted for by one iron(III) and a pair of $Fe^{2.5+}$.[229,232,236] The latter is a mixed-valence pair which can be described as an iron(II)–iron(III) pair with the odd electron delocalized over the two metal ions. This electron delocalization stabilizes the highest spin state,

i.e., favors a ferromagnetic coupling in the pair.[237,238] The ground state of the subspin state is expected to be $S = {}^9/_2$.[236] The antiferromagnetic coupling of it with the ferric ion yields a $S = 2$ ground state, as verified by EPR experiments.[233] This system may be treated similarly to the reduced Fe_2S_2 case, in the sense that we expect the proton sensing an iron ion in the mixed-valence pair to be downfield and to exhibit a Curie temperature behavior. On the other hand, protons sensing the iron(III) ion would be upfield with a pseudo-Curie temperature dependence, or slightly downfield with an anti-Curie temperature dependence. The ^1H NMR data on the reduced protein available in the literature are preliminary.[196]

A very interesting feature of the behavior of Fe_3S_4 clusters is that the fourth vacant position in the cluster may be occupied by another metal ion, like cobalt(II),[239] nickel(II),[240] or zinc(II).[241] The mixed-metal clusters constitute an interesting system to be studied by means of NMR. Some results on a model $NiFe_3S_4$ system are available.[242]

D. Fe_4S_4 Proteins

Four iron–four sulfur cubane-like clusters (see Figure 6D) may be found in proteins in three oxidation states: $(Fe_4S_4)^+$, $(Fe_4S_4)^{2+}$, and $(Fe_4S_4)^{3+}$ (see Table II). However, for a given protein, only one redox pair is active in vivo. Ferredoxins employ the $(Fe_4S_4)^+/(Fe_4S_4)^{2+}$ couple and have redox potentials ranging from −250 to −650 mV. Those proteins in which the $(Fe_4S_4)^{2+}/(Fe_4S_4)^{3+}$ couple is active possess redox potentials between +50 and +450 mV,[151,152] and they are called high potential iron sulfur proteins (HiPIPs). Owing to their low molecular weight (around 9 000) they have recently been the subject of a classical diamagnetic NMR study.[243] On the other hand, the analysis of the hyperfine-shifted signals has been useful in understanding the electronic structure of the metal clusters and in performing the sequence specific assignment of the cysteine ligands. It is appropriate to remember that X-ray structures are available for the *Chromatium vinosum* HiPIP[165,244] and HiPIP I from *Ectothiorhodopsira halophila*.[167] Even if the primary sequences of these HiPIPs present a low homology, the similarity in their tertiary structures allows a structural correspondence to be established between the coordinated cysteines which may be extended to the other HiPIPs.

In the case of oxidized HiPIPs, Mössbauer studies at 4 K are available for the ^{57}Fe-enriched proteins from *C. vinosum*[245] and from *E. halophila* HiPIP II,[246] which indicate the existence of absolutely similar clusters in both proteins. In both cases the data can be interpreted on the basis of two iron(III) and one mixed-valence pair (see Figure 14). The latter has a subspin larger than the subspin of the ferric pair. This property is essential for the understanding of the NMR data. EPR experiments indicate a $S = {}^1/_2$ ground state, which may be the result of the two subspin systems antiferromagnetically coupled.[247,248] The values of S_{34} ($S_3 + S_4$) and S_{12} ($S_1 + S_2$) might be ⟨9/2,4⟩ or ⟨7/2,3⟩, with S_{34} always larger than S_{12}.

The $S = {}^9/_2$ and 4 values for the subspin systems may be easily obtained by setting J_{12} and J_{34} respectively larger and smaller than the average J value (assuming that $J_{13} = J_{23} = J_{14} = J_{24} = J$, numbering as in Figure 14). The assumption of a larger value for J_{12} is logical since it is the coupling between the iron(III) ions. The electron delocalization in the Fe_3–Fe_4 pair introduces a ferromagnetic contribution which reduces the antiferromagnetic coupling, and the assumption of a smaller J_{34} is justified. An extension of the treatment outlined in section II.D to four centers allows a picture of the system to be obtained which reproduces nicely the NMR features. The Hamiltonian of eq 26 may be accordingly rewritten as

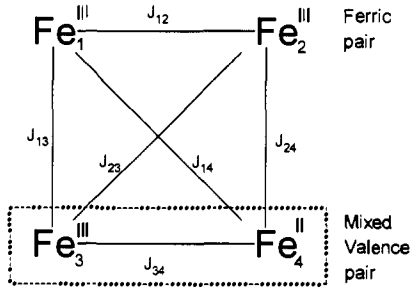

Figure 14. Exchange-coupling scheme in the $(Fe_4S_4)^{3+}$ cluster present in oxidized HiPIPs.

$$\mathcal{H} = J(\mathbf{S}_1\cdot\mathbf{S}_2 + \mathbf{S}_1\cdot\mathbf{S}_3 + \mathbf{S}_1\cdot\mathbf{S}_4 + \mathbf{S}_2\cdot\mathbf{S}_3 + \mathbf{S}_2\cdot\mathbf{S}_4 + \mathbf{S}_3\cdot\mathbf{S}_4) + \Delta J_{12}(\mathbf{S}_1\cdot\mathbf{S}_2) + \Delta J_{34}(\mathbf{S}_3\cdot\mathbf{S}_4) \quad (39)$$

where ΔJ_{12} and ΔJ_{34} are the deviations from J of the exchange coupling constants between the iron centers in the Fe_1–Fe_2 and in the Fe_3–Fe_4 pairs.

By solving eq 39 the energy levels for the different $\mathbf{S}'_i$ values are obtained.[227,249] The hyperfine coupling for each level is calculated from eq 24 by assuming that the hyperfine coupling is equal to that of the noncoupled iron ions (as in the Fe_2S_2 case). The same ground state and essentially the same distribution of excited levels are obtained using all J values equal but with J_{12} slightly larger and introducing in the treatment a parameter which describes the delocalization of one electron between the Fe_3 and Fe_4 ions. The corresponding Hamiltonian has the form:

$$\begin{aligned}\mathcal{H} = {} & [J(\mathbf{S}_1\cdot\mathbf{S}_2 + \mathbf{S}_1\cdot{}^3\mathbf{S}_3 + \mathbf{S}_1\cdot{}^3\mathbf{S}_4 + \mathbf{S}_2\cdot{}^3\mathbf{S}_3 + \mathbf{S}_2\cdot{}^3\mathbf{S}_4 + {}^3\mathbf{S}_3\cdot{}^3\mathbf{S}_4) + \Delta J_{12}(\mathbf{S}_1\cdot\mathbf{S}_2) + \Delta J_{34}({}^3\mathbf{S}_3\cdot{}^3\mathbf{S}_4)]\mathbf{O}_3 + \\ & [J(\mathbf{S}_1\cdot\mathbf{S}_2 + \mathbf{S}_1\cdot{}^4\mathbf{S}_3 + \mathbf{S}_1\cdot{}^4\mathbf{S}_4 + \mathbf{S}_2\cdot{}^4\mathbf{S}_3 + \mathbf{S}_2\cdot{}^4\mathbf{S}_4 + {}^4\mathbf{S}_3\cdot{}^4\mathbf{S}_4) + \Delta J_{12}(\mathbf{S}_1\cdot\mathbf{S}_2) + \Delta J_{34}({}^4\mathbf{S}_3\cdot{}^4\mathbf{S}_4)]\mathbf{O}_4 + \\ & B_{34}\mathbf{V}_{34}\mathbf{T}_{34} \quad (40)\end{aligned}$$

where $\mathbf{O}_3$ and $\mathbf{O}_4$ are the occupation operators for sites 3 and 4, respectively, $\mathbf{T}_{34}$ is the transfer operator between sites 3 and 4, $\mathbf{V}_{34}$ is an operator producing eigenvalues ($S_{34} + {}^1/_2$), and the ${}^j\mathbf{S}_i$ ($i,j = 3,4$) values represent the spin angular momentum operator $\mathbf{S}_i$ when the extra electron is on site j. The double exchange term B_{34} is a scalar factor proportional to the effectiveness of electron exchange in the mixed valence pair. Such an approach has similar consequences as lowering J_{34}.[237,250]

The ^1H NMR spectrum of the oxidized HiPIP II from *E. halophila* shows four hyperfine shifted downfield resonances and four upfield signals, the former set displaying a Curie and the latter a pseudo-Curie temperature dependence (see Figure 15A).[251,252] Chemical shifts spanning from 100 to −30 ppm and T_1 values between 2 and 25 ms are observed for these signals.[251,252] The first study on this protein assigned the downfield

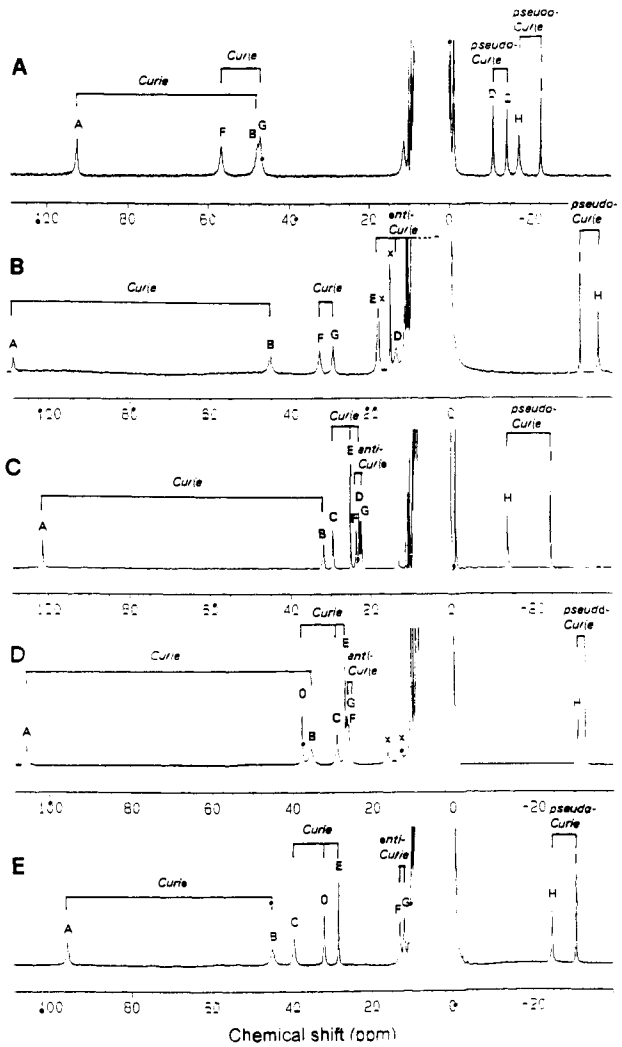

Figure 15. ^{1}H NMR spectra (600 MHz) recorded at 300 K of the oxidized HiPIPs from (A) *E. halophila* HiPIP II, (B) *R. globiformis*, (C) *E. vacuolata* HiPIP II, (D) *C. vinosum*, and (E) *R. gelatinosus*. The Curie, anti-Curie, and pseudo-Curie characteristics are indicated. Signals labeled with × are residual signals from the reduced protein. The solid lines indicate dipolar connectivities. (Reprinted from ref 259. Copyright 1993 American Chemical Society.)

signals to β-CH_2 cysteine protons, and the upfield peaks to aromatic residues in the neighborhood of the cluster and to an α-CH proton.[251] However, if the abovementioned theoretical model is taken into account,[53,253] a completely different picture appears. Protons sensing the mixed valence pair (the substate with the higher spin) will be downfield with a Curie behavior, while protons sensing the ferric pair will be shifted upfield and will have a pseudo-Curie temperature dependence. These predictions have found further support in the light of NOE experiments, which allowed the authors to assign these eight signals pairwise to the cysteines' β-CH_2 protons.[252] NOESY and COSY experiments reveal the same connectivities as well as those between β-CH_2 and α-CH protons.

A series of difference NOE experiments performed upon saturation of the hyperfine shifted signals in the *E. halophila* oxidized HiPIP II have provided the dipolar connectivities between these signals and other resonances in the diamagnetic region. For example, two signals at 6.30 and 5.58 ppm experience NOE with signal H (lettering according to Figure 15A). They are shown to be the Hζ3 and Hϵ3 proton of a Trp residue, respectively (identifiable by its spin system, cf. Figure 16). The X-ray structure of the HiPIP I isoenzyme indicates that the Hζ3 and Hϵ3 protons of Trp 45 (conserved in the HiPIP II) are close to the β2 proton of Cys 39. This has allowed the authors to assign signal H (and its geminal proton I) to Cys 39, and according to the precedent analysis to establish that this cysteine is bound to an iron(III) ion. By using this strategy for all the β-CH_2 cysteine signals, the sequence specific assignment of the bound cysteines has been performed.[254] This approach has allowed Bertini et al. to establish that Cys 39 and 71 are bound to the ferric ions, while Cys 42 and 55 are coordinated to the mixed valence pair,[254] as shown in Figure 17A.

Spectra are available also for other HiPIPs, namely those from *Chromatium vinosum*,[227,255-257] *Rhodocyclus gelatinosus*,[253,258] *Ectothiorhodospira vacuolata* HiPIP I[251] and II,[251,259] *Rhodopseudomonas globiformis*,[260] *Ectothiorhodospira halophila* HiPIP,[251] *Rhodospirillum tenue*,[195] and *Chromatium gracile*.[261] Figure 15 shows the spectra of the oxidized form of those HiPIs whose assignments are available and Table III summarizes the shifts and their assignments. An interesting feature is that the ^{1}H NMR spectra of all other HiPIPs are different from that of the *E. halophila* HiPIP II (see Figure 15). While in the *E. halophila* HiPIP II two sets of four signals each are clearly observed (one downfield and the other upfield) allowing the identification of the cysteine residues bound to the different iron pairs, in the other cases only two signals corresponding to one cysteine bound to one ferric ion are found upfield, whereas two signals of the other cysteine bound to iron(III) are slightly downfield. The latter signals experience an anti-Curie behavior.

There are several explanations to this difference based on the inequivalence of the two ferric ions. One iron(III), for example Fe_1 (see Figure 14) could experience a smaller J value with the mixed-valence pair than the other iron(III). This may be due either to an extension of the electron delocalization on Fe_1 or to a smaller involvement of Fe_1 in the antiferromagnetic couplings within the cluster.[253] Therefore, the signals of the β-CH_2 protons of the cysteines bound to Fe_1 move from an upfield position toward the downfield region.[253]

Another possibility recently proposed[259] is the presence of an equilibrium between two species differing in the valence distribution of the iron ions as pictured in Figure 18, i.e. with one iron(III) and one $Fe^{2.5+}$ being interchanged. This equilibrium would be fast on the NMR time scale. The two most downfield signals would belong to a cysteine bound to $Fe^{2.5+}$, and the two most upfield resonances would be due to the cysteines bound to iron(III). The position of the other two pairs of β-CH_2 protons would be dependent on the position of the equilibrium. This hypothesis finds further support in the fact that the sequence specific assignment of the HiPIP from *Chromatium vinosum* would indicate a different orientation of the cluster that in the *E. halophila* HiPIP II protein if the equilibrium were not considered.[256]

Reduced HiPIPs, formally with two iron(II) and two iron(III), actually possess four $Fe^{2.5+}$ ions, for which the ground state is a $S = 0$.[245,247,262] In this case, the hyperfine shifts come from excited levels (with $S \neq 0$)

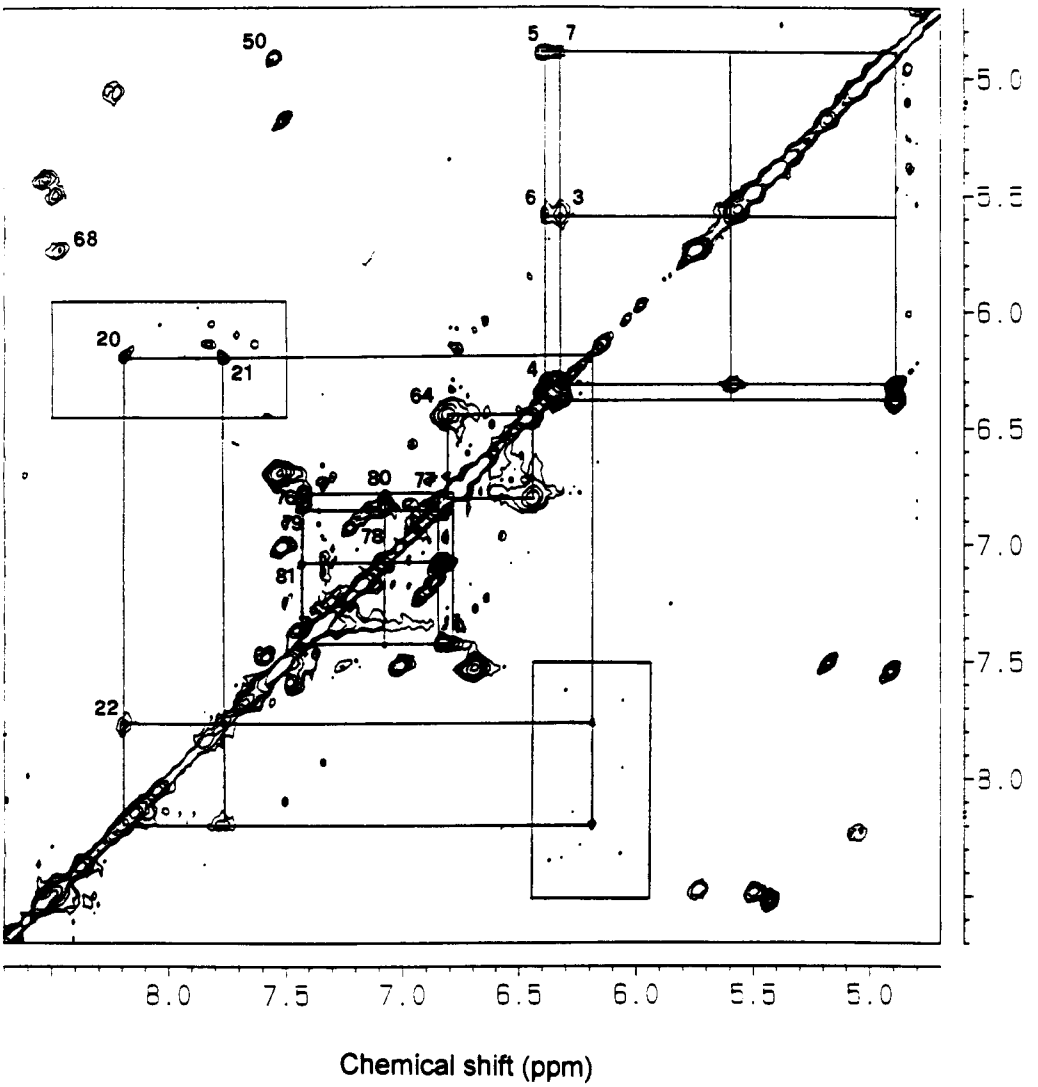

Figure 16. ^{1}H NMR TOCSY spectrum (600 MHz) of the oxidized HiPIP II from *E. halophila* in the aromatic region. The cross-peak patterns of the following residues are indicated: Trp 45 (cross peaks 3–7), Phe 60 (cross peaks 20–22), and Trp 70 (cross peaks 76–81). Cross peak 64 is between a Hϵ and a Hδ proton of Tyr 74. (Reprinted from ref 254. Copyright 1993 American Chemical Society.)

which are populated at room temperature and are always downfield and anti-Curie in character.[227] Due to the fact that this protein possesses a diamagnetic ground state, it displays a lower paramagnetism with respect to the oxidized case: in the case of the *C. vinosum* HiPIP, the reduced protein possesses a μ_{eff} of 0.84 μ_B per iron versus 1.84 μ_B per iron in the oxidized one.[219] As shown in Figure 19, the chemical shifts in these reduced HiPIPs are below 20 ppm and the lines are sharper than in oxidized HiPIPs. A correspondence between the spectra of the reduced and the oxidized protein may be achieved by means of EXSY or 1D saturation-transfer experiments,[227,253] as seen in Figure 19.

As already mentioned, the geminal β-CH_2 pairs have been initially identified by means of 1D NOE, COSY, or NOESY experiments both in reduced and oxidized HiPIPs.[227,252,253,255] In almost all these cases, these assignments were checked by EXSY or saturation-transfer experiments in samples containing both the oxidized and the reduced proteins.[227,253] The above experiments have sometimes been successful in identifying the α-CH resonances both in oxidized[256] and reduced HiPIPs.[256,258] The detection of connectivities is obviously easier in the less paramagnetic reduced protein. Figure 20 reports a COSY and a NOESY spectra of the reduced HiPIP from *C. vinosum*.[256]

The oxidation state of each iron in the oxidized protein may be recognized by means of the temperature dependence of the shifts of the β-CH_2 proton signals. In order to perform the sequence specific assignment the dipolar connectivities between any of the bound cysteines and protons in the diamagnetic region should be looked for. Finally, the identification of the type of residue to which these diamagnetic signals belong is achieved by recognition of their TOCSY cross-peak patterns. It should be kept in mind that the Mössbauer information is needed to establish whether the mixed-valence subspin system is larger than that of the iron-(III) pair. This strategy has led to the sequence specific assignment of the bound cysteine residues of the HiPIP from *Chromatium vinosum*,[256] *R. gelatinosus*,[258] *E. vacuolata* HiPIP II,[259] *R. globiformis*,[260] in addition to the HiPIP II from *E. halophila*[254] already discussed. The framing of the oxidation states of the iron ions within the protein permits one to study the valence distribution of the $(Fe_4S_4)^{3+}$ clusters within these proteins. By considering the primary sequences it is

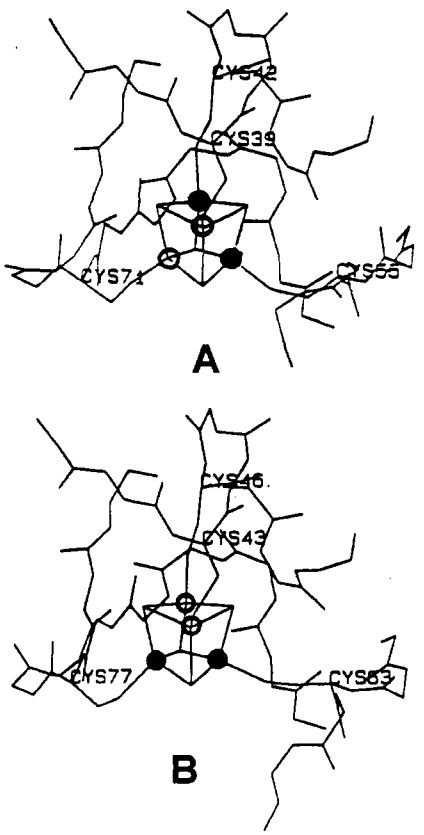

Figure 17. Positioning of the iron oxidation states in the oxidized HiPIPs from (A) *E. halophila* and (B) *C. vinosum*. Open circles indicate iron(III) ions while solid circles indicate $Fe^{2.5+}$ ions.

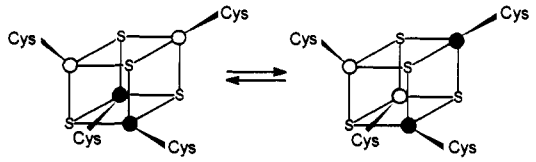

Figure 18. Schematic representation of the proposed equilibrium in the $(Fe_4S_4)^{3+}$ cluster present in oxidized HiPIPs. Open circles indicate iron(III) ions while solid circles indicate $Fe^{2.5+}$ ions.

easy to see that for example cysteine 43 in the *C. vinosum* protein corresponds to cysteine 39 in the *E. halophila* HiPIP II. It is proposed that HiPIP II from *E. halophila* is 100% in the form of Figure 17A, whereas that from *C. vinosum* is 80% in the form of Figure 17B and 20% in the form of Figure 17A.

The temperature dependence of the β-CH_2 signals of the oxidized *E. vacuolata* HiPIP II follow a nonlinear temperature dependence.[251,259] If the abovementioned hypothesis of the equilibrium depicted in Figure 18 is taken into account, the temperature dependence of the shifts should be calculated by summing the contributions of the two species. It has been shown that a small energy gap between the two energy ladders is able to reproduce this nonlinear behavior.[259]

The shift patterns of the β-CH_2 protons in reduced HiPIPs are quite similar (cf. Table IV), since all the irons are $Fe^{2.5+}$. The shift differences found for geminal protons have been ascribed to the dependence on the Fe–S–C_β–H dihedral angles.[256,260] This has been initially proposed for some nickel(II)–amino complexes.[263,264] A relationship of this type was found as follow:

$$\delta = a' \cos^2\varphi + b' \cos\varphi + c' \qquad (41)$$

where b' and c' are small and often neglected. In the case of iron sulfur proteins φ is the Fe–S–C_β–H dihedral angle (see Figure 21). For the HIPIP case, it has been observed that the β-CH_2 shift patterns are better reproduced by a $\sin^2\varphi$ [or $\cos^2(90° - \varphi)$] function instead of a $\cos^2\varphi$ function:[256]

$$\delta = a'' \sin^2\varphi + c'' \qquad (42)$$

this being valid for both oxidation states. In the reduced form the shift difference is sizable for the β-CH_2 pairs of Cys 43 and 63 (*C. vinosum* numbering), whereas it is smaller for the Cys 46 and 77 pairs in all the cases for which the specific assignment is available (cf. Table IV). This has been interpreted as a sign of a similar geometrical arrangement of the β-CH_2 moieties in all HiPIPs.[260] A further investigation[265] has lead to the proposal of the following equation for all the $[Fe_4S_4]^{2+}$ clusters:

$$\delta = a \sin^2\varphi + b \cos\varphi + c \qquad (43)$$

where $a = a'' - a'$, $b = b'$, and $c = a' + c' + c''$. The spin-transfer mechanism occurs through the overlap between the proton 1s orbital and either a p_z orbital of sulfur or the Fe–S σ bond. In the former case a is positive, and negative in the latter. For example, in the oxidized *C. acidi urici* ferredoxin values of $a = 11.5$, $b = -2.9$, $c = 3.7$ ppm have been estimated, which are

Table III. Chemical Shifts of the Hyperfine-Shifted Signals of Oxidized HiPIPs from Different Sources at 300 K

proton (label)[a]	*E. halophila* II[b]	*R. globiformis*[c]	*E. vacuolata* II[d]	*C. vinosum*[e]	*R. gelatinosus*[f]
Cys I (H,I)[g]	Cys 39	Cys 21	Cys 34	Cys 43	Cys 36
Hβ1	-22.66	-32.5	-13.9	-31.20	-30.88
Hβ2	-17.22	-37.7	-24.7	-33.01	-24.83
Cys II (F,G)	Cys 42	Cys 24	Cys 37	Cys 46	Cys 39
Hβ1	-47.16	29.2	22.4	26.41	11.83
Hβ2	56.72	32.6	23.7	25.91	12.94
Cys III (A,B)	Cys 55	Cys 33	Cys 51	Cys 63	Cys 53
Hβ1	47.85	45.6	31.9	35.32	45.08
Hβ2	92.52	108.2	101.5	105.82	95.78
Cys IV (C,D)	Cys 71	Cys 46	Cys 65	Cys 77	Cys 67
Hβ1	-14.24		22.9	37.57	31.93
Hβ2	-8.65	13.5	29.5	28.90	39.51
Hα (E)		18.2	25.1	26.75	28.39

[a] The signal label is that used in Figure 15. [b] Taken from ref 254. [c] Taken from ref 260, at pH 6.0. [d] Taken from ref 259, at pH 6.3. [e] Taken from 256, at pH 5.4. [f] Taken from ref 258, at pH 5.1. [g] The appropriate Cys numbering in each protein is specified in the columns.

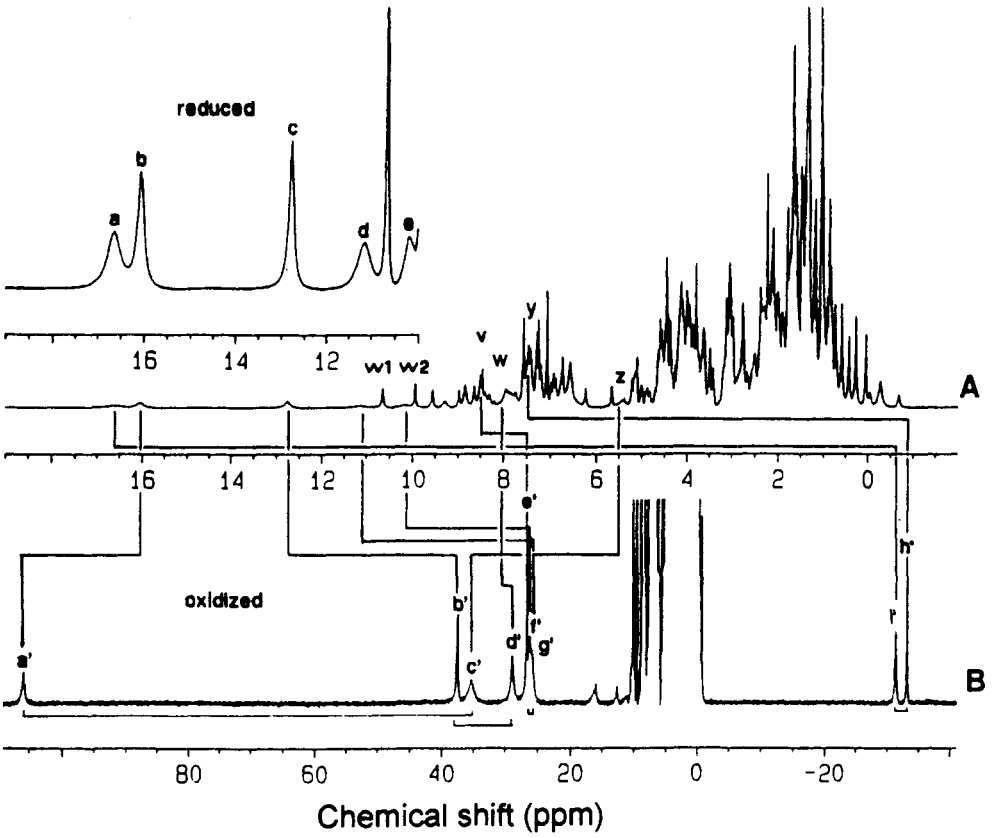

Figure 19. ^{1}H NMR spectra (600 MHz) of the (A) reduced and (B) oxidized HiPIP from *C. vinosum* recorded at 300 K. Correspondence of signals between the two oxidation states obtained by saturation-transfer experiments and NOE connectivities are also reported. (Reprinted from ref 256. Copyright 1992 American Chemical Society.)

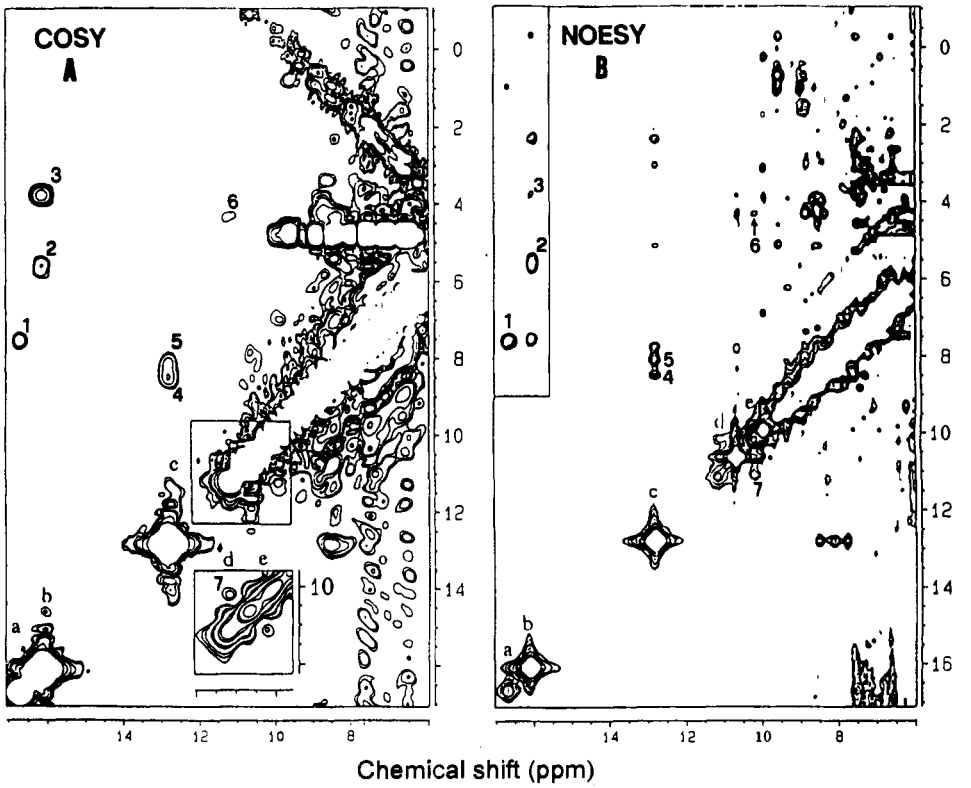

Figure 20. ^{1}H NMR (A) COSY and (B) NOESY spectra of reduced HiPIPs from *C. vinosum*, recorded at 600 MHz and 300 K. The NOESY experiment was performed with a mixing time of 10 ms. Cross peak assignments are as follows: (1) Hβ2, Hβ1 Cys 43; (2) Hβ2, Hβ1 Cys 63; (3) Hβ2, Hα Cys 63; (4) Hβ1, Hα Cys 77; (5) Hβ1, Hβ2 Cys 77; (6) Hβ2, Hα Cys 46; (7) Hβ2, Hβ1 Cys 46. (Reprinted from ref 256. Copyright 1992 American Chemical Society.)

indicative of dominant pπ mechanism, although the σ mechanism is not negligible.[265]

The electron-transfer self-exchange in partially oxidized HiPIPs is slow on the NMR time scale (at

Table IV. Chemical Shifts of the Hyperfine-Shifted Signals of Reduced HiPIPs from Different Sources at 300 K

proton	*C. vinosum*[a]	*R. globiformis*[b]	*R. gelatinosus*[c]
Cys I[d]	Cys 43	Cys 21	Cys 36
Hβ1	7.57	7.1	8.63
Hβ2	16.7	17.9	17.33
Cys II	Cys 46	Cys 24	Cys 39
Hβ1	10.16	9.4	10.6
Hβ2	11.13	11.4	11.5
Hα	4.3		
Cys III	Cys 63	Cys 33	Cys 53
Hβ1	5.52	5.0	6.12
Hβ2	16.10	15.0	14.98
Hα	3.75	4.1	3.69
Cys IV	Cys 77	Cys 46	Cys 67
Hβ1	12.77	10.8	9.35
Hβ2	8.06	8.55	8.70
Hα	8.52	8.40	7.80

[a] Taken from ref 256, at pH 7.2. [b] Taken from ref 260, at pH 6.0. [c] Taken from ref 258, at pH 7.2. [d] The appropriate Cys numbering in each protein is specified in the columns.

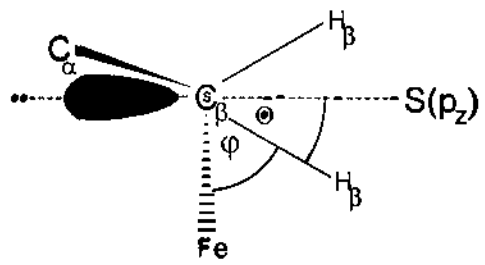

Figure 21. View of a bound cysteine residue along the C_β–S bond, showing the subtended dihedral angles φ and θ with the β-CH_2 protons.

magnetic fields between 200 and 600 MHz). This allowed the extimation of the self-exchange rates in various HiPIPs by saturation-transfer experiments.[130] Indeed, the fractional variation of signal intensity, η, is related to the pseudo-first-order exchange rate constant k' according to the following equation:[266]

$$\eta = k'/(R + k') \quad (44)$$

where R is the longitudinal relaxation rate of the signal in the reduced form and k' is the reciprocal lifetime of the reduced form. If the electron exchange reaction takes place through a second-order kinetic process, k' is related to the second-order rate constant k through the relation

$$k' = k[\mathrm{ox}] \quad (45)$$

[ox] being the concentration of the oxidized species. Values of k ranging from 10^3 to 10^6 M^{-1} s^{-1} have been obtained for HiPIPs from various bacterial sources; the differences have been discussed in terms of the total charge on the protein and of the hydrophobic character of the solved exposed area in proximity of the iron sulfur cluster.[130]

The cluster present in reduced HiPIPs is equal to that of oxidized (Fe_4S_4) ferredoxins (cf. Table II). In general, (Fe_4S_4) Fds have been the most thoroughly studied iron–sulfur proteins by means of NMR spectroscopy in the 1970s.[188-191] Some of them contain two Fe_4S_4 clusters, like the Fd from *C. pasteurianum*, whose ^1H NMR spectrum is shown in Figure 22A.[69] Packer et al. reported in 1977 similar spectra for the Fds from *C. acidi urici* and *P. asaccharolyticus* (formerly *P. aerogenes*),[267] these being highly homologous to the *C. pasteurianum* protein. As expected, the chemical shift

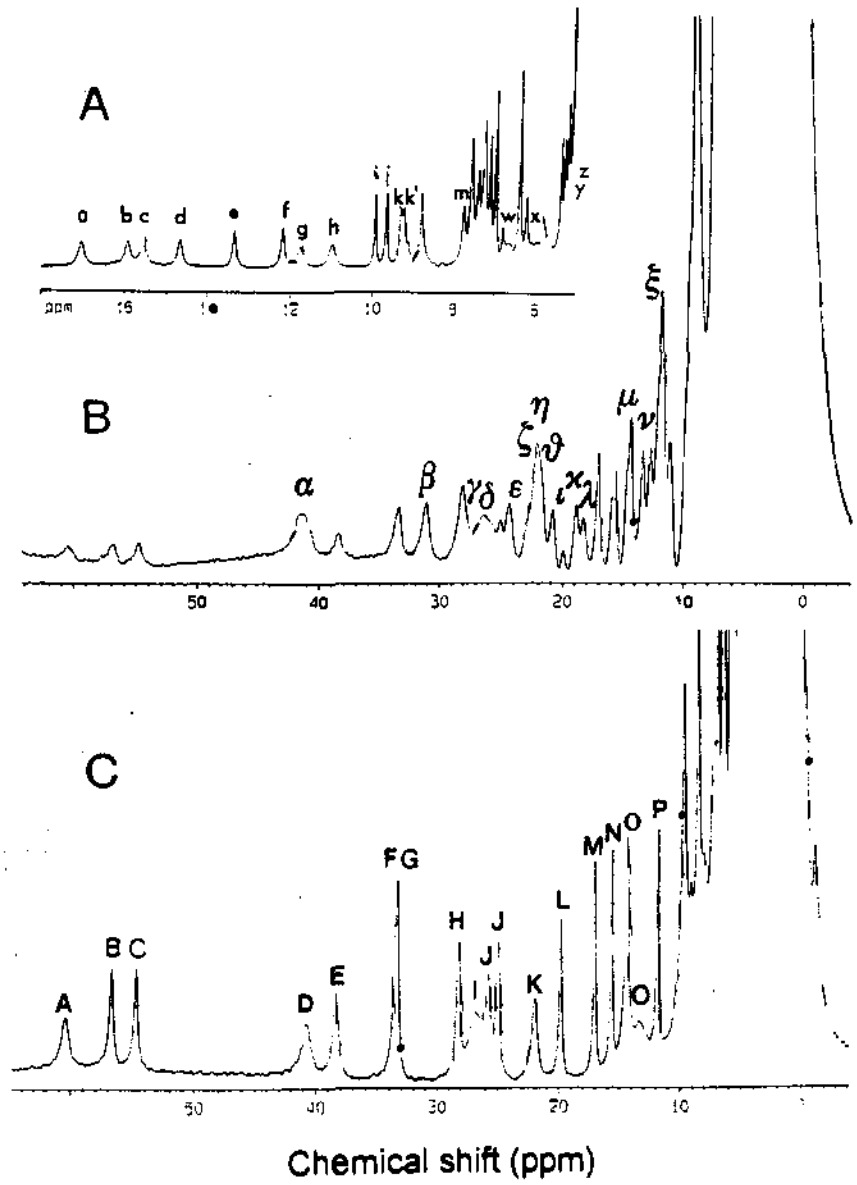

Figure 22. ^1H NMR spectra (600 MHz) of the 2(Fe_4S_4) ferredoxin from *C. pasteurianum* (A) fully oxidized, (B) partially reduced (ca. 50%), and (C) fully reduced. The signal labeling is as follows: fully reduced species, uppercase letters; fully oxidized species, lowercase letters; and partially reduced species, Greek letters. (Reprinted from ref 127. Copyright 1992 Springer-Verlag.)

range is similar to that observed for reduced HiPIPs. Eight isotropically shifted signals in the downfield region (a–h) are noted. These signals have been identified in early studies as β-CH_2 Cys protons by means of deuterium labeling in the closely related *Clostridium acidi urici* Fd.[267] The anti-Curie temperature dependence of these resonances may be reproduced by assuming a J inequivalence for two of the coupling constants in the Fe_4S_4 system, or by introducing a double-exchange term.[69,227,268]

With regard to the use of modern NMR techniques on oxidized Fe_4S_4 Fds, 1D NOE experiments gave preliminary assignments of the β-CH_2 cysteine signals in the oxidized form.[69] Later, NOESY and MCOSY experiments on the oxidized protein (see Figure 23) have allowed a complete assignment of the β-CH_2 protons of the eight coordinated cysteines, together with some α-CH protons.[269,270]

The fully reduced Fd has a $(Fe_4S_4)^+$ cluster. This cluster has been interpreted as two iron(II) ions and a mixed-valence pair, with an $S = {}^1/_2$ ground state.[262,271-274] This value arises from the antiferromagnetic coupling between the $S = {}^9/_2$ state from the mixed-valence pair and the $S = 4$ spin state of the ferrous couple. Its ^1H NMR spectrum shows 19 paramagnetically shifted signals in the 65–10-ppm range (see Figure 22C) with short T_1 values and broad lines.[127] This system is less suitable to be studied by means of 2D techniques than the oxidized protein.

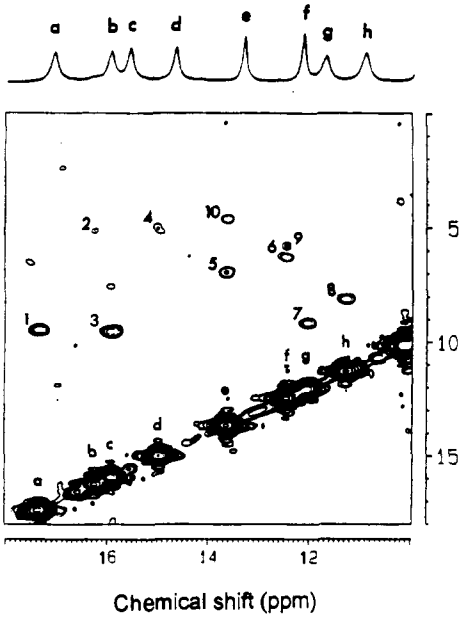

Figure 23. ^{1}H NMR COSY spectrum at 600 MHz and 300 K of the oxidized 2(Fe_4S_4) ferredoxin from *C. pasteurianum*. Cross-peak labelings are as follows: (1) a,k'; (2) b, y; (3) c, k; (4) d, z; (5) e, w; (6) f, x; (7) g, l; (8) h, m; assigned as reported in Table V. (Reprinted from ref 269. Copyright 1991 Elsevier.)

The partially reduced proteins both from *Clostridium pasteurianum* and *C. acidi urici* contain a $(Fe_4S_4)^+$ cluster and a $(Fe_4S_4)^{2+}$ cluster. The spectra of the proteins in this intermediate reduction state display a series of resonances in addition to those of the completely reduced and oxidized proteins (note in Figure 22B the signals labeled with Greek letters).[127] This is because the equilibrium between the oxidized, semireduced, and reduced forms is slow in the hyperfine-shift scale. A series of EXSY experiments performed under different experimental conditions (temperature, mixing time, oxidized-to-reduced protein ratio) have allowed the authors to correlate the β-CH_2 proton signals for 13 out of 16 cysteines (see Table V), providing the assignments for the reduced and semireduced species.[127]

The signals of the semireduced protein are not exactly the average of the shifts corresponding to the oxidized and the reduced forms. The resonances of one cluster are closer to the shift values of the oxidized species, and those of the other are more shifted toward the reduced species.[127] This is consistent with the finding of different redox potentials for the two Fe_4S_4 centers.[275] This has allowed the β-CH_2 resonances originating from different clusters to be discriminated.[127] The next step was the assignment of each Cys group to a cluster. Early ^{13}C NMR data[275] has established that cluster II is that with higher reduction potential, due to its vicinity to a Tyr residue. This observation has enabled the assignment of the hyperfine-shifted resonances to defined clusters to be made (see Table V) and to estimate the difference in redox potential between the two clusters.[127] Recently the first stereospecific, sequence-specific assignment of cysteine protons for the *Clostridium pasteurianum* and *C. acidi urici* ferredoxins has been obtained.[265] For *C. pasteurianum* the assignment is different from a previous tentative one based on the dihedral angles analysis of the β-CH_2 hyperfine shifts.[270] As reported above (see eq 43) in the most recent paper[265] a new functional form for the angular dependence of the hyperfine coupling has been also established.

Table V. Chemical Shifts of the Hyperfine-Shifted Signals on the 2(Fe_4S_4) Ferredoxin from *C. Pasteurianum* in the Different Oxidation States at 293 K, pH 8.0 (from Ref 127)

oxidized form		intermediate form		reduced form		
signal	shift	signal	shift	signal	shift	assignment
a	17.2	β	31.4	E	38.8	β-CH_2(1)–cluster II
b	16.1	α	41.5	A	60.2	β-CH_2(2)–cluster II
c	15.7	θ	21.6	F	33.7	β-CH_2(3)–cluster I
d	14.8	κ	18.9	J	25.8	β-CH_2(4)–cluster I
e	13.5	γ	27.7	B	57.0	β-CH_2(5)–cluster I
f	12.3	η	22.4	J'	25.6	β-CH_2(6)–cluster II
g	11.9	ζ	23.1	D	40.7	β-CH_2(7)–cluster I
h	11.1	λ	18.3	K	22.0	β-CH_2(8)–cluster II
i	10.0	π	11.8	N	15.8	α-CH(3)–cluster I
j	9.7	μ	14.4	M	17.2	α-CH(1)–cluster II
k	9.4	ξ	12.7	L	20.3	β'-CH_2(3)–cluster I
k'	9.3	ϵ	24.5	G	33.3	β'-CH_2(1)–cluster II
l	8.9	δ	26.1	C	54.6	β'-CH_2(7)–cluster I
m	7.9	ι	20.9	H	28.2	β'-CH_2(8)–cluster II
w	6.9	ν	13.4	I	26.9	β'-CH_2(5)–cluster I
x	6.1					β'-CH_2(6)–cluster II
y	5.1					β'-CH_2(2)–cluster II
z	4.9					β'-CH_2(4)–cluster I

The temperature behavior of the β-CH_2 signals in the reduced form is better analyzed in comparison with data from other monocluster Fe_4S_4 Fds, (see Figure 24) even if no detailed assignment is available for the latter.[192,196,219,276] All the hyperfine shifts are downfield and sizeable: half of them are of Curie and half of anti-Curie type. In order to rationalize this behavior, the proton hyperfine shifts for *C. acidi urici* have been corrected for the different φ angles by assuming that eq 43 holds for the $(Fe_4S_4)^+$ cluster and that the φ angles are the same in both reduced and oxidized species.[265] The resulting "angle-independent" shifts show that for each cluster there are two signals of both Curie and anti-Curie type far shifted and two, again of Curie and anti-Curie type, less shifted. At the moment no detailed explanation is available; however, it has been proposed that the antiferromagnetic coupling constants J for each bimetallic center are smaller than in the case of oxidized HiPIPs and that electron delocalization makes the iron ions more similar to each other than in the HiPIPs.[265] Small differences among J_{ij} values would cause a variety of temperature dependences.[127,265]

We should note at this point that NMR investigations on mononucluster Fe_4S_4 Fds consist only of 1D NMR spectra, with no detailed assignments.[192,196,219,276]

E. Seven-Iron Ferredoxins

A series of Fds known as seven-iron Fds contain one (Fe_4S_4) and one (Fe_3S_4) cluster. The X-ray structure of the *Azobacter vinelandii* seven-iron Fd is available.[176,178] The *Pseudomonas putida* and *Azobacter vinelandii* Fds (with a 85% of homology) give identical ^{1}H NMR spectra with seven hyperfine-shifted signals in the downfield region in the 30–10-ppm range (see Figure 25).[276,277] Selective deuteration experiments have demonstrated that signals A–E correspond to β-CH_2 cysteine protons.[277] Upon dithionite reduction (which alters only the three-iron center) signals A–C disappear while D and E remain.[276] This has allowed

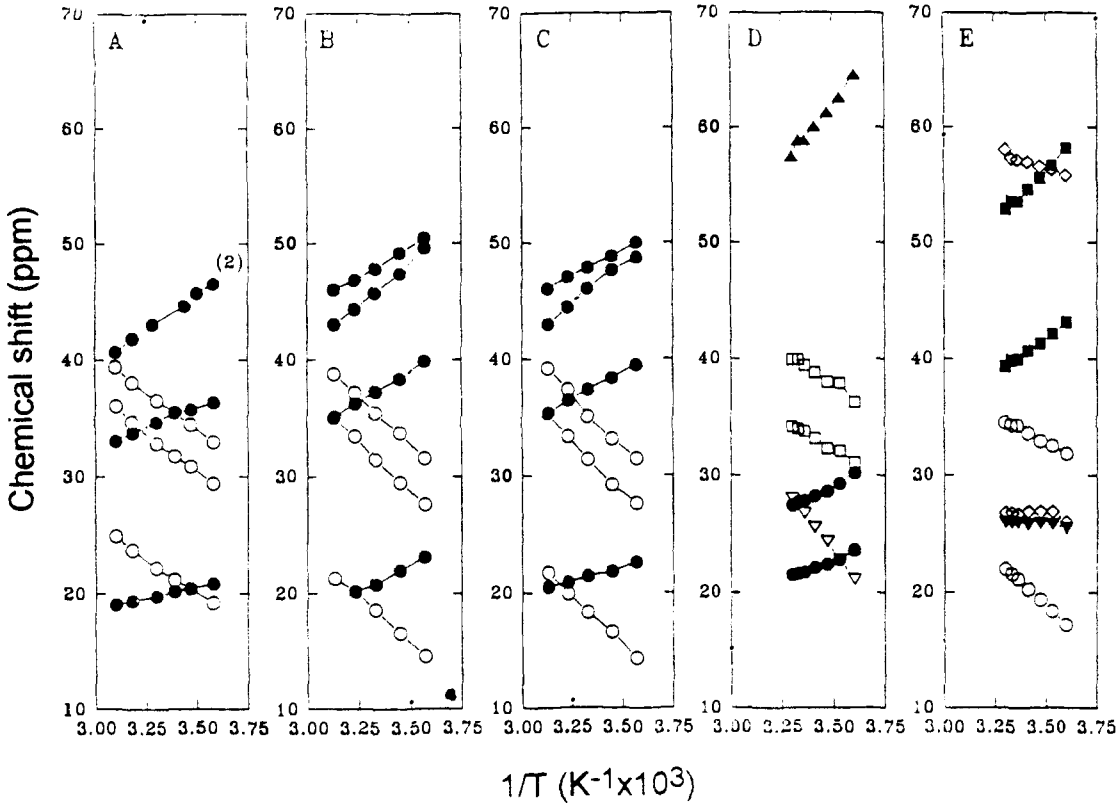

Figure 24. Temperature dependencies of the ^1H NMR hyperfine-shifted signals of ferredoxins containing Fe_4S_4 clusters in the reduced form: (A) monocluster ferredoxin from *B. polymyxa*, pH 7.0; (B) monocluster ferredoxin from *B. thermoproteolyticus* at pH 7.6, (C) monocluster ferredoxin from *B. stearothermophilus* at pH 7.6, (D) cluster II of ferredoxin from *C. pasteurianum* at pH 8.0, (E) cluster I of ferredoxin from *C. pasteurianum* at pH 8.0. Open circles denote anti-Curie behavior and solid circles indicate Curie behavior. (Reprinted from ref 127. Copyright 1992 Springer-Verlag.)

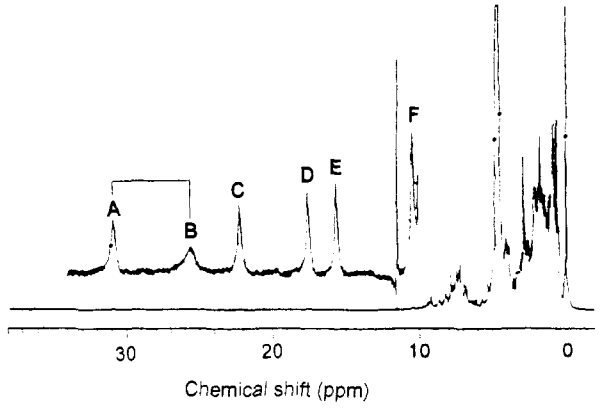

Figure 25. ^1H NMR spectrum at 400 MHz and 300 K of the native seven-iron ferredoxin from *P. putida* in D_2O. The solid line indicates a NOE connectivity. Signals A and B follow a Curie behavior, whereas signals C–F display an anti-Curie behavior. (Reprinted from ref 279. Copyright 1984 Elsevier.)

the assignment of the former resonances to cysteines bound to the Fe_3S_4 cluster, and the latter as corresponding to the Fe_4S_4 center. NOE[277] and NOESY[278] experiments showed that peaks A and B arise from a geminal pair, while C and E are nearby protons of different Cys residues. We may note that the behavior of signals A and B resembles that observed in the "unique" iron ion in the oxidized Fe_3S_4 protein from *D. gigas* (cf. signals a and b in Figure 13).[234]

The geminal protons of signals C–E and the corresponding α-CH protons have been found in the diamagnetic envelope by means of NOESY spectra. Some of these assignments have been further confirmed by heterocorrelation experiments (see section IX).[278]

When the seven-iron Fd from *Pseudomonas ovalis* is treated with a stoichiometric amount of ferricyanide, the signals corresponding to cysteines bound to the Fe_4S_4 decrease in intensity, and new resonances both in the downfield and in the upfield region appear.[279] The upfield signals in this "super-oxidized" protein were taken as indicative of a HiPIP-like Fe_4S_4 cluster. These results should be treated with caution, as the addition of excess ferricyanide may induce the conversion of the Fe_4S_4 cluster into a Fe_3S_4 cluster.[280,281] Up to now, the NMR characterization of this intermediate state of the cluster has remained uncertain.

F. Se-Substituted Iron–Sulfur Proteins

Native Fe–S clusters have been replaced by Fe–Se clusters in several proteins without significantly altering the active site structure.[282] The replacement of the sulfur atoms by selenium provides an interesting means to explore the dependence of electron-transfer mechanism on the electronic structure in iron sulfur proteins. Only two reports of ^1H NMR spectra of Se-substituted iron–sulfur proteins are available in the literature, both dealing with Fe_4S_4 proteins.[283,284]

In the case of the HiPIP from *C. vinosum*, upon Se substitution the spectrum of the protein shows the same pattern of the native one, with slightly increased shifts and shorter T_1 values (see Figure 26). The temperature dependence of the shifts is qualitatively similar to that of the native enzyme.[284] This situation is met both in the reduced and in the oxidized protein, and it parallels

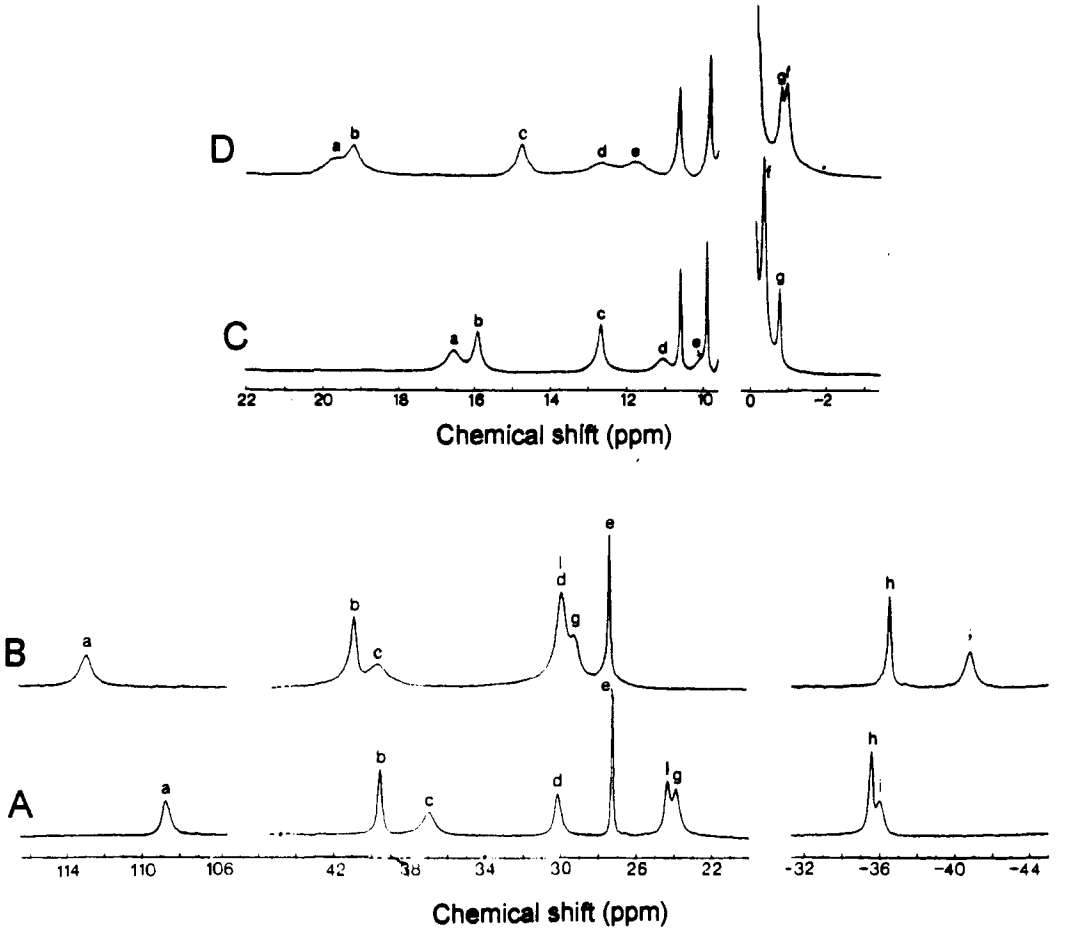

Figure 26. ^{1}H NMR spectra at 500 MHz and 298 K of the HiPIP from *C. vinosum*: (A) oxidized native protein, (B) oxidized Se-substituted protein, (C) reduced native protein, and (D) reduced Se-substituted protein. (Reprinted from ref 284. Copyright 1989 American Chemical Society.)

the behavior found in synthetic complexes. Upon substitution in $(Fe_4X_4)^+$ model systems (X = S, Se, Te) systematic trends have been observed.[88,160,285-287] The increase of the dimensions of the bridging chalcogenide results in larger Fe···Fe distances, weakening the antiferromagnetic coupling in the cluster.[288] The paramagnetism increases accordingly, and larger μ_{eff} values and hyperfine shifts are observed.[284]

Upon selenium substitution, the oxidized Fds from *C. pasteurianum* and *C. acidi urici* yield spectra similar to those observed for the native proteins (see Figure 27), but with larger downfield shifts.[283] A quite different situation is encountered for the reduced $(Fe_4S_4)^+$ case. Unusual features found in EPR and Mössbauer spectra at low temperatures have been attributed to the existence of three spin states, namely $S = {}^1/_2$, ${}^3/_2$, and ${}^7/_2$.[271,289-291] Ground states with S values larger than ${}^1/_2$ have been also found in synthetic $(Fe_4S_4)^+$ clusters as well as in the iron protein of *A. vinelandii* nitrogenase. The ^{1}H NMR spectrum is markedly different from that of the native protein (cf. Figure 27). Nineteen hyperfine-shifted signals spanning from 160 to −40 ppm are detected. In contrast with the $(Fe_4S_4)^+$ protein, all the signals but one display Curie temperature dependencies (the shift of the 65 ppm resonance is temperature independent).[283] These larger shifts have been interpreted as an indication of the existence of higher spin states also at room temperature. Magnetic susceptibility measurements indicating a μ_{eff} value of 6.4 μ_B versus a value of 4.2 μ_B for the native reduced protein

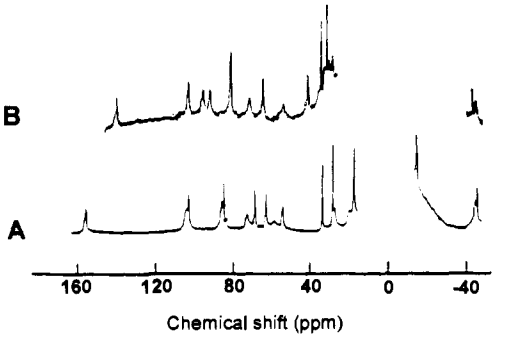

Figure 27. ^{1}H NMR spectra (250 MHz) of reduced 2(Fe_4S_4) ferredoxin from *C. pasteurianum* at 295 K: (A) Se-substituted protein and (B) native protein. (Reprinted from ref 283. Copyright 1987 American Chemical Society.)

would support this hypothesis. However, it is difficult to establish which spin states occur at room temperature. A recent theoretical model developed by Noodleman is able to describe the EPR features of $(Fe_4S_4)^+$ clusters.[66,67]

The partially reduced Fe_6Se_6 protein displays a situation similar to that found in the native one, i.e. the appearance of new signals with shifts intermediate between those of the oxidized and of the reduced proteins. However, no assignment of the β-CH_2 Cys signals is available nor a correlation of the resonances in the different oxidation states of the protein. The analysis of the electronic structure of the reduced $(Fe_4S_4)^+$ cluster warrants further studies.

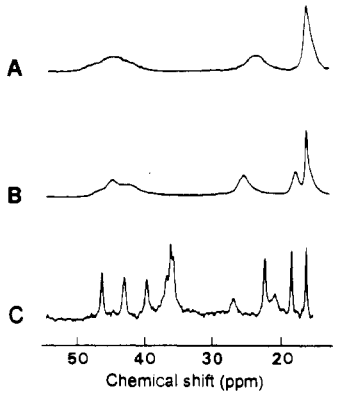

Figure 28. Downfield region of the 250-MHz ^1H NMR spectra of (A) reduced nitrogenase iron protein from *C. pasteurianum* at 295 K and (B) 325 K; and (C) reduced Fe_4S_4 ferredoxin from *B. stearothermophilus* at 325 K. (Reprinted from ref 292. Copyright 1988 American Chemical Society.)

G. Other Iron–Sulfur Proteins

Nitrogenases also contain a (Fe_4S_4) cluster, which may be present in two oxidation states: $(Fe_4S_4)^{2+}$ or $(Fe_4S_4)^{+}$, like in Fds. Figure 28 shows the ^1H NMR spectrum of the nitrogenase iron protein from *C. pasteurianum* compared with that of the *B. stearothermophilus* Fd.[292] Seven very broad downfield signals integrating for 9 to 10 protons were observed in the 50–15-ppm range, displaying both Curie and anti-Curie behaviors. The features of this spectrum reproduce qualitatively those observed in reduced monocluster Fe_4S_4 Fds, indicating a similar cluster.

The NMR investigation of iron–sulfur proteins of high molecular weight has been hitherto precluded. Unfortunately, many proteins of biological interest (hydrogenases, nitrogenases, beef heart aconitase, xanthine oxidase) fall into this group.

V. Heme Proteins

Iron–porphyrin complexes (or hemes) have a general formula (Figure 29A). Protoheme, or heme *b*, refers to the macrocycle where R is a vinyl group and represents the most common porphyrin found in heme proteins.[293] It constitutes the prosthetic group of most peroxidases, *b*-type cytochromes and globins. In systems containing *c*-type hemes the sulfur atom of two cysteine residues is bound to the inner carbon of the vinyl side chains of protoheme to make thioether bridges between the porphyrins and the polypeptide. A covalent linkage of the heme is not often found outside the *c*-type family, with the exception of lactoperoxidase and myeloperoxidase (see later).[294,295] The heme prosthetic groups of cytochrome *c* oxidase are commonly referred to as heme *a* (Figure 29B), the CO binding heme being referred to as a_3 in the enzyme.[296,297] Chlorins are porphyrins in which one of the pyrrole rings has been saturated. An unusual octacarboxylic porphyrin with partial saturation at some pyrrole rings complexed with iron forms the prosthetic group of bacterial sulfite reductase.[298]

The iron atom is coordinated to these relatively rigid tetradentate macrocycles and easily accessible to monodentate ligands in both axial coordination positions. At least three oxidation states are available to heme iron (+2/+4), although the +2 and +3 are most commonly encountered. Each of this oxidation states can exist in several spin states, encompassing all possibilities between $S = 0$ and $S = {}^5/_2$.[7]

Heme iron is present in a large variety of biological systems: essentially all prokaryotic and eukaryotic cells contain and utilize heme proteins. The three general biological functions of heme proteins are the transport of electrons (cytochromes), the transport of oxygen (globins), and the catalysis of redox reactions (cytochromes P450, peroxidases, cytochrome *c* oxidase, nitrite reductases). Despite the differences in the chemistry they support, most of these proteins share the same prosthetic group. Their different functions therefore originate from differences in the axial ligation of the iron atom and in the interaction of the protein with potential substrates.[299–303]

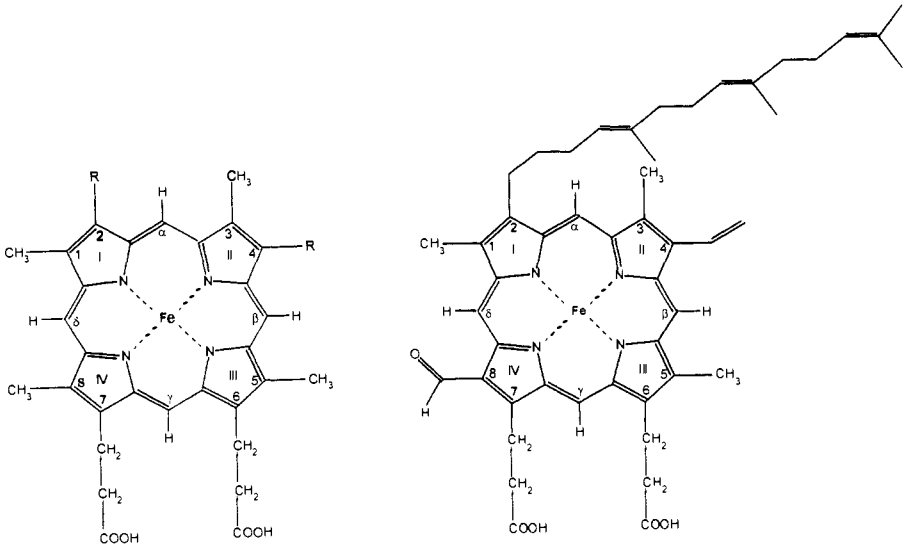

Figure 29. General formula for the heme ligand present in natural systems and (B) the heme prosthetic group of cytochrome *c* oxidase or heme *a*.

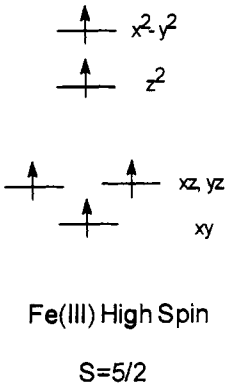

Figure 30. The electronic configuration of high-spin heme iron(III).

The power of the NMR technique in the study of these systems is well documented by an incredibly vast amount of literature.[304-307] We will focus on reviewing the results obtained for different systems according to their oxidation and spin states.

A. High-Spin Iron(III)

High-spin iron(III) represents the resting state form of many heme proteins. In this form the heme iron is pentacoordinated with His or Cys ligands, or hexacoordinated with H_2O molecule in the sixth coordination site. High spin ferric heme proteins have ^6A ground state. This means that the magnetic anisotropy is negligible and the observed hyperfine shifts are due primarily to the contact contribution.[7,308] Therefore only protons belonging to groups directly bonded to the heme iron may experience substantial hyperfine shifts. However, the ^6A ground state of iron(III) in hemes is characterized by relatively large splittings of the zero-field Kramers' doublets ($\pm^1/_2; \pm^3/_2; \pm^5/_2$). The ZFS produces a pseudocontact contribution to the shift. An estimate of it is available for model complexes.[78,308] Electron relaxation rates also depend on the magnitude of the ZFS[72] which in heme compounds is unusually large.

A general problem with hemes is that the unpaired electrons cannot be considered as localized on the metal but unpaired spin density is largely spread on the heme ring.[7,308] The electronic configuration of a high-spin d^5 system is reported in Figure 30. Unpaired electrons can delocalize on the ligand through either σ or π orbitals, the former mechanism being dominant. It follows that the shifts of heme methyl groups and α-type protons of the other heme substituents are downfield. Larger π delocalization contribution in hexacoordinate compounds can be ascribed to the coplanarity of the metal ion with the heme ligand.[309,310]

Sometimes an excited state with $S = {}^3/_2$ can be low enough in energy that substantial mixing with $S = {}^5/_2$ occurs through spin–orbit coupling.[311] When evidences of such coupling are available through EPR or NMR spectroscopies, it is said that the ground state is a quantum mechanical spin admixture. It is claimed to occur when the axial ligands are weak[312,313] or when there is only one ligand.[314,315] The same mechanism mixes also $S = {}^3/_2$ with $S = {}^1/_2$ state.

1. Metmyoglobin

The ^1H NMR spectrum of sperm whale (*Physeter catodon*) aquometmyoglobin (metMb–H_2O, MW 16 000)

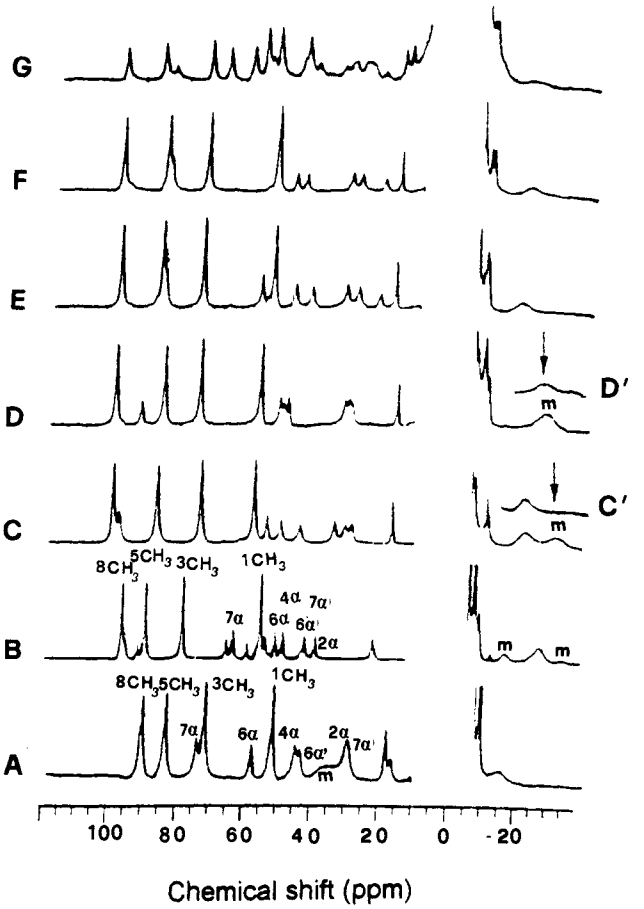

Figure 31. ^1H NMR spectra (360 MHz) of (A) sperm whale metMb; (B) *Aplysia* metMb; (C) His[E7]Phe metMb; (D) His[E7]Val metMb; (E) His[E7]Gly metMb; (F) His[E7]-Gln; (G) elephant metMb. All the spectra were recorded at 298 K in D_2O solution, 0.1 M potassium phosphate buffer pH 6.2. The insets C′ and D′ show the NMR spectra obtained on samples reconstituted with meso-$^2H_4$ hemin, which allows the meso signal assignment. (Reprinted from ref 323. Copyright 1991 American Chemical Society.)

in D_2O at 360 MHz and 298 K is reported in Figure 31A together with the resonance assignments. Four three-proton intensity signals are observed between 92 and 53 ppm. In the region 76–15 ppm many one-proton intensity signals are observed. In the upfield part of the spectrum two three-proton intensity and two one-proton intensity resonances are clearly resolved. The above assignments result from a combination of isotope labeling[87] and NOEs.[103,316] This low molecular weight heme protein is the first $S = {}^5/_2$ protein studied by means of NOE technique.[316] Iron spin magnetization follows the Curie law fairly closely, since the four heme methyls yield straight lines with intercepts at $T^{-1} = 0$ very close to the diamagnetic methyl positions. The two vinyls and two of the α-CH_2 proprionate shifts however deviate from Curie law so as to decrease slower with T^{-1} than predicted. Similar deviations are attributed to the mobility of the vinyl and propionate side chains.[87] The ^1H NMR characteristics of the high-spin metmyoglobin from mollusk *Aplysia limacina* have been also investigated and compared with those of sperm whale myoglobin.[317] The absence of a distal histidine and of coordinated water[318] differentiates *Aplysia* from the more commonly studied mammalian Mbs. The heme proton signals (Figure 31B) have been assigned by ^1H NMR using samples reconstituted with

Table VI. Heme Resonance Assignments in Various Metmyoglobin

heme proton	chemical shift		
	sperm whale[a]	*Aplysia*[a]	*G. japonicus*[b]
8-CH_3	91.7	96.8	99.9
5-CH_3	84.9	90.0	87.6
3-CH_3	73.2	79.0	76.0
1-CH_3	53.2	55.8	55.8
7-Hα	75.5	64.0	83.3
6-Hα	59.2	54.4	62.4
4-Hα	46.4	51.5	46.1
6-Hα'	44.9	48.9	37.5
7-Hα'	30.9	42.8	42.2
2-Hα	31.4	39.7	37.2
4-Hβ		-8.6	
meso-H	c	-16.6	-20
meso-H	c	-29.4	
meso-H	c	-34.4	

[a] Taken from ref 317. [b] Taken from ref 320. [c] Not detected in the hyperfine-shifted region.

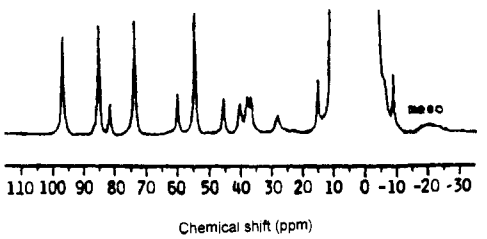

Figure 32. ^1H NMR spectrum of *Galeorhinus japonicus* metMb recorded at 270 MHz and 308 K in D_2O solution, pH 9. The meso-H signal is indicated at -20 ppm. (Reprinted from ref 320. Copyright 1990 Springer-Verlag.)

selectively deuterated hemins and NOE measurements.[317] The shift values are reported in Table VI, together with those of sperm whale metMb for comparison purposes. In spite of remarkable similarities in the downfield portions of the ^1H NMR spectra of *Aplysia* and sperm whale metMbs involving the pyrrole substituents, the overall hyperfine shift patterns differ dramatically for the meso-H shifts. The exact electronic origin of the difference in meso-H shift is not yet clear, but there are no exceptions to the correlation among the characterized models and proteins. While pyrrole substituents show very similar hyperfine shifts for penta- and hexacoordinate high-spin ferric complexes, the meso H-shifts are characteristically downfield ($\simeq$40 ppm) for the hexacoordinate systems and upfield (-20 to -70 ppm) for the pentacoordinate systems. Both the ^1H and ^2H NMR spectra of *Aplysia* metMb clearly show the absence of downfield meso-H signals and locate three of the four meso-H peaks in the region -16 to -35 ppm, consistently with the pentacoordination of the heme iron found from X-ray analysis. Also in the case of *Galeorhinus japonicus* and elephant metMbs, which possess a Gln residue at the distal site instead of the usual His residue,[319] a broad feature of the ^1H NMR spectra has been observed at around -20 ppm (Figure 32 and 31G, respectively).[320] This broad resonance has been attributed to the heme meso protons and taken as indicative of pentacoordination for the heme iron. *Aplysia* metMb has several peaks in the upfield region which exhibit large deviations from Curie behavior.[317] It must be considered that shifts alone do not determine the purity of the ground spin state, but from the analysis of the temperature dependence of the hyperfine-shifted signals useful information can be obtained. Deviations from Curie behavior must have their origin either in an equilibrium or a quantum mechanical spin admixing between different spin states or, if detected only for selected pyrrole substituents, in the internal mobility of the side chains. The temperature dependence of the chemical shifts of the meso resonances displays a deviation from the Curie behavior that is consistent with a termally accessible Kramers doublet with significant $S = {}^3/_2$ character. On the other hand, the temperature dependence of propionate and vinyl chemical shifts shows selective deviation which can be interpreted in terms of thermally induced side-chain reorientation.[317]

The influence of solvent isotope composition on ^1H NMR resonance shift and line width of heme methyls has been investigated for a variety of high-spin ferric hemoproteins (metmyoglobin, metsulfmyoglobin, methemoglobin, cytochrome *c'* from *Rhodopseudomonas palustris*, horseradish peroxidase, and cytochrome *c* peroxidase) for the purpose of detecting hydrogen-bond interactions in the heme cavity.[321] Larger hyperfine shifts and paramagnetic line widths in D_2O than in H_2O are observed for metMb and metHb possessing a coordinated water molecule, but not in *Aplysia* metMb. This suggested the existence of an influence of the distal hydrogen-bonding interactions on the heme electronic structure. A substantial isotope effect (when using H_2O or D_2O as solvent) on both shifts and line widths is observed in a variety of high-spin ferric hemeproteins when both a bound water molecule and a distal residue capable of acting as a hydrogen-bond acceptor are present. From these results the authors concluded that this isotope effect can be empirically used as a probe for the presence of such bound water. Therefore, empirical indicators for penta- or hexacoordinate ferric hemes, which were proposed to serve as probe for H_2O coordination in high-spin hemeproteins are (i) characteristic differences in the signs of the heme meso-H shifts, which are found $\simeq$30–40 ppm low-field in hexacoordinated and $\simeq$20–70 ppm upfield in pentacoordinated systems; (ii) the detection of substantial solvent isotope effects on the heme CH_3 chemical shifts. The recent successful over-expression in *E. coli* of sperm whale Mb based on synthetic gene has permitted the construction of a variety of point mutants at the key distal positions, E7 and E11.[322] The analysis of the shift pattern in the ^1H NMR spectra (Figure 31, parts C–F) of these distal mutants allowed the authors to rationalize point ii.[323] All the following considerations are based on the fact that the essentially axial dipolar shift results from the substantial zero-field splitting, D, characteristic of the ^6A state of ferric hemoproteins and is given by[308]

$$\delta_{dip} = \frac{-28g^2\beta^2}{k^2T^2}\frac{(3\cos^2\theta - 1)}{r^3}D \qquad (46)$$

where θ is the angle between the iron–proton vector **R** and the *z* axis, which is generally close to the heme normal. Detailed studies of a number of high-spin ferric complexes, have already shown that they not only exhibit positive *D* values but the magnitude of *D* also increases significantly when the axial ligand field is weakened. Hence, the loss of water at the sixth position in a ferric high-spin heme protein should manifest itself

in larger zero-field splitting and therefore larger dipolar shifts. Indeed, the difference in D values and the consequent δ_{dip} completely account for the mean −5 ppm low-field bias of the four heme methyls in *Aplysia* metMb relative to that of sperm whale metMb. The same −5 ppm low field bias is observed in the sperm whale mutant metMb His[H7]Val confirming that the His → Val substitution leads to loss of the coordinated water.[322] The proximal His F8 Hβ hyperfine shift experiences both downfield contact and upfield dipolar shifts. Since the contact shifts depends critically on orientation of the Hβ relative to the imidazole plane, comparisons are useful only among the sperm whale derivatives, where the His F8 orientation is unaltered. Since the upfield δ_{dip} is much larger in His[E7]Val than that in WT, the larger low-field shifts observed dictate an even larger His Hβ contact contribution for the mutant. This is consistent with the absence of a coordinated H_2O: a decrease in ligand field strength is expected to increase the His–Fe covalency and hence the contact shift. However, the predicted change in the dipolar shift contribution for meso-H upon loss of H_2O is a 10 ppm downfield bias; instead, a 50–80-ppm upfield bias is observed in proteins as well as in model compounds. Hence, the meso-H shifts are dominated by contact contribution changes that are not understood. In any case, in all the examples reported up to now, the characteristic change in low-field to upfield meso-H contact shifts upon loss of the sixth ligand is always accompanied by the more quantitatively understood larger D values.

An interesting paper on the effect of solvent viscosity on the NOE has recently appeared.[103] Due to the linear dependence of cross relaxation values on the correlation time (see section III) and to the independence of the intrinsic relaxation from this parameter, increased steady-state NOEs are observed with increasing viscosity. For systems that exhibit Curie spin relaxation the advantage of increased NOEs with molecular weight can still be realized if the applications are restricted to low magnetic fields, which minimize this relaxation mechanism. The relevance of these observations is obvious for the study of other larger molecular weight high spin heme proteins, where the $S = {}^5/_2$ spin state represents the active state.

2. Peroxidases Containing the Noncovalently Bound Heme

Peroxidases are an ubiquitous class of heme proteins (MW ≃ 40 000) with protoporphyrin prosthetic group and trivalent oxidation state of the iron ion in the resting state form.[300,301] In the presence of H_2O_2 they oxidize a large amount of aromatic and biological substrates. The amino acid sequence of many peroxidases of different origin have been reported.[324,325] Despite the low overall homology, some key residues in the catalytic cavity are conserved among the different species. Most of these proteins are glycosilated and therefore difficult to crystallize. For this reason the X-ray structure has been reported since many years for cytochrome *c* peroxidase (CcP) only, which is a not glycosilated intracellular protein.[326,327] The crystallographic characterization of lignin peroxidase, LiP, has been very recently reported.[328–330] In Figure 33 the active-site structure of CcP is reported. The availability of the crystallographic structure of CcP could in principle,

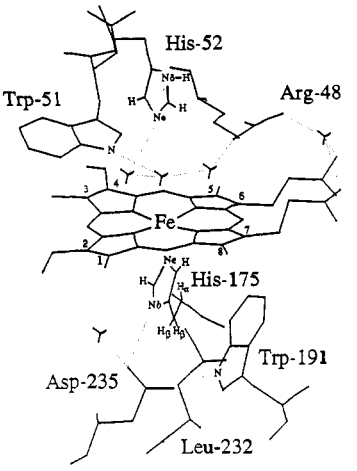

Figure 33. Active-site structure of CcP.

and has been indeed, of great help for a good NMR characterization of the solution structure. However, due to the easy availability of HRP, its higher solubility and stability with temperature, this protein has been more extensively characterized through NMR. Among large/medium-sized proteins, HRP represents the most extensively characterized system using the most advanced NMR techniques.

The ^1H NMR spectra at 200 MHz and 301 K for HRP and CcP are reported in Figure 34, parts A and B, together with those of LiP (Figure 34C) and manganese peroxidase (MnP, Figure 34D). In the NMR spectra in D_2O of HRP and CcP four three-proton intensity signals are observed in the 80–50 and 80–60 ppm range, respectively. Eight single-proton resonances are present between 65 and 25 ppm for HRP and between 55 and 35 ppm for CcP. In the upfield region some resonances are resolved in the range of −2 to −12 ppm. Since the beginning, assignments of the heme protons signals of HRP and CcP have been achieved due to the possibility of reconstituting these proteins with selectively deuterated hemes. For HRP it was possible by deuteration to assign each heme methyl groups.[85] For CcP the assignment of the four heme methyls, of 2- and 4-Hα, and of one of the β-CH_2 protons of each vinyl groups has been achieved.[331] In recent years the spectra of some peroxidases of different origin (*Coprinus*, cucumber, LiP, MnP)[332–337] and of some mutants of CcP[338,339] have been assigned, at least partially, by reconstitution with deuterated hemes and comparison with the previously reported spectra of HRP and CcP. An interesting feature of these spectra is the presence of an exchangeable signal at about 100 ppm (Table VII), assigned to the Hδ1 of the proximal His. A corresponding signal has been observed also in the spectra of metMb and methemoglobin (metHb).[340–342] Its different exchange rate with the bulk water in the different proteins might well be related to the different accessibility of the proximal cavity to the solvent.[336,340] Spectral information on the sixth coordination site of the iron ion is only available for basic cucumber peroxidase isoenzyme and HRP. In the former case (Figure 35) broad features in the −15 to −30 ppm region of the ^1H NMR spectrum have been observed and ascribed to the heme meso protons.[333] They have also been observed in the ^2H NMR spectrum of native HRP.[51] This suggests that both the enzymes contain a pentacoordinate iron(III) ion.

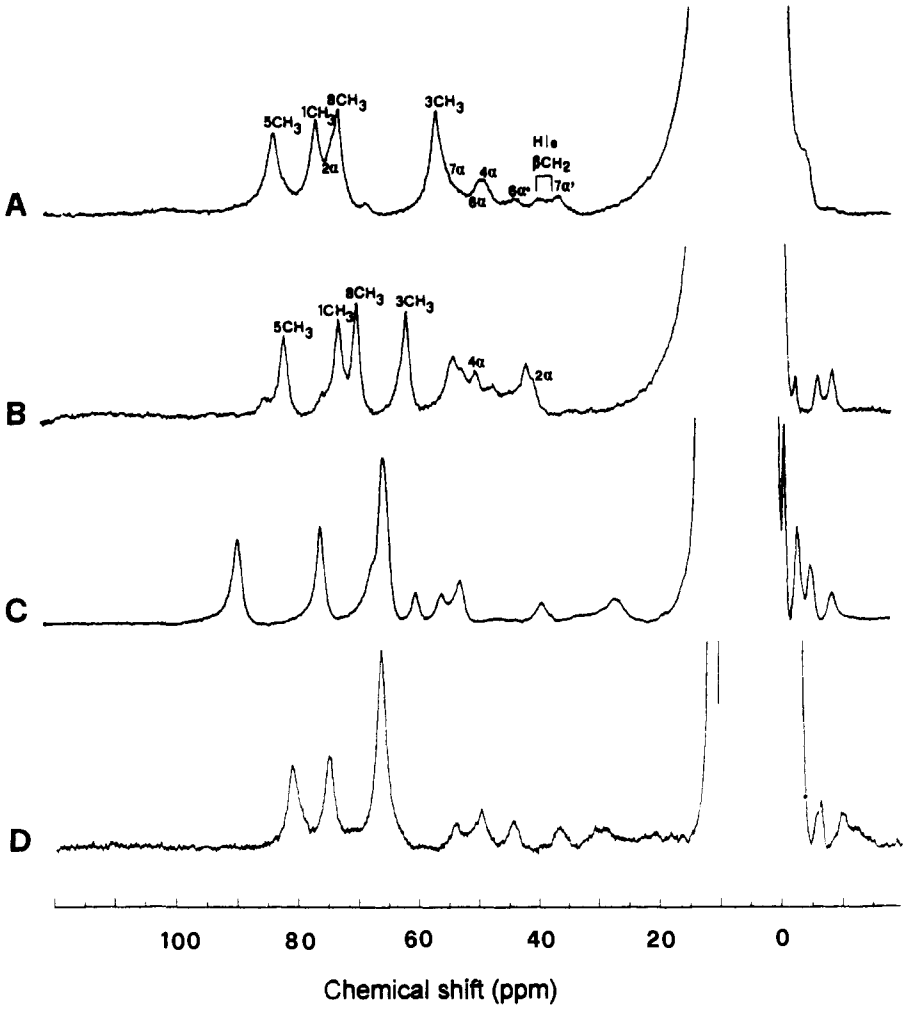

Figure 34. ^{1}H NMR spectra (200 MHz) of (A) HRP (pH 7.0), (B) CcP (pH 6.9), (C) LiP (pH 5.0), and (D) MnP (pH 6.5). All the spectra were recorded at 298 K in D_2O solution, 0.1 M phosphate buffer.

Table VII. Shift Values for the Downfield Exchangeable Signal, Attributed to the Proximal Hδ1, in Various High-Spin Heme Proteins

protein	temperature (K)	chemical shift (ppm)	ref
sperm whale Mb	308	100	340
D. dentriticum Hb	298	96	341
R. palustris cyt. *c'*	308	102	394
HRP	308	96	340
LiP	298	93	336
MnP	298	92	336
Coprinus peroxidase	294	87	332
cucumber peroxidase	298	95–100	333

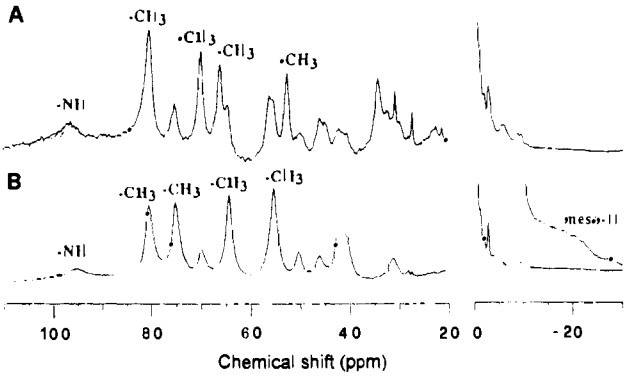

Figure 35. ^{1}H NMR spectra (600 MHz) of cucumber peroxidase: (A) acidic isoenzyme and (B) basic isoenzyme. Both the spectra were recorded at 298 K in D_2O solution, pH 8.0. The shaded signal has been attributed to the slowly exchanging NH proton of the proximal histidine. (Reprinted from ref 333. Copyright 1991 Elsevier.)

Due to the low structural information content obtainable from the NMR spectra of these high-spin systems, where the hyperfine shift is almost completely dominated by contact contribution, for most of these proteins few efforts have been devoted to an extensive assignment. In any case the applicability of NOE techniques also to these fast relaxing signals (T_1 values around 2–3 ms) has been well documented by the results obtained on HRP[343,344] (Figure 36) and on LiP[335] (Figure 37). Among high-spin peroxidases LiP represents the first example of an extensive assignment of the hyperfine-shifted signals based on NOE measurements only. Indeed, the X-ray structure has appeared more than one year later than the NMR characterization. Furthermore, a 2D study on HRP has been reported where the authors show how by NOESY and COSY spectra (Figure 38) it is possible to obtain all the information needed for the assignment of the heme and of the proximal His β-CH_2 protons without employing deuterated hemes.[345] However, as outlined in section III.B, it has been demonstrated that the cross peaks observed between the very broad signals of α-CH_2 protons of the heme propionates are due to relaxation-allowed effects rather than to scalar interactions.[137] The

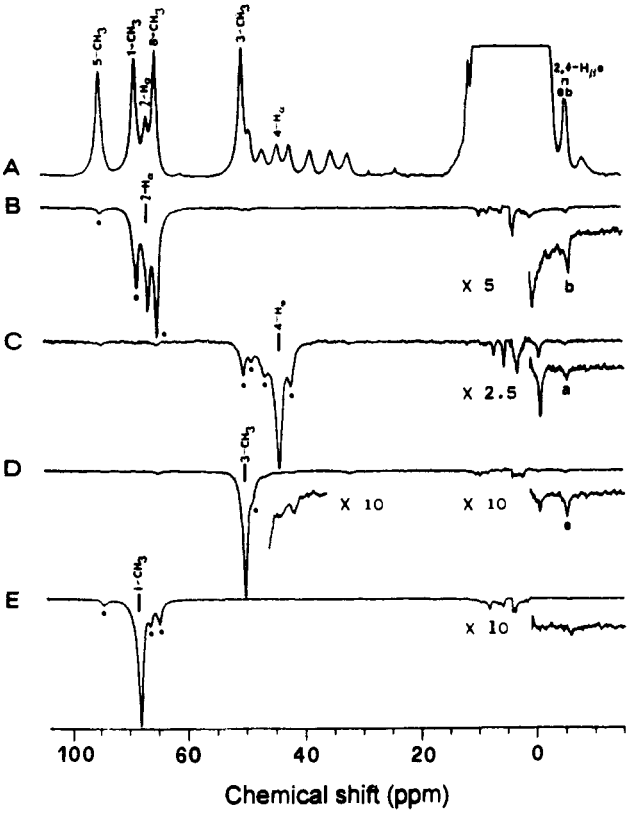

Figure 36. ^{1}H NMR spectrum (360 MHz) (A) of 3 mM HRP in D_2O at 328 K, pH 7.0, and NOE difference spectra obtained on the same sample by saturation of (B) 2-Hα, (C) 4-Hα, (D) 3-CH_3, and (E) 1-CH_3. Difference peaks due to off-resonance saturation are marked with filled circles. (Reprinted from ref 344. Copyright 1986 American Chemical Society.)

above consideration reduces the applicability of COSY experiments in heme proteins only to the low-spin species. Moreover, even in the cyanide adducts of peroxidases, cross-correlation effects may introduce dipolar contributions to cross peaks together with true scalar connectivities, e.g. between the β-CH_2 protons of the proximal histidine ligand and between the geminal protons of the heme vinyl substituents.[118]

Many other systems have been characterized by NMR spectroscopy and important structural and functional information have been obtained from the analysis of their NMR spectra, although intrinsic difficulties (like low thermal stability and low solubility of the samples) prevent the application of the most advanced NMR techniques. In the last years useful information has been obtained on the mutants of CcP. The ^{1}H NMR characterization of the mutants obtained by substituting the Asp235 residue with Asn[338] and Ala[339] shows the key role of this residue for the overall stability of the catalytic cavity. Indeed the spectra of both N235[338] (Figure 39) and A235[339] exhibit a smaller range of shifts in the downfield region (60–10 ppm). The signals observed are clearly due to at least two species, whose relative ratios strongly depend on pH conditions. One of these species shows resonances whose shifts do not exceed 40 ppm. Moreover, at variance with that reported for the other resting-state peroxidases, for the hyperfine-shifted signals of the latter species an anti-Curie behavior with temperature has been observed. These observations suggest that the mutants are characterized by a higher tendency to hexacoordination.

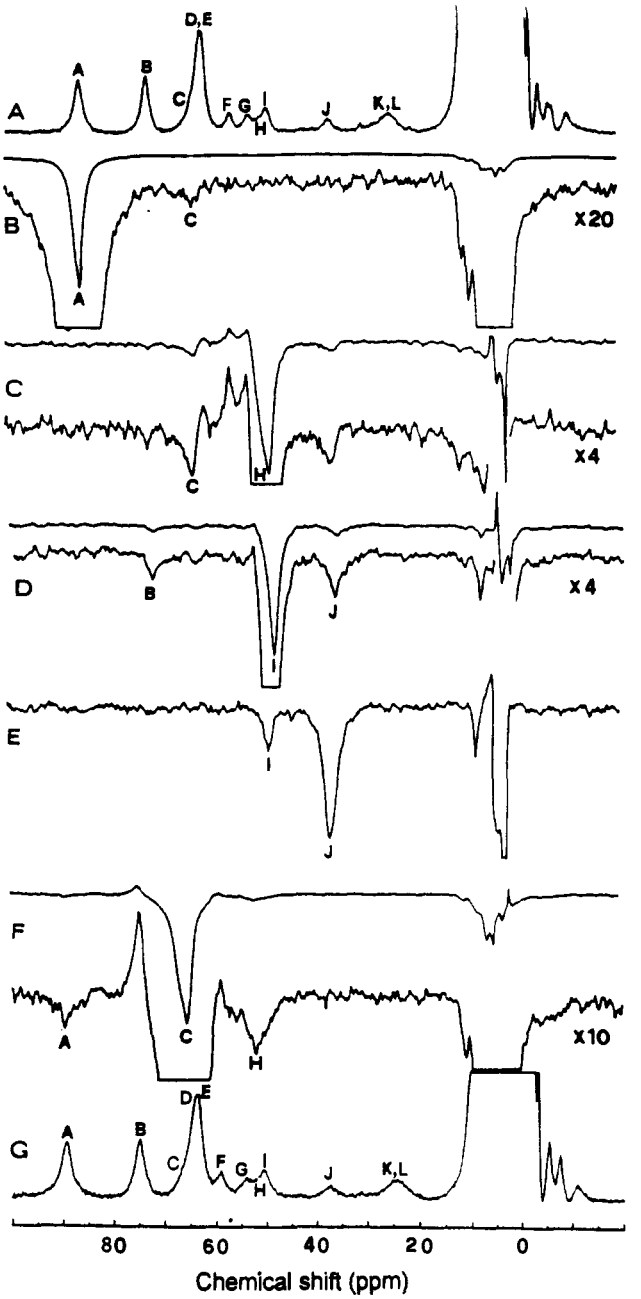

Figure 37. ^{1}H NMR spectrum (200 MHz) (A) of LiP at 308 K in D_2O solution, 10 mM sodium acetate buffer pH 5.0 and NOE difference spectra in the same experimental conditions obtained by saturation of (B) signal A, (C) signal H, (D) signal I, and (E) signal J. In F and G the NOE difference spectrum obtained at 297 K by saturation of signal C and the corresponding reference spectrum are reported. From the above NOE patterns A and B have been assigned as the two heme methyls adjacent to propionate side chains (i.e. 5- and 8-CH_3) and the couple C,H and I,J as the Hα geminal protons of the 6- and 7-propionate substituents. No discrimination between 5- and 8-CH_3 and 6- and 7-propionate resonances was obtained. (Reprinted from ref 335. Copyright 1991 National Academy of Sciences.)

The 270-MHz ^{1}H NMR spectra of CcP from *Pseudomonas aeruginosa* have also been reported.[346] This protein contains two *c*-type hemes with widely different Fe^{3+}/Fe^{2+} reduction potentials (+320 and −330 mV, respectively). The quality of the spectra is very poor, possibly due to the high molecular weight and the limited amount of the protein available. However, the data are consistent with a low spin/high spin equilibrium

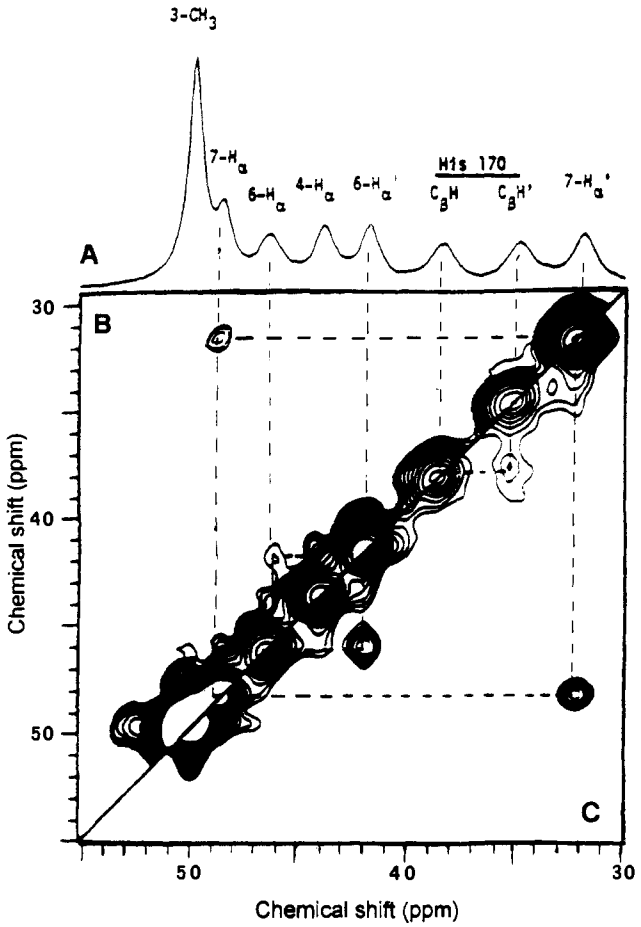

Figure 38. (A) ^{1}H NMR reference spectrum of HRP in D_2O solution at 300 MHz and 328 K, pH 7.0, and magnitude COSY (B) and NOESY (C) maps obtained in the same experimental conditions. (Reprinted from ref 345. Copyright 1991 American Chemical Society.)

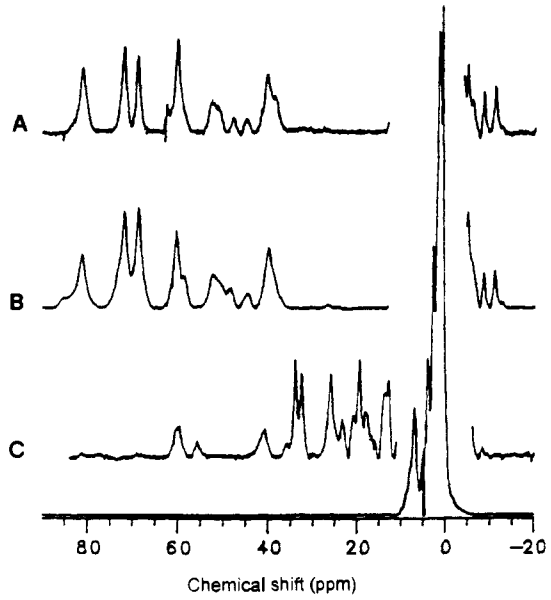

Figure 39. ^{1}H NMR spectra (261 MHz) of (A) wild-type yeast CcP, (B) recombinant MI-CcP, and (C) D235N mutant of MI-CcP. The spectra were recorded at 295 K in D_2O solution, 0.2 M potassium nitrate, and 0.05 M potassium phosphate, pH 6.8. (Reprinted from ref 338. Copyright 1990 American Chemical Society.)

of the low potential heme in both the resting and half-reduced states of the protein, whereas the high potential heme is found to be in the low-spin ferric state in the resting enzyme. Reduction of this heme perturbs the environment of the low potential heme indicating heme–heme interaction. These data are consistent with those previously reported for *Pseudomonas stutzeri* CcP.[347]

3. pH Dependence

By means of ^{1}H NMR spectroscopy different behaviors for the various heme proteins with pH have been found. The spectrum of the native ferric high-spin HRP changes depending on the pH value of the enzyme solution in three steps with pK_a around 4, 6, and 11.[348,349] In particular, above pH 10.5 new signals appear in the 20–10-ppm range, this indicating that the spin state of HRP transits from high spin to low spin with a pK_a of 11. The above behavior differs drastically from that observed for metMb. With increasing pH the heme methyl signals of horse heart metMb shift to higher field with a pK_a of 9.1. That means that the exchange time between the acidic and alkaline forms is shorter than 10^{-4} s for metMb and longer for HRP. pH dependence studies reveal that the alkaline transition occurs at pH 9.3, 9.4, 9.8, and 10.9 for HRP A_1, A_2, A_3, and C isoenzymes, respectively.[350] The pH dependence of Asian elephant metmyoglobin, where the usual distal histidine is replaced by a glutamine residue, shows some particular features.[351] At low pH the spectrum exhibits resonances in the same spectral window as sperm whale metMb, but there are many more signals suggestive of more than one species in solution (Figure 40, parts A and B). Raising the pH has no effect on the position, relative intensities, and line widths of elephant metMb peaks, although all resonances lose intensity while a new set of signals appears (Figure 40, parts C–D). This species, identified as metMb–OH^- (Figure 40E), has a spectrum very similar to that of sperm whale metMb–OH^- (Figure 40F). The pK_a is about 8.7. The two sets of resonances observed at low pH arise from two interconvertible forms of elephant metMb–H_2O. One of the two species has average heme methyl shifts slightly larger than sperm whale metMb–H_2O, while the average shift for the other species is quite a bit smaller. On this basis the authors suggested that the glutamine NH acts as a hydrogen-bond donor. The shift pattern can be justified assuming that its interaction with the water-bound molecule in the former species is slightly weaker than that between histidine and bound water in sperm whale metMb–H_2O. Analogously, in the second species the coordinated water is interacting more strongly with the distal glutamine than with the distal histidine of sperm whale Mb. *Aplysia* and *G. japonicus* metMbs exhibit an acid alkaline transition with pK_a of 7.8[317] and 10,[320] respectively. In both cases the transition time is longer than 10^{-4} s. The comparison of the pK_a values for these two pentacoordinate Mbs with those found for the hexacoordinate ones shows that the affinity of the hydroxide anion does not appear to depend on its coordination state. The kinetics of the acid alkaline transition for the pentacoordinate metMbs from *Dolabella auricularia* and *Mustelus japonicus*[352] have been investigated by saturation transfer ^{1}H NMR experiments. The former protein (pK_a of 7.8) has high sequence homology with *Aplysia limacina* Mb and the latter (pK_a of 10.0) with *G. japonicus* Mb; in both cases the acid and the alkaline forms are in slow exchange on

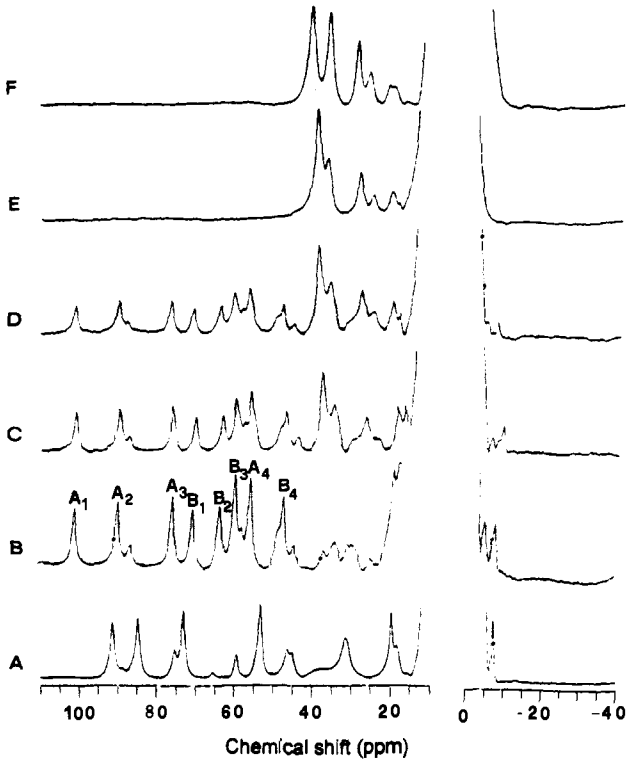

Figure 40. ^{1}H NMR spectra (360 MHz) of sperm whale metMb at pH 6.2 (A); elephant metMb at pH 6.5 (B), pH 8.6 (C), pH 9.15 (D), and pH 10.5 (E); and sperm whale metMb at pH 10.5 (F). All the spectra were recorded at 298 K in D_2O solution. The two different sets of signals labeled A_1–A_4 and B_1–B_4 originate from two distinct species. (Reprinted from ref 351. Copyright 1984 *Journal of Biological Chemistry.*)

the NMR time scale. The differences in the estimated transition rates and activation energies for the two proteins have been tentatively related to differences in the distal side residues. Upon pressurization decreased pK_a values for metMb and metHb were found.[353] It has been proposed that the decrease in pK_a originates from a contraction of the protein such that the hydrogen bond between the iron-bound water molecule and the distal histidine is strengthened and deprotonation of H_2O takes place more readily.[353]

pH-dependence studies on CcP have shown that its NMR spectrum changes according to three pK_as of about 4.1, 5.8, and above 8.[354] The second one correlates with an apparent pK_a observed in the kinetic properties of the enzyme, whereas the third one reflects the OH^- binding, which gives rise to a low-spin species.[338] In the case of the CcP N235 mutant the value of the latter pK_a decrease to about 6,[338] whereas for the A235 mutant, where the possibility of a hydrogen bond with the proximal His is completely eliminated, a further decreases to about 5 is observed.[339] Therefore, this proximal site mutation affects the pK_a for a distal-side heme ligand. The ^{1}H NMR spectrum of ferric *Coprinus cinereus* peroxidase shows only subtle changes when examined over the pH range 4.5–9. At very high pH broadening of all the signals is observed but no significant changes in the chemical shift values are seen.[332]

4. Anion Adducts

The ^{1}H NMR spectra of some anion adducts of heme proteins have been reported. The spectra of metMb–

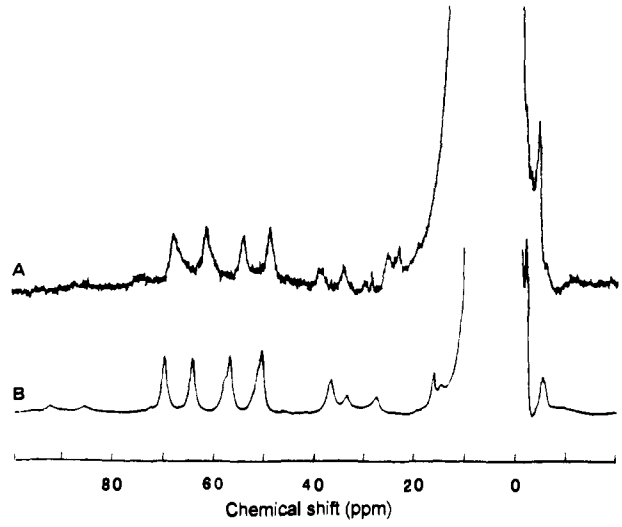

Figure 41. ^{1}H NMR spectra (300 MHz) of (A) *Coprinus* peroxidase thiocyanate in D_2O solution, pH 5.8, and (B) myoglobin thiocyanate in D_2O solution, pH 7.0. Both the spectra were recorded in 0.1 M phosphate buffer. (Reprinted from ref 332. Copyright 1989 American Chemical Society.)

NCS^-, metMb–F^-, and metMb–$HCOO^-$ are typical for ferric high-spin states.[346,355] The pH dependence of the first complex is quite distinguishable from that of metMb–H_2O, since no shift of the heme methyl peaks is observed on raising pH. Above pH 11 the spectra of this complex are almost the same as those of alkaline metMb at the corresponding pH value.[346] This suggests that the NCS^- ligand is replaced by the OH^- anion. In the case of fluoride and formate adducts the effect of pressurization on the ^{1}H NMR spectrum has been studied.[355] Upon pressurization up to 2000 atm each methyl signal of the fluoride complex tends to shift downfield, while the methyl signals of the formate complex experience slight upfield shifts. With increasing pressure also the methyl resonances of metMb shifted upfield. Iodide and thiocyanate are reported to bind HRP.[356,357] Moreover, whereas CN^-, F^-, and N_3^- anions inhibit the peroxidase activity, I^- and NCS^- are oxidizable substrates. For HRP, in the presence of iodide, both chemical shifts and line widths of the heme peripheral 1- and 8-CH_3 resonances were markedly affected by the pH change from 7 to 4 and broadened at pH 4. These results suggested that an iodide ion binds to the enzyme (but not to the iron ion as in metMb) at almost equal distance from the heme peripheral 1- and 8-CH_3 and that the interaction becomes stronger in acidic medium with protonation of an ionizable group with pK_a value of 4. The broadening of 1- and 8-CH_3 proton signals is reasoned in terms of strong quadrupole interaction of the iodide. In addition, it has been observed that the binding of iodide to the enzyme exerted no effect on the proximal histidine proton resonances.[356] Below pH 6 addition of NCS^- to native HRP induces some changes in both chemical shift and line width of only 1- and 8-CH_3.[357] The NCS^- complex of *Coprinus cinereus* peroxidase is predominantly high spin at room temperature (Figure 41A).[332] The spectrum closely resembles that of metMb (Figure 41B). At variance with HRP, no selective effects are observed on single heme substituent proton signals. The resonances display non-Curie law behavior. Slow exchange between bound and free enzyme has been

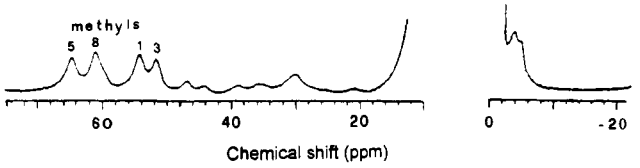

Figure 42. ^1H NMR spectrum of CcP-F^- recorded at 470 MHz and 295 K in 0.1 M potassium nitrate pH 6.95. (Reprinted from ref 331. Copyright 1983 Elsevier.)

observed. Above pH 7.6 the signals of the complex disappear.

The ^1H NMR spectrum of CcP-F^- (Figure 42) has been assigned reconstituting the protein with selectively deuterated hemes.[331] Whereas in native CcP 5- and 1-CH_3, which are on opposite pyrroles (III and I), possess larger shifts than 8- and 3-CH_3, the order of the heme methyl shift in CcP-F^- is 5 > 8 > 1 > 3. The pH dependence of the spectrum of the complex is less pronounced than that of the native protein. The 5-CH_3 resonance is the most affected and from the pH dependence of its shift values a pK_a of 5.5 has been estimated. The N235 mutant binds fluoride yielding a spectrum similar to that of the WT CcP-F^-.[338]

5. The Interaction with Substrates

^1H NMR spectroscopy has also been used for studying the interaction of peroxidases with substrates. The interaction of CcP with several cytochromes has been extensively studied.[358-360] However, the heme methyl resonance shifts of CcP are essentially unaffected by either covalent or noncovalent complexation with horse cytochrome *c*. On the other hand, meaningful information has been obtained from the analysis of the spectra of cytochromes bound to CcP (see later). A variety of aromatic molecules are known to interact with HRP. This binding produces some detectable changes in the chemical shifts of the hyperfine-shifted proton resonances on and near the heme group.[340,361,362] In particular, shift variations are observed for the 1- and 8-CH_3 resonances. A binding site close to the heme 8-CH_3 has been proposed on the basis of relaxation and NOE data.[361,363] A close inspection of the aromatic region of spectrum of different HRP isoenzymes in the presence of different aromatic molecules suggests[364-366] that the binding site includes two Phe residues. The catalytic properties of HRP are regulated by the binding of 2 mol of endogenous Ca^{2+} to the enzyme. The bound Ca^{2+} can be removed from the enzyme. The ^1H NMR spectra for native and Ca^{2+}-free HRP show quite different features for the hyperfine-shifted proton signals: particularly, the heme methyl shift values pass from 78.0, 70.4, 67.7, and 50.7 for the native enzyme to 71.3, 62.0, 62.0, and 46.0 for the Ca^{2+}-free enzyme.[367,368] The equilibrium between the two different species is slow on the NMR time scale. The shift values of the above resonance for the Ca^{2+}-free species are almost temperature insensitive within the range 9–39 °C, suggesting a different electronic state of the heme iron. The Mn^{2+} binding to MnP has been investigated. In the adduct obtained by addition of 1 equiv of Mn^{2+} drastic changes in the hyperfine-shifted resonances are observed. The two single-methyl resonances and some one-proton intensity signals become so broad that they cannot be observed. According to the Ortiz de Montellano proposal[369] and on the basis of the analogous results obtained on the cyanide adduct, the two methyl signals can be attributed to the 1- and 8-CH_3.[370] (See also section V.B.)

6. Peroxidases Containing the Covalently Bound Heme

Lactoperoxidase (LPO, MW 78 000), found abundantly in mammalian milk, but also in saliva and tears, catalyzes the oxidation of thiocyanate to a reactive species that then serves in an antimicrobial defense system. Recently, it has been shown[294] that the heme is covalently attached to the polypeptide via a disulfide bond to a cysteine residue. The ^1H NMR spectrum of resting-state LPO is reported in Figure 43: poorly resolved broad resonances are observed in the 62–20-ppm region.[371,372] In particular one intense signal is observed at 61.5 ppm, which is probably due to the CH_3 substituents of the heme. The most striking analogy of this spectrum with those of the other high-spin iron(III) hemeproteins is the presence of a broad single-proton exchangeable resonance at 104.1 ppm, assigned as Hδ1 of the proximal histidine. No changes have been observed in the LPO spectrum between pH 7 and 12. The major signal experiences an upfield shift on adding iodide,[373] suggesting the interaction of the anion with the periphery of the heme. This interaction is strengthened by protonation of an amino acid residue with pK_a 6.0. Competitive binding studies indicate that cyanide exerts no effect on iodide binding, suggesting that I^- may bind at a non-heme binding site. This is consistent with the findings on HRP reported above.[356] The same changes in the NMR spectrum of LPO have been observed in the presence of NCS^-.[374] A pK_a of 6.4 for thiocyanate binding has been found. The distance of 7.2 Å of the ^{15}N atom of thiocyanate from the ferric center estimated in the same paper is consistent with a thiocyanate ion not in direct contact with the ring peripheral group, but sufficiently close to affect the chemical shifts of some peripheral substituents. It has been found that I^- and NCS^- compete for the binding with aromatic molecules.

The spectrum of the spleen green heme protein (or myeloperoxidase), a tetramer of molecular weight 150 000 with two heavy subunits (MW 60 000) and two light subunits (MW 15 000) has been also reported (Figure 44).[375] The spectrum closely resembles that of LPO. By changing the pH from 7 to 4, the ^1H NMR spectrum of the ferric enzyme alters slightly. The major change is the position of the largest peak: it moves from 75 to 72 ppm.

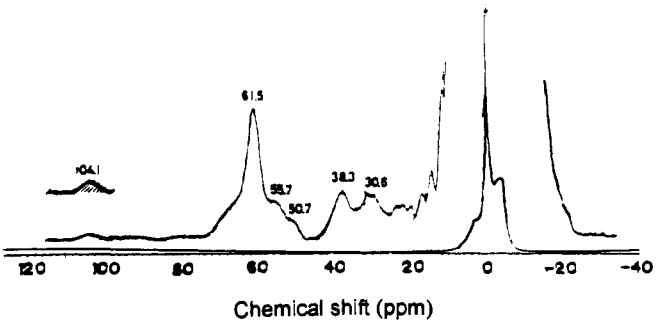

Figure 43. ^1H NMR spectrum of LPO recorded at 300 MHz and 296 K in H_2O solution, pH 7. The shaded resonance represents an exchangeable proton signal. (Reprinted from ref 372. Copyright 1986 American Chemical Society.)

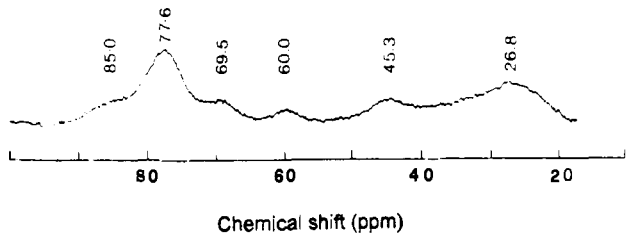

Figure 44. ^{1}H NMR spectrum (360 MHz) of the ferric half-enzyme of spleen green hemeprotein, recorded at 278 K, pH 6. (Reprinted from ref 375. Copyright 1987 Elsevier.)

7. Cytochrome P450 and Chloroperoxidase

Cytochromes P450 are an ubiquitous class of *b*-type heme proteins that catalyze the hydroxylation of a wide variety of aliphatic and aromatic molecules.[299] All P450 enzymes share a common active-site structure and reaction cycle. Among these enzymes, cytochrome $P450_{cam}$, the enzyme obtained growing *Pseudomonas putida* on *d*-camphor, can be obtained in large quantity and studied at high concentration. For these reasons it represents the best model system for understanding the detailed structure–function relationships in this class of compounds. $P450_{cam}$ is a single polypeptide chain with molecular weight about 45 000 and a protoheme as prosthetic group. The crystal structures of the camphor-bound and camphor-free species of $P450_{cam}$ have been determined.[376-378] The Cys357 residue provides the axial sulfur ligands in both forms of the enzyme. In high-spin camphor-bound state, the iron atom is pentacoordinate. The first ^{1}H NMR spectrum of high-spin ferric $P450_{cam}$ was by Keller et al.[379] The spectrum, obtained at 220 MHz and 281 K, shows four very broad lines at 66.5, 60.0, 42.0, and 37.5 ppm. More recently Lukat and Goff[380] reported a well-resolved 300-MHz 294 K ^{1}H NMR spectrum of the ferric form of $P450_{cam}$: four three-proton intensity signals are observed in the 65–35-ppm region, and some signals of intensity one are clearly apparent in the 55–30-ppm range (Figure 45A). Analogous to the other high-spin iron(III) hemeproteins, the signals of intensity three can be attributed to the four heme methyl substituents, whereas the one-proton signals should originate from the other heme substituent protons or from the axial iron ligand. The authors ruled out the latter possibility by comparing the spectrum with that of high-spin iron(II) form: they suggested that the signals of the axial cysteinate protons are not detectable due to the larger line width. The ^{1}H NMR spectrum is also available for cytochrome $P450_{RR1}$ from *Rhodococcus rhodochorus* in the presence of 2EP (2-ethoxyphenol), with characteristics similar to those of cytochrome $P450_{cam}$.[381] The line widths and T_1s seem somewhat larger than in other $S = {}^5/_2$ systems. This has been interpreted as due to a relatively small ZFS. Also the small shift range observed for the heme substituent resonance could be rationalized on the basis of a smaller ZFS.

Chloroperoxidase (CPO) is a glycoheme protein of MW 42 000 isolated from the marine fungus *Caldariomyces fumago*.[382] In addition to the usual peroxidase, catalase, and oxygenase activities.[383-365] this enzyme is able to catalyze the hydrogen peroxide dependent oxidation of I^-, Br^-, or Cl^- and the resultant formation of carbon–halogen bonds with halogen acceptors.[386] The

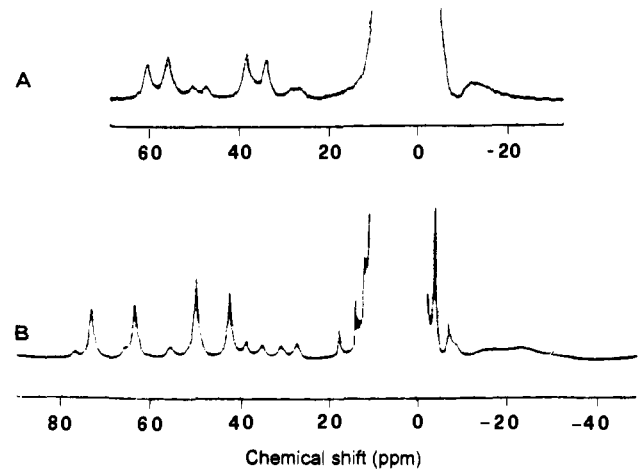

Figure 45. ^{1}H NMR spectra (300 MHz) of (A) ferric $P450_{cam}$ recorded at 294 K in H_2O solution, 0.1 M phosphate buffer pH 7.1, and (B) ferric chloroperoxidase recorded at 296 K in H_2O, 0.1 M phosphate buffer pH 5.8 (from ref 380).

catalytic cycle of these reactions involves the ferric (resting state) and higher oxidation states of the iron. Chloroperoxidase and cytochrome P450 share a number of spectral properties, suggesting that the prosthetic groups of the two enzymes are comparable.[384,365] The high-spin ferric chloroperoxidase ^{1}H NMR spectrum at 300 MHz and 296 K shows four three-proton intensity signals in the region 80–40 ppm and many one-proton resonances between 80 and 15 ppm; broad unresolved features are observed in the upfield region (Figure 45B).[380,387,388] This spectrum has a close similarity with that of ferric camphor-bound $P450_{cam}$ and with those of ferric peroxidases.

8. Cytochromes c′

Cytochromes *c′* are hemeproteins found in photosynthetic, denitrifying and nitrogen fixing bacteria, whose prosthetic group is a heme moiety covalently bound to two cysteinyl residues by means of thioether links.[389] At variance with cytochromes *c*, the iron atom is pentacoordinate: the axial ligand is a His residue exposed to the solvent. These proteins are usually found as dimers, although a monomeric cyt *c′* has been also isolated and studied. Only the X-ray structure of the cyt *c′* from *Rhodospirillum molischianum* is available,[390] and a preliminary report for the crystallization of the *Chromatium vinosum* protein has appeared.[391] Despite some spectroscopical anomalies that led Maltemp to propose that the iron atom was present in a quantum mechanical admixture of high ($S = {}^5/_2$) and intermediate ($S = {}^3/_2$) spin state,[313] NMR results seems to be indicative of the presence of an essentially high-spin iron at room temperature.[392-397] La Mar has proposed the presence of spin admixing for *Chromatium vinosum* cytochrome *c′* on the basis of the different shift values observed for the meso protons in the various cytochromes *c′*.[394] But, as stated for metMb, the position only cannot be a proof for the spin state. In Figure 46 the ^{1}H NMR spectra of various cytochromes *c′* are reported. The spectra consist of four strongly downfield shifted signals of intensity three, due to the four heme methyl groups, and eight downfield signals of intensity one, which are expected to be due to the two α-CH protons establishing the heme thioether bridge, to the

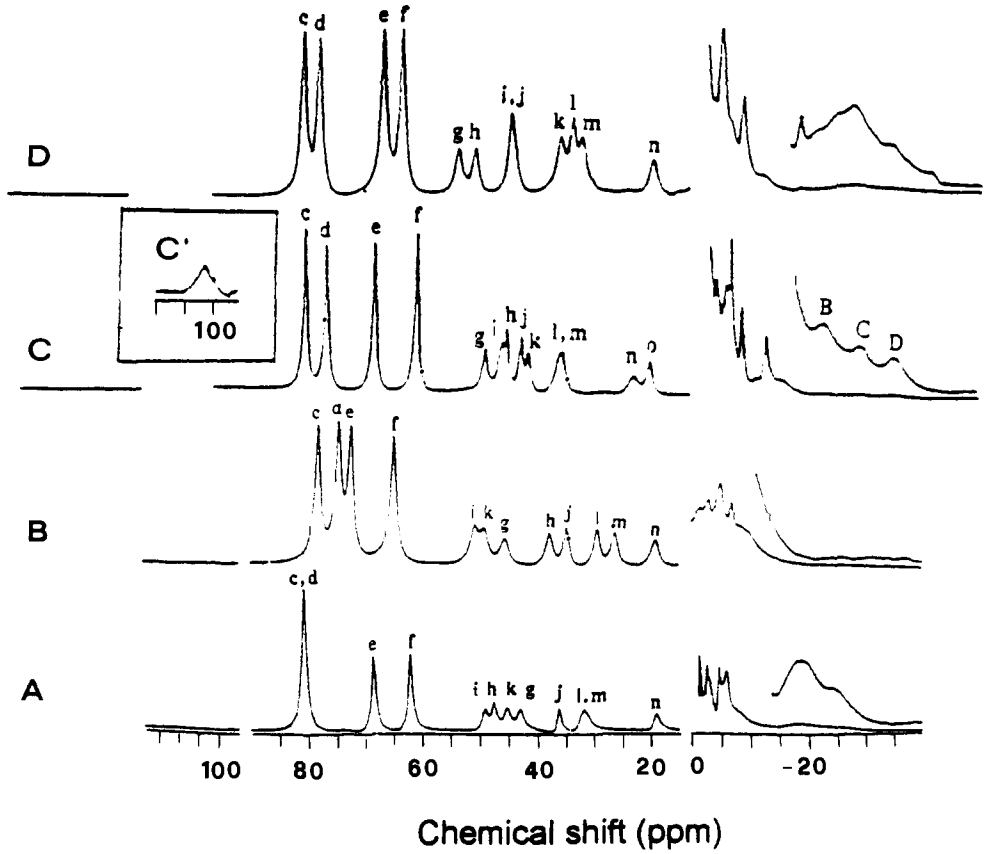

Figure 46. ^{1}H NMR spectra (360 MHz) of (A) *R. molischianum*, (B) *C. vinosum*, (C) *R. palustris*, and (C) *R. rubrum*. All the spectra were recorded at 298 K in D_2O solution, pH 5. The inset C′ shows an exchangeable proton signal observed in H_2O solution with Redfield sequence (from ref 394).

four α-CH_2 protons of the propionate side chains, and to the two β-CH_2 of the proximal histidine. At 600 MHz a sizable line broadening is induced by Curie relaxation.[396] Among high-spin heme proteins, cytochrome *c′* has been extensively characterized by 2D NMR techniques: NOESY (Figure 47) cross peaks have been clearly detected, even between signals as broad as 900 Hz and with T_1 values $\leq$ 10 ms.[396,397] Connectivities between some of these signals have been also detected in a magnitude COSY experiment at 600 MHz,[396] but they have been attributed to cross-correlation effects.[137] The analysis of the NOESY maps has allowed the assignment of most of the heme proton signals and β-CH_2 protons of the proximal His ligand, and suggested possible residues responsible for the 2 or 3 pK_as observed in the various cytochromes *c′* in the pH range 4–11. The highest pK_a is generally accepted to be due to the deprotonation of the histidine ligand.[398] The low pH value pK_a has been reported only for certain cytochromes.[396,397] The compared analysis of the pH dependencies of several cytochromes *c′* with different primary sequences has allowed the pinpointing of the residue responsible for this pK_a, i.e. Glu 10.[396,397]

9. Ferric Chlorin Containing Proteins

Sulfmyoglobin (SMb) is a green heme derivative of Mb in which the native heme has reacted with a sulfur atom leading to saturation of the aromatic skeleton. In the ^{1}H NMR spectra of SMb at least three different species have been identified, depending on preparation conditions.[399] The saturated pyrrole (pyrrole II) has been identified by deuterium labeling; it exhibits a considerably reduced contact shift.[400]

NMR spectroscopy has been successfully used to study the active site of the heme protein subunit of *E. coli* sulfite reductase,[401] where a high-spin ferric siroheme coupled to a $[Fe_4S_4]^{2+}$ cluster is present. In the ^{1}H NMR spectrum 21 hyperfine-shifted resonances are detected in the 130 to −70 ppm range, which correspond to 26 protons. Resonances arising from the β-CH_2 protons of cluster cysteines have been assigned using deuterium substitution. One of these cysteines has NOEs to the heme ring protons and has been tentatively assigned as the bridging histidine. The presence of a bridge between the siroheme and iron sulfur cluster, which cause magnetic coupling between the two, would explain the absence of the characteristic anti-Curie behavior for the resonances of the cysteine protons in $[Fe_4S_4]^{2+}$ clusters (see section IV.D).

B. Low-Spin Iron(III)

The low-spin ferric heme proteins represent an important subclass of paramagnetic metalloproteins whose ^{1}H NMR spectral parameters contain a wealth of structural information. They comprise the much-studied ferricytochromes, metcyano-myoglobins, and hemoglobins, and the cyanide complexes of resting-state heme peroxidases and cytochrome P450. Also due to the low paramagnetism of these systems characterized by $S = 1/2$, they represent the material for the first applications of new NMR techniques to paramagnetic proteins.

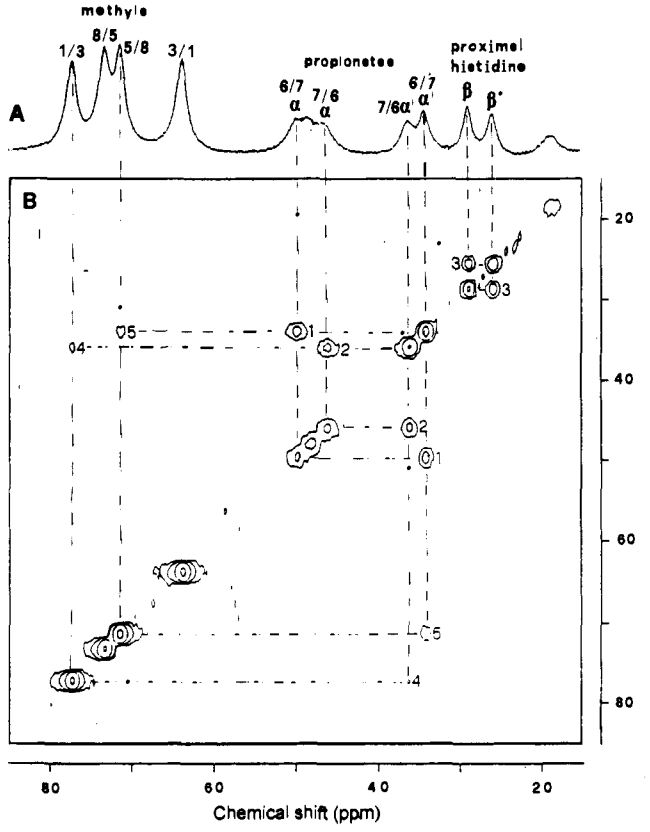

Figure 47. ^{1}H NMR reference spectrum (600 MHz) (A) and NOESY spectrum (B) of *C. vinosum* cytochrome *c'*, recorded at 300 K, pH 4.5. Cross peaks 1 and 2 individuate the two propionate α-CH_2 pairs and 5 and 4 the adjacent methyl groups. Cross peak 3 connects the proximal histidine β-CH_2 signals.

In octahedral symmetry the ground state is orbitally triply degenerate. Low-symmetry components particularly effective in heme-containing compounds split the three levels of about 500–1000 cm^{-1}. If such splitting is below $6kT$, it is believed that Orbach-type electron relaxation mechanisms are quite effective.[8] This accounts for the short electron relaxation time of these systems which can be as short as 10^{-13} s. Indeed, the nuclear T_1 values of protons of amino acid residues located around the paramagnetic center are of the order of 100–200 ms, whereas heme methyls have T_1s around 80 ms. For comparison purposes we may note that regular diamagnetic compounds have T_1s of the order of several hundred milliseconds. Low-spin heme-containing proteins have therefore been the first challenge for NMR spectroscopists toward NOE and 2D methods in paramagnetic systems.

The metal orbitals d_{xz} and d_{yz} (Figure 48) can mix with porphyrin e(π) orbitals.[7,308] The resulting molecular orbitals and the corresponding MO associated with d_{xy} are mixed through spin–orbit coupling. Thus the three Kramers' doublets no longer correspond to pure d orbitals. The highest energy Kramers' doublet, which is the one occupied by the unpaired electron of low-spin iron(III), is best represented as predominantly a mixture of the molecular orbitals containing d_{xz} and d_{yz}. Therefore no σ spin delocalization is predicted, since the unpaired electron resides in a π orbital. Moreover, a significant contribution to the hyperfine shift derives from the pseudocontact term. Different methods have been developed to estimate the pseudocontact shift contribution in low-spin heme proteins.[402–405] These will be reviewed in this section.

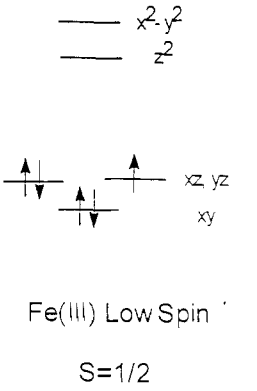

Figure 48. The electronic configuration of low-spin heme iron(III).

1. The Cyanide Adduct of Metmyoglobin

Among the various systems, the NMR characterization of the CN^- adduct of sperm whale metmyoglobin (MW 16 000) represents one of the best examples of a rigorous NMR investigation of paramagnetic metalloproteins. The ^{1}H NMR spectrum of metMb–CN^- is reported in Figure 49. Three methyl signals are observed in the region 18–13 ppm, assigned to 5-, 1-, and 8-CH_3 heme groups. Many one-proton signals are observed in the 23–9 ppm region, attributable to the α-type protons of the heme substituents and to the proximal histidine ligand protons. The resonances of some of the protons of other residues present in the active site could also be expected, due to the magnetic anisotropy of this low-spin system. In the upfield region signals are resolved in the −1 to −10 ppm range. NMR assignments for the hyperfine-shifted resonances in this system have relied primarily on comparisons with model compounds,[406–408] analysis of paramagnetic relaxation,[409,410] and by isotope labeling of heme protons.[411] In 1983–1985 some papers appeared which represented the first application of 1D NOE to a paramagnetic metalloprotein (Figure 50).[89,93,412,413] More recently, it has been demonstrated that 95% of the protons within 7.5 Å of the ferric iron of metMb–CN^- can be assigned on the basis of 2D NOESY[109] by using the X-ray crystal coordinates[414] to interpret the cross peaks. These assignments were then used to determine for the first time the orientation of the magnetic axes in solution (see later).[404] In this way two different means for the investigation of such systems have been demonstrated to be valid: NOE or NOESY and pseudocontact shifts.

From eq 4 it clearly appears that pseudocontact shifts depend on the magnetic susceptibility components χ_{xx}, χ_{yy}, and χ_{zz}. In the absence of the second-order Zeeman (soz) interaction the equation reduces to a function of the EPR **g** values:[15]

$$\left[\frac{\Delta\nu}{\nu_0}\right] = \frac{\mu_0}{4\pi}\frac{\mu_B^2 S(S+1)}{18kT}\left\{[2\mathbf{g}_{zz}^2 - (\mathbf{g}_{xx}^2 - \mathbf{g}_{yy}^2)]\frac{3\cos^2\theta - 1}{r^3} + 3(\mathbf{g}_{xx}^2 - \mathbf{g}_{yy}^2)\frac{\sin^2\theta\cos 2\varphi}{r^3}\right\} \quad (47)$$

where all the quantities are the same as defined in section II.

The measurements of **g** values are much more easily accomplished than those of χ values. However, it has

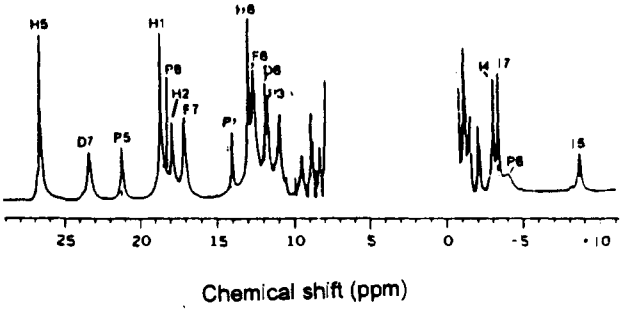

Figure 49. ^{1}H NMR spectrum (500 MHz) of metMb–CN$^-$ at 303 K in H_2O solution, pH 8.6. (Reprinted from ref 420. Copyright 1989 Elsevier.)

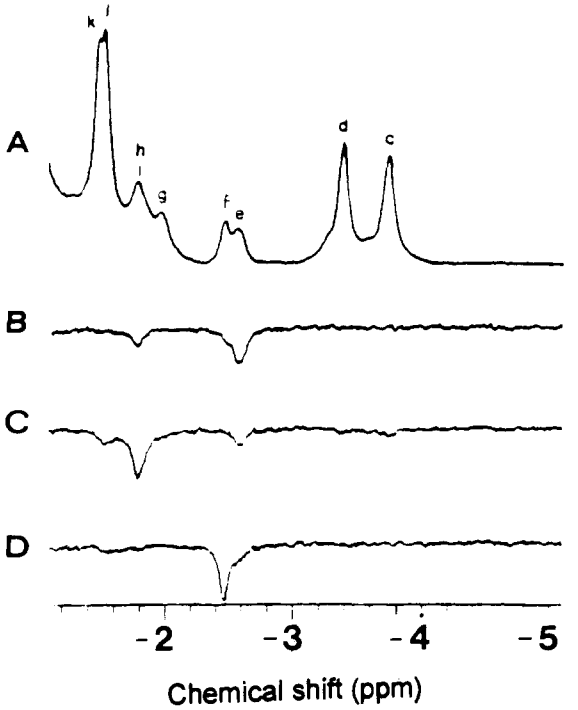

Figure 50. The 360-MHz upfield region of the ^{1}H NMR spectrum of metMb–CN$^-$ (A), and NOE difference spectra obtained by saturation of (B) 2-Hβ_{trans}, (C) 2-Hβ_{cis}, (D) peak f, showing an absence of NOE to other peaks. All the spectra were recorded at 298 K in D_2O solution, 0.2 M NaCl pH 10.4. (Reprinted from ref 412. Copyright 1984 American Chemical Society.)

been demonstrated that the use of **g** instead of χ yields results affected by a 10–30% error.[7] Horrocks and Greenberg[415] have proposed a theoretical approach to evaluate the main components of χ on the basis of the low-temperature **g** values. These values, together with the setting of approximate directions of the principal axes have been the starting point for the best fitting procedure using the dipolar shift equation.[404] The ^{1}H NMR input data are the experimental dipolar shifts of 41 signals of noncoordinated residues and the X-ray coordinates of the isostructural Mb–CO.[414] The resulting solution magnetic axes (Table VIII) differ from those proposed earlier on the basis of single-crystal EPR spectra.[416,417] Moreover, by using the pseudocontact shifts of the residues expected to be unperturbed by distal point mutations, the magnetic axes were determined for the cyanide derivative of both the His[E7]-Gly and the Arg[CD3]Gly mutants.[418] For the former mutant, the *z* magnetic axis tilt has been found to be minimally altered, but a projection of the tilt rotated of about 45° has been calculated. For the Arg[CD3]-Gly mutant a magnetic axes orientation almost indistinguishable from that found for the wild type metMb–CN$^-$ has been obtained. The proximal histidine has been taken as unchanged upon mutation. It has been found that an increase in the β angle or a more positive α angle value leads to a strong upfield bias for the proximal histidine Hδ2 and a strong lowfield bias for the Hϵ1. Therefore, the pattern of the hyperfine shifts of the proximal histidine ring protons does not only serve as a unique probe for the *z* axis tilt, as originally proposed.[404] However, it is a clear indication that the magnetic axes have been altered.[418,419]

Resonance assignments derived from the interpretation of NOEs on the basis of X-ray coordinate data have the severe limitation that the crystal structure must be available and it should be assumed to be identical to the solution structure. Analogous to the diamagnetic systems, the assignments of amino acid side chains should be independent of the crystal structure and, therefore, based on bond correlation spectroscopy (COSY or HOHAHA). For metMb–CN$^-$ preliminary COSY studies revealed cross peaks only between protons with large coupling constants (e.g. vinyl groups) and at a distance from the iron higher than 4 Å.[109,420] A subsequent paper[133] clearly demonstrates that the amino acid side chains in the heme cavity of metMb–CN$^-$ can be assigned by means of scalar correlations. For each of the residues in the heme cavity, whose protons experience significant hyperfine shifts ($\simeq$ −11 to 15 ppm) and paramagnetic relaxation ($T_1 \geq$ 20 ms and line widths $\leq$ 100 Hz), a complete identification of the spin system could be achieved by one or more bond correlation methods (double quantum filtered and magnitude COSY, HOHAHA). The only exception is the proximal His imidazole ring whose protons are as broad as $\simeq$600 Hz and whose T_1 values are about 4 ms: they can be identified only by 1D NOE experiments.[109] The assignments based on scalar correlations completely confirm the assignments previously proposed on the basis of dipolar correlations[412,413,421,422] and crystal structure analysis, except for the residue Leu F4. This inconsistency has been explained by assuming a difference between the solution and crystal orientation of the side chain.[133]

The various methods employed in the detection of the above scalar connectivities display highly variable information. Among the MCOSY, double quantum filtered COSY (DQF-COSY) and HOHAHA experiments the highest information content in terms of total number of detected cross peaks comes from the MCOSY spectrum. The major difference for the detectability of cross peaks between the MCOSY and DQF-COSY maps depends on the residue of interest. For weakly relaxed and moderately hyperfine-shifted signals, the DQF-COSY experiment is superior to MCOSY because the former can reveal cross peaks very close to the diagonal. In the case of MCOSY they are difficult to resolve because obscured by the phase-twisted line shapes of the strong diagonal. However, for the rapidly relaxed and strongly hyperfine-shifted signals MCOSY is superior to DQF-COSY. The use of the filter in the latter sequence causes the uncoupled resonances to be removed from the diagonal, but also the reduction of the intensity of the scalar connectivities between broad

Table VIII. g Tensor Parameters for Various Heme Proteins

protein	principal axes			anisotropy factors ($m^3 mol^{-1}$)		orientation		
	g_x	g_y	g_z	$\chi_\perp$	$\chi_\parallel$	α	β	γ
wild-type metMb–CN⁻								
EPR[416]	0.93	1.89	3.45			−57.5	−13	44.8
a[415]				2198	−573			
NMR[404,418]				2018	−453	10	14.5[b]	25
E7 Gly metMb–CN								
NMR[418]				2018	−409	−34	13.5	76
CD3 Gly metMb–CN⁻								
NMR[418]				[c]	[c]	11	16.0	25
	g_x[d]	g_y[d]	g_z[d]	g_{ax}[d]	g_{eq}[d]	α	β	γ
horse cyt c								
EPR[537]	1.25	2.25	3.06	6.05	−3.5	≃0	≃0	≃0
NMR[403,e]	2.25	2.59	3.32	5.15	−1.65	106	13	251
tuna cyt c								
NMR[402]	1.95	2.59	3.24	5.24	−2.91	129	11	229
NMR[403]				5.09	−2.32	99	14	246
yeast iso-1-cyt c								
NMR[480]				4.58	−2.31	[f]	9	[f]

[a] The evaluation of the magnetic susceptibilities is based on the g values and on the directions of the magnetic axes of ref 416. [b] Whereas on the basis of EPR data a z axis tilted toward the 2-vinyl position was proposed, in this case a tilt in the direction of the δ-meso position was found. [c] The $\chi_\perp$ and $\chi_\parallel$ values obtained for the wild type are used. [d] The g_i values resulting from the best fitting calculations based on NMR data would be better indicated as g_i^{eff}, as defined in the text. [e] The individual g values are estimated from the rotation-averaged magnetic susceptibility in solution and the g_{ax} and g_{eq} parameters obtained from the fitting. [f] Only the sum of α and γ is reported: $\alpha + \gamma = 366°$ indicates that g_x and g_y remain alligned along the diagonal nitrogens of the heme.

J coupled resonances. The disadvantage of HOHAHA relative to COSY variants for detecting cross peaks of strongly relaxed protons is that relaxation competes effectively with the development of coherence in the mixing time, thereby suppressing the development of significant coherence prior to detection.[133]

Yamamoto et al. demonstrated that the hyperfine-shifted heme methyl ^{13}C resonances of the ferric low-spin heme protiens are resolved upfield of the ^{13}C diamagnetic envelope[423,424] and that the ^1H–^{13}C COSY gives scalar connectivities between the heme methyl ^{13}C and the attached ^1H resonances, thus permitting the assignment of the latter even if resonating under the diamagnetic envelope. The ^1H and ^{13}C shift values for the methyl groups of the cyanide adduct of *Galeorhinus japonicus*, sperm whale, and *Aplysia limacina* metmyoglobins, horse heart cytochrome c and HRP have been compared. The differences have been explained in terms of the angle between the projection of the proximal His imidazole plane onto the heme plane and the N–Fe–N vector.[424] Combined analysis of the resonances of the heme methyl carbons and of the attached protons allows the determination of the principal magnetic axes in hemin complexes possessing magnetic anisotropy. This method, developed by Yamamoto et al., is called MATDUHM (magnetic anisotropy tensor determination utilizing heme methyls).[405,425-427] It depends neither on the availability of the crystal structure nor on the magnetic properties of the studied heme protein. According to McConnell's equation,[28,428] the contact shift (δ_c) values for the heme methyl carbons and the attached protons are directly proportional to the unpaired electron density in the p_z orbital of the pyrrole carbon to which the methyl group is bonded. To a first approximation, also the ligand-centered pseudocontact contribution to the hyperfine shift δ_{pc}^L is dependent on this unpaired electron density. Therefore, plots of the quantity $(\delta_c + \delta_{pc}^L)$ for the heme methyl carbon resonances versus the same quantity for the attached proton resonances should be linear and pass through the origin. The authors attribute deviations from a straight line to differences in metal-centered pseudocontact contribution (δ_{pc}^M) between the methyl carbon and protons. A best-fit procedure is applied to minimize the deviations of the above plot from linearity, optimizing the α, β, and γ angles and the $\chi_\parallel$ and $\chi_\perp$ values (Table VIII). Some hyperfine-shifted amino acid proton resonances in *Galeorhinus japonicus* Mb–CN⁻ have been assigned by the combined use of various 2D NMR techniques: NOESY, COSY, and relayed COSY.[405] The relayed COSY sequence has been designed to prove the connectivity between two remote nuclei A and X.[429,430] The method employs many consecutive steps where transverse magnetization is relayed from nucleus to nucleus along a path defined by a sequence of resolved couplings. The second pulse of the COSY experiment is replaced by a $90°$–τ–$180°$–τ–$90°$ sequence which may induce two consecutive coherence transfer processes. It can be shown for the AMX system with $J_{AX} = 0$ Hz that the transfer efficiency from A to X is proportional to the product $\sin(2\pi J_{AM}\tau)\cdot\sin(2\pi J_{AM}\tau)$. For *G. japonicus* Mb–CN⁻ this sequence has been successfully applied to detect connectivities of some amino acid side chains.[405] The assigned resonances were compared with the corresponding resonances in sperm whale Mb. The orientation of ThrE10 and IleFG5 residues relative to the heme in *G. japonicus* Mb–CN⁻ were semiquantitatively estimated from the analysis of their shifts using the magnetic susceptibility tensor axes determined by MATDUHM.[405] The results were compared with the crystal structure of sperm whale Mb–CO. In spite of substantial differences in the shift values between the corresponding amino acid proton resonances for the two proteins,[413] the spatial location and orientation of these amino acid residues relative to the heme of both Mbs were found to be substantially the same.[405]

A 3D ^1H NOE-NOE spectrum of metMb–CN⁻ has been obtained, which represents the first 3D experiment on a paramagnetic protein.[431]

The importance of the amino acid residues which are in van der Waals contact with the porphyrin ring was first pointed out in 1970,[432] by comparing the ^{1}H NMR spectra of different mammalian Mb–CN$^-$. The reconstitution of sperm whale and horse Mb with a series of synthetic hemins allowed the acquisition of useful information on the heme peripheral contacts. The results indicate highly hydrophobic contacts in the interior of the heme pocket. It appears that the vinyl contacts are much more important than those of propionates in determining the orientational preference in the heme pocket.[433,434]

2. Other Low-Spin Adducts of Metmyoglobin

The ^{1}H NMR spectra of the azide complex for horse, sperm whale and *G. japonicus* metMb have been reported.[348,435,436] The four heme methyl resonances are resolved in the downfield region of the spectrum in the 35–12 ppm range (Figure 51A). The resonances do not follow the Curie behavior with temperature. This has been interpreted as due to a thermal spin equilibrium between high and low spin states, fast on the chemical shift scale. The larger average (27.1 versus 24.0 ppm) and smaller spread (15.3 versus 18.7 ppm) of the heme methyl hyperfine shifts in *G. japonicus* with respect to sperm whale are consistent with a larger high-spin fraction for the former Mb. It is interesting to note that the T_1 values measured for the α-CH protons of the propionate substituents in *G. japonicus* metMb–N_3^- are of the order of 10 ms, i.e. quite close to the values obtained for the high spin complex. NOE connectivities in *G. japonicus* metMb–N_3^- (Figure 51, parts B-G) provided the assignment of the heme propionate resonances.[436] From a time-dependent NOE buildup experiment, the correlation times for the 6- and 7-propionate side chains have been estimated. These values indicate that the immobile 7-propionate group of native metMb[437] becomes mobile upon N_3^- binding.[436] With the same method, significant vinyl mobility relative to the heme has been also found in sperm whale metMb–CN$^-$.[412] The ^{1}H NMR spectrum of the metMb complex with the bulky trimethylphosphine ligand is typical for a low-spin species, with resonances in the 40–10 ppm range.[438] The most characteristic feature of this spectrum is that the methyl signal shift pattern is 5 > 8 > 1 > 3, whereas in metMb–CN$^-$, metMb–N_3^-, and metMb–imidazole the order is 5 > 1 > 8 > 3. The temperature dependence of the Mb adducts with trimethylphosphine, azide, and imidazole does not follow the Curie law. It could be consistent with a small contribution of high spin state ($S = {}^5/_2$) with increasing temperature. Some heme substituent proton resonances of metMb–N_3^-, and metMb–imidazole for *Dolabella auricularia* and *Mustelus japonicus* myoglobins have been assigned by 1D and 2D saturation transfer experiments, in the presence of the corresponding metMb forms. From the analysis of the saturation transfer extent information on the kinetics of ligand exchange have been obtained.[439] Upon pressurization the heme methyl signals of metMb–N_3^-, metMb–imidazole, and metHb–N_3^- experience an upfield shift proportional to the applied pressure.[355] It has been proposed that this shift may be due to the compression effect on the axial ligand–iron bond. This would influence the high-low-spin equilibrium in favor of the latter form. The spin state of metMb–CN$^-$, which is in the purely low-spin state, does not change at high pressure.[440] Spectral changes are observed only for specific groups. They have been related to pressure-induced structural changes in the heme crevice localized in the distal side and to possible variations in the van der Waals contacts at the heme periphery with nearby amino acid residues.

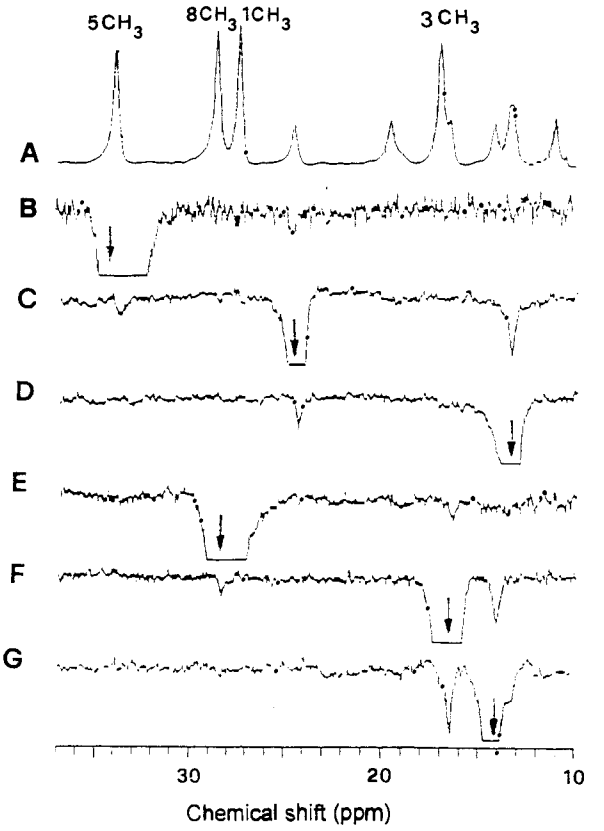

Figure 51. The 500-MHz downfield hyperfine-shifted region of the ^{1}H NMR spectrum of *G. japonicus* metMb–N_3^- (A), and NOE difference spectra obtained by saturation of (B) 5-CH_3, (C) 6-Hα, (D) 6-Hα', (E) 8-CH_3, (F) 7-Hα, and (G) 7-Hα'. All the spectra were recorded at 308 K. (Reprinted from ref 436. Copyright 1991 Springer-Verlag.)

3. Anions Adducts of Peroxidases Containing the Noncovalently Bound Heme

CcP readily binds small anionic ligands, with the resulting complexes yielding magnetic and spectroscopic data characteristic of a range of intermediate to low-spin states. The first proton hyperfine assignments for CcP–CN$^-$ (Figure 52B) have been obtained by using deuterium-enriched hemins.[84] The two large peaks that lie farthest downfield each have relative intensities of three protons. These originate from methyls in positions 3 and 8. Between 10 and 20 ppm lie six resonances with relative intensities each corresponding to one proton. Upfield, between 0 and −6 ppm there are several resonances whose relative intensities correspond to one or two protons. Among these single-proton signals only the 4-Hα, 4-Hβs, and one propionate proton have been identified through deuteration. A broad resonance is present at about −21 ppm. At variance with low-spin adducts of metMb but in analogy with all the other up to now assigned of peroxidases, 3- and 8-CH_3 are the two methyl groups which experience the large hyperfine shift. In metMb, pyrroles I and III exhibit larger

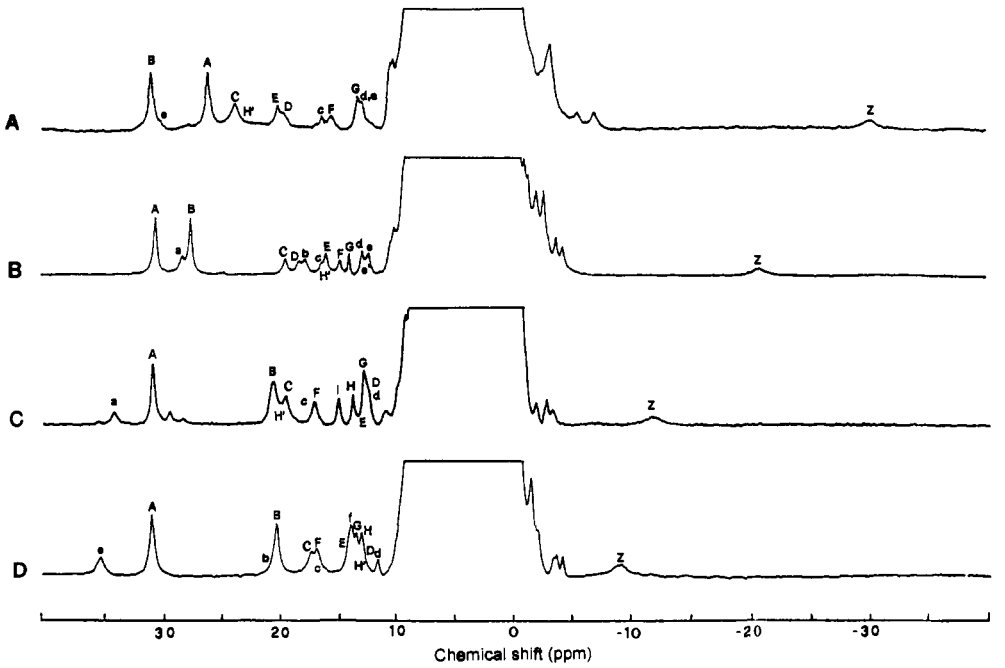

Figure 52. ^{1}H NMR spectra (200 MHz) of the cyanide adducts of (A) HRP, phosphate buffer pH 6.3, (B) CcP, phosphate buffer pH 6.3, (C) MnP, phosphate buffer pH 6.5, and (D) LiP, acetate buffer pH 5. All the spectra were recorded at 301 K. (Reprinted from ref 336. Copyright 1992 American Chemical Society.)

delocalization of unpaired spin density than pyrroles II and IV. The order is precisely reversed in peroxidases. This has been explained by the fact that there is a different orientation of the proximal ligand in the two classes of compounds (Figure 53). The 180° rotational isomerism about the α–γ axis observed in the CcP crystal structure, compared to metMb, accounts for the pairwise interchange of spin delocalization between *trans*-pyrroles. A more extensive assignment of the nonexchangeable protons of the heme substituents and of the proximal histidine for CcP–CN$^-$ has been performed through NOE measurements.[441] In the first spectrum reported in H_2O solution only four hyperfine-shifted exchangeable signals were observed, and tentative assignments for some of these were proposed.[331] More recently extensive characterization of H_2O solution of yeast CcP and recombinant proteins (MI and MKT-IGCcP) expressed in *E. coli* has been reported.[442,443] The recombinant proteins indicated by MI[442] and MKT-IGCcP[443] differ in the sequence from the wild-type CcP in that Thr 53 and Asp 152 are substituted by Ile and Gly residues, respectively. More exchangeable resonances with respect to the 1983 paper are observed. The assignments represent one of the first examples of the application of 2D NMR techniques to medium-sized paramagnetic proteins. The paramagnetically shifted exchangeable proton signals have been assigned through NOE and NOESY experiments. NOESY[442,443] (Figure 54B) and COSY[326,443] (Figure 54D) experiments in D_2O and H_2O buffered solutions have allowed the extension of the assignments to heme substituents and other residues. They are summarized in Table IX. Discrepancies exist between these assignments and those reported by Satterlee, concerning the origin of some resonances assigned to distal side residues. By comparing CcP–CN$^-$ and HRP–CN$^-$ it appears that the two systems are highly analogous. However, a more extensive exchangeable proton connectivity network is observed in CcP–CN$^-$, and small

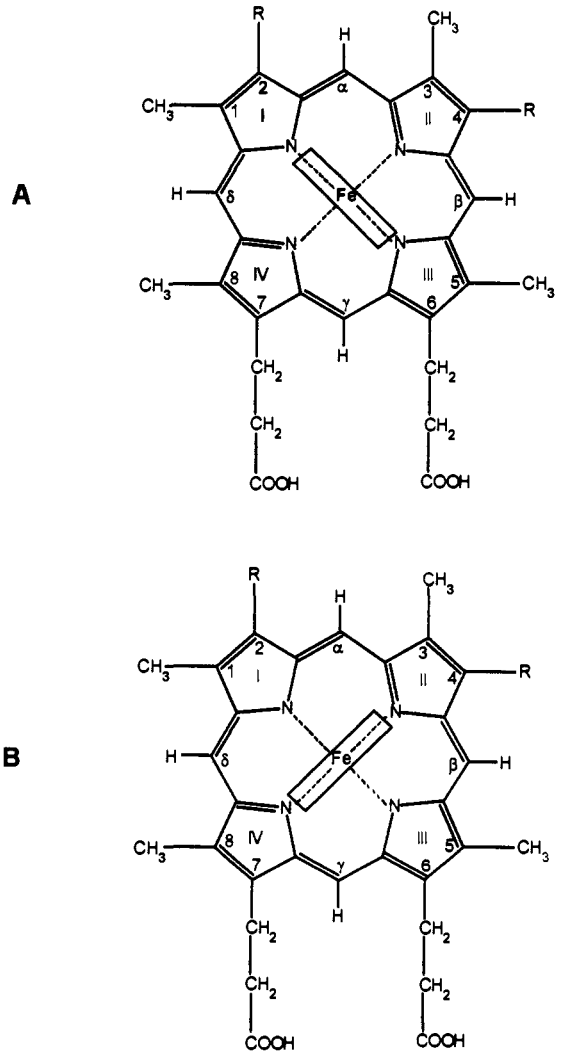

Figure 53. Relative orientations of the proximal histidine plane and heme moiety in peroxidases (A) and in globins (B).

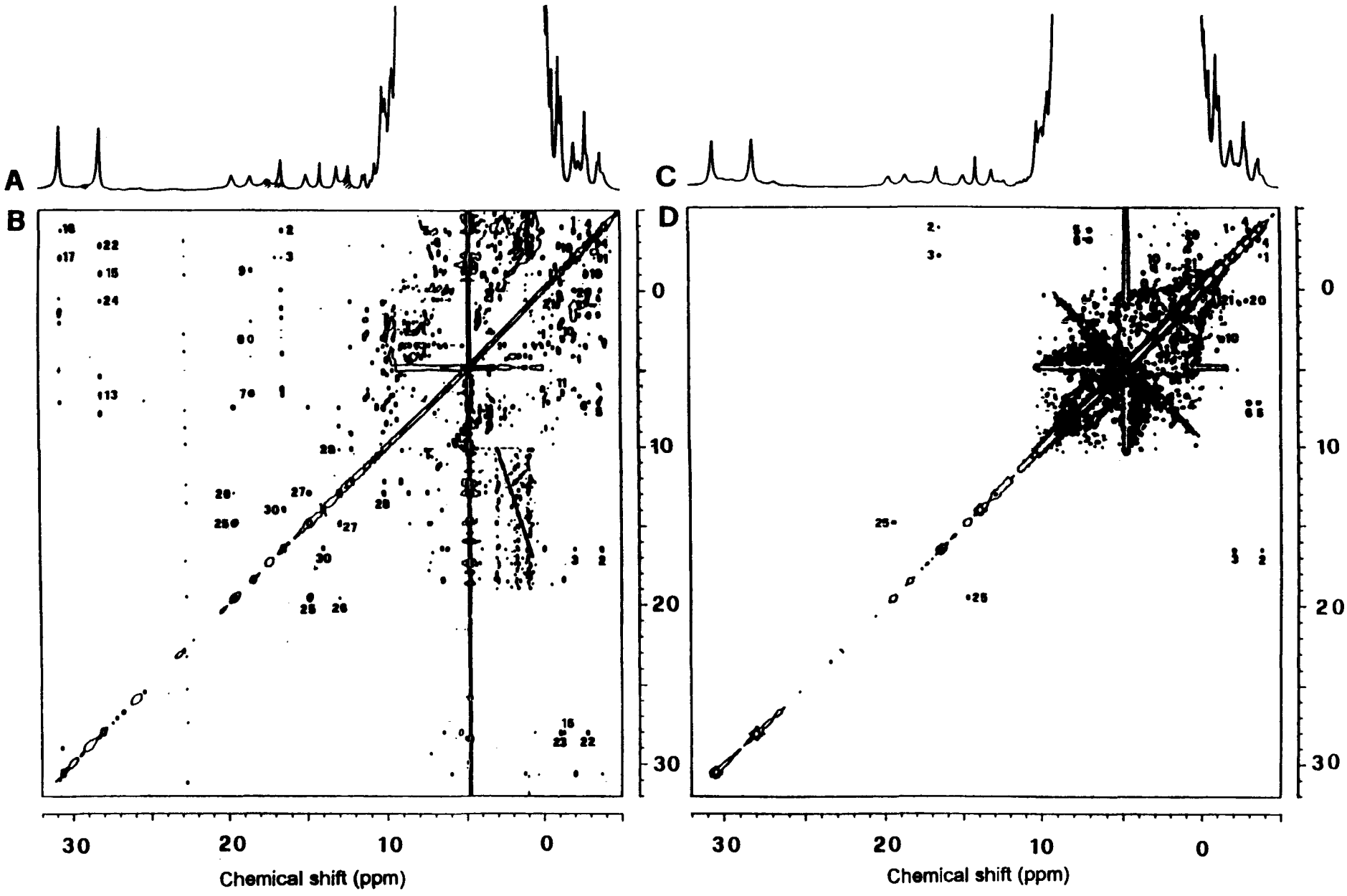

Figure 54. ^{1}H NMR spectra (600 MHz) of recombinant MKT-IGCcP-CN$^-$: (A) reference spectrum and (B) NOESY spectrum in H_2O solution; (C) reference spectrum and (D) magnitude COSY spectrum in D_2O solution. Shaded resonances in 1D spectra represent exchangeable proton signals. All the spectra were recorded at 298 K in 0.1 M phosphate buffer, pH 6.9. Corresponding cross peaks are labeled with the same numbers in both the 2D maps. Cross-peaks assignments are as follows: (1) 4-Hβ_{cis}, 4-Hβ_{trans}; (2) 4-Hα; 4-Hβ_{cis}; (3) 4-Hα; 4-Hβ_{trans}; (4) 2-Hβ_{cis}, 2-Hβ_{trans}; (5) 2-Hα; 2-Hβ_{cis}; (6) 2-Hα; 2-Hβ_{trans}; (7) 7-Hα, 7-Hα'; (8) 7-Hα; 7-Hβ'; (9) 7-Hα, 7-Hβ; (10) 7-Hβ, 7-Hβ'; (11) 7-Hα', 7-Hβ; (12) 8-CH_3, 7-Hα; (13) 8-CH_3, 7-Hα'; (14) 8-CH_3, 7-Hβ'; (15) 8-CH_3, 7-Hβ; (16) 3-CH_3, 4-Hα; (17) 3-CH_3, 4-Hβ_{trans}; (18) 3-CH_3, 4-Hβ_{cis}; (19) δ'-CH_3 Leu-232; δ-CH_3 Leu-232; (20) Hγ Leu-232; δ-CH_3 Leu-232; (21) Hγ Leu-232, δ'-CH_3 Leu-232; (22) 8-CH_3, δ-CH_3 Leu 232; (23) 8-CH_3, δ'-CH_3 Leu 232; (24) 8-CH_3, Hγ Leu 232; (25) Hβ His-175, Hβ' His-175; (26) Hβ His-175, NH_ϵ His-175; (27) Hβ' His-175; NH_ϵ His 175; (28) Hβ' His-175, Hδ1 His-175; (29) Hβ His-175, Hδ1 His-175. (Reprinted from ref 443. Copyright 1991 American Chemical Society.)

Table IX. Chemical Shift Values for Paramagnetically Shifted Resonances for the Cyanide Derivatives of MnP (298 K), LiP (301 K), CcP (301 K), and HRP (301 K)[a]

	shift (ppm)				
assignment	MnP-CN⁻ [b]	LiP-CN⁻ [c]	Ccp-CN⁻ [d]	HRP-CN⁻ [e]	signal
heme					
2-Hα	8.6	8.5	7.1	5.3	J
2-Hβ_{cis}	-3.4	-3.6	-3.7	-1.6	X
2-Hβ_{trans}	-3.2	-4.1	-3.0	-2.7	Y
α-meso	-1.1	1.1		1.9	α
3-CH_3	30.7	31.0	30.6	26.0	A
4-Hα	12.7	14.2	16.0	20.1	E
4-Hβ_{cis}	-2.8	-3.2	-3.8	-3.3	W
4-Hβ_{trans}	-1.8	-2.0	-2.1	-2.2	V
7-Hα	12.5	13.0	18.3	19.6	D
7-Hα'	8.0	9.2	6.4	9.7	I
8-CH_3	20.4	20.4	27.6	31.0	B
δ-meso	7.0	7.6		6.3	δ
proximal His					
NH_p	12.4	11.6	12.9	12.9	d
Hβ	19.5	17.4	19.4	23.7	C
Hβ'	16.9	17.0	14.8	15.6	F
Hδ1	15.1	14.0	10.2	9.9	f
Hϵ1	-11.8	-9.0	-20.6	-29.9	Z
Hδ2	20.3	13.3	15.8	23.1	H'
distal His					
Hδ1	17.0	17.0	16.5	16.3	c
Hϵ1	12.8	13.6	14.0	13.3	G
Hδ2	13.9	13.1		9.8	H
Hϵ2	34.2	35.2	28.4	31.0	a

[a] Lower case letter labeling corresponds to exchangeable protons. [b] Taken from refs 336 and 447. [c] Taken from refs 335 and 447. [d] Taken from ref 443. [e] Taken from refs 96, 363, 444, and 445.

but significant structural differences have been identified in the orientation of the proximal histidine residue of HRP–CN⁻ and CcP–CN⁻ and in the interresidue distances in the distal heme pocket of CcP–CN⁻ and MKT–IGCcP–CN⁻ as a function of the residue present at position 53.[443]

The CcP mutant D235N (Figure 55) has been studied by ^{1}H NMR spectroscopy.[338] Mutations in this position are important because the hydrogen bond between Asp235 and the proximal histidine ligand plays a crucial role for the enzymatic activity of peroxidases. The spectrum shows hyperfine shifts typical for a low-spin iron(III) system. At variance with the corresponding noninhibited species, the hyperfine shifted resonances follow the normal Curie dependence with temperature. As in the case of WT and expressed CcP and in all the other reported peroxidases, in the spectrum of the cyanide derivative only two heme methyl resonances are involved outside the diamagnetic envelope. It is interesting to note that in both D235N[338] and D235A mutants[339] the Hϵ1 signal of the proximal histidine appears at about -16 and -10 ppm, respectively.

Both WT CcP and D235N bind N_3^- with hyperfine shifts typical of low-spin species (Figure 56). For CcP-N_3^- the four methyl signals, the 2-Hα, 4-Hα and 2-Hβs protons have been assigned. The order of the methyl shifts is 3 > 8 > 5 > 1.[84,338]

Analogously to the high-spin case, an extensive NMR characterization has been performed on the CN⁻ adduct of HRP (Figure 52A). Isotope labeling, ^{1}H NMR saturation transfer between resting-state HRP and HRP–CN⁻ (Figure 57)[96] and NOE measurements[96,363,444] have been utilized for a comprehensive assignment. The three methods permitted the identification of all the 22 heme substituent resonances, including 12 resonances which are not resolved outside the intense diamagnetic envelope. Dipolar connectivities in conjunction with the available sequence homology with CcP and computer modeling of the heme pocket of HRP have led to the location and assignment of the resonances of important amino acid side chains. The application of NOESY (Figure 58A) and MCOSY (Figure 58B) techniques to HRP–CN⁻ has confirmed the assignment of all the heme resonances, of that of the proximal and distal histidines and of the distal Arg residue, Arg 38.[445] Further structural data have been obtained very recently.[446] The quantitative analysis of cross-peak intensity in NOESY spectra recorded at different mixing times has been used to obtain interproton distances. The active-site picture which sorts out from the above results is consistent with a heme moiety bearing immobile propionate side chains and 2- and 4-vinyl groups in trans and cis orientations, respectively, with a proximal histidine plane oriented along the pyrrole I and III nitrogen atoms direction, and with a distal Arg residue in almost the same positions predicted on the basis of the CcP crystal data. In Table IX analogous assignments obtained for the resonances of the heme substituents and active-site residues of LiP–CN⁻ [334,335,447] (Figure 59) and MnP–CN⁻ [336,447] (Figure 60) are reported. These results clearly demonstrate not only that the heme assignments can be inferred solely from 2D NMR data for low-spin complexes of peroxidases, but also show that it is possible to identify key catalytic residues in the heme pocket of medium/large-sized proteins. The NOESY and COSY connectivity patterns involving the 3-CH_3 and the 2- and 4-vinyl protons in the various peroxidases have allowed the determination of the vinyl orientations in the various systems. For HRP and LiP the vinyl arrangement is as reported in Figure 61A, for CcP is as in Figure 61B, whereas for MnP a fast interconversion

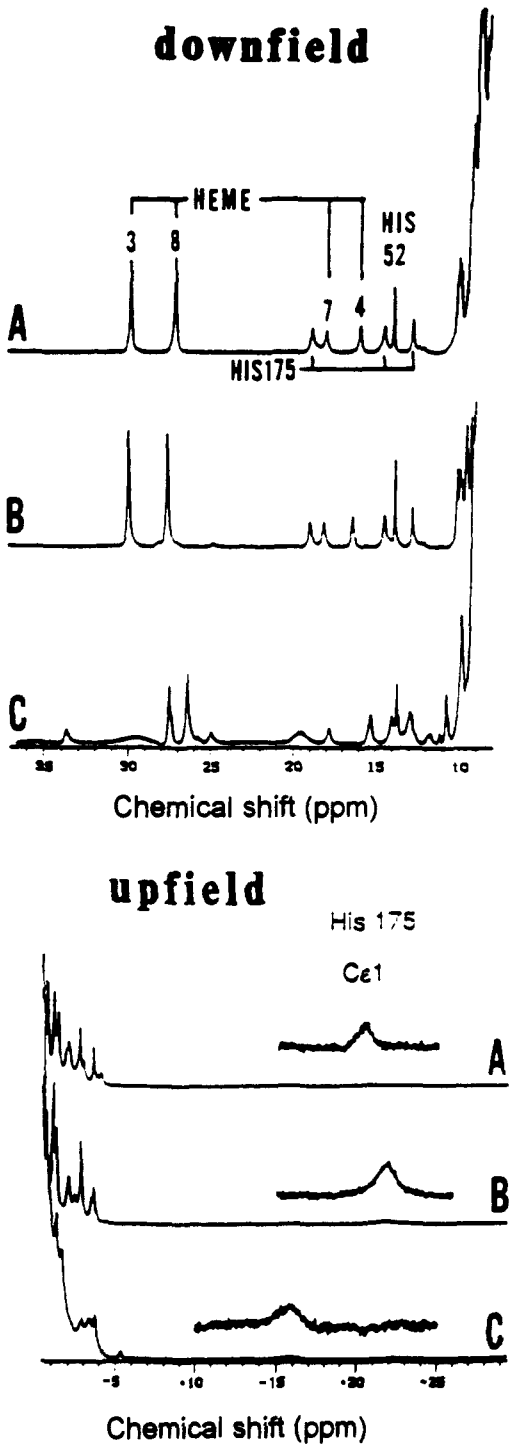

Figure 55. ^{1}H NMR spectra (361 MHz) of the cyanide adducts of (A) wild-type yeast CcP, (B) recombinant MI-CcP, and (C) D235N MI-CcP. All the spectra were recorded at 294 K in D_2O solution, 0.15 M potassium nitrate, and 0.05 M potassium phosphate. (Reprinted from ref 338. Copyright 1990 American Chemical Society.)

between the A and B conformation has been proposed.[336] From the comparison of the data reported in Table IX it appears that, besides minor shift differences for the resonances of the heme substituents, there are consistent variations in the hyperfine shift values for the proximal histidine ligand protons. In particular, the Hε1 signal varies dramatically from the −30 ppm for HRP to about −10 ppm for LiP and MnP. The shift value of the Hδ1 signal increases slightly from 9 to 15 ppm and that of the Hδ2 signal decreases from 23 to

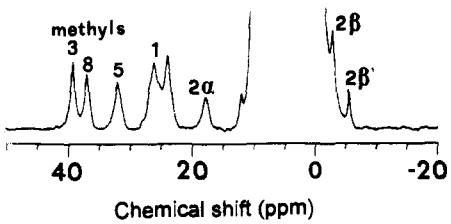

Figure 56. ^{1}H NMR spectrum of yeast CcP-N_3^- recorded at 297 K in 0.1 KNO_3, pH 7.4. (Reprinted from ref 84. Copyright 1983 American Chemical Society.)

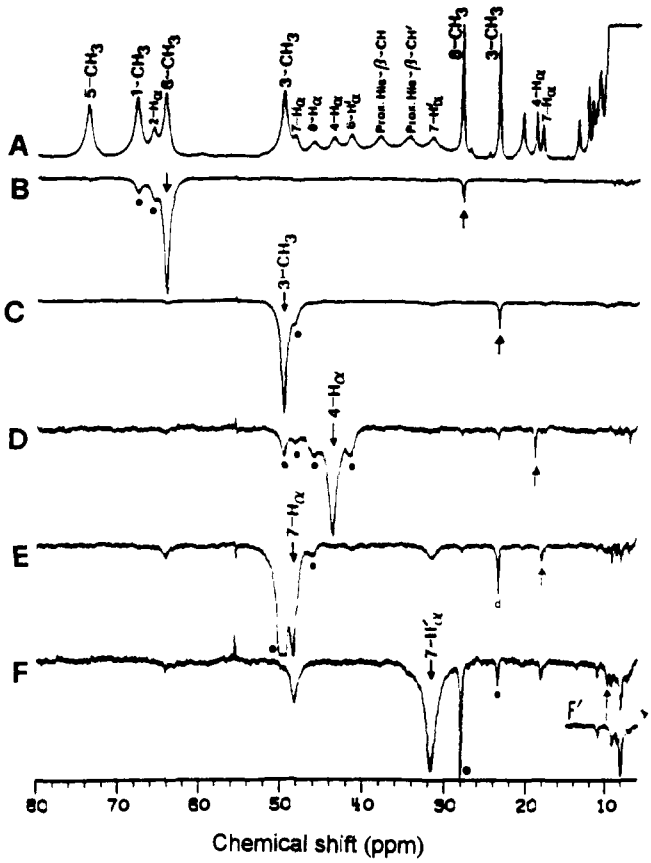

Figure 57. ^{1}H NMR spectra (360 MHz) of a mixture of HRP/HRP-CN$^-$ in the ratio 65:35 in D_2O solution (A), and (B–F) saturation-transfer difference spectra. The downward arrows indicate the saturated peaks and the upward arrows indicate saturation transfer. Difference peaks due to off-resonance saturation are marked with filled circles. All the spectra were recorded at 328 K in D_2O solution, pH 7.0. (Reprinted from ref 96. Copyright 1987 American Chemical Society.)

13 in the series HRP, CcP, LiP and then increases again to 20 ppm in MnP (see Figure 62). These shifts have been empirically correlated with the redox potential of the Fe^{3+}/Fe^{2+} couple (Figure 63), higher upfield shift values for Hε1 and higher downfield values for Hδ2 being associated with lower redox potentials. The shifts of the Hδ1, Hδ2, and Hε1 protons in metMb-CN$^-$ are 20, −5, and 10 ppm, respectively. In this case the proximal histidine has a much weaker hydrogen bond with a backbone carbonyl from Leu 89 and the Fe^{3+}/Fe^{2+} couple has a positive redox potential. Since it is generally accepted that the strength of the hydrogen bond involving the proximal His contributes to the iron ion potential, differences in the shift values for the protons of this residue may reflect different extent histidinato character in the proximal ligand. Magnetic

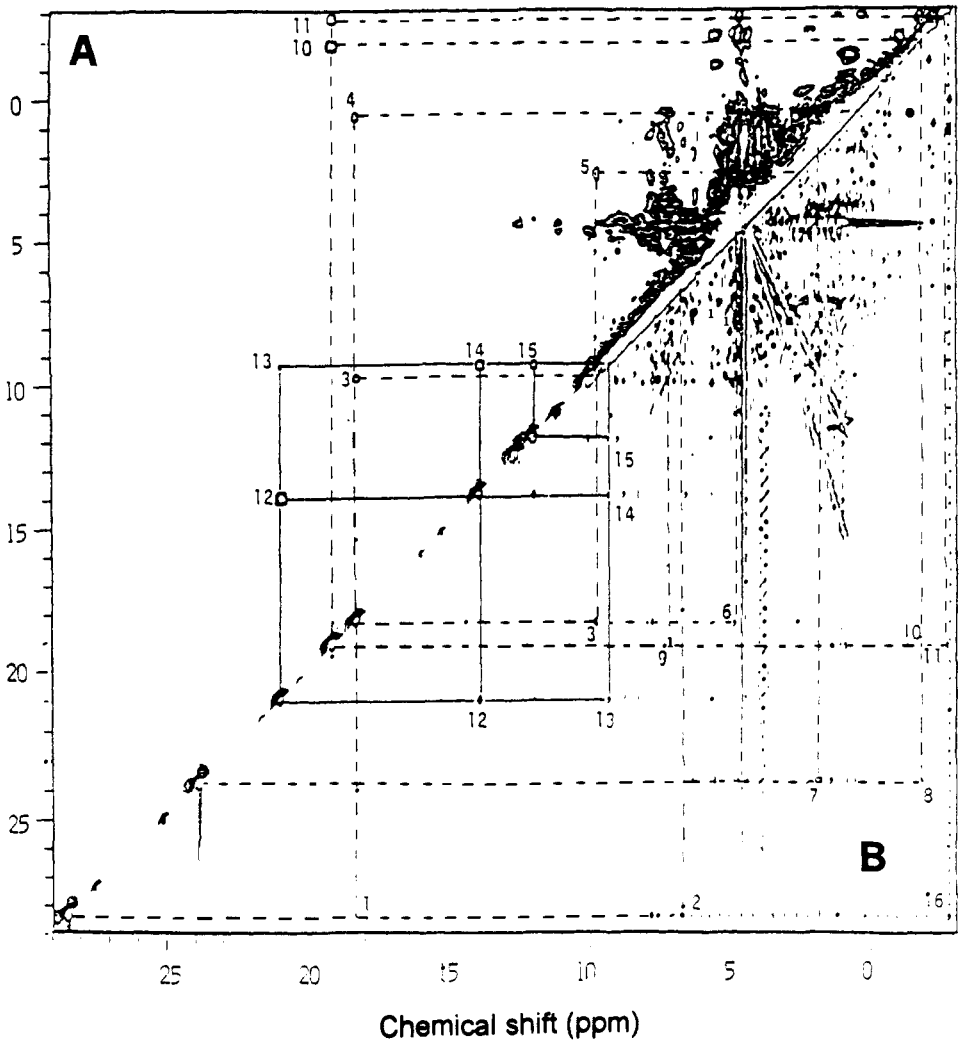

Figure 58. ^{1}H NMR magnitude COSY (A) and NOESY (B) spectra (500 MHz) of HRP-CN^- recorded at 323 K in D_2O solution, pH 7.0. The corresponding cross peaks in both the 2D maps are indicated with the same number. (Reprinted from ref 445. Copyright 1991 ESCOM.)

tensor susceptibility calculations analogous to those reported for metMb-CN^- [404] are hindered by the difficulties in extending the number of assigned protons experiencing only the pseudocontact contribution in these high molecular weight systems. However, a comparative analysis of the shift values for the ^{1}H NMR resonances of the active-site residues and for the ^{15}N NMR signal of the bound cyanide in the series HRP, CcP, LiP, MnP and D235N and D235A mutants of CcP indicates that the differences in the shift of Hϵ1 and Hδ2 of proximal His mainly reflects the different imidazolate character of this ligand.[339,447]

Wild-type recombinant HRP (isoenzyme C) and two proteins variants F41V and R38K have been characterized by ^{1}H NMR (Figure 64).[365,366,446] The recombinant proteins are expressed in non-glycosilated form and, therefore, have lower molecular weights. Whereas the spectra of the cyanide adducts of WT and recombinant HRP are essentially identical, significant differences are observed for the two mutants. Some of the hyperfine-shifted resonances have been assigned through NOESY experiments.[366] The spectra contain the same characteristic set of heme and heme-linked resonances, but many of them experience significant shifts with respect to the WT case. These shift variations are too large to be accounted for by local perturbation arising from a single substitution. In particular, the shift differences observed for the β-CH_2 protons of the proximal histidine have been proposed to originate from the degree of imidazolate character of this residue arising from substitutions made on the distal side. The proximal histidine ring protons have not been detected. Their assignment would help in confirming the above proposal.

The binding of N_3^- by HRP occurs only below pH 6.5, the bound and free enzyme forms being in rapid chemical exchange on the NMR time scale.[348] Raising the temperature causes a dissociation of the ligand from the iron-bound site of the enzyme. Also LiP is reported to bind N_3^-.[335] The spectrum of the adduct is similar to that of HRP-N_3^-.

The ^{1}H NMR spectra of the cyanide adduct of *Coprinus cinereus* and *Coprinus macrorhizus* peroxidases have been reported (Figure 65).[332] Analogously to the peroxidases, signals are observed in the 33 to −23-ppm region. Specific assignments for some heme protons have been obtained by NOE.[332,337] These NMR data show strong similarities between these fungal peroxidases and HRP. Titration of native *Coprinus cinereus* peroxidase with N_3^- shows that azide is in slow exchange on the NMR time scale.[332] The formation of the complex is highly pH dependent: at pH values higher than 7.0 peaks due to the native protein are observed in the spectrum. The spectrum of the final

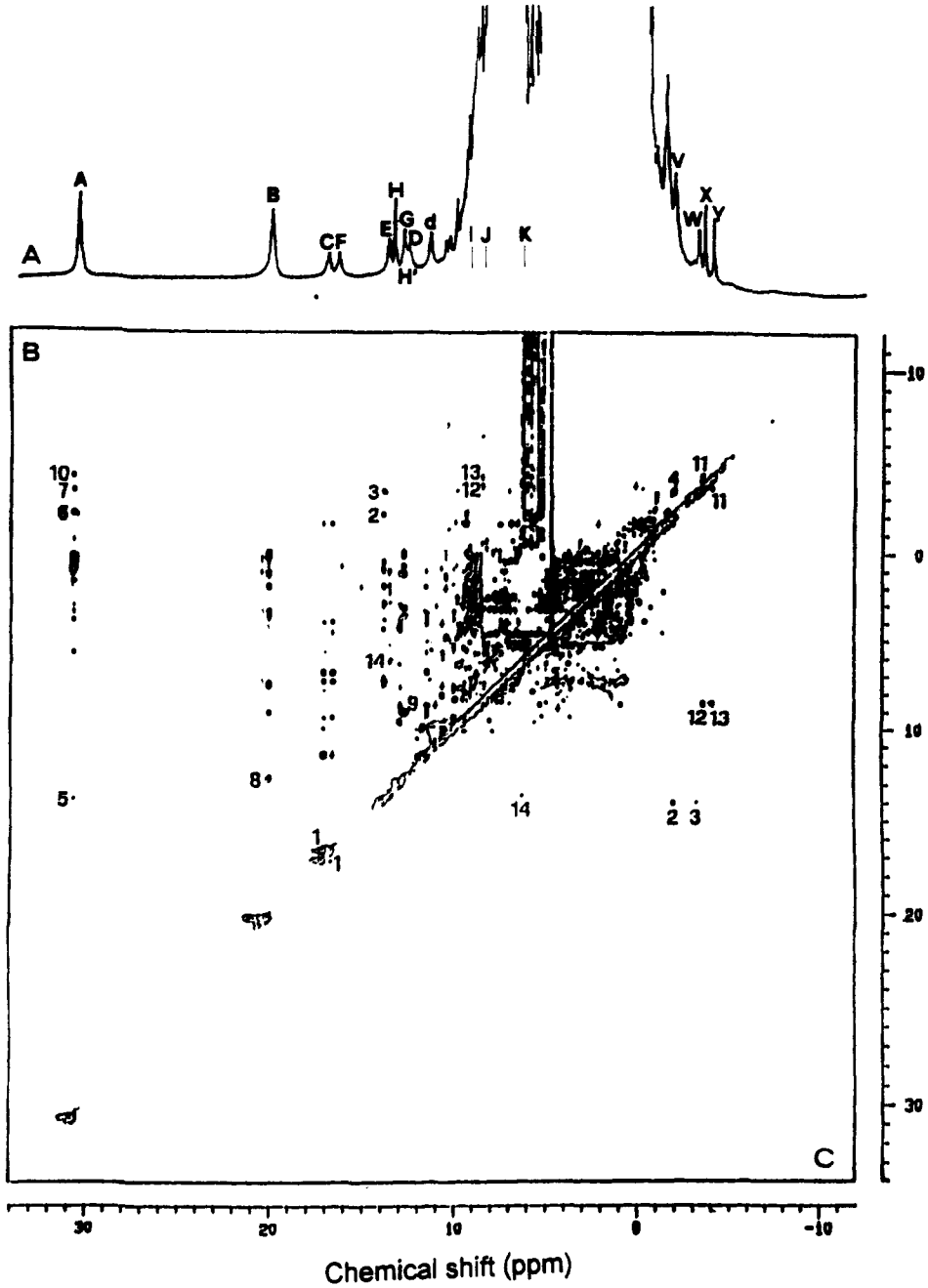

Figure 59. ^{1}H NMR spectrum (600 MHz) of LiP–CN$^-$ (A), and NOESY (B) and magnitude COSY (C) maps. All the spectra were recorded at 301 K in D_2O solution, 10 mM sodium acetate buffer pH 5. Cross-peaks assignment are as follows: (1) Hβ, Hβ' proximal histidine; (2) 4-Hα, 4-Hβ_{trans}; (3) 4-Hα, 4-Hβ_{cis}; (4) 4-Hβ_{cis}, 4-Hβ_{trans}; (5) 4-Hα, 3-CH_3; (6) 4-Hβ_{trans}, 3-CH_3; (7) 4-Hβ_{cis}, 3-CH_3; (8) 8-CH_3, 7-Hα; (9) 7-Hα, 7-Hα'; (10) 3-CH_3, 2-Hβ_{trans}; (11) 2-Hβ_{cis}, 2-Hβ_{trans}; (12) 2-Hα, 2-Hβ_{cis}; (13) 2-Hα, 2-Hβ_{trans}.

adduct obtained at pH 6.6 shows signals in the 50–20 ppm region. The temperature dependence does not follow a Curie behavior, perhaps due to a spin equilibrium between the $S = {}^1/_2$ and $S = {}^5/_2$ states.

The ^{1}H NMR spectra of the cyanide adducts of turnip peroxidase isoenzymes (P_1, P_2, P_3, and P_7) have been reported (Figure 66).[449] They closely resemble those of the other peroxidases. The spectra of the cyanide adducts of the two cucumber peroxidase isoenzymes are also typical for low-spin peroxidases (Figure 67).[333] The limited availability of protein precludes the performance of an absolute assignment of the resonances. However, spectra acquired with faster repetition rates allow the location of two broad resonances attributable to the proximal histidine Hδ2 and Hϵ1 protons. The downfield broad resonance is observed at about 23 ppm for both isoenzymes, whereas that in the upfield region is found at −30 and −27 ppm for the acidic and the basic cucumber peroxidase, respectively. Hyperfine-shifted resonances attributable to low-spin iron heme species have been reported for *Pseudomonas stutzeri* (ATCC 11607)[347] and *Pseudomonas aeruginosa*[348] cytochrome *c* peroxidases.

4. The Interaction with Substrates

Also in the low-spin case, the interaction of HRP with aromatic substrates has been studied.[361,363,366,450,451] It has been found that all these molecules bind within NOE distance of the 8-CH_3.[361,363,364,366,451] In the case of the complex formed between benzhydroxamic acid

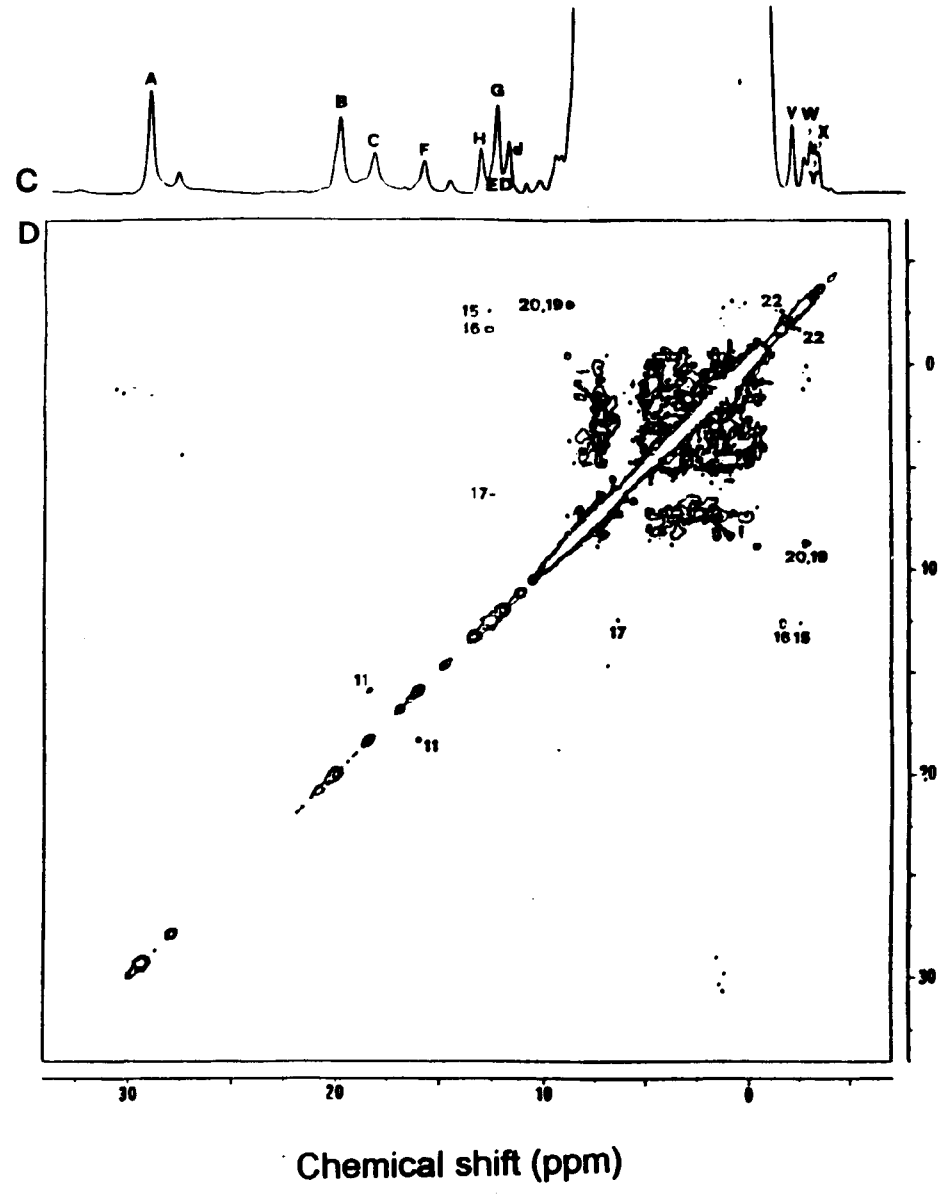

Figure 60. ^{1}H NMR spectra (600 MHz) of MnP–CN$^-$: (A) reference spectrum and (B) NOESY spectrum in H_2O solution; (C) reference spectrum and (D) magnitude COSY spectrum in D_2O solution. Shaded resonances in 1D spectra represent exchangeable proton signals. All the spectra were recorded at 307 K in 0.1 M phosphate buffer, pH 6.5. Corresponding cross peaks are labeled with the same numbers in both the 2D maps. Cross-peak assignments are as follows: (1) Hϵ2 distal His, Hϵ1 distal His; (2) Hϵ2 distal His, Hδ2 distal His; (3) 3-CH_3, 4-Hβ_{cis}; (4) 3-CH_3, 4-Hβ_{trans}; (5) 3-CH_3, α-meso; (6) 3-CH_3, 4-Hα; (7) 8-CH_3, δ-meso; (8) 8-CH_3, 7-Hα; (9) Hβ proximal His, NH_p proximal His; (10) Hβ proximal His, Hδ1 proximal His; (11) Hβ proximal His, Hβ' proximal His; (12) Hδ1 distal His, Hϵ1 distal His; (13) Hβ' proximal His, NH_p proximal His; (14) Hβ' proximal His, Hδ1 proximal His; (15) 4-Hα, 4-Hβ_{cis}; (16) 4-Hα, 4-Hβ_{trans}; (17) Hϵ1 distal His, K; (18) 7-Hα, 7-Hα'; (19) 2-Hα, 2-Hβ_{cis}; (20) 2-Hα, 2-Hβ_{trans}; (21) 2-Hα, α-meso; (22) 4-Hβ_{trans}, 4-Hβ_{cis}. (Reprinted from ref 336. Copyright 1992 American Chemical Society.)

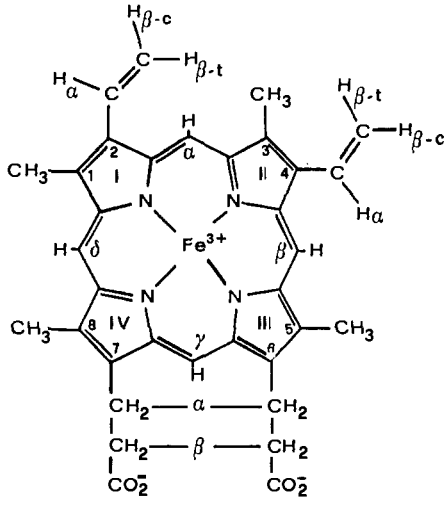

A

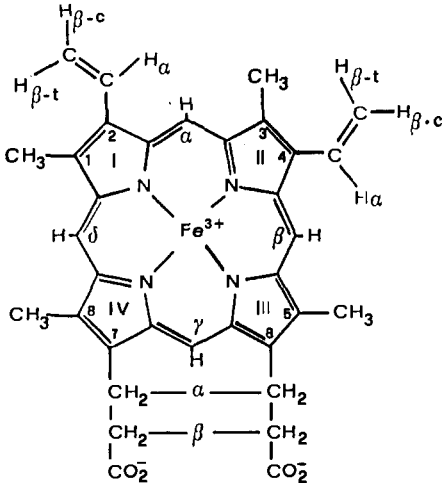

B

Figure 61. Schematic drawing of the different orientations of the 2-vinyl group found in LiP and HRP (A) and in CcP (B).

(BHA) and HRP–CN^- NOEs have been observed between the aromatic protons of the substrate and the 8-CH_3, 7-Hα, and distal histidine Hϵ1 signals.[451] A detailed analysis of the spectra of HRP isoenzyme C in the presence of different ratios of CN^- and BHA has shown that the binding of either BHA or CN^- destabilizes the binding of the other. A direct steric interaction between the two molecules is ruled out since the CN^- binds at the iron and relaxation studies place the aromatic ring of BHA at a distance higher than 8 Å from the iron. A direct electronic origin of the interaction also seems improbable: the ^1H NMR spectral characteristics of both HRP and HRP–CN^- are minimally perturbed upon BHA binding. Therefore, it has been proposed that the hydroxamic acid side chain is oriented such as to allow the hydrogen bond to the distal histidine Hϵ2. Also CN^- in peroxidases forms a hydrogen bond with the same atom. This hypothesis not only explains the competitive binding of BHA and CN^- to HRP, but also accounts for the weaker binding constant values of other substrates to resting-state HRP. Aromatic substrates with other side chains stabilize the aromatic moiety in the same

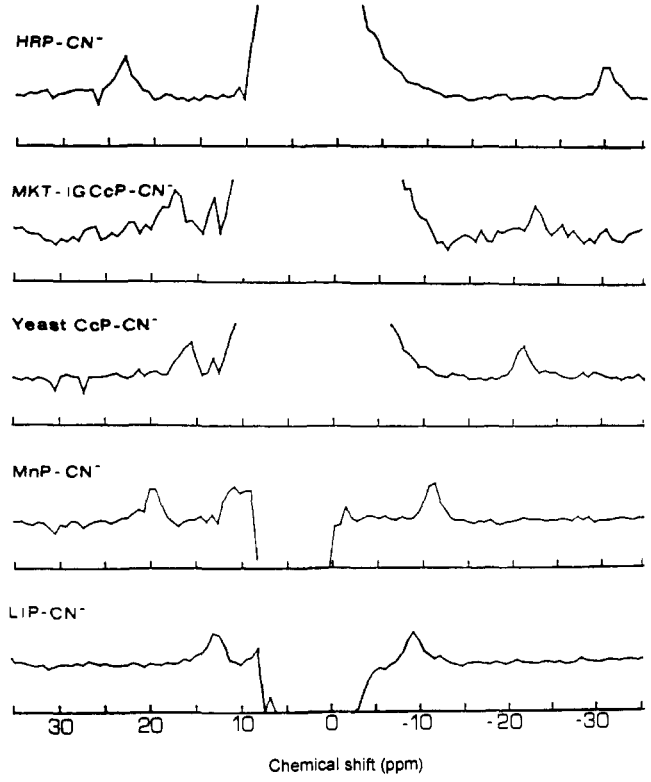

Figure 62. ^1H NMR spectra recorded at 200 MHz and 301 K of different peroxidases obtained with a super WEFT pulse sequence with a recycle delay of 10 ms and a τ value of 5 ms. The downfield signal is due to Hδ2, and the upfield signal to Hϵ1 of the proximal histidine. (Reprinted from ref 336. Copyright 1992 American Chemical Society.)

hydrophobic pocket near the heme edge, but the side chains do not have the appropriate length and/or geometry to make the hydrogen bond to the distal histidine. This is also consistent with the binding constants for these substrates being essentially unaffected by cyanide ligation. Some influence on the ^1H NMR spectra of the F41V mutant has been observed upon binding of substrates.[366]

It has been reported that the binding of ferricytochromes affects only slightly the spectrum of CcP–CN^-. Small shift variations are observed for 8- and 3-CH_3 resonances, this being consistent with the buried nature of the CcP heme.[452]

Mn^{2+} binds to MnP–CN^-. The spectrum of the final adduct shows only a few hyperfine-shifted resonances, the others being too broad to be detected. The analysis of this spectrum indicates that the Mn^{2+} binding site is within 11 Å from the heme 8-CH_3.[370]

5. The Low-Spin Adducts of Peroxidases Containing the Covalently Bound Heme

The ^1H NMR spectrum of LPO–CN^- [372,453] (Figure 68A) shows only one three-proton intensity signal around 20 ppm, attributable to a heme methyl group. In addition, other one-proton intensity signals are observed in the downfield region. By analogy with other peroxidases, the presence of a broad signal at −32 ppm suggests that the fifth ligand is a His residue. The LPO–CN^- spectrum changes in two steps depending on pH, with pK_a values of 6.4 and 11.[372] The azide binding to LPO has also been examined:[372] above pH 9 the spectrum is indistinguishable from that of the native enzyme in a ferric high-spin state. However, at

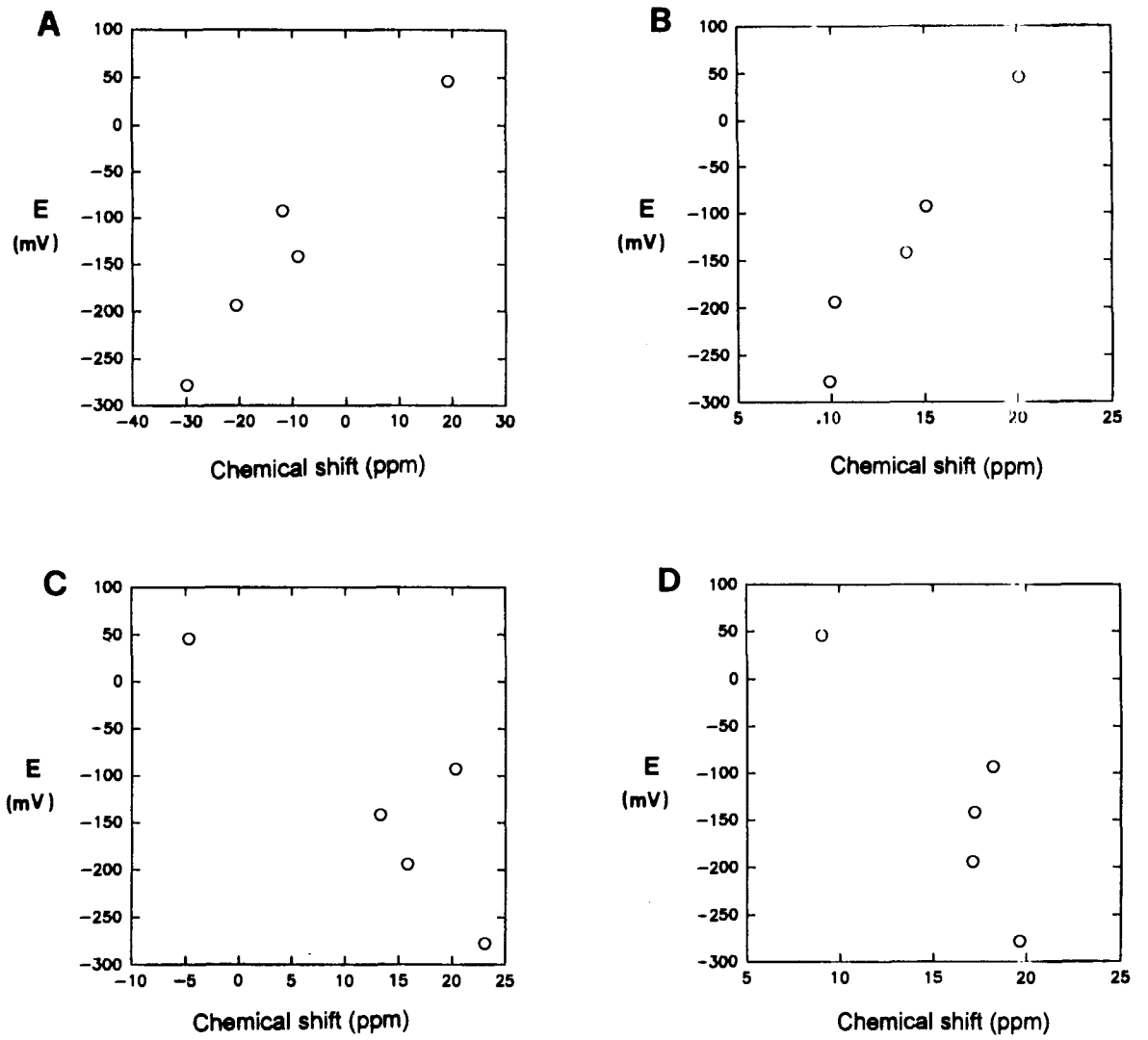

Figure 63. Relationship of the redox potential $E(Fe^{3+}/Fe^{2+})$ to chemical shift of some of the proximal histidine protons in the cyanide adducts of HRP, CcP, LiP, MnP, and Mb (in order of increasing redox potential): (A) Hε1; (B) Hδ1; (C) Hδ2; (D) mean shift of the β-CH_2.

lower pH values, signals between 50 and 10 ppm appear and increase in intensity. Below pH 7 the enzyme is completely bound to azide: in particular protonation of an ionizable group with a pK_a of 7.4 facilitates azide binding. On decreasing the pH, the signal shifts of this adduct change with a pK_a of about 6, like for the CN^- adduct. The temperature dependence of these resonances does not follow a Curie behavior, suggesting that the heme iron of LPO–N_3^- exhibits a thermal spin equilibrium. In any case the resonance assignment was complicated by the inability to reconstitute the protein with isotope-labeled or modified hemins. La Mar's group[453] successfully applied the NOE techniques to LPO–CN^-. The proposed assignments based on NOE connectivities and comparisons with HRP–CN^- yield a contact shift pattern consistent with the hypothesis that the 8-CH_3 in the hemin in LPO–CN^- is replaced by a mercaptomethylene group and with an axial imidazole plane oriented primarily along the N–Fe–N axis of pyrroles I and III.

Myeloperoxidase (MPO) is a heme-containing glycoprotein which catalyzes the formation of hypoclorous acid from chloride and hydrogen peroxide. It is a tetramer of molecular weight 120 000–160 000 and contains two heme groups that are kinetically inequivalent in primary peroxide compound formation. Identification of the chromophore present in MPO has been made difficult by the fact that it is covalently attached to the polypeptide.[295] The similarity in ^1H NMR spectral parameters for LPO–CN^- (Figure 68A) and MPO–CN^- (Figure 68B) suggests that the prosthetic groups in the two proteins are very similar.[454] Not only do MPO–CN^- and LPO–CN^- exhibit the same number of peaks with comparable shifts and relative relaxation properties, but their dipolar connectivities, and hence their relative spatial dispositions, are essentially identical. MPO is by far the largest protein to which the NOE technique has been applied (Figure 69). The reported NOE results[454] clearly show that paramagnetism does not only undermine spin diffusion and renders NOE studies more useful for large paramagnetic systems than for large diamagnetic ones, but the magnitude of NOEs actually improves with increasing molecular weight. As it appears from the spectra reported in Figure 68, at variance with the other peroxidases, in the spectra of LPO–CN^- [372,453] and MPO–CN^- [454] single-proton signals are present at unusually low-field values (35–70 ppm). In low-spin ferric heme proteins the strong perturbation of the heme electronic structure can be correlated primarily with

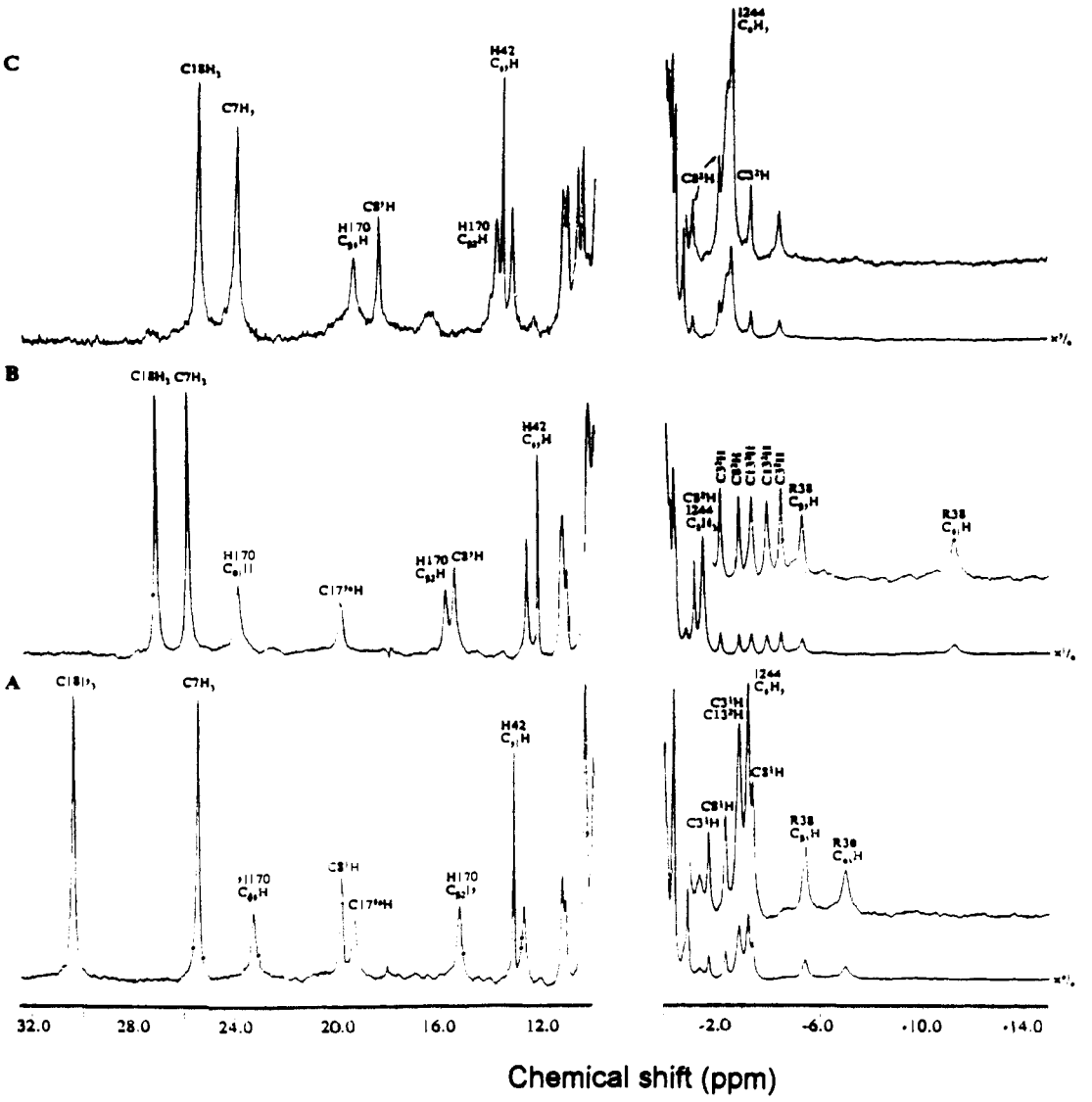

Figure 64. ^{1}H NMR spectra (500 MHz) of the cyanide adducts of (A) wild-type HRP, isoenzyme C, pH 7.6, (B) F41V mutant of recombinant HRP-C, pH 7.6, and (C) R38K mutant of recombinant HRP-C, pH 7.0. All the spectra were recorded at 303 K in D_2O solution, 20 mM potassium phosphate. The signal labeling follows the IUPAC convention for the numbering of the heme positions. (Reprinted from ref 366. Copyright 1992 Springer-Verlag.)

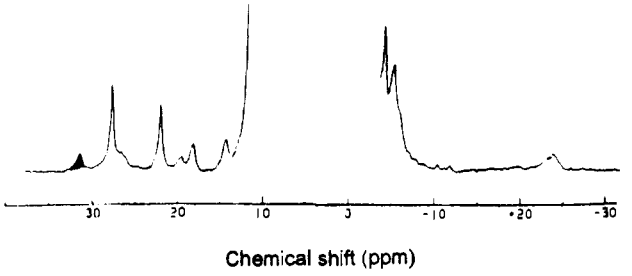

Figure 65. ^{1}H NMR spectrum (300 MHz) of the cyanide adduct of *Coprinus cinereus* peroxidase in H_2O solution, 0.1 M phosphate buffer pH 7.2. (Reprinted from ref 332. Copyright 1989 American Chemical Society.)

the orientation of the proximal His imidazole plane relative to heme pyrroles.[307,455,456] This results in large contact shifts for the substituents on opposite pyrroles. An orientation such as reported in Figure 53A would provide large low-field contact shifts for 3-CH_3 and 8-CH_3 as observed in heme *b* peroxidases, while the orientation reported in Figure 53B would provide large low-field contact shifts for 1- and 5-CH_3 as observed in metMb–CN^- and metHbA–CN^-. The observation of only a single low-field methyl for LPO–CN^- favors the hypothesis of the latter orientation with peak f due to 3-CH_3. On the basis of the analogy of the ^{1}H NMR spectra of LPO–CN^- and MPO–CN^-, the same should be valid also for the latter system. The large contact shifts observed for the methylene group giving rise to peaks a and *c* have been proposed to arise from the unusual 8-SCH_2 group. The heme α-methylene protons experience contact shifts, δ_c, related to the adjacent pyrrole carbon π spin density, ρ_π, via

$$\delta_c = \rho_\pi B \cos^2 \varphi \qquad (48)$$

where φ is the dihedral angle between the C–C–H plane and the aromatic carbon p_z axis and B is a constant. In a rotating methyl group, $\langle \cos^2 \varphi \rangle = 0.50$. In an usual methylene group, as found for hemin propionate, $\varphi \simeq 60°$, leading to $\cos^2 \varphi \simeq 0.25$, which accounts for the much smaller α-CH_2 relative to CH_3 contact shifts observed in low-spin ferric hemes. Assuming that the covalent link to the protein could lead to a 8-SCH_2 orientation for which $\varphi \simeq 30°$ and $\cos^2 \varphi = 0.75$, the resulting contact shift is $\simeq$50% larger than for a CH_3 group with the same π spin density and

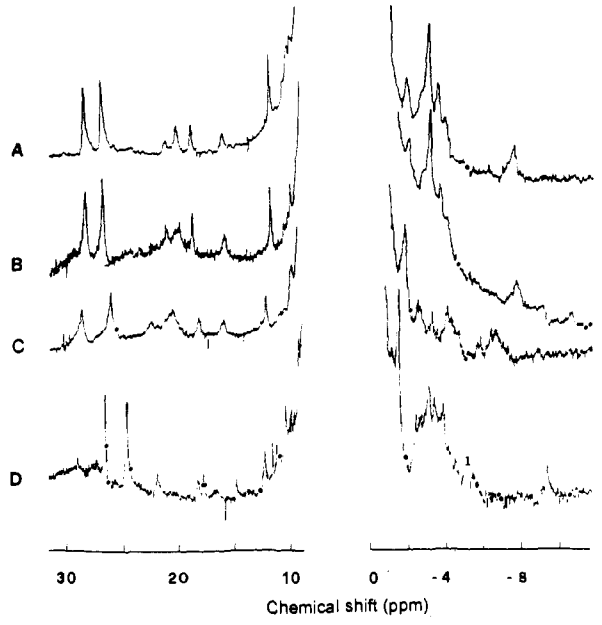

Figure 66. ^{1}H NMR spectra (270 MHz) of the cyanide adducts of turnip peroxidase: (A) isoenzyme P1, (B) isoenzyme P2, (C) isoenzyme P3, and (C) isoenzyme P7. All the spectra were recorded at 308 K, pH 7. (Reprinted from ref 449. Copyright 1975 Elsevier.)

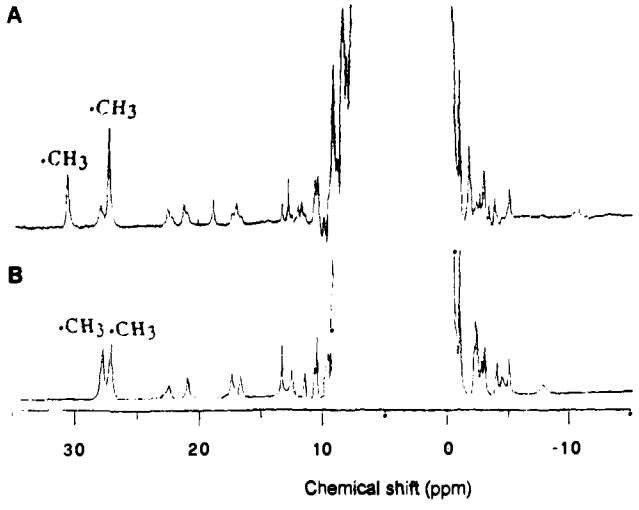

Figure 67. ^{1}H NMR spectra (600 MHz) of the cyanide adducts of (A) acidic cucumber peroxidase and (B) basic cucumber peroxidase. The spectra were recorded at 298 K in D_2O solution, pH 8.0. (Reprinted from ref 333. Copyright 1991 Elsevier.)

3 times larger than that which would result from the unusual unconstrained orientation of an α-CH_2 group.[454]

6. Low-Spin Adducts of P450 and Chloroperoxidase

The ^{1}H NMR spectrum at 220 MHz of the CN^- adduct of camphor-bound P450 has been reported (Figure 70).[379] It shows hyperfine-shifted resonances in the typical low-spin region. The 400-MHz ^{1}H NMR spectra of ferric low-spin $P450_{sec}$ complexes have been also published.[457] However, no specific assignments for the hyperfine-shifted resonances are available. Recently NOE and NOESY experiments have been performed for the substrate-free $P450_{RRI}$ (Figure 71).[381] The shift and Curie behavior of the signals indicate that the iron ion is in a low-spin state. The short nuclear relaxation rates of the hyperfine-shifted signals have been accounted for assuming a relatively larger energy separation between the three levels of the ground state for P450 with respect to peroxidases and globins.[381] CN^- binds $P450_{RRI}$ with a low affinity constant. The exchange rate is slow on the NMR time scale. The resonances here are broader with respect to the cyanide derivatives of peroxidases (Figure 72).

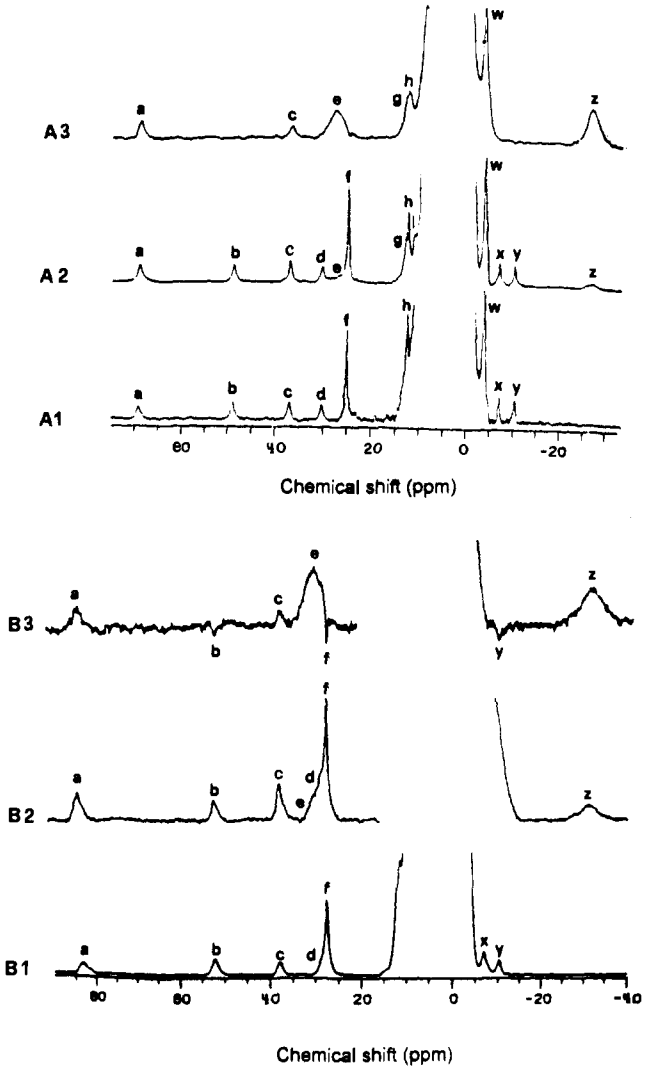

Figure 68. (A) ^{1}H NMR spectra (360 MHz) of LPO–CN^- recorded at 298 K in D_2O solution, pH 7.0, as a function of the pulse repetition rate: (A1) pulse repetition rate of 0.5 s^{-1}, (A2) pulse repetition rate of 2 s^{-1}; (A3) pulse repetition rate of 100 s^{-1}. (B) ^{1}H NMR spectra (360 MHz) of MPO–CN^- recorded at 293 K in D_2O solution, pH 7.2, as a function of the pulse repetition rate: (B1) pulse repetition rate of 3 s^{-1}; (B2) pulse repetition rate of 12 s^{-1}; (B3) pulse repetition rate of 100 s^{-1}. (Part A, reprinted from ref 453. Copyright 1989 American Chemical Society. Part B, reprinted from ref 454. 1990 *Journal of Biological Chemistry*.)

The ^{1}H NMR spectrum of ferric low spin CPO–CN^- (Figure 73A) has been reported.[387,458] Depending on the procedure of the sample preparation different ratios of two different isoenzymes may be observed. The two isoenzymes show very similar or identical chemical shift values for many hyperfine-shifted resonances. Four peaks of three-proton intensity each are present between 24 and 20 ppm, arising from two heme methyl protons of each isoenzyme. Four exchangeable protons are observed in the 17–12-ppm region. By recording the spectrum at fast repetition rates two fast relaxing peaks are observed at 39 and −20.7 ppm. In analogy

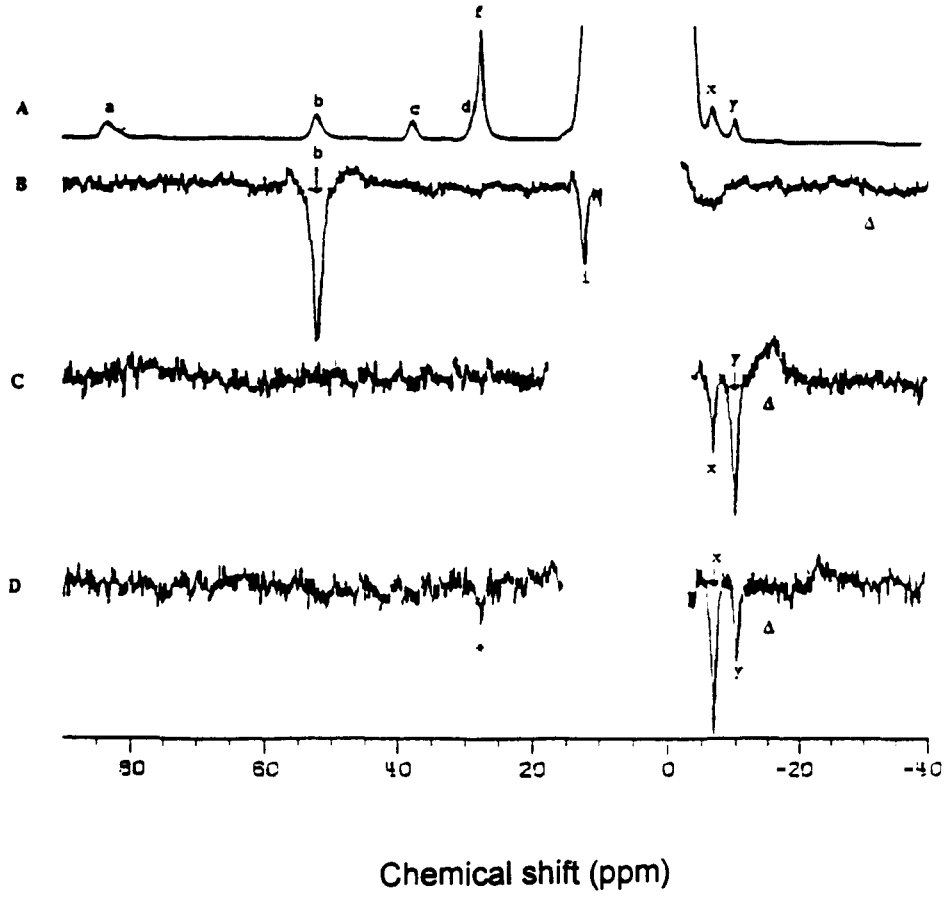

Figure 69. ^{1}H NMR reference spectrum (360 MHz) of MPO–CN$^-$ (A) and (B–D) NOE difference spectra. The downward arrows indicate the saturated peaks. All the spectra were recorded at 293 K in D_2O solution, pH 7.2. (Reprinted from ref 454. Copyright 1990 *Journal of Biological Chemistry.*)

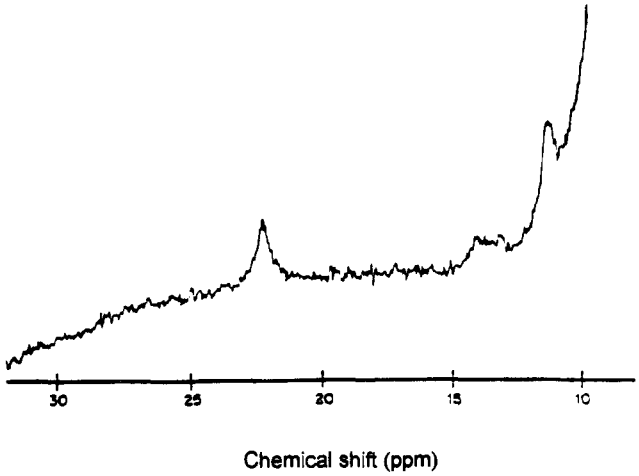

Figure 70. ^{1}H NMR spectrum (220 MHz) of the cyanide adduct of cytochrome $P450_{cam}$, recorded at 288 K in D_2O solution, 0.2 M phosphate buffer pH 7.0. (Reprinted from ref 379. Copyright 1972 National Academy of Sciences.)

with the proximal histidine ring protons in peroxidases, they exhibit large shifts and very efficient relaxation and have been proposed to be due to the β-CH_2 protons of the coordinated cysteine.[387] It is interesting to note that the T_1 values of the heme resonances in CPO-CN$^-$ are typically three times smaller than those of the cyanide adducts of peroxidases, as a consequence of axial ligation of cysteine versus histidine.[458] NOE measurements[458] (Figure 73, parts B-G) have allowed the assignment of the two more shifted heme methyl resonances to either 5- or 8-CH_3, the other two being assigned to either 1- or 3-CH_3. On the same basis the α-CH_2 resonances of the 7- or 6-propionate and the β-CH_2 resonances of the 2- or 4-vinyl have also been tentatively located. A signal with chemical shift, T_1, and line width values similar to those of the Hϵ1 proton of the distal histidine residue of peroxidases is present at 12.2 ppm. No definitive results are available to support this proposal. In any case, if a distal His residue is present it should be different from that of peroxidases in terms of hydrogen bonding with the ligated cyanide: no exchangeable signal attributable to the Hδ2 resonance of protonated histidine is observed. This finding is in agreement with a previous suggestion for the presence of a distal histidine residue. The NOE pattern and T_1 values of the resonances in the 0 to −5 ppm region are very similar to the distal arginine residue in the distal heme pocket of HRP–CN$^-$. However, this residue in CPO–CN$^-$ is close to either 1- or 3-CH_3, whereas the arginine residue in HRP–CN$^-$ is close to propionate-bearing pyrroles. The above results point to a structural similarity of the CPO pocket with that of peroxidases rather than with that of the monooxygenase cytochrome P450. The spectra obtained for CPO in the presence of various ligands (azide, thiocyanate, cyanate, nitrite) suggest that the enzyme–ligand complexes are predominantly low spin in character.[388] However the signals do not follow the Curie behavior with temperature, indicating that mixtures of high- and low-spin species are present. The adducts with azide, cyanate, and nitrite form more readily under

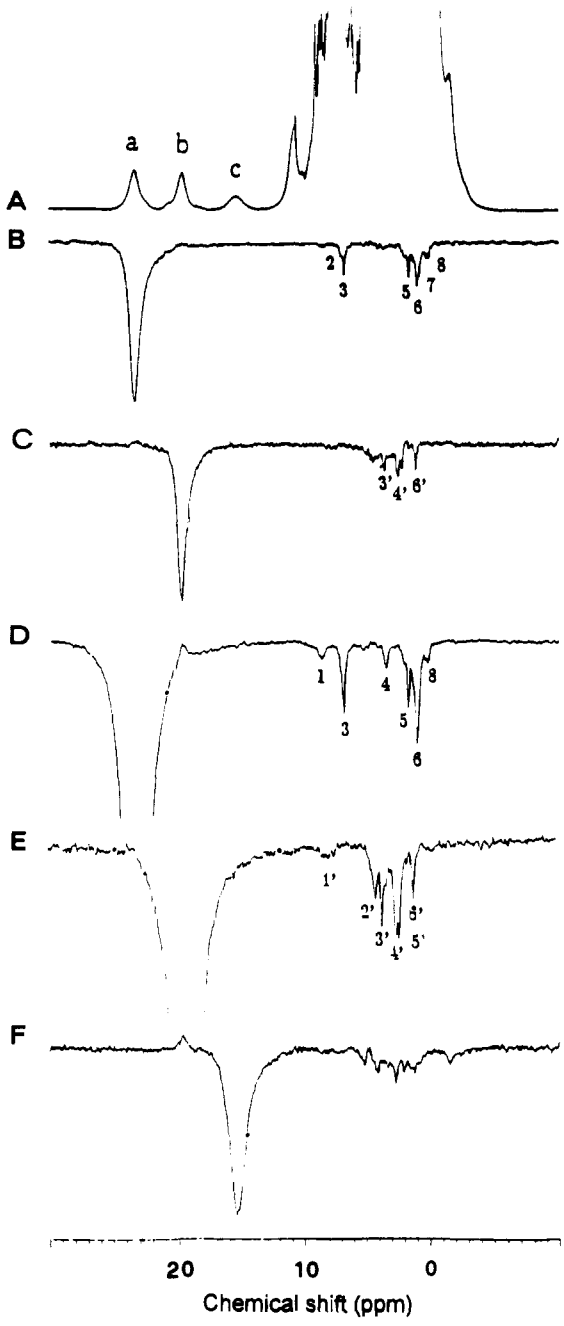

Figure 71. ^{1}H NMR reference spectrum (600 MHz) of substrate-free $P450_{RR1}$ (A) and NOE difference spectra obtained by saturation of signal a (B) and signal b (C), using a recycle time of 150 ms. NOE difference spectra obtained by saturation of signal a (D), b (E), and c (F), using a recycle time of 30 ms. All the spectra were recorded at 290 K in D_2O solution, 50 mM KCl and 0.1 M phosphate pH 7.0. (Reprinted from ref 381.)

acidic conditions. The loss of the hyperfine-shifted spectrum at higher pH is attributed to a slowing in the ligand exchange rate. In the case of thiocyanate, the complex forms only below pH 6.2. It is interesting to note that, at variance with the other heme proteins the ^{1}H NMR spectrum of the NCS^- adduct of CPO is predominantly low spin. This is consistent with the cysteine residue being a stronger ligand than histidine.[381,458]

7. Cytochromes

Cytochromes are electron-transfer proteins. The axial ligands and the heme-type which characterize the various cytochromes are reported in Table X. High resolution crystal structures are available for cytochrome b_5 and a number of variants of cytochrome c.[459-462]

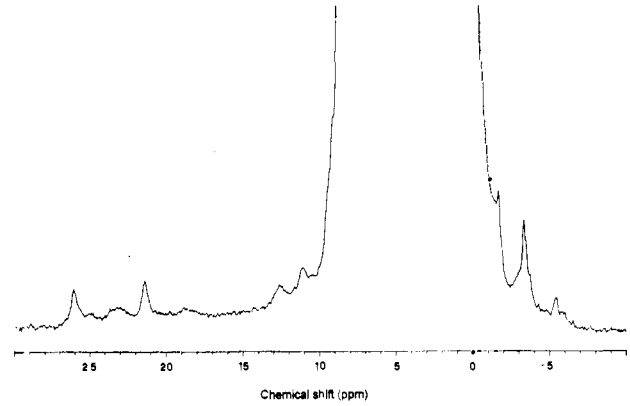

Figure 72. ^{1}H NMR spectrum (600 MHz) of $P450_{RR1}$-CN^-, recorded at 292 K in D_2O solution, 50 mM KCl and 0.01 M phosphate, pH 7.0. (Reprinted from ref 381.)

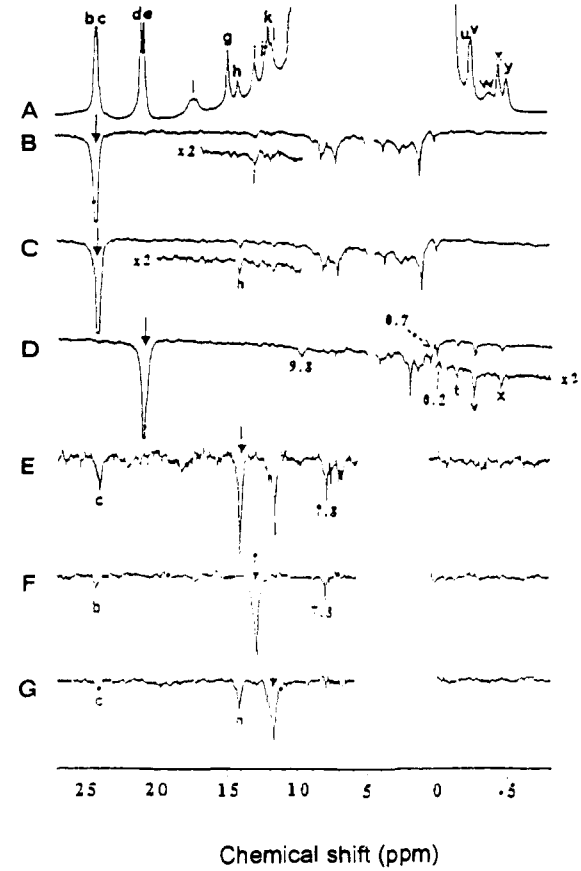

Figure 73. ^{1}H NMR reference spectrum (600 MHz) of CPO-CN^- (A) and (B–G) NOE difference spectra. The downward arrows indicate the irradiated peaks. All the spectra were recorded at 298 K in D_2O solution, 10 mM phosphate buffer, pH 6.0. (Reprinted from ref 458. Copyright 1992 American Chemical Society.)

Table X. Structural Features of Some Prosthetic Groups in Low-Spin Cytochromes

cytochrome	heme type	axial ligands
cyt c	heme c	histidine, methionine
cyt c''	heme c	two histidines
cyt c_3	heme c	two histidines
cyt b_5	heme b	two histidines

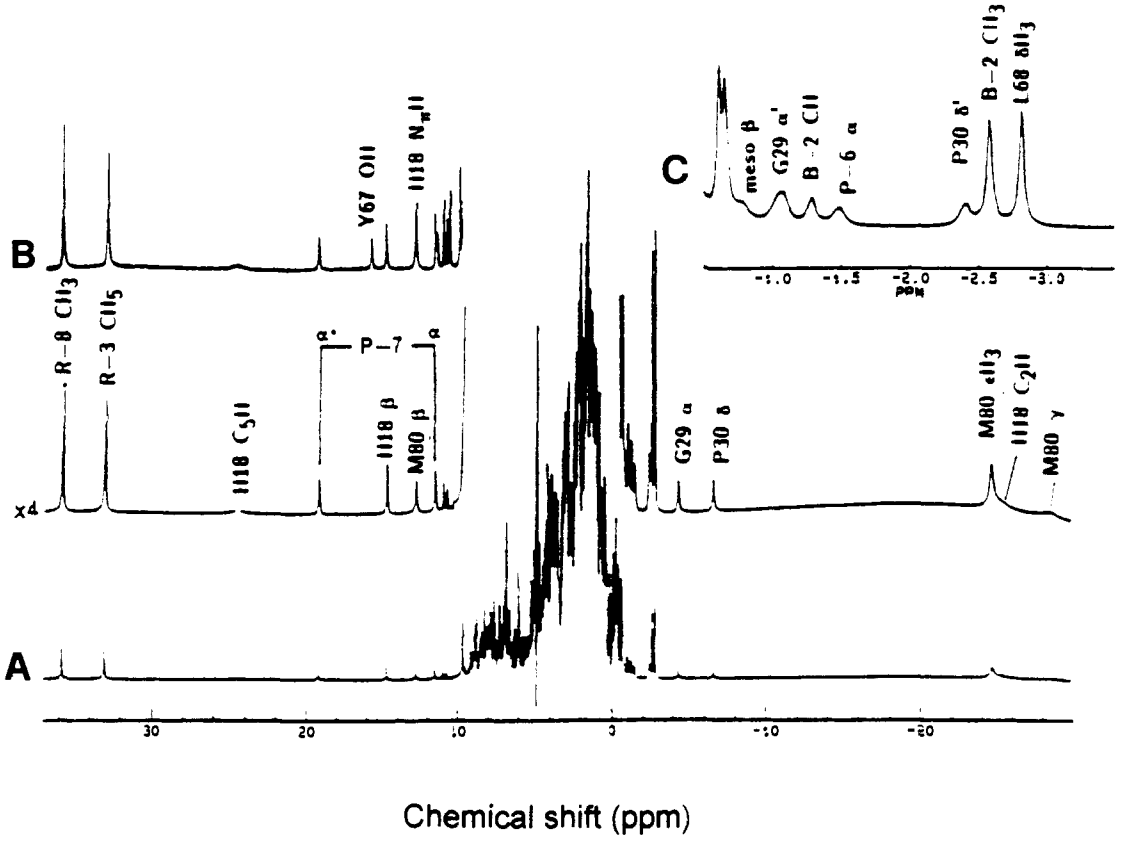

Figure 74. (A) ^{1}H NMR spectrum (500 MHz) of horse ferricytochrome *c*, recorded in D_2O solution, 100 mM phosphate and 150 mM NaCl, pH 5.7; (B) downfield region of a spectrum recorded under the same conditions in H_2O solution; and (C) expanded plot of the region between −0.5 and −3.5 ppm of spectrum A. (Reprinted with permission from ref 123. Copyright 1990 Rockefeller University Press.)

a. Strategy of Assignment in Cytochromes c. Due to their low molecular weights (around 12 000) which produce relatively narrow and well-resolved resonances, most of the cytochromes have been studied by NMR in their reduced diamagnetic forms. Using saturation transfer techniques the assignments have been subsequently transferred to the corresponding paramagnetic low-spin iron(III) species.[307] Horse ferricytochrome *c* can be taken as an example of the above procedure: historically it has been the most studied member of this important class of electron-transfer proteins. The ^{1}H NMR spectrum of horse ferricytochrome *c* is reported in Figure 74. The four ring methyl resonances had been detected in ferricytochrome *c* in early works, and the corresponding chemical shifts in ferrocytochrome *c* were determined by saturation-transfer techniques.[463,464] In the reduced protein individual assignments for the proton signals of the heme substituents have been achieved on the basis of NOE experiments.[99,465] With saturation-transfer experiments on partially reduced cyt *c*, individual assignments were obtained for the heme ring and thioether bridge methyl resonances.[465] As in all the other cytochromes reported thus far, the four heme ring methyl resonances are resolved from the diamagnetic envelope in the downfield part of the spectrum (between 7 and 34 ppm), whereas the two thioether bridge methyl signals resonate slightly upfield. Subsequent work has resulted in extensive heme and side-chain resonance assignments.[466–470] More recently, almost complete assignments for this main-chain proton resonances in both oxidation states were obtained by 2D NMR methods.[471–477] The hyperfine-shifted resonance assignments provided a basis for further analysis of the shift contributions.

An analogous characterization has been made on the highly homologous tuna cytochrome *c* (82% sequence homology).[466,469,476,478] Recently, many studies of structure and function have utilized iso-1-cytochrome *c* from the yeast *Sacchromyces cerevisiae*, due to the ease with which yeast may be genetically altered and the subsequent possibility to express the mutated proteins. Resonance assignments for the main-chain, side-chain, and heme protons for this isoenzyme and for some of its mutants have been reported in both oxidation states.[477,479–484] The NMR characterization of the mutants in which the Tyr 48 and the Tyr 48 + Trp 59 have been replaced by Phe residues, suggested the structural basis for the reduction in redox potential accompanying the amino acid substitution.[482] Tyr 48 and Trp 59 form hydrogen bond with the heme 7-propionate group. It has been found that upon mutation the shifts of the heme substituent protons are slightly affected, the most affected being the 7-propionate resonances. However, the NOE patterns obtained by irradiation of the signals of the heme substituents indicate that the protein fold around the heme is unaltered. The redox potentials of the mutants are 22 mV (Y48F) and 70 mV (Y48F + W59F) lower than the redox potential of the wild-type protein. Since NOE data do not indicate conformational changes, the differences in the redox potential have been attributed to the breaking of the hydrogen bonds involving the 7-propionate. This breaking will increase the electron density on the carboxylate, leading to an increased

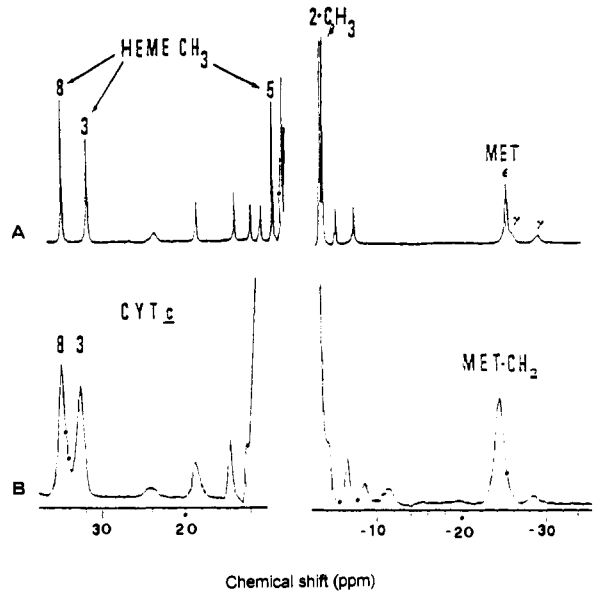

Figure 75. ^{1}H NMR spectra (361 MHz) of (A) horse ferricytochrome *c* and (B) 1:1 CcP–cytochrome *c* covalently cross-linked complex. The spectra were recorded at 296 K in D_2O solution, 10 mM KNO_3, pH 6.8. (Reprinted from ref 358. Copyright 1987 American Chemical Society.)

stabilization of the iron(III) state and hence a reduced redox potential.

The results obtained for cytochrome *c* from tuna and horse heart have been used to define the interaction sites of ferricytochromes *c* with small redox reagents[485-491] and with biological redox partners of cytochrome *c*.[358-360,492-494] In the ^{1}H NMR spectrum of the 1:1 covalently cross-linked complex between horse cytochrome *c* and yeast CcP (Figure 75) the proton hyperfine-shifted resonances of ferricytochrome *c* are broadened as expected on the basis of the increased rotational correlation time due to an effective molecular weight of about 46 000.[358] The 3- and 8-CH_3 groups are shifted closer together in the complex. Also Met 80 methyl and methylene resonances and heme 7-Hα resonances are reported to experience significant shifts upon complex formation.[358] Something similar happens in the case of the noncovalent complex,[359] but the line broadening is less dramatic, probably due to the fact that in this case cytochrome *c* is rapidly exchanging between free and complexed states. In comparison to cytochrome *c* complexes with cytochrome b_5[493] and flavodoxin,[492] the complex with CcP appears unique in that both the cytochrome *c* 8- and 3-CH_3 resonances are significantly shifted in the complex, while in the two former cases only a shift for 8-CH_3 signal has been reported. These observations suggested the idea that the interaction between cytochrome *c* and CcP involve the positively charged lysine 13 on the cytochrome surface.[359] The movement of the latter residue could cause small changes in the conformation of the axial heme ligand, Met 80, transmitted via Phe 82 residue. Because the chirality about the *c* heme-coordinated sulfur atom of Met 80 is known to be a primary factor in determining the hyperfine-shift pattern,[307] this rearrangement of residues could justify the observed shift changes. The Phe 82 residue has been shown to be invariant in all mitochondrial cytochromes *c* and located near the exposed heme edge in proximity of the 3-CH_3. Irradiation of the 3-CH_3 resonances in the ^{1}H NMR spectra of tuna, horse, and yeast iso-1-ferricytochromes *c* has been shown to give NOE connectivities to the phenyl ring protons and to the β-CH_2 protons of this residue.[300] These measurements have allowed the identification of the spin system of Phe 82 in the three cytochromes. Four different noncovalent complexes using horse, tuna, yeast iso-1- and yeast iso-2-ferricytochromes *c*, and two covalently cross-linked complexes with horse and yeast iso-1-ferricytochromes *c* with CcP have been recently studied.[494] In all the noncovalent complexes the binding of CcP induces shifts in the Phe 82 ring resonances. It is interesting to note that the complex-induced shifts of the proton resonances are different for the physiological redox partners compared to the other cytochromes. The 3- and 8-CH_3 in each complex of yeast iso-1 and iso-2-ferricytochrome *c* shift in the same direction, whereas for the horse and tuna complexes they shift closer together. The Phe 82 resonance shifts toward higher frequencies but to different extents in each case. This type of shift is consistent with a reorientation of Phe 82 away from the paramagnetic center, with structural alterations in the heme environment that are comparatively small for CcP nonredox partners. A more detailed analysis of the NMR would be now possible on the basis of the recently reported crystal structure of the CcP–cytochrome *c* complex.[495]

^{1}H NMR experiments on mixtures of reduced and oxidized proteins have been used to study the self-exchange electron-transfer processes.[128,129,496-508] Electron self-exchange rates were determined either by saturation-transfer methods[128,129] or by measuring electron exchange induced line broadening. In the latter case the inverse state lifetime is proportional to the induced line broadening. The influence of ionic strength, pH, anion binding, and site-specific chemical modifications on the exchange rate have been analyzed.[128,129,497,498] ^{1}H NMR studies of the electron self-exchange rates in the hexametaphosphate–cytochrome *c* aggregates showed that anion-induced protein self-association lowers the overall kinetic barrier to electron exchange from heme to heme.[498] Differences among cytochromes *c* of different origins have been interpreted in terms of an active role of the polypeptide chain in the electron-transfer process.[496] Meaningful differences have been also observed between cytochrome *c* and b_5 and cytochrome c_{551}.[497,499]

Salt-dependent structure changes have been detected for some residues in horse heart cytochrome *c*.[509] By 2D NMR techniques a structural description of oxidized horse cytochrome *c* at acidic pH and high ionic strength have been obtained, measuring the extent of hydrogen exchange for 44 amide protons. The transition from the native to the acidic form result in the loss of some specific interactions, including some salt bridges and at least one axial ligand (Met 80).[510] The spectrum of the cyanide adduct has been also reported.[463]

Due to the incredibly vast amount of literature available for cytochromes, we will discuss here mostly the papers in which assignments are based only on the paramagnetic species. Indeed, the topic of this review is to illustrate what kind of information can be obtained from the NMR spectra of paramagnetic compounds and to discuss the technical details in optimizing NMR experiments for these particular systems. Moreover,

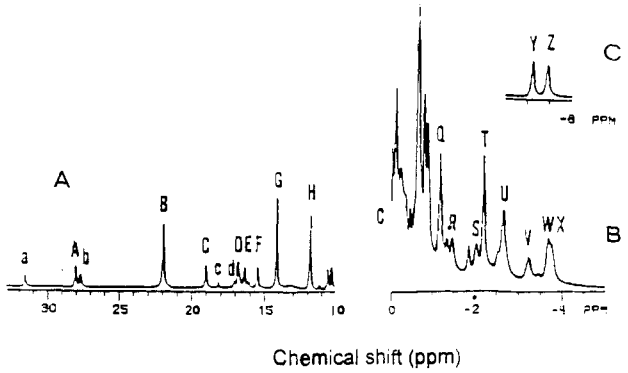

Figure 76. Resolved portions (A–C) of the 500-MHz ^{1}H NMR spectrum of ferricytochrome b_5 recorded at 293 K in D_2O solution, pH 6.2. (Reprinted from ref 524. Copyright 1986 American Chemical Society.)

a general discussion on the shift patterns observed in the various low spin iron(III) cytochromes (independently of the assignment procedure) will be included with the aim of elucidating which factors affect both the contact and the pseudocontact contributions.

b. The Oxidized Cytochrome b_5. Among the various cytochromes, the most extensive assignments based only on the iron(III) species have been obtained for the ferricytochrome b_5. Cytochrome b_5 is found both as a membrane-bound protein in mammalian liver microsomes as well as a soluble form in erythrocytes. The trypsin-solubilized fragment of cytochrome b_5 from bovine liver microsomes contains the heme prosthetic group and consists of 84 amino acids. It retains the full reactivity.[511] It has been reported to form 1:1 solution complexes with cytochrome *c*,[493,512,513] myoglobin,[514] and hemoglobin.[515] In the former two complexes the binding is clearly detected by ^{1}H NMR spectroscopy: highly selective perturbations only for a small number of resonances are observed.[493,513,514]

The hyperfine-shifted portion of the ^{1}H NMR spectrum of ferricytochrome b_5 is reported in Figure 76. Assignments for all four heme methyl groups, the 2-vinyl protons, two of the four propionate β-methylene protons and a few amino acid side chains in the vicinity of pyrroles I and II have been obtained by saturation transfer from the reduced forms and by reconstitution with isotope-labeled hemes.[516–518] Analogously to HRP,[519] CcP,[520] and globins,[521–523] the reconstitution of apocytochrome b_5 with hemin has demonstrated that in solution exists an equilibrium involving two forms of the protein which differ in the orientation of the heme.[517] Since the isomer with the X-ray-determined orientation dominates in solution (about 9:1 ratio), only the signals of the major component have been assigned. NOE experiments allowed the assignment of the heme propionate protons.[524] The pattern of the α-methylene proton hyperfine shifts for both propionates is inconsistent with the orientation obtained from the X-ray crystal data, suggesting specific rotation for each side chain. The above assignments have been extended by NOESY experiments.[108]

The shift of 6-propionate protons experiences a dramatic pH dependence, with a pK_a of 5.9.[524] The 6-propionate side chain has been found by X-ray crystal analysis to be solvent exposed.[525] By addition of increasing amounts of Gd^{3+}, selective broadening of the β-methylene protons of 6-propionate has been detected and attributed to selective binding of the cation to the carboxyl groups of this side chain.[524] This is consistent with the exposed nature of this heme substituent. One- and two-dimensional ^{1}H NMR methods have defined cation-binding domains on the surface of the tryptic fragment of microsomal b_5.[526] The addition of $Cr(en)_3^{3+}$ to solutions of ferricytochrome b_5 reveals at least three distinct sites (indicated as I, II, and III) on the surface of the protein to which highly charged cations may bind. Site I contains the exposed 6-propionate group and a series of carboxylate residues. Sites II and III are located away from the heme edge region. By DQF-COSY experiments the 6-propionate resonances have been found to be selectively perturbed upon complex binding. Selective effects on these resonances have been observed also in the case of complex formation between ferricytochrome b_5 and cytochrome c^{493} or myoglobin.[514] The binding of cytochrome *c* to cytochrome b_5 has been studied by 1D and 2D ^{1}H NMR spectroscopy.[513] A line broadening is observed throughout the spectrum of ferricytochrome b_5, as expected from the increased correlation time for the complex. The chemical shifts of the hyperfine-shifted resonances of cytochrome b_5 are consistent with a single high-affinity cytochrome *c* binding site on the surface of cytochrome b_5 and at least one secondary binding site of lower affinity. In the DQF-COSY experiments, the only cross peaks substantially altered by complex formation were those attributable to the heme propionates of cytochrome b_5. In the binary complex between ferricytochrome b_5 and ferricytochrome *c*, $Cr(en)_3^{3+}$ broadens many cytochrome b_5 resonances.[526] Cytochrome *c* shows significant line broadening of resonances in the presence of the complex. Although the pattern of line broadening of resonances at sites II and III is unaltered by complex formation, cytochrome *c* selectively shields some residues at site I, the heme edge site. This has been explained assuming that cytochrome *c* can bind to the residues at site I in many orientations each of approximately equal stability. Thus on average it shields Gly 42 and Glu 43 but leaves the heme propionate more accessible.

The ^{1}H NMR spectra of the soluble fragment of bovine native and wild-type rat ferricytochrome b_5 reconstituted with a variety of chemically modified hemes have been analyzed.[527,528] The relative proportion of the two heme orientations obtained by 180° rotations about the α–γ meso axis varied widely. The unpaired spin density distribution in the heme π system leads to substituent hyperfine-shift patterns diagnostic of the heme orientation in the protein matrix. The analysis is based on the assumption that the unpaired spin distribution in a heme is caused mainly by the rhombic perturbations due to the axial His bonding and, therefore, is indicative of the position of the substituent in the protein matrix and does not depend on the particular heme. The resulting range of chemical shifts for the methyl–, vinyl–, propionate–, and pyrrole–hydrogen substituents as a function of individual positions in the protein matrix is diagramed in Figure 77 and has been proposed as an useful guide to rapid determination of orientation of other chemically modified hemins in cytochrome b_5 or for native hemin in cytochrome b_5 mutants. The slightly different shifts patterns for bovine versus rat cytochrome b_5 with the

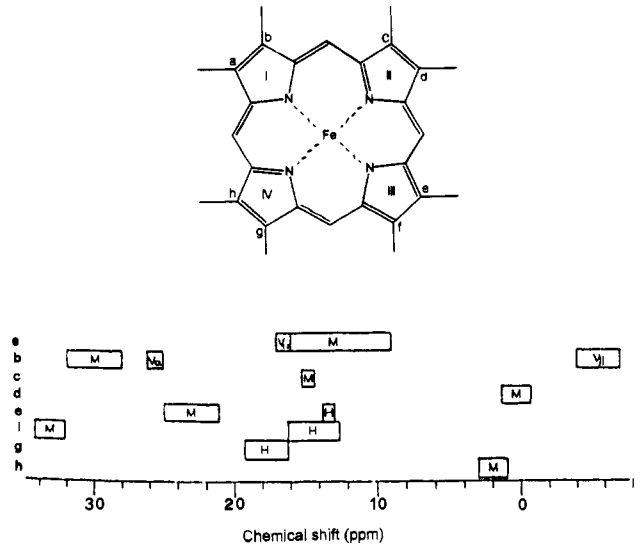

Figure 77. Empirical correlation of chemical shifts for methyls (M), vinyls (V_i), and propionate α-CH_2 (H) with positions in the protein matrix; a–h indicate the heme positions according to the reported scheme (from ref 528).

same hemin in the same orientation must reflect small differences in the peripheral contacts due to the substitution near the heme-binding site. The major determinant of the heme orientation has been proposed to be a repulsive interaction between a vinyl and a hydrophobic cluster of amino acid residues.[527] Moreover, it has been shown that for a stable holoprotein the axial iron–His bonds are essential and that the protein matrix cannot accommodate carboxylate side chains at interior positions in the heme binding pocket.[528] Therefore, the heme pocket interior in cytochrome b_5 appears much less polar and less sterically accommodating than that of myoglobin.

c. Cytochrome c_3. Cytochromes c_3 from *Desulfovibrio vulgaris*, Miyazaki F and Hildenborough, have been widely characterized by ^{1}H NMR spectroscopy.[529–534] They are tetraheme iron proteins of molecular weight around 13 000. The iron ions are coordinated by *c*-type hemes and bisligated by histidines. The redox mechanism was shown to be a four consecutive one-electron process. It has been found that the intramolecular electron exchange rate is fast on the NMR time scale, but the intermolecular electron exchange is slow.[531] Therefore, five sets of spectra corresponding to the five macroscopic oxidation states can be observed (Figure 78).[532] In the intermediated oxidation states, each heme methyl group exhibits only one resonance in the NMR spectrum with a chemical shift depending on the ratio between the molar fraction of the oxidized and reduced states of that particular heme. By NOE, NOESY, COSY, and TOCSY experiments assignments of many hyperfine-shifted signals have been obtained for the fully oxidized form in both cytochromes c_3.[533,534] One- and two-dimensional saturation-transfer experiments allowed the determination of the chemical shifts of the heme methyl groups in the five macroscopic oxidation states (Figures 79).[531]

d. Factorization of the Hyperfine-Shift Contributions in Cytochromes. For cytochromes, the availability of the assignments of most of the residues in both the oxidized and reduced forms provides an opportunity to examine the origin of redox-related structural

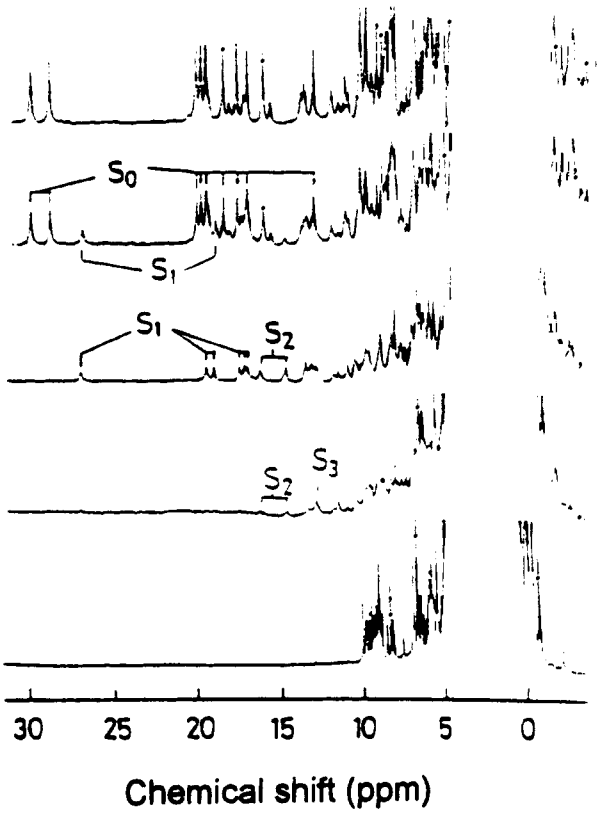

Figure 78. ^{1}H NMR spectra (500 MHz) of cytochrome c_3 from *Desulfovibrio vulgaris*, Miyazaki F, in a variety of redox stages: from fully oxidized (top) to fully reduced (bottom). The heme methyl signals are labeled on top. S_i is the macroscopic oxidation state. All the spectra were recorded at 303 K. (Reprinted from ref 532. Copyright 1990 American Chemical Society.)

differences in solution. Fermi contact shifts are restricted to nuclei of the heme group and its immediate ligands, i.e. the two axial ligand residues, and the two heme-bound cysteines for *c*-type cytochromes. The shift of these residues contains information on the distribution of the unpaired electron. The measured chemical shift differences for nonbound residues are largely dominated by the pseudocontact contribution operative in the low-spin iron(III) systems. However, there may also be contributions due to conformational differences of some groups, which will affect the diamagnetic shift. The pseudocontact contribution can be estimated given the orientation, magnitude, and anisotropy of the magnetic susceptibility tensor. Keller and Wüthrich[535] applied for the first time the method developed by Kurland and McGarvey[16] to determine the orientation of the **g** tensor in cytochrome b_5, using liquid helium temperature **g** values. Subsequently, a most advanced procedure has been employed to analyze the structures of a variety of cytochromes *c* using ^{1}H NMR. Methods analogous to that above described for sperm whale metMb–CN^- have been commonly and satisfactorily used for various cytochromes, mainly by Williams et al.

The first of these papers is dated 1985.[402] The difference in chemical shift between the two oxidation states in tuna cytochrome *c* has been estimated and analyzed on the basis of the previously reported **g** values of the oxidized form. The structures of both ferri- and ferrocytochrome *c* are available with high resolution and have been found to be similar.[461,536] Only small

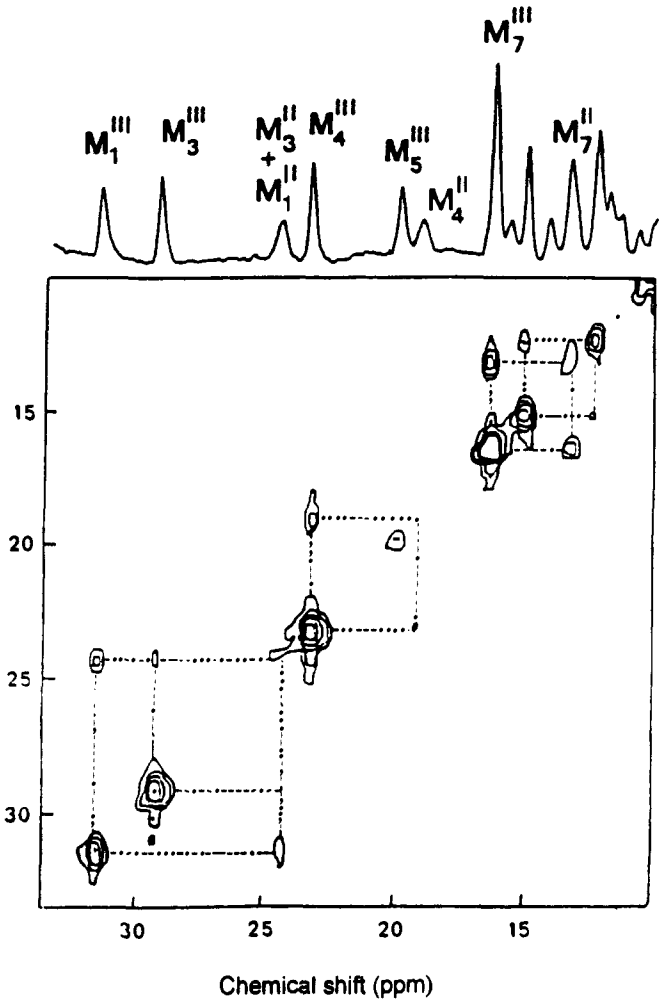

Figure 79. ^{1}H NMR EXSY spectrum (300 MHz) of *Desulfovibrio gigas* cytochrome c_3, recorded at 290 K. (Reprinted from ref 531. Copyright 1984 Academic.)

changes in the orientation of amino acid side chains at the protein–solvent interface and changes of internuclear distances within the protein around the heme propionate groups were observed. Susceptibility tensor components are unavailable for tuna cytochrome *c*, whereas the magnitude and the orientation of the principal components of the **g** tensor in a single crystal at 4.2 K for horse cytochrome *c* have been reported.[537] In order to calculate pseudocontact shifts at room temperature, an effective **g** tensor was defined:

$$\mathbf{g}_i^{\text{eff}} = \frac{\sum_j \mathbf{g}_i^j \exp(-E_j/kT)}{\sum_j \exp(-E_j/kT)} \qquad (49)$$

where j is allowed to vary over all the occupied electronic states and $\mathbf{g}_i^j$ represents a **g** tensor component of the jth electronic states. Approximate tetragonal and rhombic distortion values and spin–orbit coupling constant were obtained for cytochrome *c* by fitting the **g** values calculated for the lowest Kramers doublet to the experimental values obtained at 4.2 K, where only this energy level is occupied. This procedure allows the calculation of the orbital diagram for the iron(III) in ferricytochrome *c* (Figure 80). By using these calculated levels, the **g** values for the first excited Kramers doublet were obtained. Substitution in eq 49 then allowed the effective $\mathbf{g}_i^{\text{eff}}$ values at higher temperature to be calculated. This procedure is equivalent

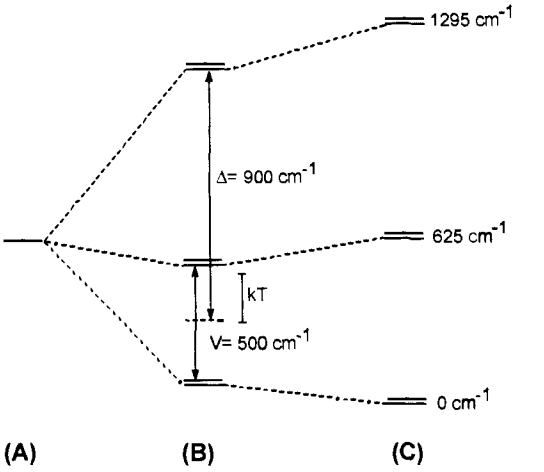

Figure 80. The orbital diagram for the electronic state of iron(III) in ferricytochrome *c*: (A) the ^{2}T state of the low-spin iron(III) ion in octahedral crystal field; (B) the ion in a rhombic and tetragonally distorted crystal field; (C) as B with the inclusion of spin–orbit coupling. The energy levels were calculated with the following parameters: Δ = 900 cm^{-1} (tetragonal distortion), V = 500 cm^{-1} (rhombic distortion), and λ = −340 cm^{-1} (spin–orbit coupling) (from ref 402).

to calculating the first-order Zeeman (foz) contribution to the magnetic susceptibility tensor. Further refinement was possible by allowing these states to mix under the influence of the external magnetic field. This perturbation, the second-order Zeeman (soz) effect, alters both the $\mathbf{g}_i^{\text{eff}}$ values and the energies of each level. The foz- and soz-corrected $\mathbf{g}_i^{\text{eff}}$ values have been used for the calculation of the pseudocontact term. In order to refine the orientation of $\mathbf{g}^{\text{eff}}$ tensor in solution and to evaluate the theoretical corrections made to the measured low-temperature **g** values, 21 methyl groups of 14 residues have been chosen. Separate shifts were calculated for each proton of a methyl group and subsequently averaged before comparison with the experimental data. It was found that the calculated pseudocontact shifts are relatively insensitive to the choice of the $\mathbf{g}^{\text{eff}}$ tensor magnitude. The starting orientation of the $\mathbf{g}^{\text{eff}}$ tensor was chosen with the z axis perpendicular to the plane defined by the four heme pyrrole nitrogen atoms, and the x and y axes in the direction of the I and III, and II and IV pyrrole nitrogens, respectively. The $\mathbf{g}^{\text{eff}}$ tensor orientation under the solution conditions was determined with a systematic rotation of the principal axes through the three Euler angles during the best-fit procedure. The final result of this procedure yielded a z axis displaced from the pyrrole nitrogens normal approximately in the direction of the bond between the axial Met 80 sulfur and the heme iron. The orientation of the z axis has been proposed to arise from the donation effect of the π-electron density from the sulfur ligand to the partially occupied d_{yz} orbital of iron(III). The pseudocontact contributions have been calculated for all the nonbound residue protons assigned in the NMR spectra of both oxidation states and compared with the observed hyperfine shifts. The overall protein fold and the position of most of the heme-packing residues are shown to be invariant between the crystal and solution. However, three regions of the protein (at the C terminus, around the heme propionate, and at the heme crevice near the thioether-2) are proposed to undergo confor-

mational changes upon the removal of crystal-packing constraints.

On the basis of the nearly complete assignment obtained for both horse ferro- and ferricytochrome *c*, the above calculation has been recently repeated.[403] The newly available main-chain resonance assignments[124,473,474] were used rather than the side-chain resonances utilized by Williams et al., since main-chain protons can often be more precisely placed in the structure. A different approach was used for the data analysis, and was extended to distinguish both crystal versus solution differences from oxidized versus reduced structural differences in solution. The much larger number of assigned proton resonances with respect to the above paper of Williams, allowed the authors to fit directly all five independent tensor parameters ($g_{ax}^{eff} = (g_z^{eff})^2 - {}^1/_2[(g_x^{eff})^2 + (g_y^{eff})^2]$; $g_{eq}^{eff} = (g_x^{eff})^2 - (g_y^{eff})^2$; and the three Euler angles α, β, and γ). Again, the optimal fit resulted in a *z* axis for the g^{eff} tensor congruent with the Met 80 S–Fe bond and passing through the sulfur atom at 0.07 Å from its apparent center of mass. The *x* and *y* axes closely match the natural heme axes defined by the pyrrole nitrogens. The g^{eff} tensor in tuna ferricytochrome, previously computed by Williams et al.[402] using 21 assigned methyl groups as a reference set, was recalculated by the present method for the two crystallographically independent molecules (inner and outer) in the unit cell of the tuna ferricytochrome *c* crystal, using as reference the reported redox-dependent shifts of 12 assigned C_α protons.[466,538] The parameters found are impressively similar to the horse protein g^{eff} tensor refined with many more protons (64 protons). The magnitudes of the three principal g^{eff} values cannot be individually determined by the present calculation alone, but require a third constraint from an independent measurement. With the value of the reported rotation-averaged susceptibility of horse ferricytochrome c in solution at 20 °C these individual g^{eff} values have been obtained. The g^{eff} values are close to those calculated by Williams et al. using the foz and soz corrections, indicating the importance of the latter contribution.[402] The refined g^{eff} tensor was used to calculate pseudocontact shifts at over 400 positions (for a total of 600 assigned protons) in horse ferricytochrome *c*. The list of protons was then screened for redox-dependent chemical shift changes that could not be explained by the pseudocontact contribution. Only small structural adjustments due to redox-dependent strain rather than sizable structural displacements or rearrangements are proposed.

The analysis of the pseudocontact shift contribution allowed the evaluation of the true contact shifts for the heme group and its covalently linked residues and ligands.[403] The contact shifts around the heme reveal a highly asymmetric distribution of unpaired electron spin. Substituents on one diagonal (pyrroles II and IV) exhibit much larger downfield shifts than those on the other (pyrroles I and III). Unpaired electron spin density appears not to extend significantly into the Cys 14 and Cys 17 substituents or even their bridging groups. Among the iron ligands, the Hγ and Hϵ of Met 80, which are two bonds away from the sulfur atom, show large upfield contact shifts, while the Cβ experience very small contact contribution. Similarly, for the His ligand the most affected protons are the two nonexchangeable protons of the imidazole ring.

Pseudocontact shifts for protons of yeast iso-1-cytochrome *c* have been also calculated[480] by using an optimized g^{eff} tensor and the X-ray crystallographic coordinates of the reduced form of yeast iso-1-cytochrome. The optimization has been performed on the five parameters g_{ax}, g_{eff}^{eff}, α, β, and γ. The optimized g^{eff} tensor components differ little from the values determined by others.[402,403] The β angle was tilted by 9° from the heme normal, i.e. it has been found again to be tilted in the direction of the Met 80–Fe axis. g_x^{eff} and g_y^{eff} remain aligned along the pyrrole nitrogens of the heme. Although the agreement between experimental and calculated values is very good, there are places along the backbone where differences are very much greater than the experimental error in paramagnetic shift (±0.02 ppm). This has been explained by slight movement of the heme and small rearrangements of a few residues. Moreover, considerable changes in a few hydrogen bonds have been proposed.[480]

The NMR characterization of the F82S and N52I variants of yeast iso-1-cytochrome *c* in both oxidation states has been also reported.[483] Changes in the chemical shifts of heme and amino acid protons upon substitution of serine for phenylalanine at position 82 are analyzed in terms of ring current, contact, and pseudocontact shifts. Changes in NOEs are then discussed in terms of structural changes. Calculation of the pseudocontact shifts for the mutant were made by using the derived proton coordinates from the crystal structure of the reduced wild-type protein. The five calculated tensor parameters are essentially the same as for the wild-type protein. Changes in chemical shift between homologous protons of the two reduced variants have been explained by a direct and an indirect effect. The former results from the substitution of phenylalanine by serine at position 82, while the latter by reorganization of other diamagnetic fields. However, in the case of the oxidized protein there is a greater number of protons that exhibit significant differences. These protons are mainly located in a region characterized by a greater flexibility in the oxidized state also in the case of the wild type. The mutation at position 82 appeared to increase the conformational differences between the oxidized and reduced proteins. From the results obtained on the F82S mutants the authors suggested that the shift probe has the highest sensitivity for changes in hydrogen bonding, the NOE approach being less sensitive or even misleading due to changes in relaxation properties. Also in the case of the N52I mutant[484] the five best fit tensor parameters do not differ significantly from those reported for the other ferricytochromes *c*. From the comparison of the chemical shift data for the oxidized and reduced mutant with the corresponding forms of the wild-type protein, major regions of change can be located: the mutant and the wild-type protein differ in many respects, independently of the oxidation state. There are a small number of discrepancies between the observed and the calculated shifts in the mutant with respect to the wild-type protein, suggesting a smaller redox state change in the N52I variant. It was previously proposed for the wild-type protein that the redox state change is coupled with a rearrangement of a proton network which runs through the cytochrome *c* molecule.[480] The N52I

substitution breaks this hydrogen-bond network. Indeed, the smaller extent of variations observed between the reduced and oxidized form in the mutants seems to support the breaking of this coupling between the redox state of the iron center and the protein rearrangement.

The assignments for the ferricytochrome b_5 have been extended to provide approximately 260 proton resonances.[539] With the same procedure employed for the cytochrome *c* case, $\mathbf{g}^{eff}$ tensor components and axes have been calculated and used to evaluate the pseudocontact shifts. At variance with the cytochrome *c* case, the possible redox-linked conformational changes have been found to be minimal. Some local mobility has been detected for certain residues.

It should be pointed out that all the above calculations assume no change in the position of the heme group with oxidation state. The $\mathbf{g}^{eff}$ tensor fitting procedure will obscure any change in the heme position. However, from the dipolar shift equation it is clear that for a given value of $\mathbf{r}$ there is extreme sensitivity of the shift at those angles where the shift changes sign. The inspection of the sign changes for the observed and calculated pseudocontact shift values along the amino acid sequence has been proposed as a method to determine heme position variation.[484] For cytochrome b_5 there is only one disagreement in the location of a sign change along the amino acid sequence between calculated and experimental values out of a total of 12 such changes.[540] This has been taken as indicative of a fixed heme position in the two oxidation states. For wild-type cytochrome *c*, where the shift changes sign 30 times along the sequence, there are sign differences between calculated and observed values in 15 locations.[483] The authors suggested that in this case the heme moves slightly from the reduced to the oxidized state. On the basis of the few discrepancies in sign observed for the N52I mutant, only small changes in the heme position have been proposed for the mutant.[484]

The above reported approaches separate directly the effects of structural differences between either the oxidized and reduced forms in solution but could suffer from differences between the oxidized or the reduced protein in solution and in the crystal. An alternative method proposed to calculate the magnetic axes in horse heart oxidized cytochrome *c*[427] is based on the MATDUHM procedure described for *G. japonicus* metMb–CN^-. The angle between the *z* axis and the heme normal was found to be 9.5° and the *z* axis forms angles of 9.9° and 12.5° with the Fe–His 18 and Fe–Met 80 bonding vectors, respectively. Therefore the orientation of the *z* axis with respect to the heme appears to be different from that above reported. This disagreement may be explained in terms of the nature of the two methodologies. In MATDUHM only the heme methyl groups are used in the calculation, while the other procedure is based on a large subset of nonbound residue proton assignments. A novel approach which employs a large number of ^1H and ^{13}C shifts has been recently proposed.[541] The basic idea is that, if there is a conformational change on going from the reduced to the oxidized state, there will be a difference in the diamagnetic screening constant which will be reflected in a deviation from the fitting of the pseudocontact shift through eq 47. The diamagnetic shift of ^{13}C resonances is much more sensitive to the environment than that of ^1H resonances. Using sets of data obtained at different temperatures the authors proposed a separation of diamagnetic and paramagnetic contributions, the former being *T* independent. The susceptibility tensor parameters resulting from this fitting procedure are in good agreement with those obtained from studies of protons alone.

Pseudocontact shift calculations have been mainly developed over the last few years because the determination of reliable magnetic susceptibility tensor values and orientations requires extensive assignments for non-heme bound residues. These can be accomplished with the new high-field instruments and advanced 2D techniques. On the contrary, a rationalization of the contact shift contribution for the protons of the heme substituents has been attempted since the beginning of the paramagnetic NMR. The contact shift is the main shift contribution for these nuclei. The various proposed explanations for the contact shift patterns observed in the different low-spin heme proteins have been summarized and discussed by Satterlee.[307] The factors contributing to the contact shifts in the various heme positions are due to the heme ligand orientation and heme peripheral contacts. The latter have been investigated in those systems which contain noncovalently bound heme, by reconstituting the apoproteins with selectively modified hemins and have been reviewed in the single cases. The interaction with the axial ligands has been proposed as the dominating effect in determining the heme methyl shift pattern.[455,456,542,543] As discussed above, for low-spin globins and peroxidases, it is widely accepted that the orientation of the proximal histidine plane defines the electron-spin delocalization on opposite pyrroles. Models are available that demonstrate the capability of coordinated imidazole to spread pairwise the heme methyl resonances, when the rotational mobility of the coordinated imidazole is restricted.[307] In the case of *c*-type cytochromes, the orientation and conformation of the methionine ligand has been proposed to affect the unpaired spin density distribution on the heme *c*.[307] A correlation between the methionine chirality with the identity of the high-frequency heme methyl resonance pair for a large number of cytochromes has been found, suggesting that the imidazole plane of the proximal ligand retains the same orientation in the various proteins.[307] Moreover, a linear correlation has been found between the chemical shift of the methionine ligand methyl signal and the sum of the chemical shifts of the four heme methyl signals.[544] A theoretical explanation for this correlation is complicated by the nonnegligible contribution of the pseudocontact term to the shift of the heme methionine methyl. However, an analysis of the EPR spectra shows that the $\mathbf{g}_z$ value, which is the primarily responsible for determining the pseudocontact contribution to the methionine methyl chemical shift, is essentially the same for different cytochromes *c*. For this correlation the chirality of the methionine ligand is not important because proteins of known chirality appears in random position in the plot. Also the strength of Fe–S bond does not vary significantly in the different proteins. The orientation of the lone pair has been proposed to be the determining factor.[544] Changes in the orientation of the lone pair

result not only from changes in the chirality but also from a simple rotation about the Fe–S bond. The asymmetry in the distribution of the delocalized unpaired electron onto the heme macrocycle in horse cytochrome *c* has been calculated using the ^{13}C Fermi contact shifts.[545] (See also section IX.) The calculation makes use of the magnetic susceptibility tensor previously obtained to determine the pseudocontact shift contributions.[541] Whereas the total spin delocalization is almost temperature independent, the asymmetry of the distribution changes significantly with temperature.[545] This is the origin of the anti-Curie effect observed in ^1H NMR spectra of several cytochromes.[503,545–549] In those proteins methyls 3 and 8 exhibit a normal Curie behavior with temperature, whereas the shift of methyls 1 and 5 increase with temperature. This anti-Curie effect has been explained by a Boltzmann distribution between the two partially filled molecular orbitals containing the d_{xz} and d_{yz} iron orbitals, with an energy difference of 3 kJ M^{-1}.[545] For *b*-type cytochromes some features of the EPR spectra have been proposed to be due to variable relative orientations of the two axial histidine planes. Whereas in cytochrome b_5 the two planes are nearly parallel,[550] for b_{566}, b_{562}, b_{559}, and b_6 an almost perpendicular relative arrangement for the two aromatic rings has been proposed on the basis of results obtained for model compounds[551] (and references therein). In the case of cytochrome c_3 from *Desulfovibrio vulgaris* (Hildenborough) the different heme methyl shift patterns for the various hemes have been proposed to be determined by the different orientations of the axial histidine ligands.[534] Hemes I and IV are both characterized by almost coplanar axial imidazole rings, but whose orientations with respect to the heme plane differ by almost 180°. These two hemes display a pairwise inverted order of the chemical shift for the methyl groups: 8 > 1 > 5 > 3 versus 5 > 3 > 8 > 1. It is interesting to note that these heme methyl shift patterns differ from those commonly shown by other heme systems characterized by the pairs 8,3 and 5,1 or 5,1 and 8,3.[7,307] However, it should be considered that the spin distributions on individual hemes can be complicated by cross interactions.

e. Cytochrome c Oxidase. Bovine mitochondrial cytochrome *c* oxidase is a dimeric metalloprotein (MW 2 × 200 000) of the mitochondrial inner membrane. Owing to the large molecular weight this system has not yet been studied by NMR. Only a spectrum of the cyanide bound adduct of the monomeric form of cytochrome *c* oxidase has been reported.[552] It consists of two very broad resonances centered at 30.5 and 24.8 ppm, attributed to methyl substituents of heme *a*.

8. Ferric Chlorin Containing Proteins

^1H NMR has been used to study the hyperfine-shifted resonances of the sulfite reductase from *Desulfovibrio vulgaris* (Hildenborough).[553] The active site is constituted by a siroheme chromophore connected to a ferredoxin-like Fe_4S_4 cluster through a sulfur ligand. The heme iron atom is hexacoordinate low spin in the *Desulphovibrio vulgaris* species (Figure 81A). The spectrum is reported in Figure 81B–D. Seven downfield shifted single proton resonances are present in the 25–12-ppm region. A broad resonance is present at 90 ppm. In the upfield region several signals are detected in the −2 to −14 ppm range. No specific assignments are available. However, this shift range is typical for low-spin heme iron and oxidized ferredoxin species, except for the resonance at 92.5 ppm. It has been proposed that this signal originates from a proton of a β-CH_2 group of a cysteine ligand and that its shift is the effect of the coupling between the siroheme and the Fe_4S_4 cluster on a cysteine proton characterized by a very small Fe–S–C–H dihedral angle. Also the absence of the anti-Curie behavior typical for oxidized ferredoxin cysteines has been attributed to the magnetic coupling. The lack of methyl resonances in the downfield region has been explained by negligible spin density on the pyrrole rings to which the methyl groups are bound, the pyrroles being partially saturated. The presence of the broad upfield signal at −13 ppm has been taken as indicative of a histidine residue as the sixth axial ligand of the siroheme iron.

C. High-Spin Iron(II)

The iron(II) ion in high spin state ($S = 2$) is present in pentacoordinate porphyrin systems.[554] In model compounds, the intermediate spin state $S = 1$ has been observed in the absence of axial ligands.[554] The presence of a $S = 1$ ferrous state in a natural system has been proposed only for one-electron-reduced sulfite reductase from *E. coli*.[401] In this case, however, the prosthetic group is not a porphyrin but a reduced hydroporphyrin. The binding of two axial nitrogens or of one nitrogen and one sulfur axial atom produces low-spin diamagnetic species.[554] Diamagnetic species are obtained also upon dioxygen or carbon monoxide binding in the sixth coordination site.[554,555] The small phenyl proton shifts observed in synthetic tetraphenylporphyrin derivatives has been taken as an indication of negligible pseudocontact shift contributions.[308] For model compounds large downfield pyrrole proton and α-CH_2 shifts and small upfield meso proton shifts have been observed. These data have been interpreted as due to a large amount of σ delocalization onto the pyrrole position and a moderate amount of π delocalization onto the meso position.[308] A shift pattern characterized by a large amount of σ delocalization onto the pyrrole positions and moderate π delocalization to the meso positions has been also found in high-spin iron(III). Two possible electronic configurations have been proposed for high-spin iron(II) (Figure 82, parts A and B) on the basis of the fact that both low-spin iron(III) and intermediate spin iron(II) appear to have d_{xy} lower in energy than d_{xz} and d_{yz} and also on the basis of ^{13}C data, scheme A seems more probable.[308,406,556,557] However, the large variability in shift patterns may be related to different electronic ground states. Assignments of the individual methyl groups revealed that the spread of the methyl signals increases as the electron-withdrawing power of the 2,4 substituents increases.[406,556]

The far downfield region of the ^1H NMR spectra of sperm whale deoxyMb and deoxyHb A are reported in Figure 83. La Mar et al.[406] have attributed some of the downfield signals to the proximal histidine ligand, on the basis of the results obtained for model compounds.[406,556] In the case of sperm whale deoxyMb, a relatively narrow exchangeable proton was observed at 78 ppm and attributed to the Hδ1 of the proximal

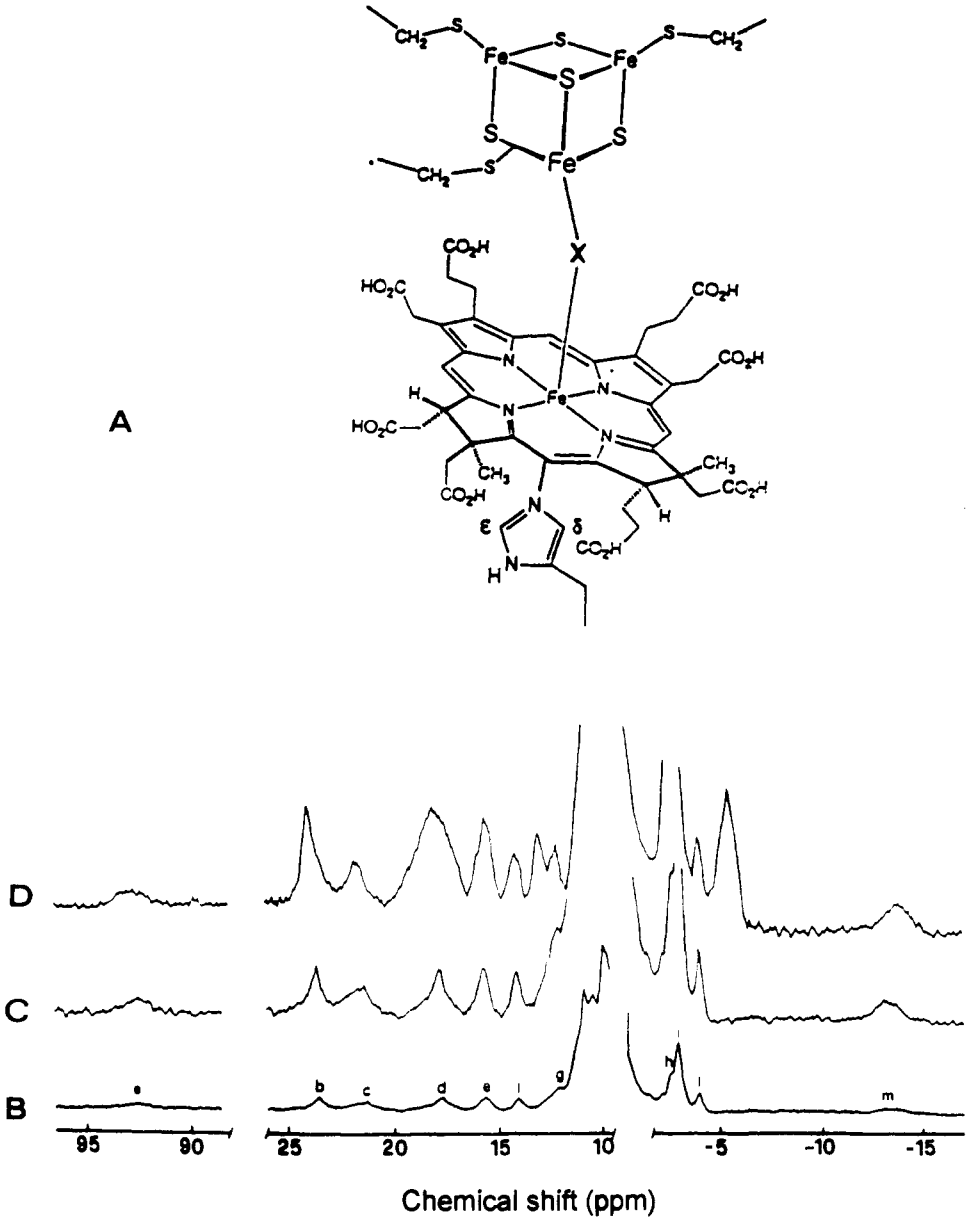

Figure 81. (A) Schematic representation of the exchange-coupled $[Fe_4S_4]$–siroheme in the active site of assimilatory sulfite reductase (*Desulfovibrio vulgaris*) with the proposed histidine axial ligand (the bridging unit X has been proposed as sulfite) and 500-MHz ^1H NMR spectra at 296 K in 0.1 M sodium phosphate buffer, pH 7.0: (B) in D_2O solution; (C) spectrum as in B but with a 4-fold increased vertical scale; and (D) in H_2O solution. (Reprinted from ref 553. Copyright 1990 American Chemical Society.)

ligand.[406] A broad resonance at 46 ppm, with relative intensity of two protons was proposed to originate from the Hδ2 and Hε1 of the same residue. Analogous exchangeable signals were detected at 75.9 and 63.9 ppm for deoxyHb A and attributed to the proximal histidine Hδ1 in the two subunits.[406] The resolution of two such Hδ1 signals in deoxy Hb A has been taken as a direct evidence for slight structural differences in the α and β subunits. The comparison of the spectra of the synthetic hybrids, $\alpha_2(\beta^+CN)_2$, $(\alpha^+CN)_2\beta_2$ of hemoglobin A and the natural valency hybrids of the Boston, Iwate, and Milwaukee deoxyhemoglobins have led to the unambiguous assignment of the two proximal histidine Hδ1 signals at 64 and 76 ppm to individual α and β subunits, respectively.[342] With the same method the assignment of the hyperfine-shifted signals in the 18–6-ppm range to the α and β chains of the normal human adult deoxyHb has been accomplished.[558] A single-proton intensity nonexchangeable resonance detected

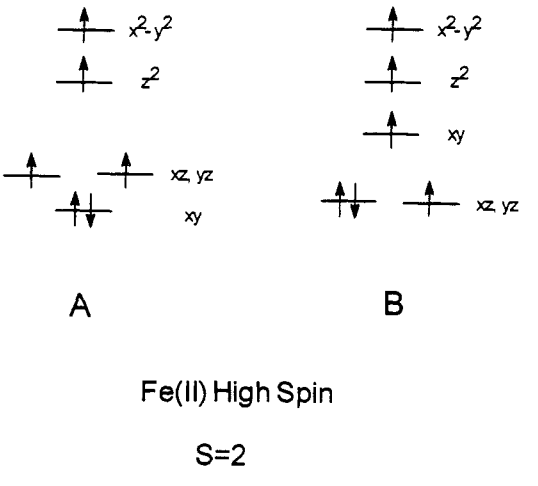

Figure 82. Proposed electronic configurations for the high-spin heme iron(II).

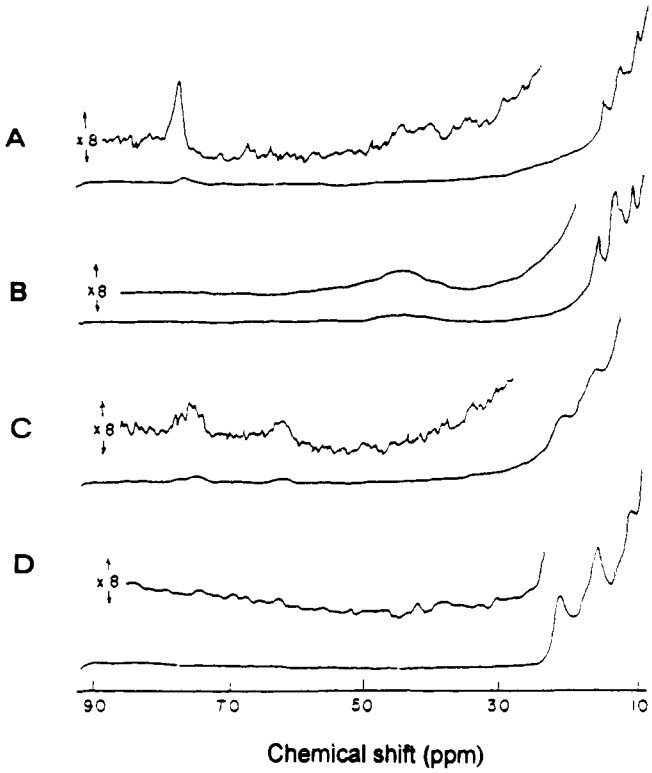

Figure 83. ^1H NMR spectra (99.5 MHz) of (A) sperm whale deoxymyoglobin in H_2O solution, 0.2 M NaCl pH 6.8; (B) sperm whale deoxymyoglobin in D_2O solution, 0.2 M NaCl pH 7.0; (C) deoxyhemoglobin A in H_2O solution, 0.2 M NaCl pH 6.0; and (D) deoxyhemoglobin A in D_2O solution, 0.2 M NaCl pH 6.3. All the spectra were recorded at 298 K. (Reprinted from ref 406. Copyright 1977 Academic.)

in the extreme downfield region of the spectra of Boston and Iwate Hbs has been tentatively proposed to originate from the coordinated tyrosine of the mutated α chains.[342] The ^1H NMR spectra of three monomeric deoxyHbs of *Chironomus thummi thummi* have been assigned by deuterium labeling. The assignments for two of these Hbs are reported in Table XI.[86] It is interesting to note that two of the heme methyl resonances appear downfield and the other two upfield. Moreover, the exchangeable proximal histidine proton experiences a hyperfine shift (90–95 ppm) larger than those observed in deoxyMb or tetrameric deoxyHb, suggesting a stronger iron–imidazole bond. Indeed, studies on model compound have pointed out that the shift of this proton arises primarily from iron–imidazole σ bonding.[406,556] Minor peaks indicative of heme rotational disorder have been detected,[86] as in the Hb–CN$^-$ case.[522,523]

From the pH dependence of the hyperfine-shifted signals of the heme substituents in *C. thummi thummi* Hbs, an apparent pK_a around 8 has been found, which indicates that the T $\leftrightharpoons$ R transition, as modulated by the Bohr proton, is being observed.[86] The proximal histidine environment remains essentially unaffected by the T $\leftrightharpoons$ R transition. On the contrary, a correlation between Hδ1 shifts and protein structure was found for the tetrameric Hbs. For three chemically modified Hbs which exhibit the R $\leftrightharpoons$ T transition, the Hδ1 shifts for the two subunits are the same in the R state, but that of the α subunit decreases by 10–12 ppm upon converting to the T structure. This has been interpreted

Table XI. Observed Shift Values at 298 K for Native Monomeric Deoxyhemoglobins of the Insect Larve *Chironomus thummi thummi* (from Ref 86)

	chemical shift (ppm)	
heme proton	Hb III	Hb IV
proximal His[a]		
Hδ1	92.2	91.0
Hδ2	*b*	32[c]
Hϵ1	*b*	51[c]
heme[d]		
2,4-Hα	21.11	21.59
6,7-Hα[e]	18.15	18.95
1-CH_3	14.30	16.2[f]
3-CH_3	13.64	15.9[f]
5-CH_3	−2.35	−3.58
8-CH_3	−3.75	−6.25
2,4-Hβ[g]	12.2	13.9

[a] The assignments are based on the comparison with model compounds. [b] Insufficient signal-to-noise to observe the signal. [c] The shifts were measured at 318 K, where the resolution is considerably improved. [d] The assignments are based on selective deuteration experiments. [e] No direct proof for this proposed assignment is available. [f] Assigned in analogy with the Hb III isoenzyme. [g] Deuterium labeling of vinyl Hβs reduces the intensity of the composite peak at about 12 ppm, suggesting that at least one Hβ resonates in this region.

in terms of some strain imposed on the Fe–N bond in the α subunit, with the result that less σ spin density is transferred to the imidazole.[559] The effects of pH have been studied also for Ru–Fe hybrid Hbs.[560] Selective effects on the exchangeable proton shift values for the different subunits have been detected also upon pressurization.[353] The importance of a hydrogen bond between a Tyr and an Asp residue at the subunit interface, considered a key interaction for the allosteric transition of Hb, has been studied. The ^1H NMR spectra of the ferrous forms of mutants in which the Tyr have been substituted by Phe and His show a substantial downfield bias as compared with native Hb A. This has been proposed to originate from a less strained configuration which favors the electron-spin delocalization from the iron to the imidazole.[561] The shift values observed for the Hδ1 proton in various Hbs have been summarized by Satterlee.[307] However a comparison between different proteins is difficult because the Hδ1 shift reflects a combination of changes in bond distances, angles, and NδH hydrogen bonding, whose effects are difficult to factorize.

In reduced Mb from different sources two heme CH_3 and the α-CH_2 signals have been identified in the downfield region by ^1H and ^2H NMR spectra on protein reconstituted with specifically deuterated hemes,[562] by 1D and 2D ^1H NOE experiments,[563,564] and protein-decoupling ^{13}C NMR experiments.[565] The spectrum of *Aplysia limacina* deoxyMb is reported in Figure 84. At variance with sperm whale and horse deoxyMb, one downfield and three upfield heme methyl resonances are detected.[566]

Temperature and pH dependence studies on the hyperfine-shifted resonances of sperm whale and horse deoxyMb have been formed.[567] Recording the spectra at different temperatures allowed the resolution of many overlapping signals: most of them follow a T^{-1} dependence, but exhibit intercepts significantly outside the diamagnetic envelope. Above pH 7 the shifts are essentially independent of pH. The fitting of the pH

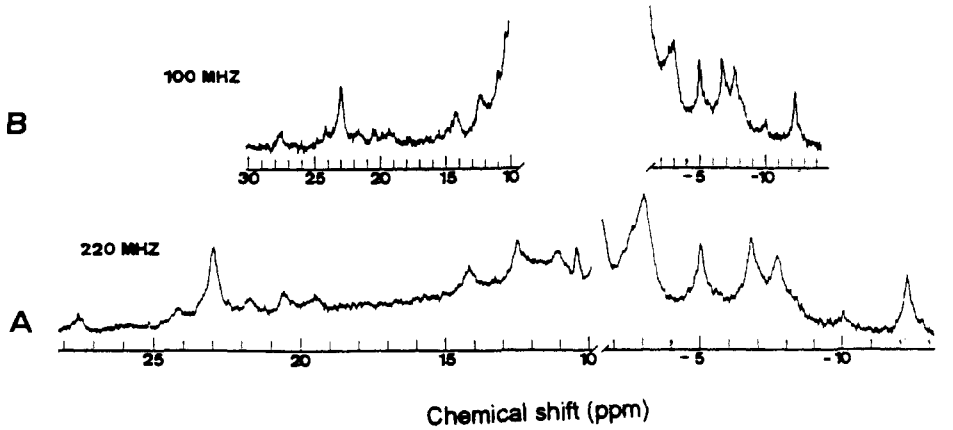

Figure 84. ^1H NMR spectra of *Aplysia* myoglobin recorded at 295 K in D_2O solution: (A) 220 and (B) 100 MHz. (Reprinted from ref 566. Copyright 1977 American Chemical Society.)

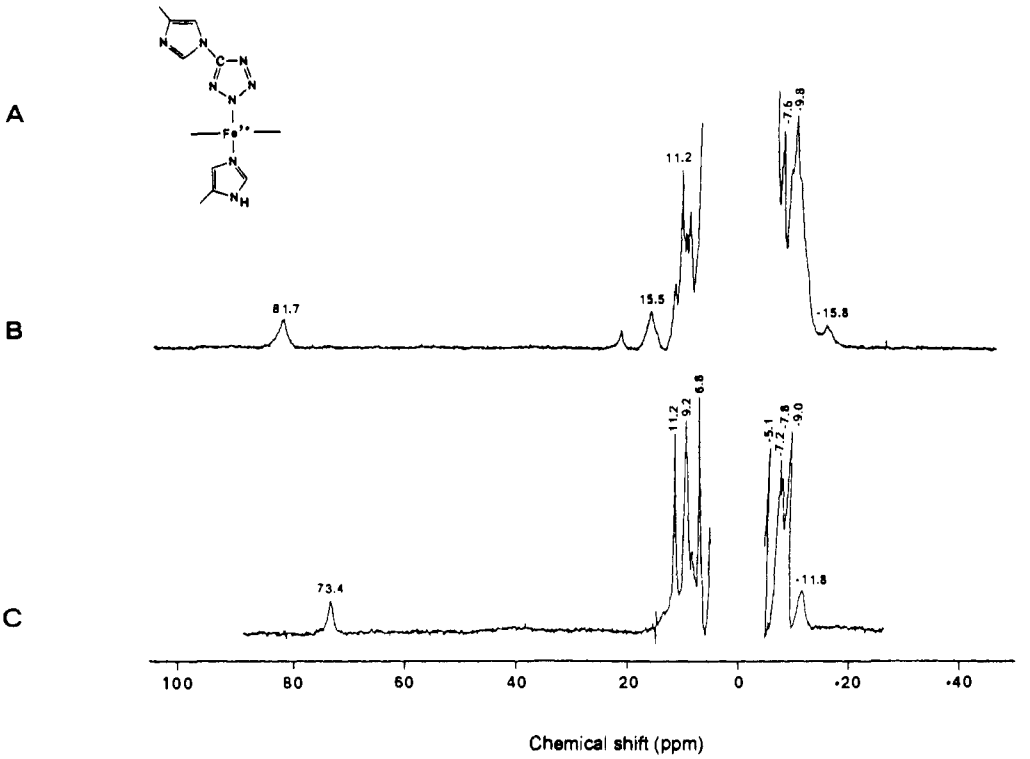

Figure 85. Schematic representation of *N*-tetrazole Mb, and 300-MHz ^1H NMR spectra of the deoxy forms of (B) *N*-tetrazole Mb and (C) native Mb. Both the spectra were recorded at 296 K in H_2O solution, pH 7. (Reprinted from ref 568. Copyright 1992 American Chemical Society.)

dependence of the signals below pH 7 resulted in pK_a values of 5.7 and 5.6 for sperm whale and horse Mb, respectively. The area of the exchangeable proton remained constant up to pH 9.5, indicating a pK_a for its deprotonation greater than 10.

Chemical modification of Mb by a stoichiometric amount of BrCN afforded a modified species in which the ϵ nitrogen of the distal histidine is N-cyanated. It has been reported that further addition of azide produces a ferric low spin complex in which a *N*-tetrazole-substituted His is present and coordinated to the heme iron (Figure 85A).[568] The ^1H NMR spectrum of the species obtained by addition of dithionite is typical for the deoxy form and is reported in Figure 85B. An exchangeable proton signal at 81.7 ppm corresponds to the proximal histidine Hδ1 at 73.4 ppm of the native deoxyMb (Figure 85C). The spectrum clearly indicates that the tetrazole ring dissociates from the heme iron upon reduction to produce a pentacoordinate species.[566] It is noteworthy that a modification in the distal cavity is reflected in an 8.3 ppm difference in the shift of a proximal histidine proton.

An estimation of the electron relaxation time values for deoxyHb and deoxyMb has been reported. From the field-independent part of T_2^{-1}, a τ_s value of 6×10^{-12} s has been proposed for both the proteins.[569] Moreover, on the basis of T_1 measurements a τ_s value of 7×10^{-13} has been estimated for deoxyHb[570] and deoxyMb.[563] It is important to consider that in both cases the ligand-centered contributions have been completely neglected.

The ^1H NMR spectrum of ferrous HRP has been partially assigned by using selectively deuterated hemes.[571] The vinyl Hα and the 5-, 8-, and 3-CH_3 resonances have been located in the downfield region in the 25–10 ppm range. The spectrum changes with pH according to a pK_a of 7.5. The alkaline and the acidic forms are in slow exchange on the NMR time scale. This is clearly apparent from the spectrum

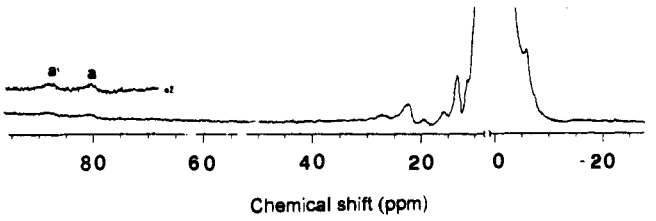

Figure 86. ^{1}H NMR spectrum (200 MHz) of ferrous HRP recorded at 298 K in H_2O solution, pH 7.5. (Reprinted from ref 571. Copyright 1982 American Chemical Society.)

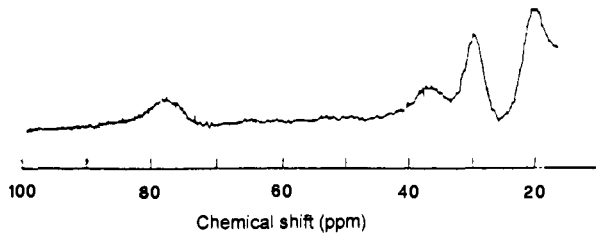

Figure 87. ^{1}H NMR spectrum (200 MHz) of the reduced form of spleen green heme protein recorded at 298 K, pH 5.0. The upfield region has never been reported. (Reprinted from ref 375. Copyright 1987 Elsevier.)

reported in Figure 86: the proximal histidine Hδ1 signals of both the forms are clearly detected in the region 90–75 ppm. Their shift values have been taken as an indication of the degree of hydrogen bonding between the proximal ligand and the proximal aspartate. The 7–8 ppm higher shift in the alkaline species has been taken as proof of a stronger hydrogen bond in the acidic than in the alkaline form of the protein. This is based on the assumption that the fractional decrease in the interaction of the Hδ1 with the imidazole spin density is larger than the fractional increase in iron-to-imidazole σ spin transfer.[571] In deuterioheme reconstituted HRP two resonances have been detected at 41 and 57 ppm and attributed to the Hδ2 and Hϵ1 proximal histidine protons in analogy with model compounds.[571]

Examination of reduced *Coprinus* peroxidase by NMR spectroscopy reveals that the protein is pentacoordinate in the reduced state. Resonances are observed at 67.0, 22.7, 21.7, 17.7, −2.8, and −6.6 ppm. The signal at 67 ppm is due to an exchangeable proton assigned as NHδ1 of the proximal His.[332]

The 200-MHz ^{1}H NMR spectrum of ferrous spleen green heme protein is reported in Figure 87.[375] By analogy with the other heme proteins, the resonance at 18 ppm has been tentatively attributed to a heme methyl group and the signal at 76.1 to the Hδ1 of the proximal histidine.

High-spin ferrous P450 is formed by electron transfer to the high-spin ferric state during the catalytic cycle. The first NMR spectrum (at 220 MHz) of ferrous P450 was reported by Keller et al.:[379] they observed three resonances in the region 27–17 ppm. A more extensive study on this species has been recently performed.[380] In the spectrum obtained at 300 MHz (Figure 88) four three-proton intensity resonances are observed in the 30 to −15-ppm region. Other signals of intensity one are observed in the same shift range. Particular attention has been devoted to a broad signal at 279 ppm. On the basis of comparison with the proton NMR spectra for high-spin porphirinatoiron(II) thiolate model compounds, this proton resonance is assigned to the axial β-CH_2 cysteinate protons, but it was not possible to decide if this signal with a line width of several thousand hertz is due to one or two of these β-methylene protons.[380] Specific assignments for the hyperfine-shifted signals in cytochrome P450 are not available. The application of 1D NOE and 2D NOESY experiments is more difficult than in the Mb case due to the shorter relaxation times.[563] The faster longitudinal relaxation rates have been proposed to be due to electron relaxion times about 2.5 times longer than in Mb,[563] whereas Curie relaxation strongly contributes to the transverse relaxation times in this higher molecular weight protein.

The 300-MHz ^{1}H NMR spectrum of reduced chloroperoxidase does not have as many features resolved as its cytochrome $P450_{cam}$ counterpart:[380] two broad signals are observed in the spectrum obtained at pH 5.8 and 296 K at about 25 and −7 ppm (Figure 89). A very broad resonance is observed at about at 205 ppm. The use of a particular shaping function facilitates observation of a very broad feature at 250 ppm. At variance with $P450_{cam}$, there are detectable changes in the NMR spectrum between pH 4.1 and 6.7. The shift differences for the large downfield resonances and the different behaviors with pH have been proposed to reflect subtle differences between the active sites of cytochrome P450 and chloroperoxidase.[380]

The spectrum of the reduced cytochrome *c* oxidase has been also reported: the only paramagnetic metal center is represented by the a_3 heme moiety. Poorly resolved broad resonances are present downfield in the 40–10 ppm range. An exchangeable proton attributed to the proximal histidine Hδ1 has been detected at 73.5 ppm.[572]

Among hexacoordinate cytochromes, which upon reduction yield diamagnetic species, cytochrome *c″* from *Methylophilus methylotrophus* represents an exception. On the basis of low-temperature EPR and MCD data, ferricytochrome *c″* has been found to possess two axial histidine ligands, with perpendicular orientation of the imidazole rings.[573] Upon reduction, a ^{1}H NMR spectrum typical for a high-spin heme iron(II) species is obtained, indicating that one of the axial histidines is detached from the coordination site.[574,575] The spectrum is reported in Figure 90: several broad resonances are observed in the 35 to −20 ppm region. Three-proton intensity signals are present at 28.6 and 26.9 ppm; a six-proton intensity resonance at −14.8 ppm has also been observed and attributed to two overlapping methyl signals. An exchangeable proton signal has been observed at 83 ppm, indicative of the histidine nature of the axial ligand. Analogous to deoxymyoglobin and deoxyhemoglobin,[576] temperature-dependent line broadening has been detected for the hyperfine-shifted resonances. The spectrum is virtually unchanged between pH 5.2 and 7.1. Above pH 12 the spectrum shows signals with chemical shift range typical for diamagnetic compounds. This has been explained by hydroxide ligation in the sixth coordination site.[575]

The ^{1}H NMR spectra of several reduced cytochromes *c′* are available. The ^{1}H NMR spectrum of *Rhodospirillum rubrum* species is reported in Figure 91: three three-proton intensity resonances are present

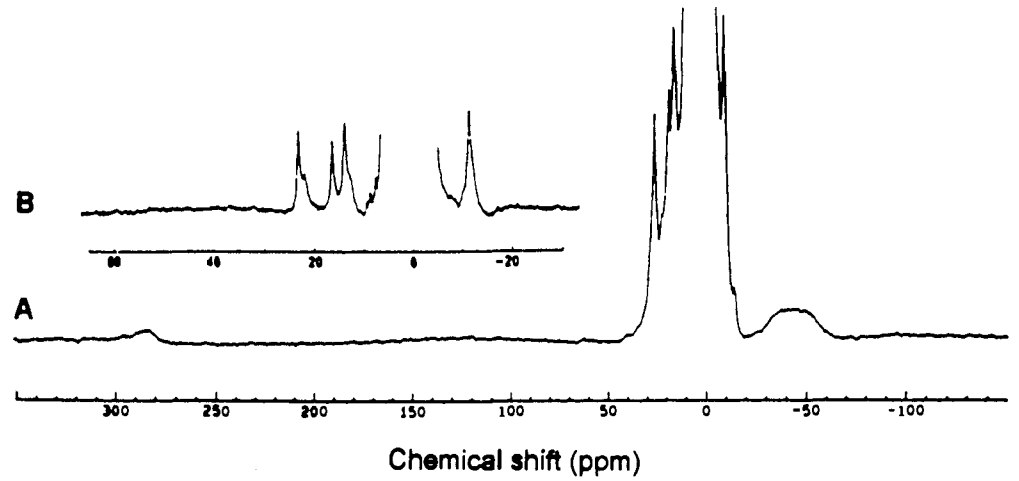

Figure 88. (A) ^{1}H NMR spectrum (300 MHz) of ferrous cytochrome $P450_{cam}$ recorded at 294 K in H_2O solution, 0.1 M phosphate buffer and 0.1 M KCl, pH 7.1, and (B) and expanded view of the 70 to −30 ppm region (from ref 380).

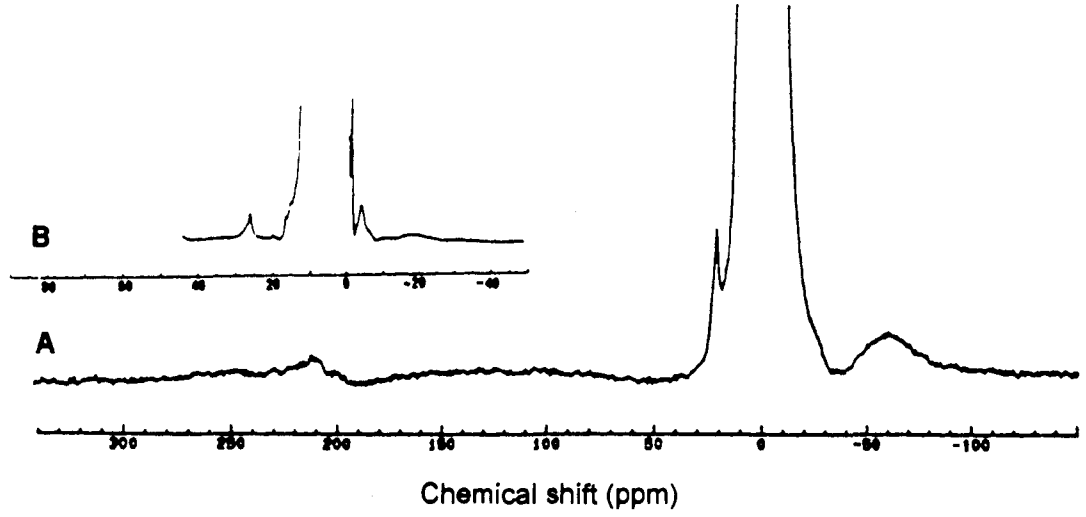

Figure 89. (A) ^{1}H NMR spectrum (300 MHz) of ferrous chloroperoxidase recorded at 296 K in H_2O solution, 0.1 M phosphate buffer, pH 5.8, and (B) and expanded view of the 90 to −50 ppm region (from ref 380).

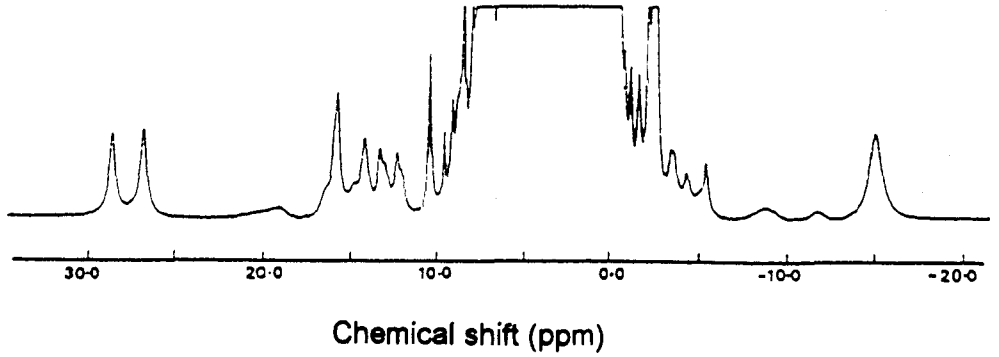

Figure 90. ^{1}H NMR spectrum (500 MHz) of ferrous cytochrome *c″*, recorded at 310 K at pH 6.4. (Reprinted with permission from ref 574. Copyright 1988 Elsevier.)

upfield and one downfield.[392,393] Ferrocytochrome *c′* from *Rhodopseudomonas palustris* has been reported to possess an analogous spectrum.[392] The two broad resonances observed at 33 and 52 ppm in *Rhodospirillum rubrum* and *Rhodopseudomonas palustris*, respectively, have been proposed to originate from Hε1 or Hδ2 protons of the proximal histidine.[392] In the case of *Rhodospirillum rubrum*, an exchangeable signal has been observed at 93 ppm.[393] In the case of *Chromatium vinosum* ferrocytochrome *c′* methyl signals have been observed at 18.5, −7.5, −12.2, and −16.6 ppm at pH 7.2.[396] At pH values lower than 7 an exchangeable single proton resonance is present at 104 ppm. Again, in the *Rhodocyclus gelatinosus* ferrocytochrome c′, there are three methyl resonances in the upfield region and the fourth one in the downfield part of the spectrum (Figure 92A). Five additional signals of intensity one are present in the downfield region.[397] Nonselective T_1 values in the 60–20-ms range have been measured at 600 MHz for the proton signals of the heme substituents. Assignments of the hyperfine-shifted resonances have been obtained by NOESY experiments (Figure 92B) and confirmed by means of saturation transfer experiments from the oxidized species. These experiments

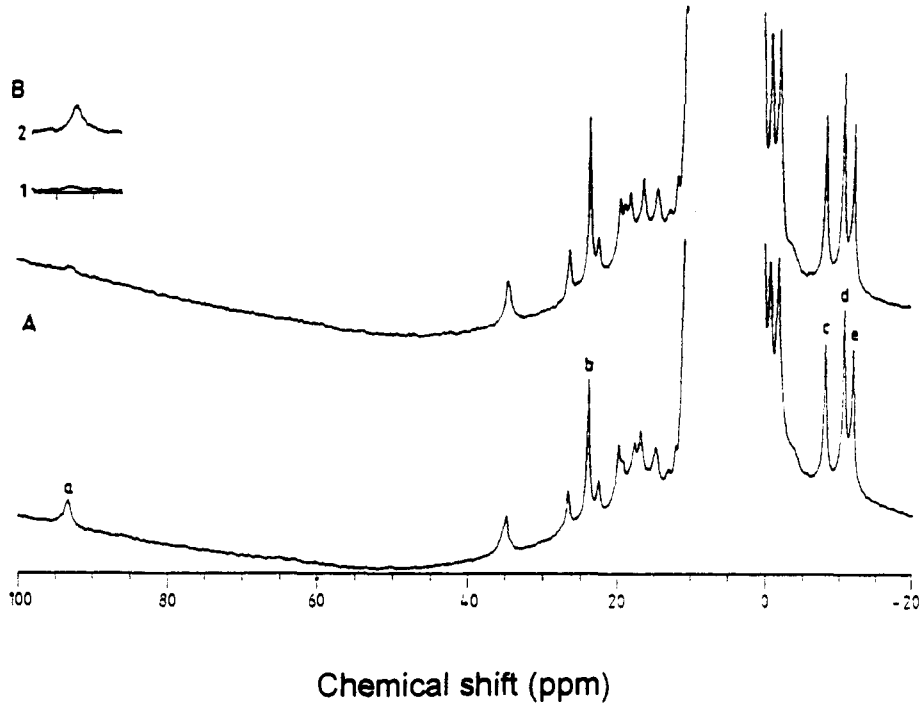

Figure 91. ^1H NMR spectra (200 MHz) of reduced *Rhodospirillum rubrum* cytochrome *c'*. The spectra were recorded at 298 K in H_2O solution at (A) pH 5.4 and (B) pH 5.9. The inset in B shows the 98–86 ppm region recorded at 360 MHz using the Redfield pulse sequence, with and without presaturation of the H_2O signal. These results demonstrate that the disappearance of the exchangeable signal at high pH is due to saturation transfer from the water via base-catalyzed proton exchange. (Reprinted from ref 393. Copyright 1981 American Chemical Society.)

represent the first 2D spectra of a ferrous high-spin protein.[397]

A comparison of the shift patterns in the different ferrous heme proteins indicates that in such cases in which the proximal histidine is oriented like in Figure 53B (i.e. Hb and Mb), two downfield and two upfield, or two downfield, one almost diamagnetic and one upfield methyl resonances are observed. This suggests a pairwise effect on the methyl groups as found in the ferric low-spin case, and therefore a significant π contribution to the shift. For HRP and cytochromes *c'* the situation is not exactly reversed, as expected on the basis of the 180° different orientation of the proximal histidine (Figure 53A). This suggests some fine modulations in the balance of σ and π contributions.

D. Other Oxidation States

Peroxidases perform the oxidation of their substrates according to the following catalytic cycle:

$$\text{ferriperoxidase} + H_2O_2 \rightarrow \text{compound I} + H_2O$$

$$\text{compound I} + AH_2 \rightarrow \text{compound II} + AH^{\bullet}$$

$$\text{compound II} + AH_2 \rightarrow \text{ferriperoxidase} + AH^{\bullet} + H_2O$$

where compound I and compound II are two and one oxidizing equivalents above the resting ferric state, respectively. The nature of these reaction intermediates has been extensively studied by several spectroscopic techniques. In the case of HRP electronic absorption spectroscopy,[577] magnetic susceptibility,[578] Mössbauer,[579–581] and resonance Raman[582,583] are all consistent with a compound II containing a low-spin (S = 1) iron(IV)–oxo species (ferryl group). A more complicated picture comes out for the electronic structure of HRP compound I. In this case magnetic susceptibility values of about 4 Bohr magnetons are indicative of $S = {}^3/_2$ ground state,[578] whereas the Mössbauer spectrum yields the same iron isomer shifts for both compounds I and II,[579–581] indicating that a low-spin iron(IV) is present also in compound I. The electronic absorption spectrum of compound I resembles that of a porphyrin cation radical.[577] Indeed, a radical has been detected by EPR and its considerable line width was attributed to the interaction with the paramagnetic iron center.[581,584] Several efforts have been devoted to the ^1H NMR characterization of these compounds, and particularly to the elucidation of the electronic structure of compound I. Models have been extensively investigated.[585–589]

The ^1H NMR spectrum of HRP compound I, obtained by addition of H_2O_2 to the ferric enzyme solution, is reported in Figure 93B. With respect to the native ferric state (Figure 93A) the resonances experience an upfield bias on going from ferric HRP to compound I. Three-proton intensity signals are observed at 76.1, 72.1, 59.1, and 50.1 ppm. Several one-proton intensity signals are resolved in the 50–11 and 0 to −22 ppm regions. The assignments of the heme resonance reported in Figure 93B have been obtained by selective deuteration and NOE experiments.[343,344,590] The line widths of these signals are rather narrow, compared with those for native HRP. Upon addition of *p*-cresol to the compound I solution, the spectrum of compound II is obtained (Figure 93C), characterized by a broad signal at about 14 ppm. The same spectrum is obtained also by addition of other aromatic substrates.[591–593] The

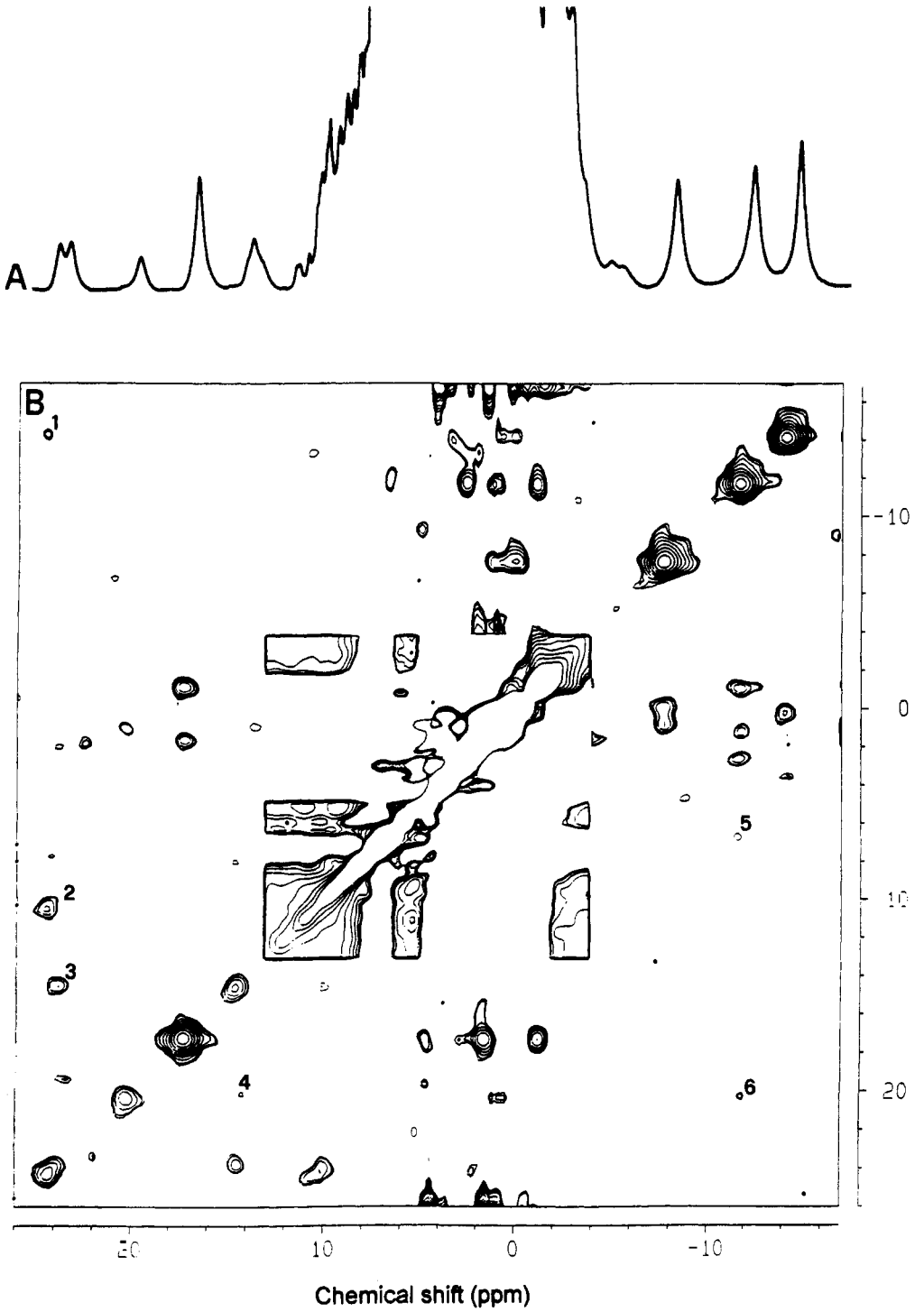

Figure 92. ^{1}H NMR reference spectrum (600 MHz) (A) and NOESY spectrum (B) of *Rhodocyclus gelatinosus* ferrocytochrome *c'*, recorded at 295 K, in D_2O solution pH 5.2. Cross peaks assignments are as follows: (1) 8-CH_3, 7-propionate Hα; (2) 7-propionate Hα, 7-propionate Hα'; (3) proximal histidine Hβ, proximal histidine Hβ; (4) 6-propionate Hα, 6-propionate Hα'; (5) 3-CH_3, proton of a Phe residue; (6) 5-CH_3, 6-propionate Hα. (Reprinted from ref 397. Copyright 1993 American Chemical Society.)

resonances of both compound I and II follow the normal Curie behavior in the 280–305 K temperature range.[592,593] The pH-dependent shifts for these intermediates afforded a pK_a value of 5.6, as in the case of the native ferric HRP.[591,593]

In Figure 94A the spectrum of sperm whale Mb treated with H_2O_2 is reported. Three hyperfine-shifted resonances are resolved in the downfield region, labeled a, b, and c. This spectrum closely resembles that of HRP compound II (Figure 94C).[591-593] For sperm whale Mb reconstituted with hemin deuterated at the meso position (Figure 94B), resonances a and b decrease in intensity by approximately 80%, corresponding to the degree of deuteration of the meso position.[594] On this basis a and b have each been assigned to a pair of unresolved meso protons. Comparison of the trace of HRP compound II (Figure 94C) with that of HRP compound II reconstituted with meso-deuterated hemin (Figure 94D) again shows that the downfield resonances a and b decrease in intensity. It has been proposed that a represents a single meso proton and b results from the remaining three.[594] On the basis of their much

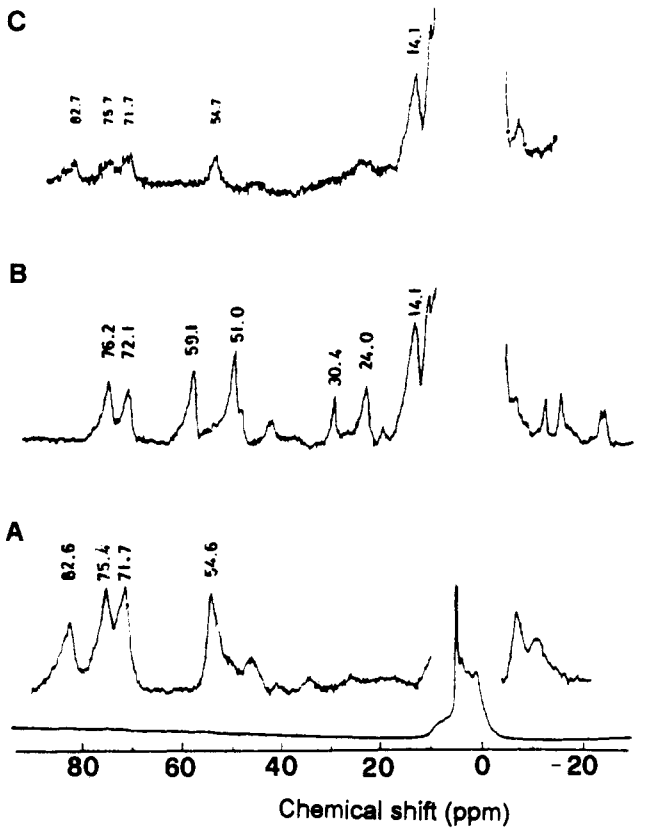

Figure 93. ^{1}H NMR spectra (220 MHz) of (A) resting-state ferric HRP, (B) HRP compound I, and (C) HRP compound II, contaminated with that of the resting enzyme. All the spectra were recorded at 293 K in H_2O solution, 2 mM borate buffer pH 9.2. (Reprinted from ref 592. Copyright 1978 American Chemical Society.)

smaller line widths, peaks c and d have been proposed to arise from amino acid residues. The unique spectral feature of showing only the resonances of the meso protons shifted outside the diamagnetic region has been found only for low-spin iron(IV)–oxo porphyrins possessing an axial imidazole.[594] Moreover, two broad resonances have been detected in the case of Mb at about −11 and −16 ppm and attributed to Hδ2 and Hε1 of the axial imidazole, in analogy with ferryl iron(IV) model compounds.[595] Therefore, the ^{1}H NMR data for H_2O_2-treated Mb and HRP compound II have been interpreted as a definite evidence for the presence of an iron(IV)–oxo species.[594,595]

For compound I the lack of hyperfine-shifted resonances due to non-porphyrin protons is proof of negligible pseudocontact shift contribution.[590] The spectrum was first reported by Morishima,[591-593] but the interpretation was very tentative. It was noted the similarity in the pyrrole-H shifts in high-spin iron(III) and iron(IV) model complexes and the fact that the heme methyl shifts in HRP and HRP compound I are similar. Later, by reconstituting HRP with deuteriohemin, La Mar et al. clearly demonstrated that the similarity in the methyl shifts of compound I and the shifts in high-spin iron(IV) model compounds is a coincidence not recognizable in deutero-HRP compound I.[596] The large downfield methyl and upfield proton shifts in deutero-HRP compound I (Figure 95B) have been proposed to be consistent with extensive spin delocalization primarily in the π system, as may be expected for a free radical. The differences in line widths between the spectra of HRP compound I and deutero-HRP compound I has been attributed to a different orbital ground state for the porphyrin radical in the two species. Indeed, while the a_{2u} orbital places the spin density on the meso position, the a_{1u} orbital puts the spin density primarily on the pyrrole Cαs, the latter accounting for the larger methyl resonance line width in deutero-HRP compound I.[596] By using selectively deuterated hemins the hyperfine-shifted signals in deutero-HRP compound I have also been assigned.[590] Whereas in HRP compound I the methyl shifts decrease in the order 8 > 3 > 5 > 1, for deutero-HRP compound I the order is 3 > 1 > 5 > 8. The pairwise interchange in the relative positions of 1-CH_3 and 3-CH_3 and 5-CH_3 and 8-CH_3 has been attributed to the fact that the heme orientations in HRP and deutero-HRP differ by 180° rotation about the α–γ meso axis.[519] While the hyperfine-shift pattern cannot eliminate iron(V), the resulting $^2A_{2g}$ ground state is very unlikely to lead to the rapid electron-spin relaxation implied by the highly resolved NMR spectra.[72,597] In HRP compound I, an effect is also observed on the line widths of methyl resonances 3 and 8.[590] This observation again favors the hypothesis of a porphyrin cation radical rather than an amino acid radical. A breakdown of the contact and dipolar relaxations in both HRP and deutero-HRP compound I showed that both compounds experience essentially identical contributions. Their differential line broadening has been accounted for by also assuming very similar electronic structures for both the iron and the free radical, without involving different orbital ground states for the radical in the two cases.[590]

The reported ^{1}H NMR spectra of HRP reconstituted with ruthenium(II) mesoporphyrin or deuteroporphyrin π cation radicals (Figure 96) show close resemblances with those of HRP compound I.[598,599] This is further support for the hypothesis that the large hyperfine shifts of the heme peripheral protons in HRP compound I result mostly from the π cation radical center. The temperature dependence of ruthenium(II) mesoporphyrin HRP provides apparent intercepts at $T^{-1} = 0$ beyond the diamagnetic region,[599] as in the case of the corresponding model compounds.[600] This behavior has been explained by assuming that the π cation radical in the protein is not in a single electronic state, but is an admixture of the two different electronic states, $^2A_{1u}$ and $^2A_{2u}$, (Figure 97) as for ruthenium porphyrin cation radical models. This leads to the proposal that the native HRP compound I is characterized by a cation porphyrin radical in the $^2A_{1u}$ state, mixed to some extent with the $^2A_{2u}$ state.[599] This suggestion is supported by the finding that extremely broadened ^{2}H NMR signals for HRP compound I reconstituted with mesohemin deuterated at the meso positions are detected around 20–15 ppm.[51]

The shift values of the hyperfine signals in ruthenium(II) mesoporphyrin HRP change with pH with a pK_a of 6.0,[599] which may correspond to that of 5.6 reported for HRP compound I.

The oxidation of the ruthenium(II) myoglobin did not yield the corresponding cation radical, in accordance with the fact that Mb affords compound II but not compound I.[599] This suggests that a characteristic heme environmental structure of HRP may serve to stabilize

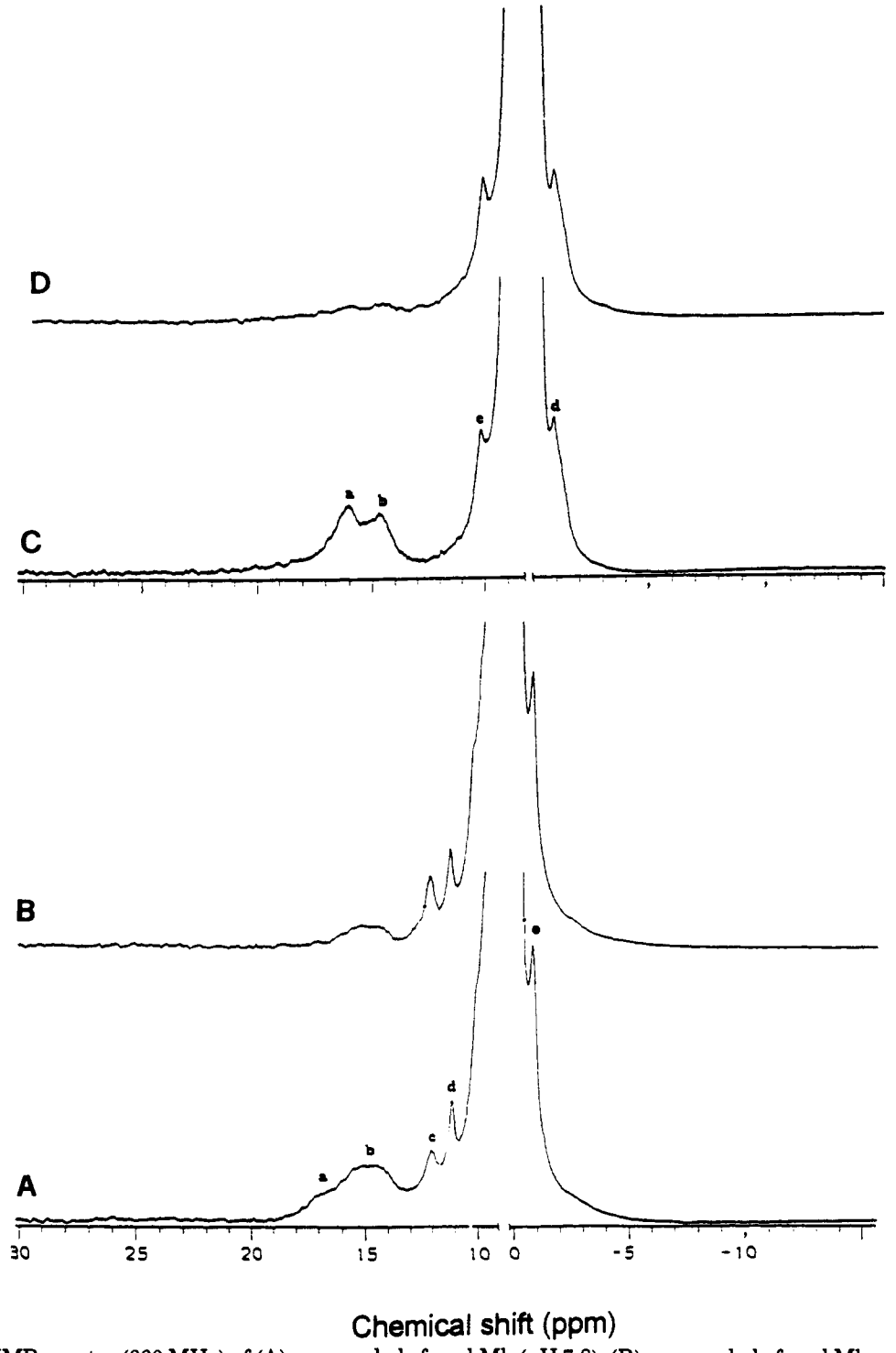

Figure 94. ^1H NMR spectra (360 MHz) of (A) sperm whale ferryl Mb (pH 7.8), (B) sperm whale ferryl Mb reconstituted with hemin deuterated at the meso position (pH 7.8), (C) HRP compound II (pH 9.2), and (D) HRP compound II reconstituted with hemin deuterated at the meso position (pH 9.2). All the spectra were recorded at 298 K in D_2O solution, 0.2 M NaCl. (Reprinted from ref 594. Copyright 1983 American Chemical Society.)

the porphyrin π cation radical through the heme proximal or distal side, or a combination of both.

NOE experiments have been successfully applied to HRP compound I.[343,344] The short T_1 values ($\simeq$8 ms) for the heme resonances allowed very rapid data acquisition, making possible the detection of small NOEs even in relatively unstable reactive intermediates such as compound I. The trans and cis configurations have been established for the 2- and 4-vinyl groups, respectively,[344] as found in resting HRP and in HRP-CN^-. The previously unassigned α-CH_2 protons of the heme propionate side chains have been located.[343] From an estimation of the NOE effect on the adjacent heme methyls and based on the fact that the predominant methylene proton contact shift is strongly dependent on the rotational position of the side chains, the orientation of the propionate groups has been determined. It has been proposed that the compound I formation is accompanied by a 5° rotation of the 6-propionate, the 7-propionate being essentially unaltered.[343] Since the benzhydroxamic acid substrate has been found to be located near the 7-propionate group,

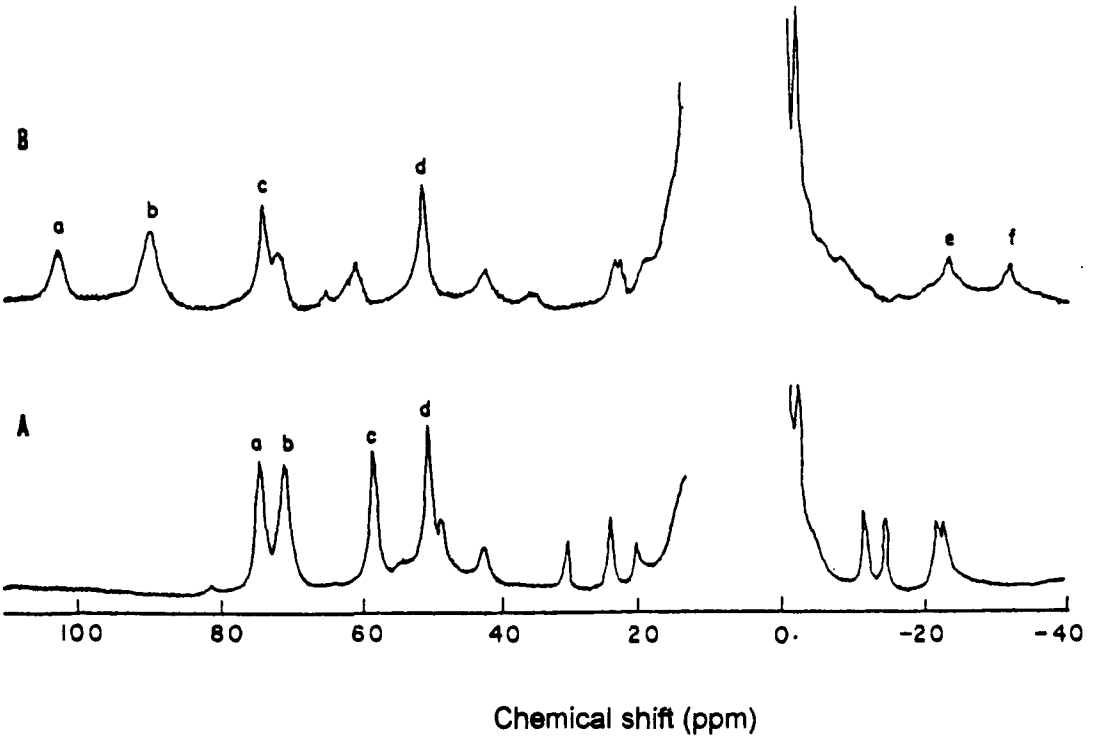

Figure 95. ^{1}H NMR spectra (360 MHz) of (A) HRP compound I and (B) deutero-HRP compound I. The spectra were recorded at 298 K in 0.2 M NaCl, pH 7.0. (Reprinted from ref 596. Copyright 1980 American Chemical Society.)

it seems that the substrate binding site is not significantly altered upon formation of compound I. The absence of NOEs to the peak at 21 ppm indicated that it cannot arise from a heme proton. Due to negligible pseudocontact shift, it has been proposed that it arises from the proximal histidine residue.[343] The similarity of its relaxation properties relative to those of the proximal histidine β-CH_2 in resting HRP suggested that this signal arises from a β-CH_2 proton. Studies on model compounds have demonstrated that the iron center cannot be entirely responsible for the substantial histidine β-CH_2 contact shift.[587,588] On this basis it was proposed that the cation radical in HRP compound I is not localized solely on the porphyrin but exhibits significant delocalization onto the axial histidine.[343]

The spectrum of CcP compound I (Figure 98B) is quite different from that of HRP compound I,[601] but similar to HRP compound II, and to the hydrogen peroxide forms of metMb and soybean leghemoglobin.[602] This is consistent with the interpretation that the second oxidizing equivalent in CcP resides on an amino acid residue spatially separated from the heme ring. By ENDOR measurements the cation radical has been recently localized on Trp 191.[603] Trp 191 is parallel to and exhibits π–π contacts with the proximal histidine imidazole ring. All the above reported NMR results are consistent with a picture in which the reaction of CcP with peroxide yields initially a porphyrin-centered cation radical as in HRP. Its delocalization onto the proximal histidine proposed for HRP might allow it to move onto the Trp 191 ring in CcP.

CcP compound II cannot be formed stoichiometrically from CcP compound I because all reducing agents reduce both species at comparable rates. As found by other techniques, the formation of compound II can be inferred from biphasic spectroscopic behavior, i.e. neither the disappearance of compound II resonances nor the appearance of the heme methyl signals of the ferric enzyme titrate linearly with increasing concentration of the reducing substrate.[601]

No significant changes in line widths or chemical shift values have been detected for the hyperfine-shifted ferricytochrome *c* heme methyl resonances upon oxidation of CcP in the complex formed by the two proteins.[601]

The ^{1}H NMR spectrum of the species obtained upon addition of 1 equiv of H_2O_2 to *Coprinus* peroxidase shows four methyl signals at 85.1, 71.7, 61.5, and 48.4 ppm and signals of intensity one in the region −22 to −27 ppm (Figure 99). Under conditions required for obtaining a proton NMR spectrum *Coprinus* peroxidase compound I has a half-life of approximately 12 min.[332]

VI. Non-Heme, Non-Iron–Sulfur, Iron Proteins

Excluding the heme and iron–sulfur proteins, which have been thoroughly studied by means of NMR spectroscopy, iron is also present in metalloenzymes bound to oxygen atoms.[59,604,605] Among them, we can distinguish those containing only one iron atom per unit from those possessing a binuclear oxo-bridged iron center.[59,60,604,606] In order to understand the NMR spectra of these proteins, many of mono- and dinuclear iron model compounds have been synthesized and studied.[607-614]

Typical iron ligands in these proteins are His, Tyr, Glu, and Asp residues. The observed hyperfine shifts of signals corresponding to iron ligands are expected to be mainly contact in origin. In phenolate ligands, unpaired spin density delocalizes via a π mechanism. This results in an alternation of the sign of the contact shifts of the *ortho*, *meta*, and *para* ring protons.[78,608,611]

Among the mono-iron proteins, the existence of the aromatic-degrading **catechol dioxygenases** should be

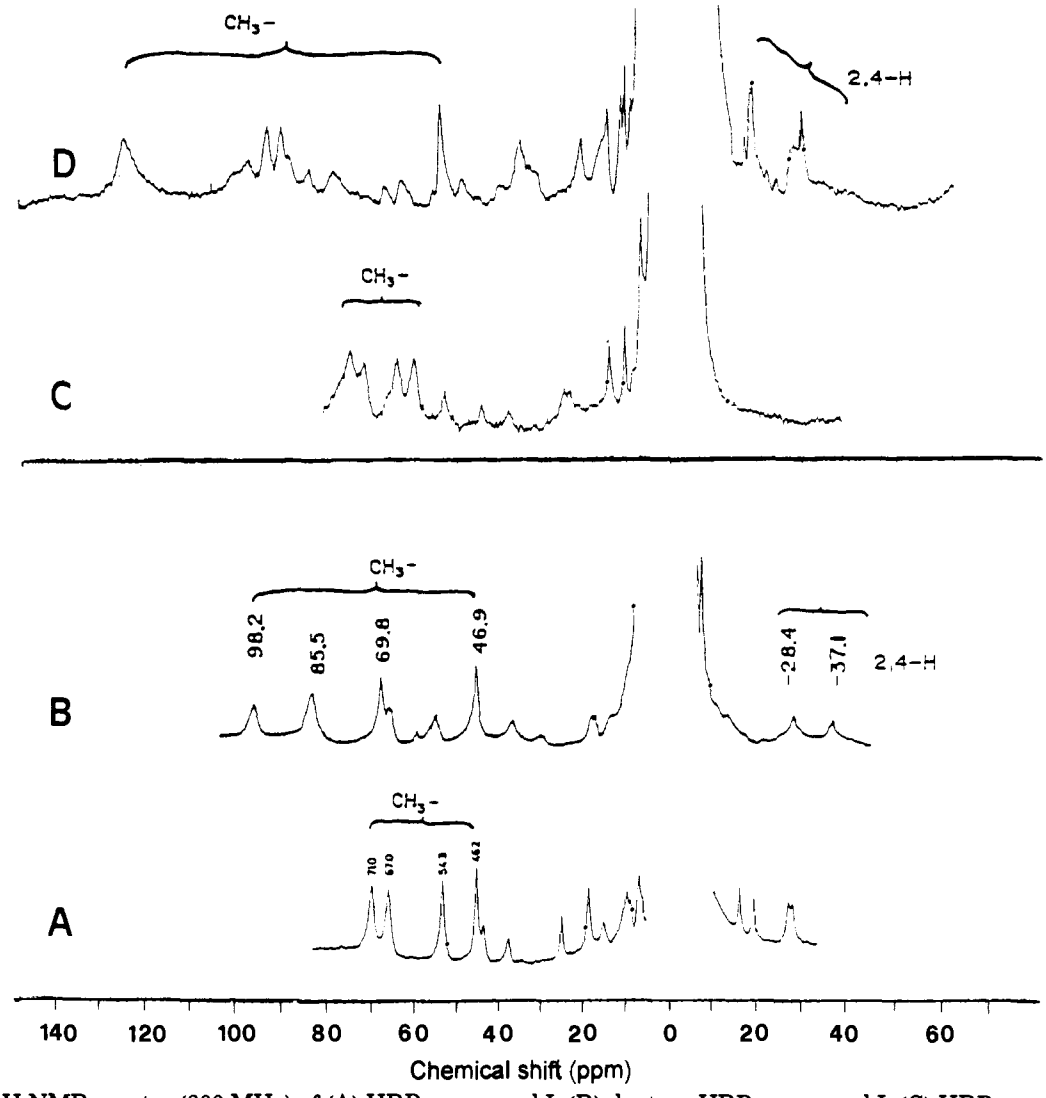

Figure 96. ^{1}H NMR spectra (300 MHz) of (A) HRP compound I, (B) deutero-HRP compound I, (C) HRP reconstituted with ruthenium(II) mesoporphyrin, and (D) HRP reconstituted with ruthenium(II) deuteroporphyrin. All the spectra were recorded at 283 K in 0.1 M phosphate buffer, pH 7.0. (Reprinted from ref 599. Copyright 1986 American Chemical Society.)

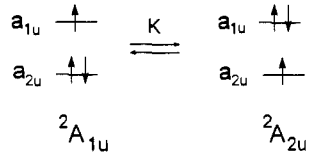

Figure 97. The $^2A_{1u}$ and $^2A_{2u}$ configurations proposed for the porphyrin cation radical.

mentioned. These can be classified in extra- and intradiol dioxygenases.[605] Only the latter, which contain pentacoordinate high-spin iron(III) center,[605,615] have been studied by means of NMR. The iron ligands are two tyrosinates, two histidines, and a water molecule, as shown by an X-ray study.[615] The NMR spectrum of the intradiol dioxygenase exhibits four very broad ill-defined paramagnetically shifted signals (Figure 100A). This is due to the slow relaxing characteristics of high-spin iron(III) and Curie relaxation effects which are operative in such a large protein (MW 63 000). Upon substrate binding the spectra display narrower lines.[616,617] (See Figure 100, parts B and C.) Ring protons from the aromatic substrate are not observed, probably due to the vicinity of the iron ion. Neither signals for the tyrosinate ligands seem to be detectable, since the characteristic upfield–downfield shift pattern of a metal-bound phenolate moiety is not observed. Relying on this observation and by comparison with the shifts observed in model complexes,[608,609,611,612] it was suggested that the-hyperfine shifted signals could arise from β-CH_2 groups of the bound His and Tyr residues.

The enzyme **isopenicillin N synthase** (IPNS) (MW 38,400) contains a high-spin non-heme iron(II) center. Its structure is still unknown. Its ^{1}H NMR spectrum has revealed the existence of three signals corresponding to exchangeable protons at ca. 65 ppm, suggesting the presence of three His residues bound to the iron ion and a two-proton signal at 42 ppm.[618] The interaction of the enzyme with its natural substrate and with NO has been monitored by ^{1}H NMR spectroscopy, allowing the authors to propose a structure of the active site and a catalytic mechanism.[619] One of the His residues seems to be detached from the metal ion upon binding of both the substrate and NO. Since the resonances in the native proteins are too broad to perform NOE experiments, the iron(II) ion has been replaced by cobalt(II) (see section VII).[619]

When discussing binuclear oxo-bridged iron proteins, some of their interesting properties should be mentioned. They are capable of performing oxygen trans-

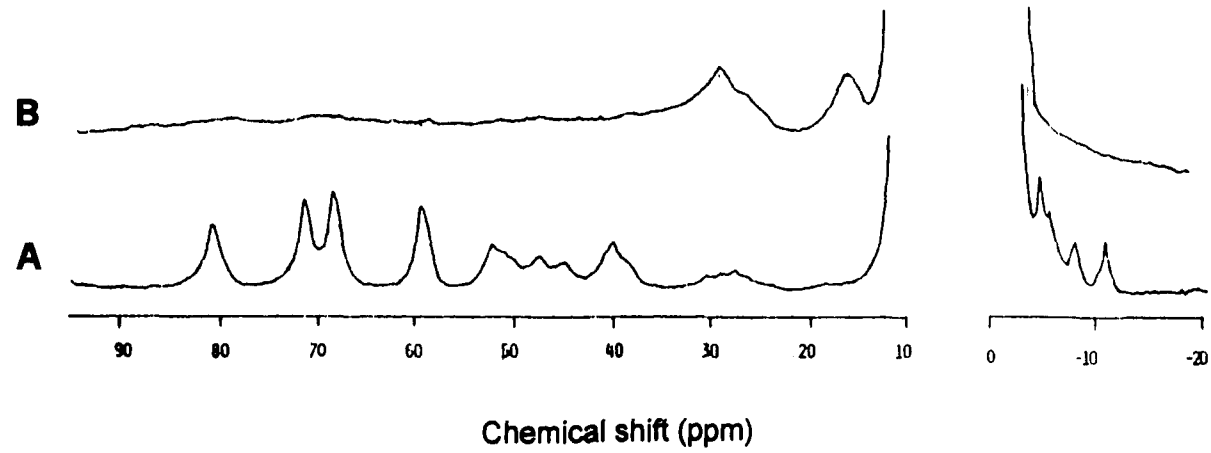

Figure 98. ^{1}H NMR spectra (360 MHz) of (A) resting-state ferric CcP and (B) CcP compound I. The spectra were recorded at 284 K at pH 7.4. (Reprinted from ref 601. Copyright 1981 *Journal of Biological Chemistry.*)

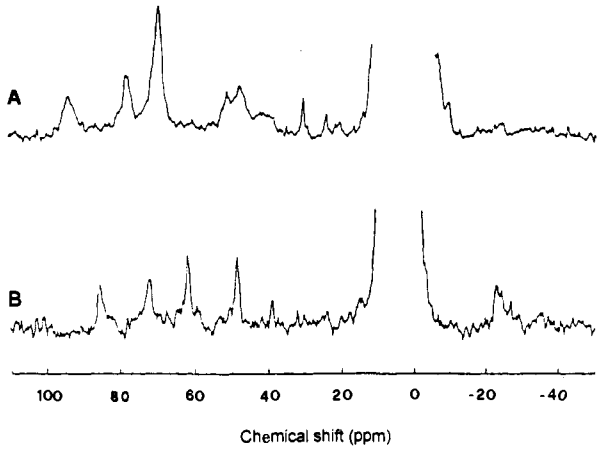

Figure 99. ^{1}H NMR spectra (300 MHz) of (A) *Coprinus* peroxidase and (B) *Coprinus* peroxidase compound I. (Reprinted from ref 332. Copyright 1989 American Chemical Society.)

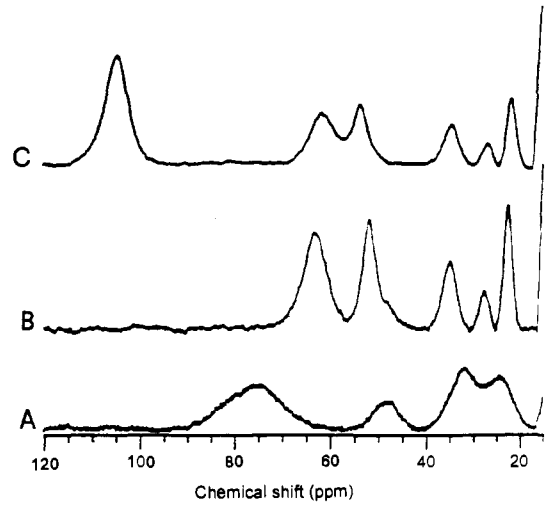

Figure 100. ^{1}H NMR spectra (300 MHz) of (A) native catechol 1,2-dioxygenase (CTD) and its complexes with (B) catechol and (C) 4-methylcatechol. The spectra have been recorded in D_2O solutions. (Reprinted from ref 616. Copyright 1987 American Chemical Society.)

port, oxygen activation, and insertion into an unactivated C–H bond, phosphate hydrolysis, and electron transfer.[59,60,604] Their active sites consist of mono- or bis(μ-carboxylato)(μ-oxo)diiron units. Examples in-

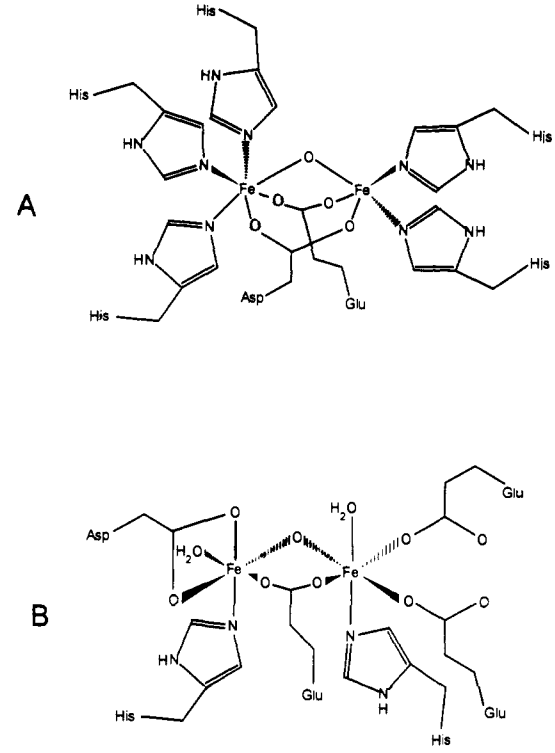

Figure 101. Schematic view of the active sites of (A) hemerythrin and (B) ribonucleotide reductase, resulting from their X-ray structures.

clude hemerythrin, ribonucleotide reductase, and purple phosphatases. (See Figure 101.) As in the case of iron–sulfur proteins, the bridging anions facilitate the antiferromagnetic coupling between the metal ions and the iron ions may be found in different oxidation states. The iron ions generally display either hexa- or pentacoordination; in the latter case a potential coordination site for the binding of substrates is available.

The assignment strategy undertaken by Que and coworkers for the study of these proteins relied heavily on the comparison with chemical shifts observed in mononuclear iron complexes. As already discussed in this review, the antiferromagnetic coupling of two iron ions reduces the $\langle \mathbf{S}_a \rangle$ in the polymetallic center, resulting in smaller contact shifts for the bound ligands with respect to mononuclear systems. Hence, for a proper comparison with values of monoiron models, using this approach, the observed chemical shifts in

proteins are scaled up to shift values for $J = 0$ (uncoupled system).

In **hemerythrin** (Hr),[60,606,620,621] the two iron ions are bridged by an oxo group and two carboxylate moieties as determined by the X-ray structure.[622,623] The ions are also coordinated to five histidines: two to one iron and three to the other (see Figure 101A). A sixth coordination site remains vacant in one of the iron ions, which may be occupied by peroxide or other small anions. This system may exist in three formal oxidation states: [iron(II),iron(II)] (deoxy), [iron(II),iron(III)] (semimet), and [iron(III),iron(III)] (oxy and met). All of them have been characterized by NMR spectroscopy.

The 300-MHz NMR spectra of metHr and oxyHr feature three sets of very broad, poorly resolved paramagnetically shifted signals[624,625] in the 30–10 ppm range (see Figure 102A). Two of them (A and B) belong to solvent-exchangeable protons, and they have been attributed to NH protons of the bound histidines. Their chemical shifts (20–12 ppm) are smaller than those observed in mononuclear iron(III) complexes (100–80 ppm),[609] as expected from the strong antiferromagnetic coupling present in metHr ($J = 268\ cm^{-1}$). The identity of signal C (at 11 ppm) as belonging to a methylene group of a bridging residue has been suggested by analogy with binuclear acetate-bridged models. (The acetate methyl resonance in $[(HBpz_3Fe)_2O(OAc)_2]$ is at 10.5 ppm.[610]) When azide binds to metHr, the signals belonging to the NH histidine protons present different shift values, always in the same range (cf. Figure 102B).

In deoxyHr (containing two iron(II) ions) the NH histidine proton signals are found in the 65–40 ppm region (see Figure 102C).[625] *MCD* measurements have indicated for deoxyHr a weaker antiferromagnetic coupling ($J = 60\ cm^{-1}$) than that in oxyHr ($J = 154\ cm^{-1}$).[626] This explains why the shifts are only slightly smaller than those observed in high-spin iron(II) mononuclear imidazole complexes (79–57 ppm).[609] Further unassigned upfield signals are also detected in the deoxy form. Anion binding is known to weaken the antiferromagnetic coupling. In the case of azide, the binding completely decouples the ferrous ions.[626] This fact can be qualitatively monitored by NMR by comparing the shifts with those observed in mononuclear iron(II)–imidazole complexes.[609]

By means of one-electron reduction of metHr or one-electron oxidation of deoxyHr, mixed-valent [iron(III),iron(II)] semimetHr forms are obtained, which give low-temperature EPR spectra characteristic of a $S = {}^1/_2$ ground state,[627] again indicating an antiferromagnetic coupling. The NMR spectrum of the azide adduct of semimetHr displays two exchangeable signals at 72 and 54 ppm in a 2:3 ratio (see Figure 102D).[625] By comparison with iron(III) and iron(II) model compounds and by assuming that the ligands coordinated to a certain metal ion will be influenced by that ion only (a good approximation in weakly coupled systems), it has been proposed that the reduced iron ion is the one bound to three histidines.

Ribonucleotide reductase B2 from *E. coli* contains two identical subunits of MW 39 000, each containing a dinuclear iron center.[628] Its ^1H NMR spectrum[629] shows an exchangeable signal at 24 ppm (similar to the value observed in metHr) and a nonexchangeable resonance at 19 ppm, the intensity ratio of the peaks being 3:1. The reduced protein (diferrous) exhibits proton NMR resonances at 45 and 57 ppm in a 1:1 ratio,[630] the first being exchangeable and probably attributable to a histidine ligand. The nonexchangeable signals could arise from methylene protons of nonbridging carboxylate ligand residues. The lines are very broad owing to the protein size, and the quality of the spectra is poor. All spectroscopic data pointed to an active site similar to that of hemerythrin but with fewer histidine ligands,[628,630] as has been recently shown by the X-ray structure of the enzyme.[631]

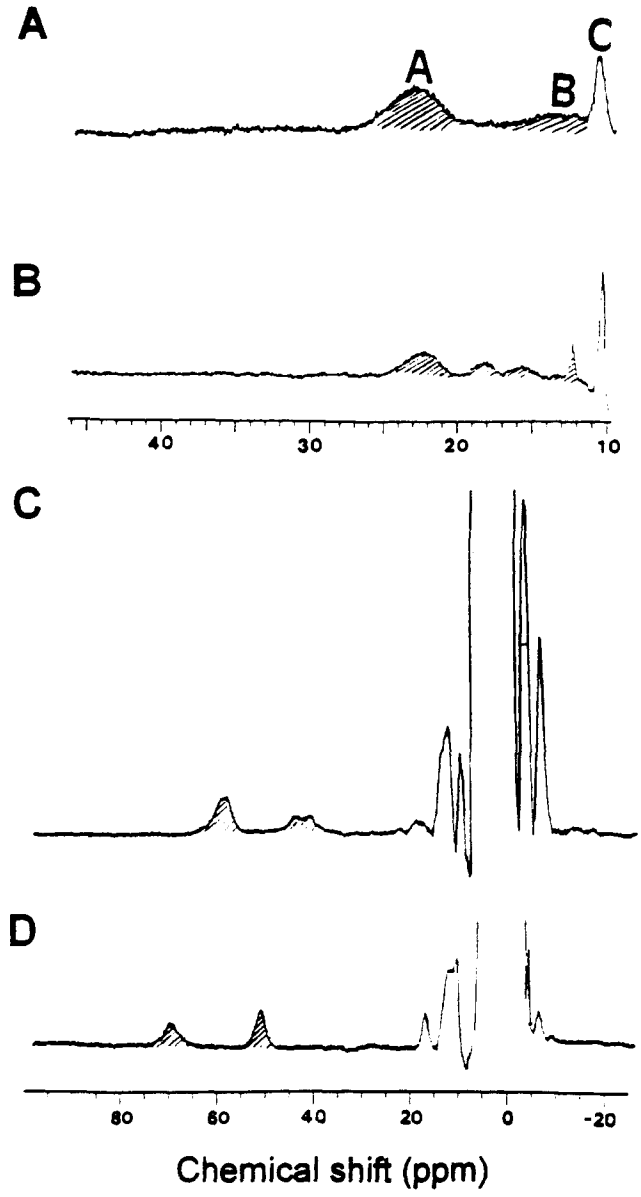

Figure 102. ^1H NMR spectra (300 MHz) of (A) *Phascolopsis gouldii* metHr at 303 K, (B) *P. gouldii* metHr–N_3 adduct at 303 K, pH 7.5, (C) *P. gouldii* deoxyHr at 313 K, and (D) *P. gouldii* semimetHr–N_3 adduct at 313 K. All the spectra were recorded in H_2O solutions. The shaded signals correspond to exchangeable protons in D_2O solutions. (Part A, reprinted from ref 624. Copyright 1984 American Chemical Society. Part D, reprinted from ref 625. Copyright 1986 American Chemical Society.)

The most important results from NMR studies of diiron oxo proteins have appeared recently and regard **purple acid phosphatases** (PAPs).[59,632,633] The most extensively studied in this group are uteroferrin (Uf) and that from bovine spleen (BSPAP), both of medium

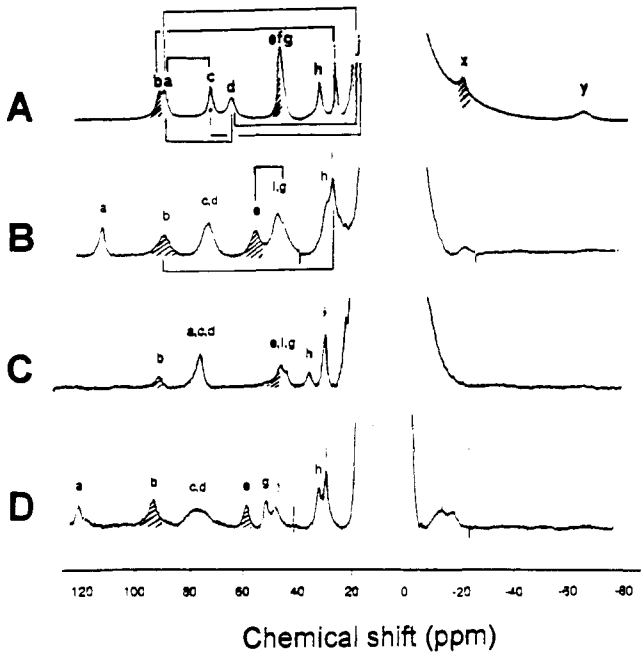

Figure 103. ^1H NMR spectra (300 MHz) of (A) reduced uteroferrin, (B) reduced uteroferrin-WO_4^{2-} complex, (C) reduced bovine spleen purple acid phosphatase (BSPAP), and (D) reduced BSPAP-WO_4^{2-} complex. All the spectra were recorded in H_2O solutions at pH 4.9 and 303 K. The shaded signals correspond to exchangeable protons in D_2O solutions. The solid lines indicate dipolar connectivities as results from NOE experiments. (Part A, reprinted from ref 609. Copyright 1983 *Journal of Biological Chemistry*. Part D, reprinted from ref 638. Copyright 1992 American Chemical Society.)

molecular size (35 000). The diiron center may exist in the purple oxidized (two iron(III) ions, EPR silent) or in the pink reduced (one iron(III) and one iron(II), with a $S = {}^1/_2$ ground state) form, both of them always displaying an antiferromagnetic coupling.[634,635] No X-ray data are available for any purple acid phosphatase, thus the possible structure of the active site has been proposed on the basis of spectroscopic data only.

In the oxidized diferric Uf, no hyperfine-shifted signals could be detected in the 100 to −80 ppm spectral window.[609] This fact has been attributed to the slow-relaxing properties of iron(III). On the other hand, the spectrum of reduced Uf shows 10 well-resolved hyperfine-shifted signals which correspond to 13 protons, three of them exchangeable in a D_2O solution. (See Figure 103 A.) In this case, the electronic relaxation time is dominated by the faster relaxing iron(II) ion and allows the detection of the hyperfine-shifted signals. The spectrum of reduced BSPAP is similar to that of Uf (cf. Figure 103C), except for the fact that it does not display upfield signals. Both proteins are known to bind inorganic anions like molybdate and tungstate. The spectra of the tungstate adducts are shown also in Figure 103, parts B and D.

The observed hyperfine-shifted signals can be ascribed to the metal-bound residues. In an early NMR study an assignment for Uf was proposed by comparison with mononuclear iron(II) and iron(III) complexes.[609] A saturation-transfer effect observed between signals c and d (lettering according to Figure 103) suggested that they corresponded to the Hδ1 and Hδ2 protons respectively of a bound tyrosine experiencing a dynamic exchange by an aromatic ring flipping. Their shifts were also consistent with a Tyr bound to an iron(III) ion. The nonexchangeable upfield signal y was assigned to an Hε Tyr proton because of the sign and magnitude of its shift.[609] Later,[636] it was observed that the T_1 values of signals a and j corresponded to protons farther from the metal center and (as demonstrated by a NOE experiment) dipolarly connected. These signals were attributed to the β-CH_2 protons of the bound tyrosine. All this information led to the proposal that only one Tyr residue was bound to the iron(III) ion, the other signals being assigned to two histidine residues each bound to a different iron ion. Signals corresponding to a bridging residue were not expected to be observed because of their vicinity to the two metal ions. This has been possible, however, upon replacement of one of the iron ions by cobalt(II),[637] as will be discussed in section VII. Further NOE experiments on the native enzyme Uf and on its tungstate adduct[638] (see spectrum on Figure 103B) allowed the authors to confirm and to correct some previous assignments. Table XII summarizes these assignments. In all these cases, the identification of the oxidation states of the metal ions was performed by comparison of the observed shifts with model mononuclear complexes and by calculating the expected reduced shift by the effect of the magnetic coupling.

A recent report[614] shows the applicability of 2D techniques on small paramagnetic diiron model compounds. No 2D NMR experiments on native diiron-

Table XII. ^1H NMR Chemical Shifts of Reduced Uteroferrin (Uf), Bovine Spleen Phosphatase (BSPAP), and Their Tungstate Adducts at 303 K

	chemical shift (ppm) (T_1)				
signal	Uf[a]	BSPAP[b]	Uf-WO_4^{2-} [a]	BSPAP-WO_4^{2-} [b]	tentative assignment[b]
a	86.6 (19.5)	69.5	112.7 (27.5)	115.8	Fe(III)-Tyr Hβ1 (Hβ2)
b	88.4 (3.8)	83.2	88.3 (7.7)	89.2	Fe(III)-His Hδ1
c	70.0 (7.7)	69.5	72.1 (11.0)	73.4	Fe(III)-Tyr Hδ1 (Hδ2)
d	62.4 (7.3)	69.5	72.1 (11.0)	73.4	Fe(III)-Tyr Hδ2 (Hδ1)
e	44.0 (-)	39.9	54.5 (13.3)	54.5	Fe(II)-His Hε2
f	43.5 (6.8)	39.9	46.4 (16.2)	43.8	-
g	43.5 (6.8)	39.9	44.2 (11.2)	47.0	Fe(II)-His Hδ2
h	29.5 (5.9)	30.0	28.1 (13.0)	28.3	-
i	23.4 (11.3)	24.0	23.7 (20.6)	25.1	Fe(III)-His Hβ1
j	15.1 (20.2)	-	-	12.0	Fe(III)-Tyr Hβ2 (Hβ2)
x	-24.5 (2.6)	-	-23.7 (6.0		-
y	-68.0 (-)		-72.0 (-)		Fe(III)-Tyr Hε1 (Hε2)

[a] Taken from ref 636. [b] Taken from ref 638.

oxo proteins have been reported up to this point. This is not an easy task since these proteins are of medium size, and considerable line broadening due to Curie relaxation effects is observed at high fields. For example, the line widths of the hyperfine-shifted signals in reduced uteroferrin range from 400 to 1400 Hz at 300 MHz.[636]

VII. Cobalt(II) Proteins

Cobalt(II), although not naturally present is metalloenzymes, has been recognized as a useful paramagnetic probe owing to its spectroscopic properties, as already pointed out in section II.C as far as electron relaxation times are concerned. Cobalt(II) substitution has proved useful in the study of metalloproteins which may otherwise be difficult to study using NMR.[639-642] Difficulties arise in medium- or large-sized zinc enzymes and also in proteins containing copper.

Zinc(II) is diamagnetic, and the ^{67}Zn isotope has a magnetic moment which is too low to be observed by NMR at the concentration of metalloproteins.[643,544] Owing to the similarities of the coordination chemistry of zinc(II) and cobalt(II), cobalt(II)-substituted enzymes retain all or part of the activity of the native proteins and represent ideal models of the latter systems.[639,640] Cobalt(II) substitution induces hyperfine shifts on protons belonging to residues in the active site, avoiding the problem of signal overcrowding encountered in medium- or large-sized enzymes.

In the case of copper(II) proteins, the slow relaxation properties of the metal ion induce such a large broadening on the NMR signals of nearby protons that they are rendered undetectable.[645] Again, cobalt(II) substitution allows the detection of hyperfine-shifted signals near the metal site.

Cobalt(II) is a d^7 ion, which may be high spin ($S = {}^3/_2$) or low spin ($S = {}^1/_2$).[7] The low spin form is generally present under strong-ligand conditions. This situation can be encountered in planar complexes, like cobalt(II) porphyrins[646,647] or when two simultaneous cyanide ligands are coordinated.[648] High-spin cobalt(II) is found in tetrahedral, pentacoordinate, and octahedral complexes.

A. High-Spin Cobalt(II)

High-spin cobalt(II) is usually found when replacing the metal ion in zinc enzymes. It displays electronic relaxation times in the 10^{-11}–10^{-12}-s range, depending on the coordination geometry. Tetracoordinate cobalt(II) has an orbitally nondegenerate ground state, whereas pentacoordinate cobalt(II) possesses low-lying excited states, so that a shorter relaxation time is expected. The latter situation also holds for pseudooctahedral coordination. In the tetracoordinate case the longer τ_s will therefore give rise to broader lines and shorter T_1s with respect to penta- or hexacoordinate systems.[6,649,650]

Residues coordinated to cobalt(II) yield proton resonances experiencing large contact shifts. Regarding pseudocontact shifts, one should recall that the magnetic anisotropy of the cobalt(II) ion increases in the following order: tetrahedral, pentacoordinate, octahedral.[651] Hence, the pseudocontact contribution to the observed shifts will increase in the same direction.

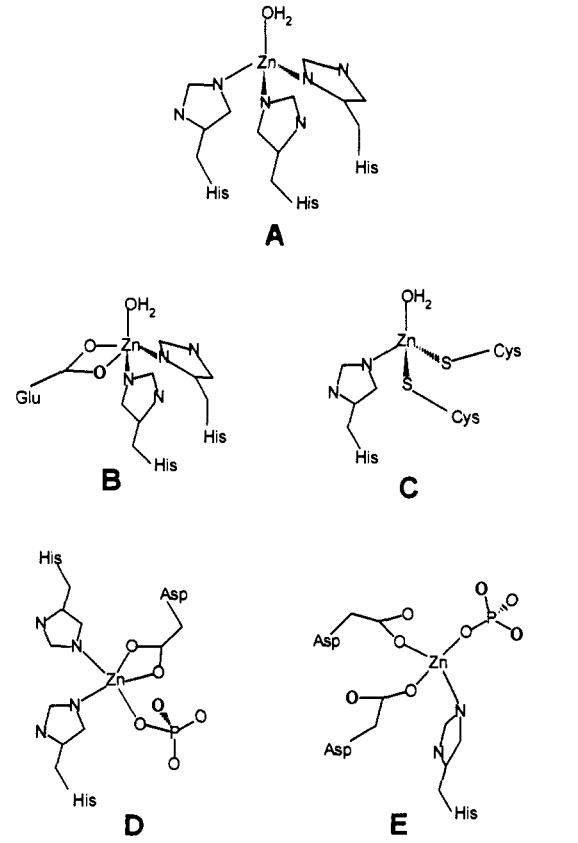

Figure 104. Schematic representations of the active sites of the following zinc enzymes: (A) carbonic anhydrase, (B) carboxypeptidase A, (C) liver alcohol dehydrogenase, and (D) site A and (E) site B in alkaline phosphatase, as resulting from their X-ray structures.

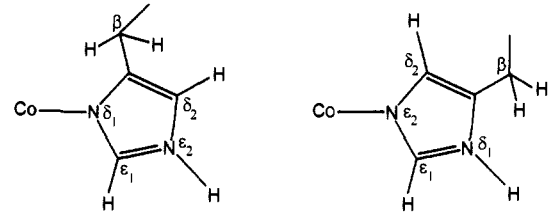

Figure 105. Possible modes of coordination of a histidine residue to a metal ion.

The pseudocontact shifts may in some cases be large, as will be discussed later.

Figure 104 shows the active site of four zinc enzymes which have been subject to cobalt(II) substitution. These will be discussed here. They are carbonic anhydrase (CA), carboxypeptidase A (CPA), liver alcohol dehydrogenase (LADH), and alkaline phosphatase (AP). Histidines are common metal ligands in zinc enzymes. The first NMR studies of cobalt(II)-substituted zinc enzymes have in many cases enabled the assignment of the signals corresponding to the bound histidines to be made. This has generally been achieved by comparison with spectra of model complexes or of other cobalt(II)-substituted zinc enzymes.

Ring histidine protons in *ortho* positions with respect to the cobalt(II) ion display broader signals than *meta* protons, sometimes being beyond the limit of detectability. Histidines may be bonded to the metal ion through the Nδ1 or through the Nϵ2 nitrogen atom (see Figure 105). Residues bound through the Nδ1 nitrogen have one *ortho*-like proton (Hϵ1, nonexchangeable) and

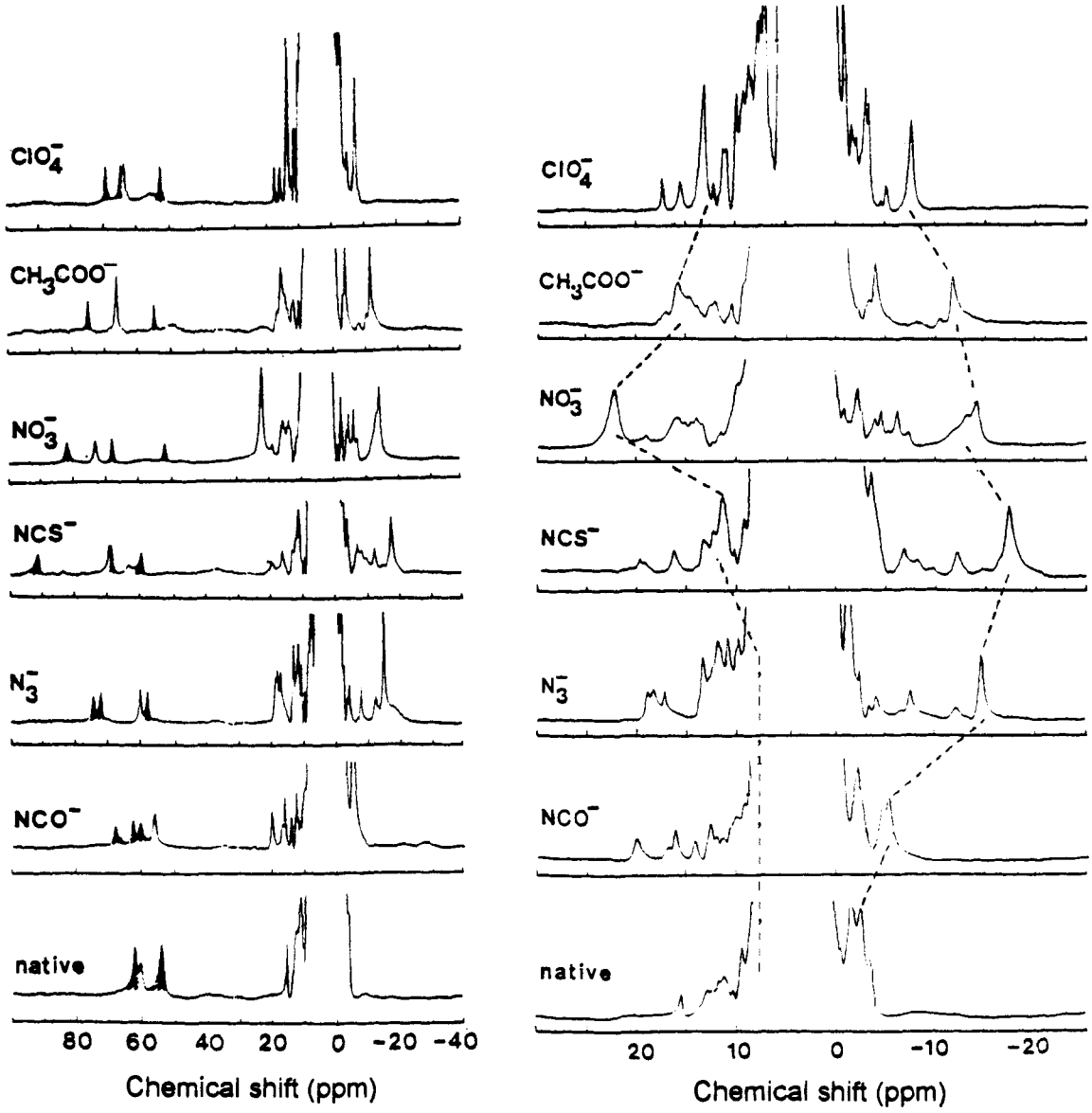

Figure 106. ^{1}H NMR spectra (200 MHz) of several adducts of cobalt(II)-substituted bovine carbonic anhydrase II. All the spectra were recorded in H_2O solutions at 300 K. The shaded signals correspond to exchangeable protons in D_2O solutions. The dashed lines correlate the signals of the methyl groups of the residues Thr 199 and Thr 200 in the different adducts. (Reprinted from ref 656. Copyright 1990 Gordon & Breach.)

two *meta* protons (Hδ2 and Hϵ2), while the opposite situation is encountered for the case of Nϵ2-bound histidines. The resonances corresponding to histidine-ring protons may be differentiated in *meta*-like and *ortho*-like protons according to their line widths. Those associated with the imidazole NH protons of histidines bound to the cobalt(II) ion may be recognized by their solvent exchangeabilities. This method, however, has in some cases led to erroneous assignments. The recent application of NOE and 2D experiments to these systems has led to a rigorous assignment for many of these resonances.

Carbonic anhydrase (CA hereafter) is a hydrolytic medium size (MW 30 000) zinc enzyme[652,653] in which the metal ion is tetrahedrally coordinated to three histidine residues and a water molecule.[654] Many anions and neutral molecules bind to the metal ion, either by adding to the coordination sphere as a fifth ligand or by replacing the water molecule, yielding a tetrahedral adduct. An equilibrium between the two species sometimes occurs.[655-657] The X-ray structure is not only available for the native enzyme,[654,658,659] but also for a number of tetra- and pentacoordinate adducts.[660-664] The NMR analysis of the diamagnetic zinc protein has been hitherto hampered by the size of the enzyme. A recent work[665] discusses the applicability of 2D techniques to medium-sized proteins, with CA as an example.

Cobalt(II)-substituted CA (CoCA hereafter) represents an ideal system in which to monitor protein residues present in the active-site cavity.[655,666] The ^{1}H NMR spectrum of native CoCA at pH 6.0 shows three well-shifted paramagnetic signals in the 70–50 ppm range, corresponding to four protons (three of them exchangeable in D_2O, see Figure 106).[667] The four shifted resonances were assigned in an early work to protons of the coordinated histidines by comparison with model complexes.[667] The three exchangeable signals correspond to "*meta*"-like NH protons. The nonexchangeable proton is identified as the Hδ2 proton of His119, which is the only histidine bound to the metal ion through its Nδ1.

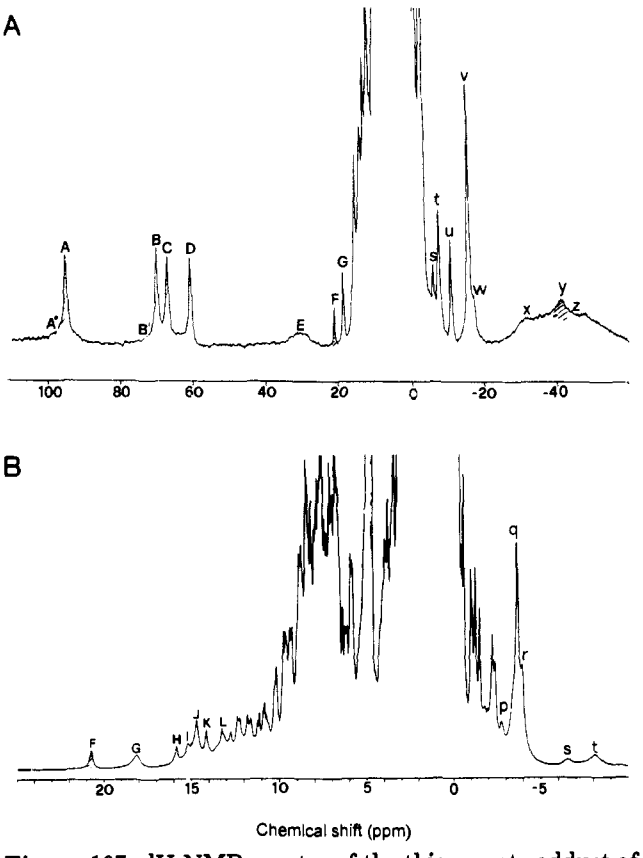

Figure 107. ^1H NMR spectra of the thiocyanate adduct of cobalt(II)-substituted human carbonic anhydrase II at (A) 200 and (B) 600 MHz. All the spectra were recorded in H_2O solutions at pH 6.7 and 300 K. The shaded signals indicate protons that are exchangeable in a D_2O solution.

When the enzyme is inhibited by anions yielding pentacoordinate adducts, the higher magnetic anisotropy of the metal ion induces larger dipolar shifts. This is reflected in a larger spread of the histidine signals. In addition, a set of hyperfine-shifted signals is observed near the diamagnetic envelope both in the downfield and in the upfield regions (see Figure 106).[656,667] Tetracoordinate adducts produce spectra more akin to that of the native enzyme. For the above reasons, pentacoordinate adducts are the most suitable for investigation by NMR.

Although the T_1 values of the histidine ring protons have a large contribution of ligand-centered mechanisms, longer times (15–30 ms) are observed in pentacoordinate adducts owing to the shorter τ_s, when compared with those present in tetrahedral adducts (less than 10 ms).[656] The T_1 values of these signals have thus been used as an indication of the coordination number of the cobalt(II) ion. In the case of the low-activity HCA I isoenzyme,[668] different coordination geometries have been recognized in the high- and low-pH species by this means.

A further insight into the assignment of noncoordinated residues in the active site of this enzyme has been recently gained by means of NOE and 2D NMR experiments on different pentacoordinate adducts of some bovine[669,670] and human[671] isoenzymes. Spectra recorded on different adducts may be correlated by cross titration,[656,669] allowing the extension of the assignments from one adduct to the others. Figure 107 shows the spectra of the thiocyanate adduct of the human isoenzyme II (HCA II) at 200 and 600 MHz. We may distinguish three types of hyperfine-shifted resonances in these spectra. First, signals A–D, which display large downfield chemical shifts and are broadened by up to 1200 Hz at 600 MHz. A second group is constituted by seven very broad signals which are barely detectable at 200 MHz (some of them, i.e. signals B′, E, x, y and z, are shown in Figure 107A) but may be observed at lower fields. Finally, the signals falling in the 20 to −20-ppm range, which become well resolved in the 600-MHz spectrum (cf. Figure 107 B).

The identity of signal B as belonging to a His residue has been confirmed by the fact that this signal is absent in a spectrum of a protein sample in which all the His ring protons had been deuterated.[671] NOE experiments on this signal have indicated that signal A is the Hε2 proton of the same His residue.[669] The very broad signals found both in the upfield and in the downfield regions of the spectrum had initially been assigned as the *ortho* protons of the coordinated histidines,[667,672] due to their large line widths (up to 1500 Hz at 200 MHz). Some of these signals are absent in spectra recorded in a protein sample in which all the His residues are deuterated. NOE experiments have been performed on some of these very broad signals providing information for their assignment to specific histidine residues.[671]

Regarding the signals corresponding to non-bound residues, their assignment is of relevance for the estimation of the χ tensor parameters. This depends on the possibility of assigning a reasonable number of signals corresponding to nonbound residues. The calculation of pseudocontact shifts (already discussed in section V) has been seldom performed on non-heme proteins. This is due partly to the smaller number of assignments of nonbound residues available for these systems and partly to the intrinsically lower symmetry of non-heme metal centers.

The ^1H NMR spectra of pentacoordinated adducts usually show two readily identifiable methyl resonances (one upfield, one downfield) coming from nonbound residues. Their positions in the spectra of different adducts are correlated by means of dashed lines in Figure 106. They had been first tentatively assigned to the methyl groups of two Thr residues residing in the active-site cavity.[656,670] The upfield resonance is absent in the spectra of the human isoenzyme I where one of these residues is replaced by a His.[669] Both methyl groups are approximately at the same distance from the metal center (5.6 and 5.9 Å respectively), so that the opposite sign of their shifts is due exclusively to the orientation of the χ tensor. These assignments were later verified by recognizing the spin patterns of these residues.[669,671] However, the pseudocontact shift of the different protons of a certain residue may be quite different, and it is not always possible to find complete spin patterns outside the diamagnetic envelope.

In a further stage, NOE experiments in the formate and acetate adducts have been performed by irradiating the inhibitor signals. The combined use of NOE and 2D experiments has led to the docking of the anions in the hydrophobic pocket of the active site.[670] Recent studies on the bovine[669] and on the human II isoenzymes[671] have applied the following assignment strategy.

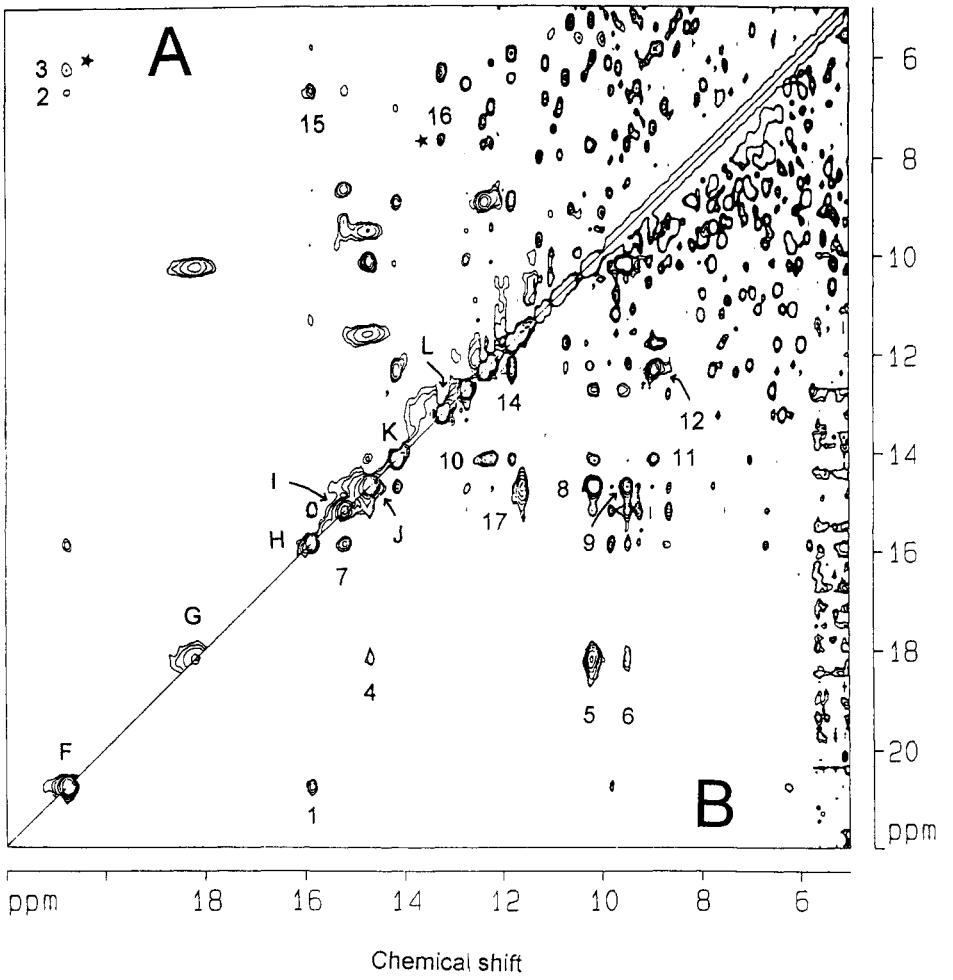

Figure 108. ^{1}H NMR NOESY spectra (600 MHz) of the thiocyanate adduct of cobalt(II)-substituted human carbonic anhydrase II in H_2O solution at 290 K. The cross peaks marked with stars are absent in the corresponding experiments performed on a protein in which all the histidine residues were deuterated. The upper left triangle (A) corresponds to an experiment performed with a mixing time of 20 ms, whereas the lower right triangle (B) corresponds to an experiment performed with a mixing time of 100 ms. Cross-peak labeling is as follows: (1) Hδ1 His107, NH_p His107; (2) Hδ1 His107, Hβ1 His107; (3) Hδ1 His107, Hε1 His107, F H; (4) Hγ2 Glu117, Hβ1 Glu117; (5) Hγ2 Glu117, Hγ1 Glu117; (6) Hγ2 Glu117, Hβ1 Glu117I; (7) NH_p His107K, NH_p Glu106; (8) Hβ1 Glu117, Hγ1 Glu117; (9) Hβ1 Glu117, Hβ2 Glu117; (10) NH_p Ile146, Hα1 Gly145; (11) NH_p Ile146, Hα2 Gly145; (12) Hα1 Gly145, Hα2 Gly145; (13) NH_p Gly145, Hα2 Gly145; (14) Hα1 Gly145, NH_p Gly145; (15) NH_p His107, Hβ1 His107; (16) Hβ1 His96, Hα His96; (17) NH Gln92, NH Gln92.

By irradiating signals A–D, a series of NOEs are observed in the 20 to −20 ppm region. The identification of the signals dipolarly connected with A–D may be obtained by means of 2D experiments (see Figure 108). The combined use of 2D NMR and isotope labeling techniques, assisted with the aid of computer graphics analysis of the crystallographic structure has enabled the assignment of a number of signals corresponding to nonbound residues sensing the paramagnetic center.[671] Table XIII summarizes a series of assignments for the thiocyanate adduct of the human II isoenzyme.

By these means, an orientation of the magnetic susceptibility tensor has been proposed for different pentacoordinated adducts.[669,671] The different shifts found for the same residues in various inhibitor derivatives may be accounted for by assuming different $\Delta\chi$ values rather than by changing the orientation of the χ tensor.

Cobalt(II)-substituted **carboxypeptidase A** (CoCPA hereafter) is another example in which the zinc ion has been replaced by cobalt(II). In CPA the metal ion is bound to two His and a Glu residue, as determined by crystallographic methods (see Figure 104B).[673,674] The ^{1}H NMR spectrum of Co(II)CPA (see Figure 109A) displays four well-defined isotropically shifted signals in the downfield region, one of them being exchangeable and therefore assigned to a Hε2 proton of a coordinated histidine. The NH belonging to the second bound histidine is not detected, probably due to fast exchange with the bulk solvent. Two sharp signals at 52 and 45 ppm have been scribed to the Hδ2 protons of His 69 and 196. The fourth (broader) signal at 56 ppm and two further peaks (barely detectable) at 75 and 40 ppm have been attributed to the Hε1 protons and a γ-CH_2 proton of the bound Glu residue.[675–677] A NOE experiment has indicated that signals a and c belong to the same His residue (unpublished results from this lab). Many derivatives of CoCPA have been investigated with amino acids and anions.[676–678] However, the protein is soluble only in viscous high ionic strength solutions, and therefore, the signals are broad and no 2D NMR spectra have been performed on it.

Liver alcohol dehydrogenase (LADH) is a dimeric zinc enzyme of molecular weight 80 000 containing two zinc ions in each subunit. The metal ion is coordinated to a His, two Cys residues and a water molecule in a

Table XIII. Signal Assignments for the Thiocyanate Adduct of Human Carbonic Anhydrase II from *E. coli* (Taken from Ref 671)

signal	chemical shift[a]	assignment
A′	123[b]	*ortho*-like His proton[c]
A″	95[b]	*ortho*-like His proton[c]
A	94.1	Hε2 His 119[d]
B	69.2	Hδ2 His 119[c,d]
C	66.4	Hδ1 His 96[d]
D	60.2	Hδ1 His 94[d]
E	31.3[b]	Hε1 His 96[c,d]
F	20.76	Hδ1 His 107[d,e,f,j]
G	18.19	Hγ2 Glu 117[d,e,g]
H	15.85	NH pept. His 107[e,f,j]
I	15.17	NH Glu 106[e,f,j]
J′	14.68	Hβ1 Glu 117[e,g]
J″	14.74	Hε2 Gln 92[e,f]
K	14.14	NH Ile 146[d,e,f,j]
L	13.22	Hβ1 His 96[d,e]
M	13.30	Hβ2 His 96[d,e]
O	12.35	Hα1 Gly 145[d,e,g,j]
Q	11.79	NH Gly 145[e,f]
R	11.63	Hε2 Gln 92[d,e]
S	10.19	Hγ1 Glu 117[d,e,g]
T	9.48	Hβ2 Glu 117[e,g]
U	8.90	Hα2 Gly 145[d,e,g]
V	7.74	Hβ2 His 94[d,e]
W	7.63	Hα His 96[d,e]
X	6.65	Hβ1 His 107[d,e]
Z	6.21	Hε1 His 107[c,e]
m	−1.61	Hβ Val 207[e,h]
n	−1.85	Hβ1 Ser 29[d,e]
o	−2.30	γ-CH_3 Val 207[e,h]
p	−3.00	Hβ Thr 199[d,e]
q	−3.71	γ-CH_3 Val 207[e,h]
s	−6.58	Hβ1 His 94[d,e]
t	−8.13	Hα Thr 199[d,e]
u	−11.18	Hζ2 Trp 209[d,i]
v	−16.16	γ-CH_3 Thr 199[d,e]
x	−31[b]	Hδ2 His 94[c,d]
z	−42[b]	NH Thr 199[d]

[a] At 600 MHz, except where indicated. [b] At 200 MHz. [c] Assigned by means of spectra of a sample with selectively deuterated His ring protons. [d] Assigned by means of NOE experiments. [e] Assigned from NOESY spectra. [f] Identified as an NH proton by spectra in a ^{15}N-labeled sample. [g] Assigned from COSY spectra. [h] Assigned from TOCSY spectra. [i] Assigned by means of spectra on a sample with selectively deuterated Trp ring protons. [j] Assigned from a HMQC ^{15}N–^1H spectrum.

distorted tetrahedral geometry (see Figure 104C).[679] The ^1H NMR spectrum of Co_2Zn_2LADH (see Figure 109B–C) displays six very broad well-shifted downfield signals (one of them, c, corresponding to an exchangeable proton),[680] spanning from 280 to 70 ppm. These resonances are detectable only at low fields and possess T_1 values of ca. 1 ms. Signals d, f, and e would originate from the Hε1, Hδ1, and Hδ2 protons of the bound histidines respectively, as suggested by comparison with the spectra of CoCA and CoCPA. Signals a (intensity two), b, and c were attributed to the β-CH_2 protons of the bound cysteines. A set of sharper hyperfine-shifted signals (better resolved at higher fields) are present near the diamagnetic envelope, both in the upfield and in the downfield regions (see Figure 109C).[680]

Copper, zinc **superoxide dismutase** (Cu_2Zn_2SOD hereafter), a dimeric protein of MW 32 000, has been extensively investigated by using cobalt(II) as a spectroscopic probe.[681–685] The copper(II) ion is bound to four His and the zinc(II) ion is coordinated to three His through their Nδ1 atoms and one Asp residue (see Figure 110A), as shown by its X-ray structure.[682,686] The metal

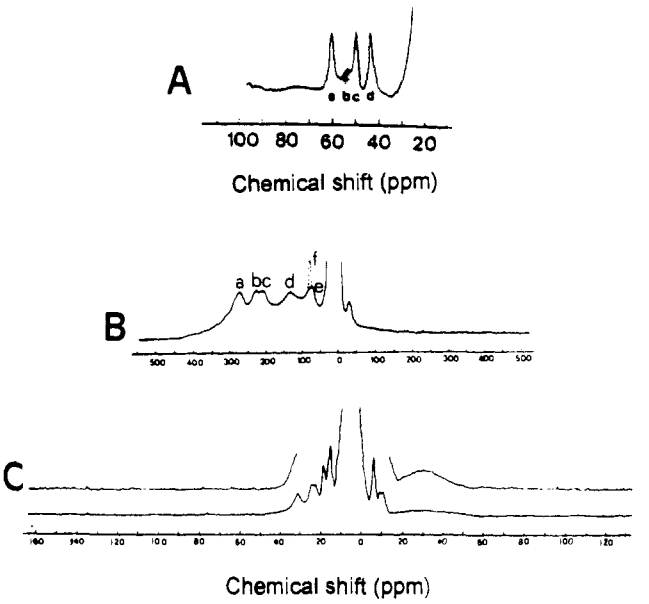

Figure 109. (A) ^1H NMR spectra (90 MHz) of cobalt(II)-substituted CPA at pH 6.0 and 300 K (the shaded signals indicate protons that are exchangeable in a D_2O solution), (B) ^1H NMR spectra (60 MHz) of Co_2Zn_2 LADH at pH 8.3 in D_2O (the dashed signal is present in a H_2O solution), and (C) 300-MHz spectrum, of Co_2Zn_2 LADH in D_2O. (Part A, reprinted from ref 676. Copyright 1988 American Chemical Society. Part C, reprinted from ref 680. Copyright 1984 American Chemical Society.)

ions are 6.3 Å apart, with the imidazolate ring of His 63 serving as bridging ligand. This protein may be obtained from different sources and the human enzyme has been cloned and overexpressed in yeast and *E. coli*. The numbering of the residues used throughout this review corresponds to the human enzyme.

The protein can be deprived of both native metal ions.[685,687] Addition of one equivalent of cobalt(II) at pH 5.0 provides a derivative in which the cobalt(II) ion is bound to the zinc(II) site.[883,687] The ^1H NMR spectrum of E_2Co_2SOD (where E stands for empty and the subscript 2 indicates the dimeric nature of the protein) is reported in Figure 111A.[56] The resonances in the 60–30 ppm region correspond to metal-bound residues. Three Hδ2 His protons are detected (signals A, C, and D), as well as two exchangeable NH protons (B and G). The third NH is probably in fast exchange. The spectrum recorded in a protein expressed in *E. coli* with the His residues deuterated in the Hε1 position (*ortho*-like) is similar to that reported in Figure 111A, indicating that the signals corresponding to these protons are broadened beyond detection at 200 MHz.[147] NOE experiments have suggested that signals E and F correspond to a geminal pair, probably the β-CH_2 group of the coordinated Asp83.[147]

If copper(II) is added to a solution of this derivative, a Cu_2Co_2–enzyme is obtained[685] which has almost the same biological activity as the native enzyme.[684,685] Upon treatment with dithionite, a reduced enzyme containing copper(I) is obtained. The spectrum of the $Cu^I_2Co_2$SOD derivative (Figure 111B) is similar to that of E_2Co_2SOD but in this case three signals corresponding to exchangeable protons are found.[688] Since cobalt(II) is the only paramagnetic probe, the detection of three NH protons has been taken as a proof of the detachment of the bridging His from the copper site upon reduction

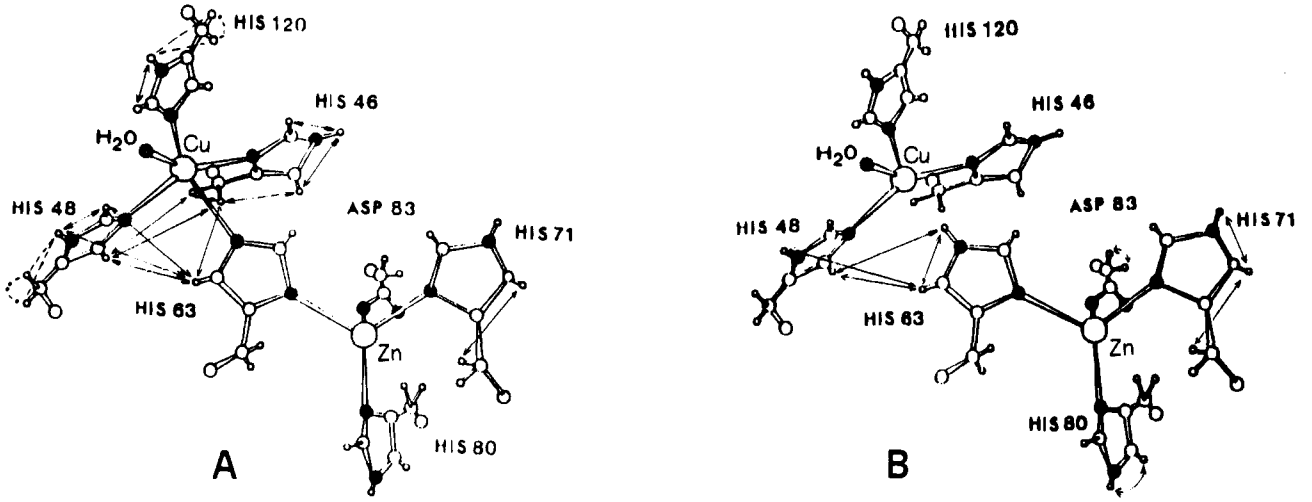

Figure 110. Schematic view of the active site of Cu_2Zn_2SOD in the (A) native form, as it appears from the X-ray analysis and (B) reduced form, adapted from the X-ray structure. The solid lines denote dipolar connectivities detected by means of NOE experiments, whereas the dashed lines indicate additional dipolar connectivities as determined by means of a NOESY experiment.

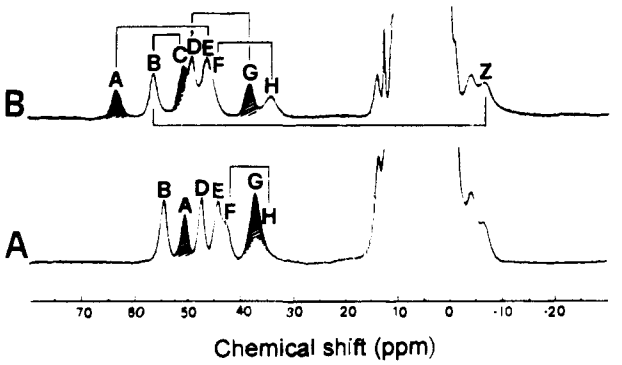

Figure 111. ^1H NMR spectra (200 MHz) of (A) bovine E_2-Co_2SOD and (B) bovine $Cu^I_2Co_2SOD$ in H_2O solutions. The solid lines connect resonances exhibiting NOEs. All the spectra were recorded in H_2O solutions at pH 5.5 and 300 K. The shaded signals indicate protons that are exchangeable in a D_2O solution. (Reprinted from ref 147. Copyright 1990 American Chemical Society.)

of the enzyme (see Figure 110).[688] The loss of the bridging ligand in the reduced protein had been previously proposed on the basis of the absorption spectrum of the cobalt(II) derivative[889] and from EXAFS data.[690] This is also consistent with the following NMR investigation of the reduced $Cu^I_2Co_2$-SOD and the oxidized Cu_2Co_2SOD.

A thorough NMR study of $Cu^I_2Co_2SOD$ has allowed the pairwise assignment of the *meta*-like CH and NH protons of all the bound histidines.[691] Their T_1 values are very short, ranging from 1 to 3 ms. The *ortho*-like protons escape detection at 200 MHz. Through both NOE and NOESY experiments a tentative assignment of the hyperfine-shifted signals has been performed, which is reported in Table XIV. A number of protons which do not experience contact shifts but do experience pseudocontact shifts have been assigned. Analysis of the pseudocontact shifts has provided the orientation and an estimate of the anisotropy of the magnetic susceptibility tensor.[691]

The magnetic coupling present in the oxidized Cu_2Co_2SOD[692] reduces the electron relaxation time of copper(II). This has made possible the detection of hyperfine-shifted signals of protons bound to copper(II) in a copper protein.[56] The spectrum of Cu_2Co_2SOD in

Table XIV. ^1H NMR Chemical Shifts, T_1 Values, and Assignments of the Hyperfine-Shifted Signals in $Cu^I_2Co_2SOD$

signal	chemical shift[a]	T_1[b] (ms)	assignment[c]
A	63.2	1.4	Hε2 His 63
B	55.5	1.8	Hδ2 His 71
C	49.4	2.4	Hε2 His 71
D	48.7	2.4	Hδ2 His 80
E	45.5	1.5	Hδ2 His 63
F	44	≤1.5	Hβ1 (Hβ2) Asp 83
G	38.8	1.3	Hε2 His 80
H	33.2	1.1	Hβ (Hβ1) Asp 83
Z	−6.4	1.4	Hβ2 His 71

[a] Measured at 300 K. [b] Measured at 200 MHz and 300 K, from ref 691. [c] Assigned on the basis of NOE experiments and X-ray data, from ref 691.

H_2O is reported in Figure 112A. It shows a number of hyperfine-shifted signals equal to the number of protons attached to the ligands of both metal ions. The signals belonging to the copper domain are sharper than those belonging to the cobalt(II) domain probably on account of the different S values of the metal ions. The abovementioned criteria plus an analysis of the nuclear relaxation times provided a tentative assignment which was eventually corrected by means of an NOE study.[56,91] The problem with the analysis of nuclear relaxation times is that large electron delocalization effects are present on the imidazole rings. This prevents the safe application of the qualitative rule according to which the larger the relaxation rate, the shorter the distance.[91] The T_1 values of these signals are in the 1–5-ms range. A systematic NOE study later allowed a safe assignment of the hyperfine-shifted signals of this derivative by comparison of the NOE-calculated interproton distances with those observed in the X-ray structure (see Table XV).[92] Owing to the short nuclear relaxation times, small NOEs are expected although spin diffusion is expected to be negligible. A full analysis of different NOE techniques has been performed on this system demonstrating the superiority of steady-state methods with respect to transient NOE experiments.[97] ^1H NMR spectra performed on a protein with the His residues deuterated in the Hε1 position has indicated that the only *ortho*-ring protons observable are those of the

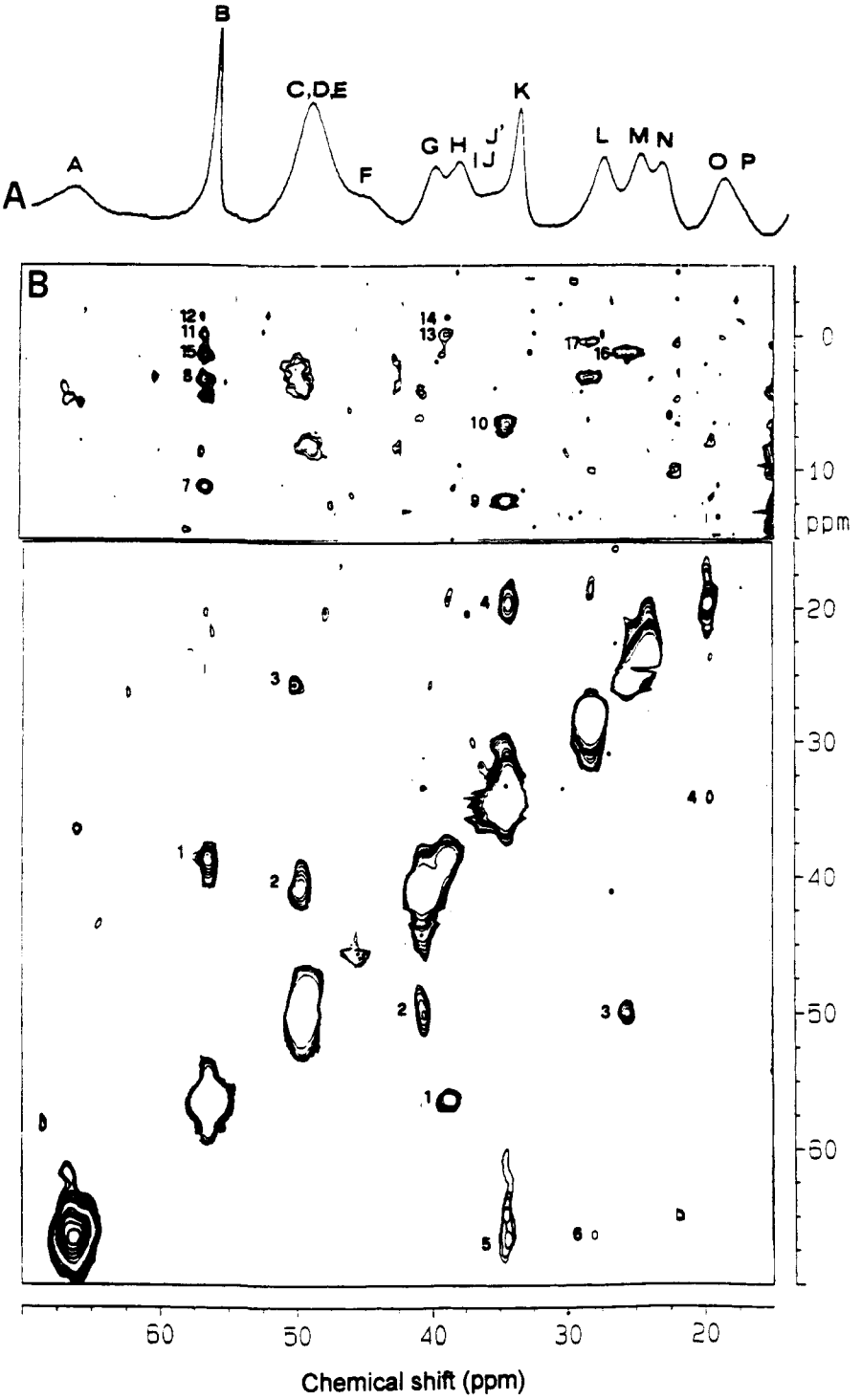

Figure 112. ^1H NMR spectra (600 MHz) of Cu_2Co_2SOD: (A) 1D spectrum and (B) NOESY spectrum. All the spectra were recorded in H_2O solutions at 300 K. Signals B, C, F, J, and K correspond to protons that are exchangeable in a D_2O solution. The NOESY spectrum was performed using a mixing time of 4 ms. Cross-peak labelings are as follows: (1) B, H; (2) C, G; (3) C, M; (4) K, O; (5) A, K; (6) A, L; (7) B, d′; (8) B, k′; (9) K, c′; (10) K, i′; (11) B, n′; (12) B, o′; (13) H, n′; (14) H, o′; (15) B, l′; (16) M, l′ (assigned as reported in Table XV). (Reprinted from ref 693. Copyright 1993 Societa Chimica Italiana.)

copper(II) site, confirming the NOE-based assignment.[147]

Recent NOESY spectra (see Figure 112B)[693] have allowed the extension of the assignment somewhat further from the donor groups of the metal ions. The β-CH_2 groups of all the His residues bound to copper(II) have been identified, except the bridging His 63. The proton pairs for which NOE have been detected are indicated with solid arrows in Figure 110A. Properly performed NOESY experiments have yielded the same connectivities plus those reported in dashed arrows in Figure 110A.

The assignment of the signals of Cu_2Co_2SOD has allowed the authors to monitor changes in the coordination sphere when anions have been added to the protein as well as when mutations have been introduced through site-directed mutagenesis. Azide binds copper(II) and exchanges fast on the NMR time scale, so that through a simple titration the spectrum of the azide derivative can be fully assigned.[56,91,694] It appears

Table XV. ^{1}H NMR Chemical Shifts, T_1 Values, and Assignments of the Hyperfine-Shifted Signals in Cu_2Co_2SOD Belonging to the Protons of Coordinated Residues

signal	chemical shift[a]	T_1[b] (ms)	assignment[c]
A	66.2	1.5	Hδ2 His 63[d,e]
B	56.5	7.8	Hδ1 His 120[d,e]
C	50.3	4.2	Hε2 His 46[d,e]
D	49.4	3.8	Hδ2 His 71[d]
E	48.8	4.6	Hδ2 His 80[d]
F	46.7	2.1	Hε2 His 80 (His 71)[d]
G	40.6	3.5	Hδ2 His 46[d,e]
H	39.0	1.8	Hε1 His 120[d-f]
I	37.4	1.7	Hβ1 (Hβ2) Asp 83[d]
J′	35.6	1.7	Hβ2 (Hβ1) Asp 83[d]
J	35.4		Hε2 His 71 (His 80)[d]
K	34.5	8.0	Hδ1 His 48[d,e]
L	28.4	4.3	Hδ2 His 48[d,e]
M	25.3	2.7	Hε1 His 46[d-f]
N	24.1	2.9	Hδ2 His 120[d]
O	19.6	1.9	Hε1 His 48[d-f]
P	18.7	1.6	Hβ1 His 46[d]
Q	−6.2	2.4	Hβ2 His 71[d]
R	−6.2	2.4	Hβ2 His 46[d]
a′	14.05		Hε2 His 43[e]
b′	12.85		Hδ1 His 43[e]
c′	12.30		Hβ2 His 48[g]
d′	11.21		Hβ2 His 120[g]
e′	10.29		Hε1 Trp 30[e]
f′	8.63		Hε1 His 43[e]
g′	7.38		Hζ1 Trp 30[e]
h′	7.06		Hδ1 Trp 30[e]
i′	6.40		Hβ2 His 48[g]
k′	3.13		Hβ1 His 120[g]
l′	1.23		β-CH_3 Ala 140[e]
m′	0.53		γ1-CH_3 Val 118[e]
n′	0.28		Hγ1 Arg 143[e]
o′	−1.51		γ2-CH_3 Val 118[e]

[a] Measured at 300 K. [b] Measured at 200 MHz and 300 K, from ref 92. [c] Proton-labeling according to Figure 110. [d] Assigned on the basis of NOE experiments and X-ray data, from ref 92. [e] Assigned from NOESY spectra, from ref 693. [f] Assigned by means of selective deuteration of the Hε1 His protons, from ref 147. [g] Assigned by means of NOESY and COSY spectra, from ref 693.

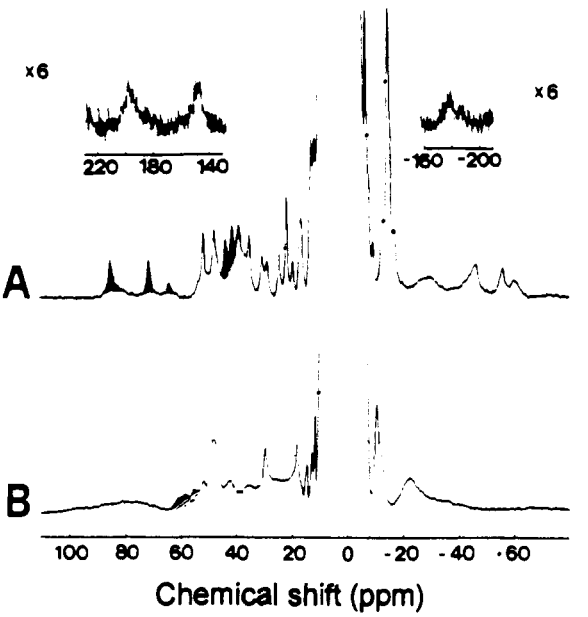

Figure 113. ^{1}H NMR spectra (90 MHz) in H_2O of (A) bovine Co_2Co_2SOD and (B) bovine Co_2Co_2SOD in the presence of a 10-fold excess of phosphate. All the spectra were recorded in H_2O solutions at pH 7.4. The shaded signals indicate protons that are exchangeable in a D_2O solution. (Reprinted from ref 704. Copyright 1987 American Chemical Society.)

that upon azide binding the hyperfine coupling with the protons of His 48 is drastically reduced. Such reduction is largest in the cyanide derivative[695,696] and is smallest with the fluoride derivative.[697] Models of anion binding are available on a spectroscopic basis[696] while the SOD community still waits for an X-ray structure of an anion derivative.

The change in hydrophobicity of the cavity obtained by site-directed mutagenesis regulates the presence of water semicoordinated to copper(II). The hyperfine shifts of His 48 in the copper(II) site are sensitive to mutations in the 137 position.[698] The Ile 137 mutant in particular,[699] apparently without semicoordinated water, displays the largest hyperfine coupling between the unpaired electron and the protons of His 48. Mutants in which the Arg 143 residue is replaced display similar spectra. However, a decreasing affinity to anion binding[700,701] has been observed after replacement of Arg 143 with residues bearing a positive, neutral, or negative charge. In summary, in the SOD case, ^{1}H NMR has proved to be a unique spectroscopic tool in monitoring changes in the active site.

Upon addition of cobalt(II) to the apoenzyme at pH 7.4, a Co_2Co_2 derivative is obtained in which even the copper(II) site is occupied by cobalt(II).[683] The cobalt(II) ion in the copper(II) site is pentacoordinate, and it has a shorter electron relaxation time than the other cobalt(II), which is in a pseudotetrahedral environment. The exchange magnetic coupling between the two ions is shown by the absence of any EPR signal.[702] The ^{1}H NMR spectrum of Co_2Co_2SOD is very rich in hyperfine-shifted signals, which are relatively sharp (see Figure 113A).[703-705] A tentative assignment is available, but the investigations were performed before the application of NOE techniques to this enzyme. Upon additon of phosphate, the NMR spectrum of Co_2Co_2SOD becomes broader (cf. Figure 113B). It was suggested that the phosphate may bridge the Arg 143 residue and the cobalt(II) ion in the copper(II) site by breaking the Co–Co bridge.[704] As a result two tetrahedral cobalt(II) centers are obtained without magnetic coupling. At pH > 10 the influence of phosphate on the NMR spectra vanishes and the spectra resemble those taken in the absence of phosphate.[705]

Alkaline phosphatase (AP) is a dimeric enzyme of MW 94 000 possessing three metal sites in each monomeric unit. These sites are naturally occupied by two zinc(II) and one magnesium(II) ions. The X-ray structure reveals that sites A and B are 3.9 Å apart, whereas sites B and C are 4.2 Å apart.[706] The spectrum of the $Co_2Co_2Mg_2$ enzyme (with the cobalt(II) ions in the A and B sites) is reported in Figure 114A.[58,707] Four signals corresponding to exchangeable protons are observed (e, g, h, and o), initially attributed to Hε2 protons of bound histidines. A more refined crystallographic structure of AP[706] has recently shown that only three His residues are actually bound to the metals in sites A and B. It is reasonable to suppose (from their chemical shifts) that signals e, g, and h correspond to the His NH protons. The fourth exchangeable signal may origin from an exchangeable proton of any other residue experiencing only a pseudocontact shift.[707] The nonexchangeable signals a, c, d, j, k, and l have been

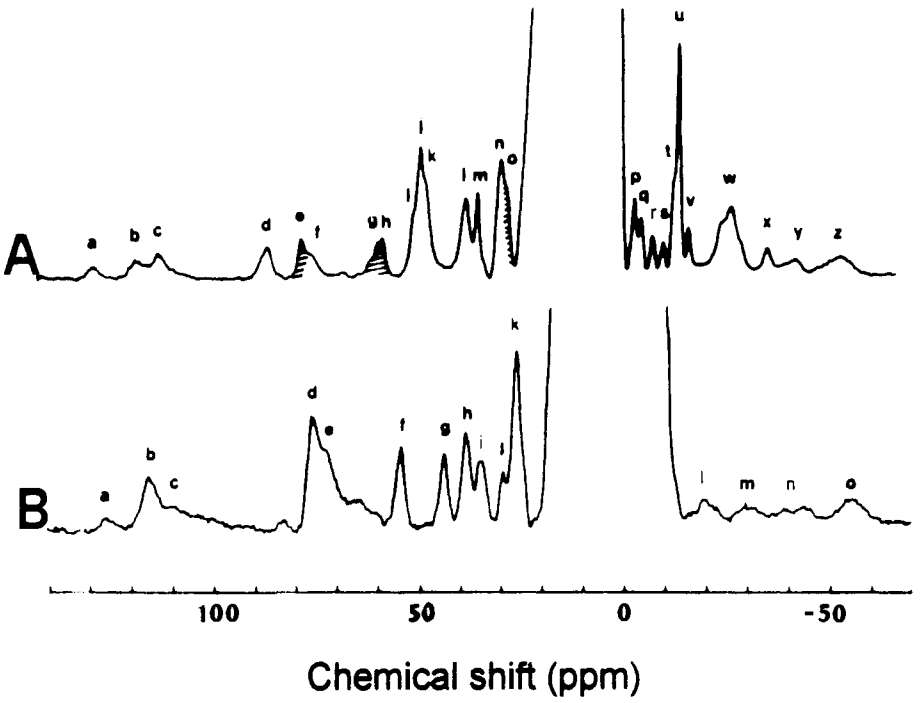

Figure 114. ^1H NMR spectra (90 MHz) of (A) $Co_2Co_2Mg_2AP$ and (B) $Cu_2Co_2Mg_2AP$ in H_2O. All the spectra were recorded in H_2O solutions at 301 K and pH 6.0–6.3. The shaded signals indicate protons that are exchangeable in a D_2O solution. (Reprinted from ref 707. Copyright 1988 American Chemical Society.)

ascribed to the Hε1 or Hδ2 protons of the His residues by considering their shifts and T_1 values.[58,707] The remaining signals are sharper and have longer T_1 values and could correspond to nonligated residues experiencing pseudocontact shifts.

The spectra of $Cu_2Co_2Mg_2AP$ show signals of protons of residues coordinated both to the copper(II) and to the cobalt(II) ion (see Figure 114B). Even if the magnetic coupling between these metal ions is small, it allows the detection of signals of the copper(II) ligands. Some signals display shifts very similar to others observed in Co_2Co_2AP, so that they have been taken as belonging to the B metal site.[707]

The use of zinc replacement by cobalt(II) has been recently attempted in the **zinc finger peptide** CP-1.[708] The location and assignment of the metal-bound and contiguous residues has not been performed in this case. However, the assignment of several nonbound residues and the calculation of the pseudocontact shifts was useful to obtain the orientation and anisotropy of the χ tensor in the molecular frame. These studies are aimed at the use of this information for refining 3D structures in solution.

Azurin (Az) is a blue copper protein of MW 14 000 on which studies have been made by substituting the native metal ion with cobalt(II).[709] A recent crystallographic study yielded the structure of native azurin resolved to 1.93 Å,[710] which is shown in Figure 115A. The copper(II) ion adopts a distorted trigonal bypiramid geometry, being bound to two His and a Cys residue, and more weakly coordinated to a Met and a Gly residue. A preliminary study of cobalt(II)–Az reported the detection of several hyperfine-shifted signals, expected to arise mainly from the coordinated residues.[709] A recent preliminary study has given some clues for their assignment.[711] Two well-shifted signals (a and b, see Figure 115B) are solvent exchangeable and present NOE and NOESY connectivities with signals c and d, assigned to the Nε2 and Nδ2 protons of the two bound histidines respectively. The upfield signal at −7.9 ppm (integrating for three protons) has been assigned to the bound methionine. Intense NOE and NOESY connectivities have been observed between the pairs of signals e,k and f,j, which remain unassigned at this moment.

Stellacyanin is a blue Cu protein in which the metal ion is coordinated to at least two histidines and a cysteine.[712,713] Since its X-ray structure is not available, spectroscopic methods are of help in elucidating the structure of the active site. ^1H NMR spectra of the native enzyme were recorded, but no paramagnetically shifted proton resonances were observed.[712,714] In the spectrum of the Co(II)-substituted protein,[713] several hyperfine-shifted signals may be observed, as shown in Figure 115C. A proposal for the origin of the hyperfine-shifted signals was made on the basis of their T_1 values and pH dependencies, but a thorough assignment is not available.

As we previously noted in section IV, **rubredoxin** bears only one iron ion which is tetrahedrally coordinated, so that even in the ferrous state it is very difficult to detect the signals corresponding to the bound cysteines.[204,715] Replacement of the iron by cobalt(II) renders the ^1H NMR spectrum rich in isotropically shifted signals: seven well-shifted signals in the 270–85 ppm region, and a considerable number of peaks in the 10–50 ppm region as well as in the upfield region are observed (see Figure 116).[208] The far downfield resonances were tentatively assigned to the β-CH_2 groups of the bound cysteines[208] on the basis of their large chemical shifts only. The application of NOE and 2D techniques would be desirable in this protein in order to obtain a full assignment of the hyperfine-shifted signals.

The replacement of the iron(II) ion by cobalt(II) in **uterferrin** yields a catalytically active species with

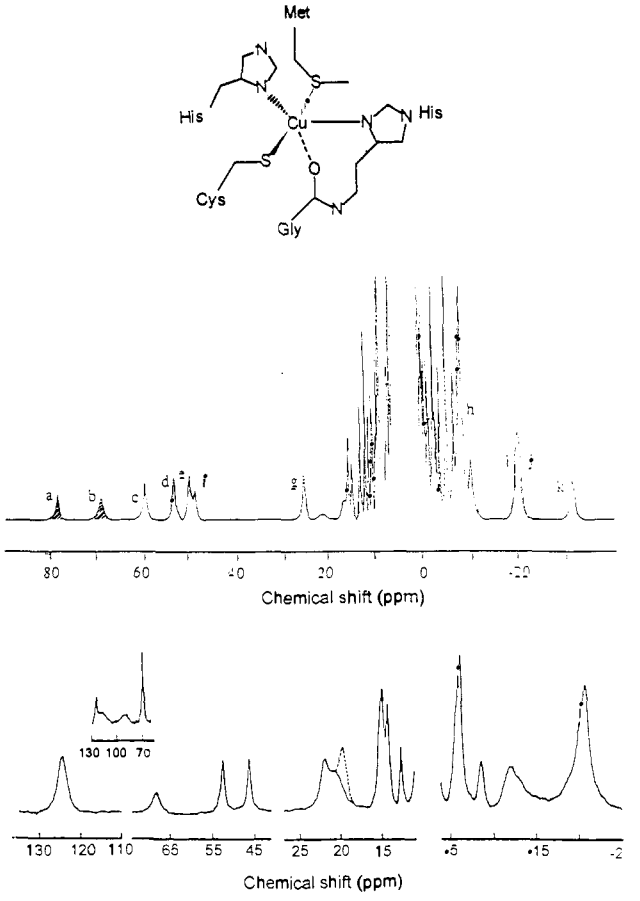

Figure 115. (A) Schematic view of the metal site of native azurin, as results from its X-ray structure; (B) 400-MHz ^1H NMR spectrum of *Pseudomonas aeruginosa* cobalt(II)-substituted azurin in H_2O at pH 4.7 and 298 K (the shaded signals indicate protons that are exchangeable in a D_2O solution); (C) 270-MHz ^1H NMR spectrum of cobalt(II)-substituted stellacyanin from *Rhus vernicifera* at pH 7.3 in an unbuffered D_2O solution at 303 K (the dotted peak at 19 ppm is present in the spectrum recorded in a H_2O solution). Part B, reprinted from ref 764. Copyright 1993 Chemical Society of London. Part C, reprinted from ref 713. Copyright 1989 American Chemical Society.)

isotropically shifted signals displaying T_1 values 2–4 times longer than those of the native enzyme. This fact has allowed a NOESY experiment[637] to be performed and allowed the identification, as in reduced Uf, of the β-CH_2 and two aromatic protons of the tyrosinate ligand and a histidyl NH (see Figure 117). The further identification of three paramagnetically shifted signals giving a NOESY pattern attributable to an aspartate or glutamate residue has yielded the first evidence of a coordinated carboxylate for these proteins.

The iron(II) ion of **isopenicillin N synthase** (IPNS) has also been replaced by cobalt(II).[619] This metal derivative displays sharper isotropically shifted proton signals than the native enzyme. A signal integrating for three exchangeable protons is seen at 78 ppm, and two signals corresponding to nonexchangeable protons are found at 32 and 21 ppm. NOE experiments[619] have shown that these two signals do not belong to the bound His, but to other metal-bound residue and correspond to nearby protons. This has been taken as indicative of the presence of a carboxylate ligand.

Ovotransferrin (Otf) is an iron-binding protein of MW 78 000 which can also bind 2 equiv of cobalt(II), in sites apparently undistinguishable. The metal ion is in an octahedral environment bound to an aspartate, two tyrosines, a histidine, and a synergistic ion, as shown by its X-ray structure.[716,717] The 60-MHz spectrum of cobalt(II)–Otf–bicarbonate shows signals spanning from 120 to −100 ppm (see Figure 118A).[718] Two exchangeable downfield signals were initially assigned to histidine NH protons in the belief that two His residues were bound to the iron ion. Similarly, two signals in the 70–60 ppm range were attributed to *meta*-like histidine protons owing to their shifts and T_1 values. The recently refined X-ray structure[716,717] has shown that only one His residue is bound to the iron ion. The second exchangeable signal may therefore come from a nearby residue sensing only a pseudocontact shift. Four upfield signals with short T_1 values may originate from *ortho*-like protons of the bound tyrosines. The spectrum of the cobalt(II)–Otf–oxalate complex[719] displays a higher number of downfield signals and fewer upfield signals. No precise assignments for them are available.

Lectins are cell-agglutinating proteins which contain one manganese(II) and 1–2 calcium(II) ions per monomeric unit. The manganese site may be occupied by cobalt(II). Cobalt(II) lectins display ^1H NMR spectra with shifts ranging from 100 to −40 ppm (see Figure 118B).[720] The spectra of cobalt(II)-substituted concanavalin A, lentil, and pea lectins have been correlated one another by means of the temperature dependencies of their shifts. Three exchangeable signals are observed, but only one may be attributed to a bound His.

Metallothioenins are metal-storage proteins, rich in cysteine residues, to which several divalent metal ions can bind forming two clusters of structure M_4S_{11} and M_3S_9 (see Figure 119).[721] The Cd_7 derivative has been the object of numerous studies, and its solution structure has been solved by NMR spectroscopy.[715,722,723] Cobalt(II) binding to the apoprotein leads to a final uptake of 7 equiv. The CO_7 derivative yields a well-defined NMR spectrum over a very broad spectral window (ca. 350 ppm),[724] as shown in Figure 120A. The signals display T_1 values between 1 and 7 ms. These resonances were shown to experience not only contact shifts but also a pseudocontact contribution due to an anisotropic χ tensor. Upon comparison with the ^1H NMR spectrum of the Cd_4Co_3 derivative, it was

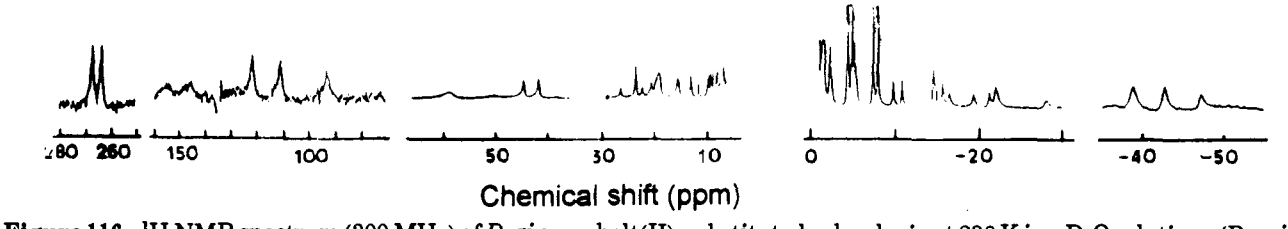

Figure 116. ^1H NMR spectrum (300 MHz) of *D. gigas* cobalt(II)-substituted rubredoxin at 298 K in a D_2O solution. (Reprinted with permission from ref 208. Copyright 1991 Elsevier.

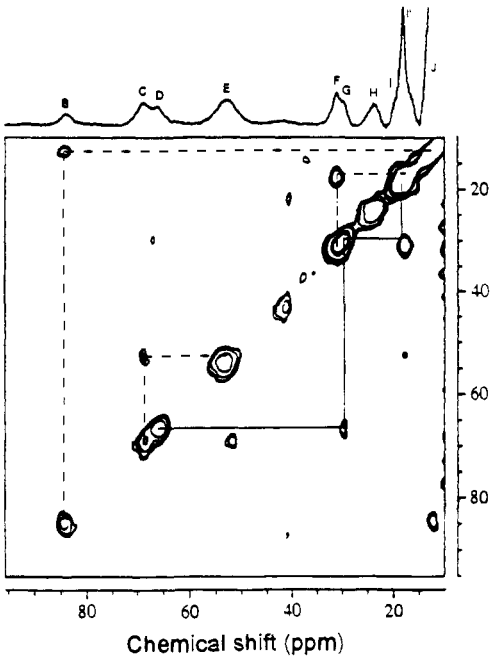

Figure 117. NOESY spectrum (360 MHz) of iron(III), cobalt-(II)-uteroferrin in a buffered D_2O solution (100 mM acetate, 200 mM NaCl, pH 5.3) at 313 K. The spectrum was acquired using a mixing time of 15 ms. (Reprinted from ref 637. Copyright 1992 American Chemical Society.)

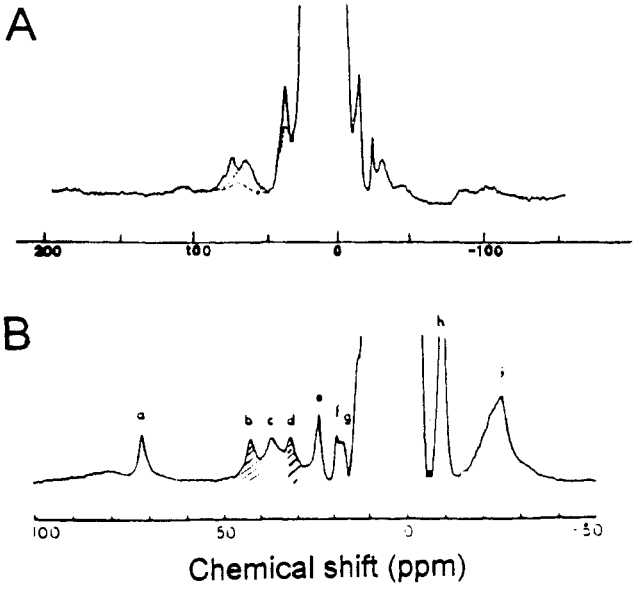

Figure 118. ^1H NMR spectra (90 MHz) of (A) cobalt(II)-(bi)carbonate ovotransferrin complex at pH 8.3 and (B) cobalt-(II) concanavalin A at 300 K. The spectra were recorded in H_2O solutions. The shaded signals indicate protons that are exchangeable in a D_2O solution. (Part A, reprinted from ref 718. Copyright 1984 Springer-Verlag. Part B, reprinted from ref 720. Copyright 1987 *Journal of Biological Chemistry*.)

concluded that the well-resolved spectrum arises from the four-metal cluster. The temperature dependencies of the shifts follow a Curie behavior, except for six of them which display an anti-Curie temperature dependence. This behavior has been rationalized by a theoretical model of the exchange coupling interactions in the cluster.[725] By assuming that J_{12} is zero (the subscripts follow the numbering of Figure 119), cobalt ions 1 and 2 will display a lesser extent of antiferromagnetic coupling than ions 3 and 4. This subsystem

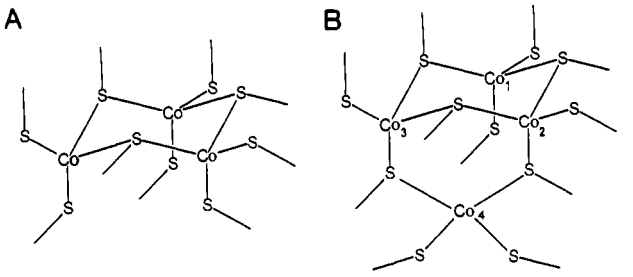

Figure 119. Schematic drawing of the (A) three- and the (B) four-metal clusters in Co_7-metallothionein.

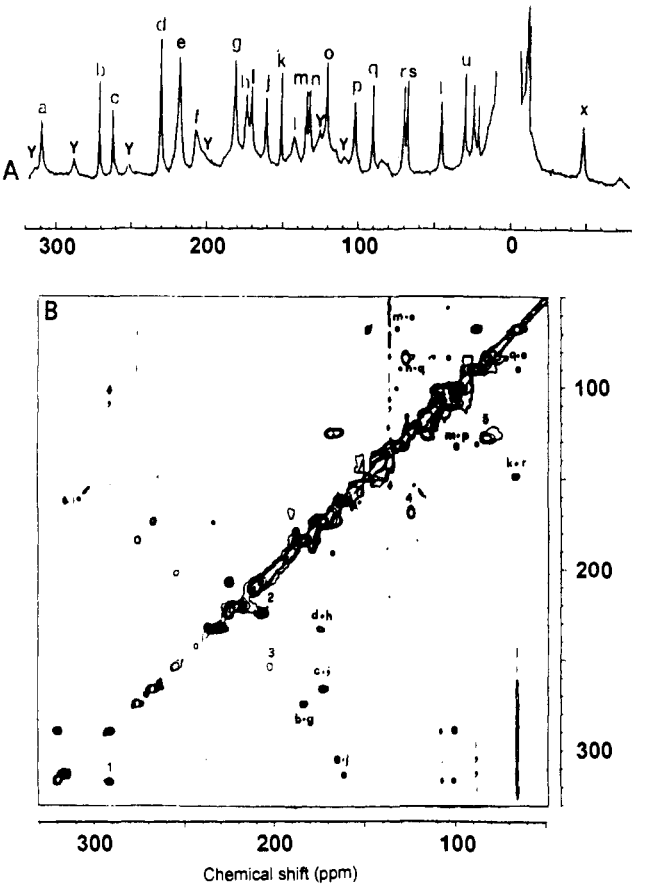

Figure 120. ^1H NMR spectra of Co_7-metallothionein. Part A is a 200-MHz 1D spectrum in D_2O at 300 K. Signals labeled with Y, of fractional intensity, probably belong to some secondary Co_4 cluster species. All signals display a Curie temperature behavior except signals k, m, and p–s which present an anti-Curie temperature dependence. Part B is a 600-MHz NOESY spectrum recorded at 290 K with a mixing time of 7 ms. (Reprinted from ref 102. Copyright 1993 Springer-Verlag.)

will have low-lying excited states with larger spins than the 3–4 subspin system, and it will force the 3–4 pair to be aligned against the external field, for which their protons should exhibit an anti-Curie behavior. The six anti-Curie signals thus correspond to the cysteines binding exclusively the cobalt(II) ions 3 and 4, and to the one bridging them.

In spite of the extremely short T_1 and T_2 values and the broad spectral window needed to cover all the resonances, NOE and NOESY spectra were successful in assigning the β-CH_2 signals of nine of the eleven cysteines of the Co_4S_{11} cluster[102] (see Figure 120B). The spectral window used for the NOESY experiment (250 000 Hz) is the largest ever reported in a 2D study.

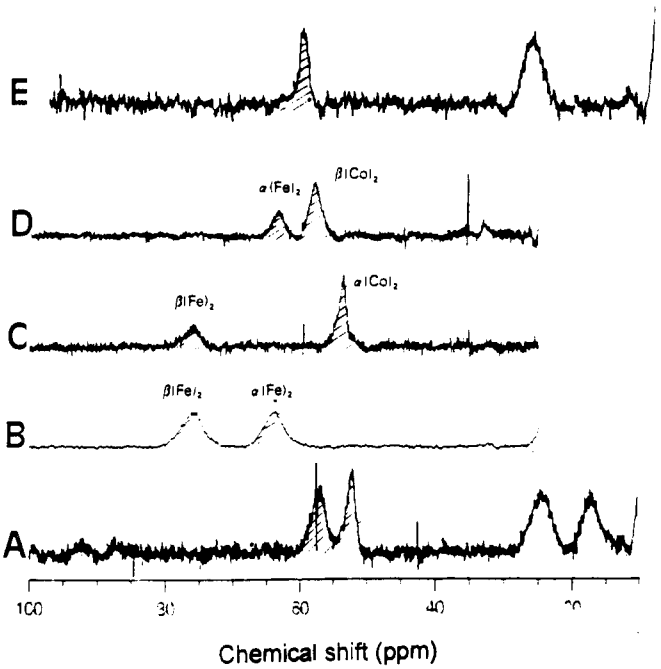

Figure 121. ^{1}H NMR spectra (270 MHz) of (A) deoxyCo–Hb; (B) deoxyFe–Hb; (C) deoxyCo_2^α – Fe_2^β – Hb, (D) deoxyFe_2^α – Co_2^β – Hb, and (E) deoxyCo–Mb. The spectra were recorded in H_2O solutions at 296 K and pH 7.0. The shaded signals indicate protons that are exchangeable in a D_2O solution (from ref 647).

Owing to the low molecular weight of this protein, the use of a solvent mixture to increase the viscosity of the solution was necessary in order to obtain sizable NOEs. This information and the abovementioned theoretical model have allowed the sequence specific assignment of some β-CH_2 cysteine signals.

B. Low-Spin Cobalt(II)

Cobalt-substituted heme proteins are examples of low-spin ($S = 1/2$) cobalt(II) proteins. In tetracoordinate planar systems, the first excited level is far away in energy, so that the metal ion displays long electronic relaxation times (10^{-9}–10^{-10} s) which give rise to broad NMR signals. In the cases of pentacoordination, the first excited level increases in energy, and the NMR spectra become even worse. With regard to the hyperfine shifts, the magnetic anisotropy is higher in tetracoordinate systems, the dipolar contribution is thus large. In the case of pentacoordinate low-spin cobalt(II), however, the hyperfine shift is mainly contact in origin. Cobalt(II)-substituted globins would fall into the latter category.

Deoxycobalt(II)–hemoglobin shows two broad resonances at 58.4 and 53.8 ppm, both solvent exchangeable, attributable to the NH protons of the proximal histidines in the two different subunits of the protein (see Figure 121).[647] The histidine NH protons belonging to the α and β subunits have been identified by performing the spectra on the hybrid derivatives Co_2^α – Fe_2^β – Hb and Fe_2^α – Co_2^β – Hb (cf. Figures 121, parts B–D). The ^{1}H NMR spectrum of deoxycobalt(II)–myoglobin shows an exchangeable signal at 62.2 ppm (see Figure 121E). The nonexchangeable resonances in the 30–15 ppm range have been ascribed to the meso protons.[647]

VIII. Other Ions

A. Nickel(II)

Nickel(II) is a d^8 ion, which may be present in different spin states depending on the coordination geometry.[7] Nickel(II) is paramagnetic ($S = 1$) when it adopts an octahedral or a tetrahedral geometry, but diamagnetic in tetracoordinate planar complexes. Thus, the pseudotetrahedral and the square planar geometries of tetracoordinate nickel(II) complexes may be distinguished by the presence or absence of paramagnetism. Pentacoordinate nickel(II) complexes may be high ($S = 1$) or low spin (diamagnetic) depending on the nature of the donor atoms. Pseudotetrahedral nickel(II) has a 3-fold orbitally degenerate ground state, which accounts for shorter electronic relaxation times than for analogous octahedral complexes. Hence, sharp and well-resolved NMR spectra are obtained for pseudotetrahedral nickel(II) complexes. Where hyperfine shifts are concerned, the larger magnetic anisotropy in tetra- and pentacoordinate complexes induces large dipolar contributions; negligible in the case of octahedral nickel(II).

Nickel(II) has been used, like cobalt(II), as a spectroscopic probe for metalloenzymes which proved difficult to study ordinarily. This is true for zinc enzymes in which, as already discussed in section VII, the metal substitution introduces paramagnetism into the active site; or for some paramagnetic metalloenzymes in which the native metal ion displays long relaxation times, which broaden beyond detection the NMR signals of protons near the paramagnetic center. Almost all the systems which will be discussed in this part of the review have also been subject to cobalt(II) substitution and have been mentioned in the preceding section.

Nickel(II)-substituted **carbonic anhydrase**[726,727] has been less studied than its cobalt(II) analogue, in part due to the fact that upon introduction of the nickel(II) ion, the enzyme retains only a low percentage of its activity. Figure 122, parts A and B, shows the spectra of nickel(II)–CA and its nitrate adduct.[728] The shaded signals correspond, as in cobalt(II)–CA, to the histidine NH protons, and signal d is the Hδ2 proton of His119, as confirmed by NOE measurements.[728,729]

Nickel(III)-substituted **carboxypeptidase A** displays a ^{1}H NMR spectrum with three far downfield shifted signals, as in the case of the analogous cobalt(II)-substituted enzyme (cf. Figures 109A and 122C).[730] Signal a (see Figure 122C) belongs to a NH proton of a His residue and the two other signals are attributable to the *meta*-like protons of the two coordinated histidines.[730]

^{1}H NMR investigations are available for nickel(II)-substituted superoxide dismutase with the nickel in the zinc site.[57,731,732] The systems investigated are E_2Ni_2SOD, $Cu^I_2Ni_2SOD$, Ag_2Ni_2SOD, and $Cu^{II}_2Ni_2SOD$. The signals are sharper than in the analogous cobalt(II) derivatives because nickel(II) has $S = 1$ and cobalt(II) is an $S = 3/2$ ion, and probably also because the electron relaxation times of nickel(II) are shorter (a value of 3×10^{-12} s has been estimated at 300 MHz).[57] Analogously, the signals corresponding to protons in the copper domain have longer T_1 values that the corre-

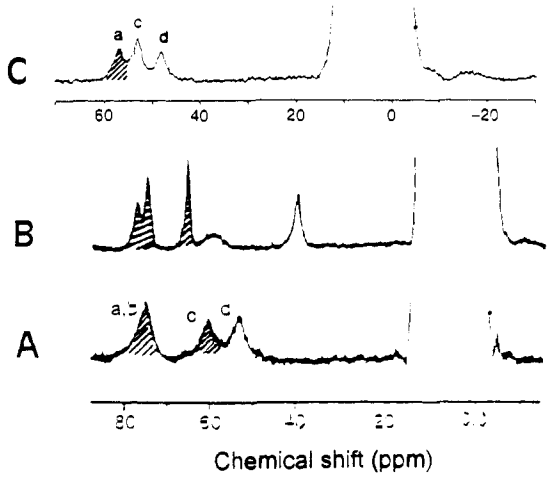

Figure 122. ^{1}H NMR spectra (200 MHz) of (A) NiCA at pH 6.2, (B) the NiCA–NO_3^- adduct, and (C) NiCPA at 293 K, pH 7.0. All the spectra were recorded in H_2O solutions. The shaded signals indicate protons that are exchangeable in a D_2O solution. (Part B, reprinted from ref 728. Copyright 1991 Chemical Society of London. Part C, reprinted from ref 730. Copyright 1992 Chemical Society of London.)

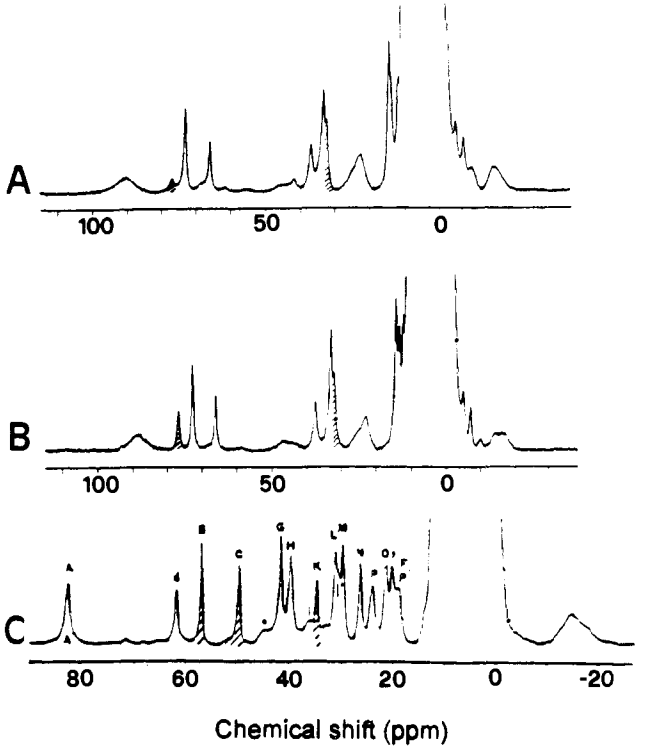

Figure 123. ^{1}H NMR spectra in H_2O solutions at 296 K of (A) $Cu^I_2Ni_2SOD$, recorded at 200 MHz, (B) Ag_2Ni_2SOD, recorded at 200 MHz, and (C) Cu_2Ni_2SOD, recorded at 300 MHz at pH 6.5. The shaded signals indicate protons that are exchangeable in a D_2O solution (from ref 57).

sponding ones in the Cu_2Co_2SOD derivative. The $Cu^I_2Ni_2SOD$ and Ag_2Ni_2SOD derivatives yield very similar spectra, with hyperfine-shifted signals arising only from the nickel(II) ligands (see Figure 123, parts A and B). As in the $Cu^I_2Co_2SOD$ case, three hyperfine-shifted signals corresponding to NH protons were detected, indicating again that His 63 is detached from the copper site. Only tentative assignments are available for the other signals.[57]

The ^{1}H NMR spectrum of $Cu^{II}_2Ni_2SOD$ displays many well-resolved signals (cf. Figure 123C), with T_1 values ranging from 3 to 30 ms.[57] A NOESY experiment is available on this system[732] which clearly displays cross peaks between protons 2 to 4 Å apart. The five NH His protons were pairwise assigned to their vicinal CH ring protons (see Table XVI).

Table XVI. ^{1}H NMR Chemical Shifts, T_1 Values, and Assignments of the Hyperfine-Shifted Signals in $Cu^{II}_2Ni_2SOD$ Belonging to the Protons of Nickel(II)-Coordinated Residues

signal	chemical shift[a]	T_1[b] (ms)	assignment[c]
A	83.9	3.9	Hδ2 His 63[d]
A′	84.0		Hϵ1 His 63[d]
D	62.6	14.8	Hδ2 His 71[d]
E	30.2	3.1	Hδ2 His 80[e]
F	19.4		Hϵ2 His 71[d]
α	12.50		Hβ2 His 48[d]

[a] Measured at 300 K, from ref 732. [b] Measured at 300 MHz and 303 K, from ref 57. [c] Proton labeling according to Figure 110. [d] Assigned from NOESY spectra, from ref 732. [e] Tentative assignment, from ref 732.

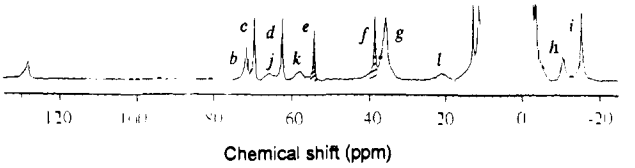

Figure 124. ^{1}H NMR spectrum (200 MHz) of *Pseudomonas aeruginosa* nickel(II)–azurin in a H_2O solution at 298 K and pH 4.7. The shaded signals indicate protons that are exchangeable in a D_2O solution. (Reprinted from ref 734. Copyright 1982 American Chemical Society.)

^{1}H NMR spectra of the two derivatives Ni_2Zn_2SOD are Ni_2Co_2SOD, i.e. with nickel(II) bound in the copper site, have been reported.[733] The spectra of three exchangeable signals in the spectrum of Ni_2Zn_2SOD has been taken as indicative that at least three histidine residues are coordinated to nickel(II), in addition to the bridging one, which does not provide an imidazole NH. In the spectrum of Ni_2Co_2SOD four exchangeable proton resonances are observed, one of which is not influenced by the presence of N_3^- and therefore attributed to the cobalt coordination domain. On this basis the authors proposed a binding environment for nickel(II) very similar to that of copper(II) in native SOD.[733]

When copper(II) is substituted by nickel(II) in **azurin**, the protein yields a well-resolved spectrum (see Figure 124). The first NMR study on nickel(II)–Az led to the determination of the pseudotetrahedral geometry of the nickel(II) ion.[734] Nine hyperfine-shifted signals were detected in the 125 to −20 ppm range in a D_2O solution. In this initial work, only the assignment of the methionine methyl group was proposed because of its intensity. Recently, Moratal Mascarell et al.[735] detected two further signals in the H_2O spectrum, attributable to the NH of the histidine ligands. As in the cobalt(II)-substituted protein, NOE and NOESY experiments have allowed the assignment of the Hδ2 and Hϵ2 protons of one of the bound histidines and a β-CH_2 geminal pair attributable to the metal-bound methionine.

Ni(II)-substituted **rubredoxin** presents a well-resolved NMR spectrum (see Figure 125)[208] with hyperfine shifts spanning from 350 to −30 ppm. The eight more-shifted downfield signals in the 350–150-ppm range were tentatively assigned to the β-CH_2 cysteinil protons, as

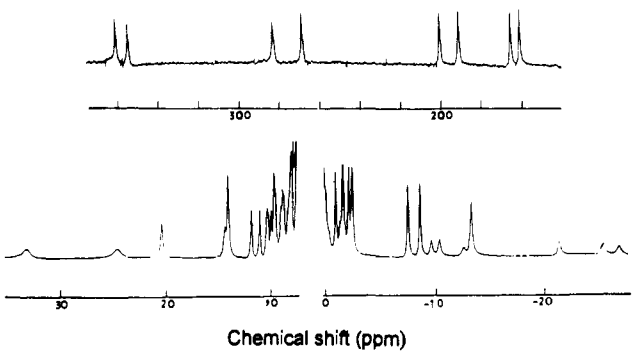

Figure 125. ^{1}H NMR spectrum (300 MHz) of *D. gigas* nickel(II)–rubredoxin at 298 K in a D_2O solution. (Reprinted from ref 208. Copyright 1991 Elsevier.)

done for cobalt(II)–Rd,[208] but a definitive assignment is as yet not available.

A recent communication[736] reported preliminary NMR spectra of the nickel(II) complexes of two zinc finger peptides. A set of relatively sharp hyperfine-shifted signals was detected both in the upfield and in the downfield region of the spectra, even if these were performed using a rather narrow spectral window. The paramagnetism was taken as an indication of the pseudotetrahedral geometry of the complexes, in agreement with the electronic spectroscopy data.

B. Ruthenium(III)

Ruthenium(III) is a d^5 ion which generally gives hexacoordinate complexes. It displays electron relaxation times in the 10^{-11}–10^{-12}-s range. The attachment of pentaammineruthenium(III) to surface histidines of proteins affords semisynthetic multisite metalloproteins which may be used for studying intramolecular electron transfer across long distances.[737] This procedure has been applied to paramagnetic metalloproteins like myoglobin,[738] ferricytochrome *c*,[737] and HiPIPs.[261]

The $Ru(NH_3)_5^{3+}$ species is paramagnetic ($S = {}^1/_2$) and induces hyperfine shifts on the proton signals of the protein histidines coordinated in the sixth coordination position. In the case of sperm whale myoglobin, ^{1}H NMR spectroscopy has been used to monitor possible changes of the protein conformation in the heme site.[738] The spectra of Ru-labeled apomyoglobin, metaquomyoglobin, metcyanomyoglobin, metazidemyoglobin, and deoxymyoglobin have been recorded.[738] The heme shifts remain unaltered upon ruthenium binding. Both a line broadening and a shortening of the T_1 values of the heme signals are noticed in the ruthenium derivatives, these being sizable in the low-spin cases. Since the shortest heme–ruthenium distance is ca. 12 Å, it is unlikely that this could be due to a dipolar relaxation induced by the ruthenium(III) ion.

Ruthenium(III) labeling in a HiPIP has also been studied by ^{1}H NMR spectroscopy. This true case for both the oxidized and reduced HiPIP from *Chromatium gracile*.[261] The Ru-modified proteins display ^{1}H NMR spectra similar to those of the native ones, with small shifts on the hyperfine-shifted signals. Two solvent-exposed histidine residues were labeled with ruthenium(III) and their pK_a values were characterized by means of a pH titration.[261]

C. Lanthanides(III)

Lanthanides have been used as paramagnetic probes, as both shift and relaxation agents, for some decades.[739,740] Lanthanide(III) ions have electron-relaxation times falling in the 10^{-12}–10^{-13}-s range (cf. Table I) owing to the availability of low-lying excited states. This is not the case for gadolinium(III) which, being a d^7 ion, displays a long τ_s value (see Table I). The short electron-relaxation times are reflected in small line broadenings in ^{1}H NMR spectra.

It is generally assumed that f orbitals do not play a great part largely in covalent bonding when the lanthanide(III) ions are coordinated. The electron delocalization onto the ligands is therefore expected to be small. The contact contribution to the shift is generally limited to the nuclei directly coordinated to the metal ion, as it is negligible for nuclei a few bonds away from the paramagnetic center.[741,742] Some methods to separate the contact and the pseudocontact contributions are available in the literature.[742–744] As far as ^{1}H NMR is concerned, the negligible contact contribution to the shifts results in a smaller shift range for the hyperfine-shifted signals.

The small electron delocalization allows one to use the metal-centered approximation for the lanthanides with a higher degree of accuracy than for the first row transition metal ions. Ligand field effects cause magnetic susceptibility anisotropy in the metal ions. Bleaney has derived a treatment which allows the estimation of the pseudocontact shift. A set of parameters ($\mathbf{D}_x$, $\mathbf{D}_y$, and $\mathbf{D}_z$) is used which take into account the ligand field splitting.[745] Provided that $\mathbf{D}$ is larger than the Zeeman energy and smaller than kT, the following general expression may hold:

$$\left(\frac{\Delta\nu}{\nu_0}\right) = -\frac{\mu_0}{4\pi}\frac{\mathbf{g}_J^{\,2}\,\mu_B^{\,2}\,J(J+1)(2J-1)(2J+3)}{60(kT)^2} \times \frac{\mathbf{D}_z(3\cos^2\theta - 1) + (\mathbf{D}_x - \mathbf{D}_y)\sin^2\theta\cos 2\Omega}{r^2} \quad (50)$$

where r, θ, and Ω are polar coordinates with respect to the principal directions of the $\mathbf{D}$ tensor, and $\mathbf{g}_J$ is given by

$$\mathbf{g}_J = 1 + \frac{J(J+1) - L(L+1) + S(S+1)}{2J(J+1)} \quad (51)$$

Sometimes an axial symmetry can be assumed that yields this simplified equation:

$$\left(\frac{\Delta\nu}{\nu_0}\right) = -\frac{\mu_0}{4\pi}\frac{\mathbf{g}_J^{\,2}\,\mu_B^{\,2}\,J(J+1)(2J-1)(2J+3)}{60(kT)^2} \times \frac{\mathbf{D}_z(3\cos^2\theta - 1)}{r^3} \quad (52)$$

The most extensive use of lanthanides(III) as paramagnetic probes has been in calcium-binding proteins, since they have ionic radii similar to that of calcium(II).[740] Therefore they can substitute calcium(II) without major conformational alterations. Lysozyme[746,747] and parvalbumin[748–750] have been investigated in this way.

Carp parvalbumin possesses two calcium binding sites, and both can be occupied by lanthanides(III).

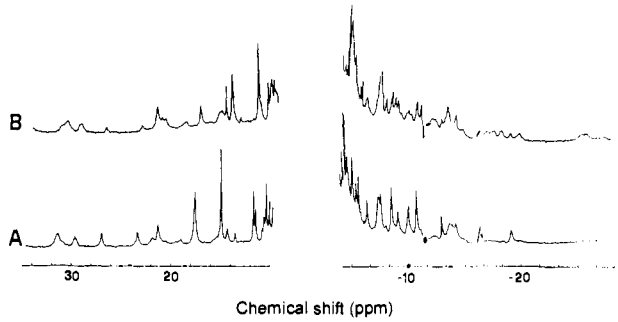

Figure 126. ^1H NMR spectra (270 MHz) of carp parvalbumin in a D_2O solution at 303 K with the addition of ytterbium(III) in an ytterbium(III)/protein ratio of (A) 1.1 and (B) 2.0. (Reprinted from ref 749. Copyright 1981 American Chemical Society.)

The metal affinity is high and the ^1H NMR spectra are in the slow-exchange regime. This is not the case for lysozyme and trypsin, in which the metal binding proceeds in the fast-exchange limit. Ytterbium(III) has been preferentially used as paramagnetic probe for parvalbumin because the contact contribution to NMR parameters is the smallest with respect to the other lanthanides.[743] During the titration of the calcium-saturated protein with ytterbium(III) the two binding sites are sequentially occupied by the lanthanide ion, and signals corresponding to the two binding sites may be recognized (see Figure 126).[748,749] The identification of the two binding sites, however, has not been performed by NMR but by X-ray analysis and visible spectroscopy.[749] The spectra show more than 20 hyperfine-shifted signals spanning from 35 to −20 ppm, with T_1 values from 30 to 300 ms. The signals are not too broad (80–300 Hz at 200 MHz), but do exhibit a sizable Curie line broadening at high fields due to the large J value of ytterbium (7/2). The pseudocontact shifts of five unequivocally assigned resonances plus the shifts of six methyl groups were used to estimate the orientation and principal values of the magnetic susceptibility tensor in solution.[750] By this means, a series of signals corresponding to residues in the first binding site were tentatively assigned.[750] Owing to their relatively long T_1 and T_2 values make lanthanide(III) containing systems suitable for a 2D NMR. Two-dimensional NMR studies on small lanthanide(III) complexes have been available for several years,[125,751] whereas only recently a 2D NMR study on rabbit parvalbumin substituted with Yb^{3+} at the Ca^{2+} EF site has been performed.[752] Using as starting point the X-ray structure of the homologous carp protein, a stepwise sequence-specific assignment of the hyperfine-shifted resonances has been performed. A first set of signals has been assigned on the basis of well-defined connectivity patterns and used to make a preliminary determination of the χ tensor parameters. This parameter has been then used to identify further connectivity patterns in the 2D maps and, in turn, to improve the reliability of the magnetic susceptibility tensor parameters. Thanks to the application of this cyclic procedure all the hyperfine-shifted resonances have been assigned.[752]

The binding of a series of lanthanide(III) ions to human serum apotransferrin has been studied by ^1H NMR spectroscopy.[753] Signals in the 80 to −100 ppm range are observed for several lanthanides (see Figure 127). Titration of apotransferrin with these ions revealed the inequivalence of the two naturally occurring binding sites.

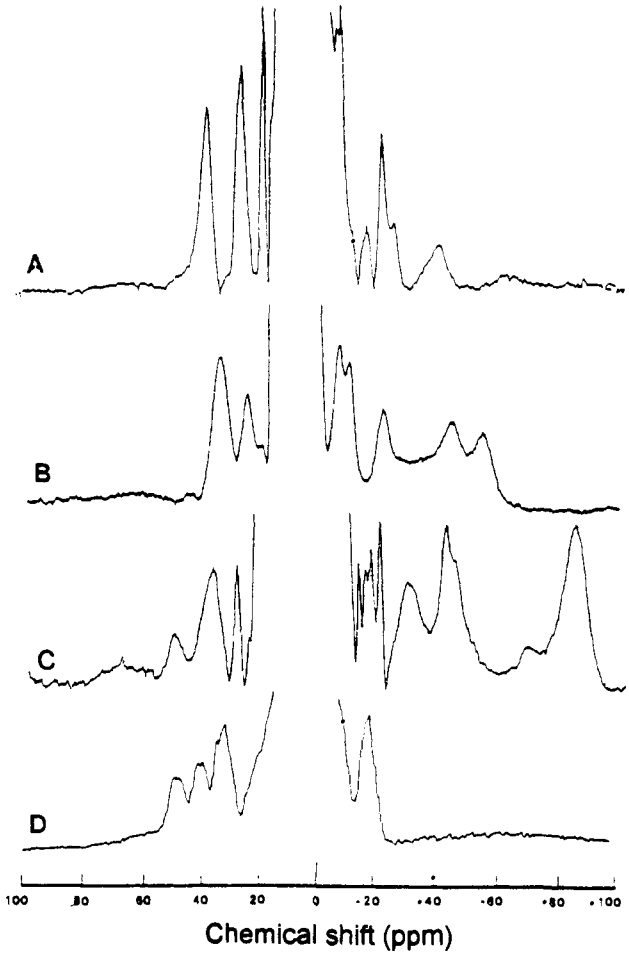

Figure 127. ^1H NMR spectra (90 MHz) of (A) Tm_2–transferrin, (B) Tb_2–transferrin, (C) Dy_2–transferrin, and (D) Yb_2–transferrin. (Reprinted from ref 753. Copyright 1991 Elsevier.)

IX. Heteronuclei

Heteronuclear NMR studies of paramagnetic metalloproteins are far less common than ^1H NMR investigations. This is due to the lower giromagnetic constants and lower natural abundances of ^{13}C and ^{15}N (see section III.B), which are the heteronuclei present in proteins. Nowadays, proteins enriched on ^{13}C and ^{15}N can be easily obtained (see section III.C). The low natural abundance of ^{15}N may be exploited when selective labeled proteins are required, since there is much less interference from natural abundance background than is the case for ^{13}C.

The ^{13}C NMR spectra of the oxidized and reduced forms of the ^{13}C-enriched Fe_2S_2 Fd I from *Anabaena variabilis* were reported in 1983.[194] Two broad resonances at 75 and 168 ppm are noted in the oxidized protein, while the spectrum of reduced Fd displays 11 additional resonances. The proton multiplicity of each carbon was determined by a simple comparison of the proton-coupled and proton-decoupled spectra. Five sharp signals corresponding to nonprotonated carbons were observed near the carbonyl region, tentatively assigned to carbonyl carbons near the paramagnetic

center. The other six broader signals, spanning from 125 to 70 ppm, appeared as multiplets in the proton-decoupled spectrum. However, owing to their large line widths, it was not possible to establish their multiplicities. They were tentatively assigned to α and β cysteinyl carbons. Four of them showed a Curie temperature dependence, whereas the other two displayed an anti-Curie behavior. We now know that this fact arises from the antiferromagnetic coupling in the cluster and, as done for the ^1H spectra (see section IV), signals with a Curie behavior may be ascribed to the iron(III)-bound cysteines and the others to the residues bound to the ferrous ion.

The sequence-specific assignment for the diamagnetic ^1H, ^{13}C, and ^{15}N resonances from the *Anabaena* 7120 Fe_2S_2 Fd has been recently performed. It was also noticed that the hyperfine-shifted ^1H, ^{13}C, and ^{15}N resonances showed drastic differences in the two oxidation states, a phenomenon unobserved in the diamagnetic region. The assignment of the heteronuclear hyperfine-shifted resonances could be useful, especially for comparison with the spectrum of the oxidized protein.

The recognition of ^{13}C spin systems is useful in characterizing amino acid residues.[754,755] These patterns are more easily detectable than ^1H spin systems since the $^{13}C(^{13}C)DQC$ experiment utilizes the $^1J_{CC}$ (ca. 50 Hz), which is considerably larger than normal ^1H–^1H couplings. In addition, the relaxation rate enhancements on ^{13}C signals due to the paramagnetic center are 16 times smaller than those on ^1H resonances (for ^1H and ^{13}C nuclei at the same distance from the paramagnetic center). Markley has detected ^{13}C spin systems for residues near the paramagnetic center of the *Anabaena* 7120 Fd whose ^1H spin systems were not complete.[150]

In the ^{15}N NMR spectrum of oxidized *Anabaena* 7120 Fd[225] nine broad signals were found shifted downfield with respect to the amide nitrogen region. These were assigned to peptide backbone nitrogens. Even if the ^{15}N lines are sharp, the broadening induced in the attached ^1H signals has precluded the detection of scalar connectivities in the $^1H(^{15}N)$ SBC for these resonances. The chemical shifts of these signals are almost independent of temperature.

Some Fds containing two Fe_4S_4 clusters were studied by ^{13}C NMR spectroscopy in 1978.[756] Sixteen signals present in the spectrum of the apoprotein were absent in the native Fd. In turn, 13 new resonances were found in the 120–80-ppm region, which were thus identified as signals corresponding to the α and β carbons of the bound cysteines. Seven-iron Fds from *Ps. putida* and *A. vinelandii* have been grown in a medium with ^{13}C-enriched cysteines in the β position.[278] Those resonances bound to the Fe_4S_4 cluster have been recognized according to their shifts, which are in the 120–90 ppm range, i.e. in a range similar to that observed for the *C. acidi urici* Fd.[756] On the other hand, those corresponding to the Fe_3S_4 cluster fall in the 180–150 ppm range. Curie and anti-Curie temperature dependencies have been observed for the ^{13}C signals of cysteines bound to the three iron cluster, as in the ^1H NMR spectrum (section IV). A HMQC ^{13}C–^1H experiment[278] allowed the correlation of two cysteinyl carbon signals with their respective protons. Cross peaks were detected for fast-relaxing protons (T_1 = 8 ms), confirming the ^1H NMR assignments. In a recent HMQC experiment performed in the 2(Fe_4S_4) Fd from *C. acidi urici*, all the α and β cysteinyl carbon resonances have been located.[265]

When discussing ^{13}C NMR studies on heme proteins, we will only consider here the assignment of signals sensing a contact contribution, i.e. belonging to the heme moiety and to the axial ligands. Extensive ^{13}C assignments are available for nonbound residues in cytochromes, so that the carbon shifts have been useful in order to estimate the orientation of the magnetic susceptibility tensor.[541,757] This subject has been already discussed in section V.B.

In low-spin heme proteins, the spin density is delocalized in the $3e_\pi$ MO of the porphyrin ring, and hence the ^1H and ^{13}C contact shifts for the heme substituents in α positions are expected to be of comparable magnitude but of opposite sign.[7] On the other hand, the pseudocontact contribution is expected to be of the same sign for both nuclei. The heme carbon resonances are not easily detectable, and their shifts do exhibit a sizable ligand-centered contribution.[7,758]

By considering that the ^{13}C and ^1H contact shifts of the α heme substituents are due to a hyperconjugation mechanism from the π electron system, eq 9 may be reformulated as:[7]

$$\left(\frac{\Delta\nu}{\nu_0}\right)_{con} = \frac{2\pi\mu_B \mathbf{g}}{3\gamma_N kT} S(S+1)\, Q_{CX}\, \rho^\pi \qquad (53)$$

where Q_{CX} is the experimental hyperfine-coupling constant (in hertz) and ρ^π is the π spin density on the heme carbon atom to which the substituent is attached. The value of Q_{CX} for protons is highly sensitive and difficult to determine, so that ^{13}C contact shifts are more valuable in providing information about electron delocalization in the heme ring, as we will discuss later. As already mentioned, the contact contribution is expected to be opposite in sign with respect to the proton resonances. For this reason, the heme methyl and α-propionate carbon resonances are found resolved upfield of the ^{13}C diamagnetic envelope. Table XVII reports the ^{13}C and ^1H heme resonances for a series of low-spin iron(III) heme proteins.

Santos and Turner reported the first assignment of ^{13}C heme methyl resonances at natural abundance for horse heart ferricytochrome *c* in 1986.[757,759] Two of these resonances were assigned to specific methyl groups by means of a heterocorrelation ^{13}C,^1H experiment. The other two were identified by polarization transfer experiments, whereas the methyl group of the axial ligand Met 80 was assigned using difference spectra with selective proton decoupling. Recently Timkovich has attempted a series of inverse detection HMQC experiments on horse heart ferricytochrome *c* and cytochrome c_{551} from *Pseudomonas aeruginosa*,[760] assigning the heme methyl, α-CH_2 propionate, and some vinyl ^{13}C resonances. The previous assignments for the heme methyls have been confirmed, all of them detected by means of a 2D experiment. However, for horse heart cytochrome *c*, the heterocorrelation cross peak for the broad methyl signal of Met 80 (110 Hz at 360 MHz) could not be detected. Yamamoto has also detected the four ^{13}C heme methyl signals by means of a ^1H–^{13}C COSY spectrum in the ferricytochrome *c* cyanide complex.[761]

Table XVII. ^{13}C and ^{1}H Chemical Shifts of the Heme Methyl Groups in a Series of Low-Spin Iron(III) Heme Proteins

	cytochrome c		cytochrome c_{551}		cyt c cyanide		metCN-SWMb[a]		metCN-GJMb[b]	
methyl group	^{13}C[c]	^{1}H[c]	^{13}C[d,e]	^{1}H[d]	^{13}C[f,g]	^{1}H[h]	^{13}C[f,i]	^{1}H[f,i]	^{13}C[f,i]	^{1}H[k]
1-CH_3	−17.4[f]	7.11	−46.9	24.80	−39.5	12.94	−39.3	18.77	−29.0	1
3-CH_3	−53.6[j]	31.76	−21.8	13.47	−19.3	7.72	−13.0	5.00	−17.5	6
5-CH_3	−24.1[f]	10.11	−54.3	31.25	−46.2	19.53	−60.5	27.63	−49.5	2
8-CH_3	−68.0[j]	34.57	−35.91	17.17	−50.8	17.50	−33.2	12.97	−25.8	1

[a] Metcyano sperm whale myoglobin. [b] Metcyano *Galeorhinus japonicus* myoglobin. [c] Taken from ref 759, chemical shifts at 303 K. [d] Taken from ref 760, chemical shifts at 305 K. [e] By a HMQC experiment. [f] By a ^{1}H–^{13}C COSY experiment. [g] Taken from ref 761, chemical shifts at 308 K. [h] Taken from ref 761, chemical shifts at 308 K. [i] Taken from refs 423 and 424, chemical shifts at 295 K. [j] By selective decoupling of assigned proton resonances. [k] Taken from ref 405, chemical shifts at 308 K.

Heteronuclear decoupling experiments have allowed La Mar and co-workers to assign the vinyl carbon resonance in a series of paramagnetic myoglobin derivatives reconstituted with selectively ^{13}C-labeled hemin.[565] Later, Yamamoto performed the ^{13}C–^{1}H heterocorrelation spectra of the sperm whale[423] and *Galeorhinus japonicus* metMb–CN^-,[424] locating all the heme methyl resonances. Since the ^{13}C heme methyl resonances are well resolved, the detection of the ^{13}C–^{1}H connectivities made it possible to locate the proton 3-CH_3 resonance, which lies in the diamagnetic envelope. All the heme substituent ^{13}C resonances of sperm whale metMb–CN^- have been recently assigned by means of HMQC experiments, which have proved to be more effective than direct detection methods, because they provide both a higher spectral resolution and shorter experimental times. A sizable contact contribution has also been found in the shift of the β carbon of the distal His residue of sperm whale metMb–CN^-.[762]

If the ^{13}C heme shifts and the orientation and magnitude of the magnetic susceptibility tensor are available, the spin density in the heme-ring carbons may be calculated by factorizing the contact contribution and using eq 53. The calculation of the spin densities at two different temperatures has allowed Turner to explain the anti-Curie behavior of the ^{1}H and ^{13}C methyl signals of horse ferricytochrome *c*.[545] The factors determining the spin density distribution in the heme ring in hemoproteins have already been discussed in section V, when considering the ^{1}H shifts, and do apply also for ^{13}C shifts. The influence of the orientation of the proximal His ligand is more notorious in the case of carbon shifts. In the case of sperm whale and *Galeorhinus japonicus* metMb–CN^-, the following ^{13}C methyl pattern has been found: 3-CH_3 > 8-CH_3 > 5-CH_3 > 1-CH_3,[423,424] which corresponds to an orientation of the proximal His ring along pyrroles II and IV. In the case of the peroxidases HRP–CN^- and LiP–CN^-, the different orientation of the proximal His is reflected in a reversal of the carbon shift trend: 1-CH_3 > 5-CH_3 > 8-CH_3 > 3-CH_3.[762]

Inverse detection HMQC ^{15}N–^{1}H experiments have been recently successfully performed on some cobalt(II)-substituted zinc enzymes. For example, in ^{15}N-enriched cobalt(II) carbonic anhydrase eight NH moieties of residues not bound to the metal have been characterized, with proton line widths ranging from 80 to 150 Hz.[671] It has been also possible to find the nitrogen NH resonances of copper-bound histidines in Cu_2Co_2SOD by using Δ delays of the order of the T_2 values of the proton signals, i.e. of 1.5 ms.[763]

Inverse detection techniques, particularly HMQC experiments, have proved to be applicable to paramagnetic metalloproteins, even if its development is still new. However, it is expected that in the near future it will be as useful as it has been for diamagnetic biomolecules.

X. Perspectives

It is still a common belief that it is impossible to record the NMR spectra of paramagnetic molecules (not only of paramagnetic proteins) because the lines are too broad, the field homogeneity low, cross peaks in 2D experiments lacking, etc. In line with this, the groups of researchers working in the NMR of metalloproteins are very small. Therefore, the advancements are relative slow. The present review shows how much has to be done to proceed with the assignment and to establish proton–proton distances within the systems here discussed. New paramagnetic proteins are becoming available and the utility of substituting zinc with paramagnetic metal ions like cobalt(II) is more and more apparent. Furthermore, we should consider in the number of paramagnetic proteins, the mutants obtained through DNA recombinant techniques. Molecular biology is of particular help to NMR: it may provide large quantity of samples through overexpression and samples labeled with ^{2}H, ^{13}C, or ^{15}N nuclei. ^{13}C- and ^{15}N-labeled proteins will allow the development of HMQC experiments and 3D spectroscopies. We also expect improvements in hardware and software: very large spectral widths in 2D experiments can nowadays be obtained by using ADCs having a lower number of bits; particularly shaped probes can be used to shorten the 90° pulse; the introduction of nuclear relaxation in the simulation of 2D or 3D spectra may become important to plan experiments. New pulse sequences must be planned to suit the particular nature of the NMR experiment on paramagnetic molecules. Therefore, the number of suitable systems is growing and the advancement of the techniques is such that the tridimensional structure in solution can be obtained just like for the diamagnetic proteins of the same size. Furthermore, local information around the metal can be obtained even for proteins of large sizes. Molecular dynamic simulation techniques have been shown to be applicable to systems containing open-shell metal ions.

Acknowledgments. Professors Claudio Luchinat and Lucia Banci are gratefully acknowledged for keeping at the present level an NMR lab in Florence working on NMR of paramagnetic proteins. A.J.V. thanks the ICGEB (International Centre for Genetic Engineering and Biotechnology) for a postdoctoral fellowship, as well as Fundacion Antorchas for further support.

Note Added in Proof

Some relevant papers in the field of iron–sulfur proteins have been recently produced. Sadek et al. have reported on the successful application of TOCSY experiments to *Clostridium pasteurianum* ferredoxin (Sadek, M.; Brownlee, R. T. C.; Scrofani, S. D. B.; Wedd, A. G. *J. Magn. Reson.* **1993**, *101*, 309). Bertini et al. have completed a study on the electronic structure of $Fe_4Se_4^{3+}$ clusters in *C. vinosum* HiPIP and *E. halophila* HiPIP II (Bertini, I.; Ciurli, S.; Dickiy, A.; Luchinat, C. *J. Am. Chem. Soc.*, in press). Finally, Markley et al. have prepared an interesting review on structure–function studies of Fe_2S_2 ferredoxin where the most significant results of the application of NMR techniques to the *Anabaena* 7120 heterocyst and vegetative ferredoxins and mutants are summarized (Holden, H. M.; Jacobson, B. L.; Hurley, J. H.; Tollin, G.; Oh, B.-H.; Skjeldal, L.; Chae, Y. K.; Cheng, H.; Xia, B.; Markley, J. *J. Bioenerg. Biomemb.*, in press).

References

(1) Cohn, M.; Mildvan, A. S. *Adv. Enzymol.* **1970**, *33*, 1.
(2) Bertini, I.; Luchinat, C.; Messori, L. In *Metal ions in biological systems*; Sigel, H., Ed.; Marcel Dekker, Inc.: New York, 1987; Vol. 21, p 47.
(3) Koenig, S. H.; Brown, R. D., III. In *Metal ions in biological systems*; Sigel, H., Ed.; Marcel Dekker, Inc.: New York, 1987; Vol. 21, p 87.
(4) Luchinat, C.; Xia, Z. *Coord. Chem. Rev.* **1992**, *120*, 281.
(5) Dwek, R. A. *Nuclear Magnetic Resonance in Biochemistry: Applications to Enzyme Systems*; Oxford University Press: London, 1973.
(6) La Mar, G. N., Horrocks, W. D., Jr., Holm, R. H., Eds. *NMR of Paramagnetic Molecules*; Academic Press: New York, 1973.
(7) Bertini, I.; Luchinat, C. *NMR of Paramagnetic Molecules in Biological Systems*; Benjamin/Cummings: Menlo Park, CA, 1986.
(8) Banci, L.; Bertini, I.; Luchinat, C. *Nuclear and Electron Relaxation*; VCH: Weinheim, 1991.
(9) Bertini, I.; Banci, L.; Luchinat, C. *Methods Enzymol.* **1989**, *177*, 246.
(10) Banci, L.; Bertini, I.; Luchinat, C.; Piccioli, M. In *NMR and biomolecular structure*; Bertini, I., Molinari, H., Niccolai, N., Eds.; VCH: Weinheim, 1991; p 31.
(11) Banci, L.; Bertini, I.; Luchinat, C.; Messori, L.; Turano, P. *Appl. Magn. Reson.* **1993**, *4*, 461.
(12) Banci, L.; Piccioli, M.; Scozzafava, A. *Coord. Chem. Rev.* **1992**, *120*, 1.
(13) Noggle, J. H.; Schirmer, R. E. *The nuclear Overhauser effect*; Academic Press: New York, 1971.
(14) Neuhaus, D.; Williamson, M. *The nuclear Overhauser effect in structural and conformational analysis*; VCH: New York, 1989.
(15) McConnell, H. M.; Robertson, R. E. *J. Chem. Phys.* **1958**, *29*, 1361.
(16) Kurland, R. J.; McGarvey, B. R. *J. Magn. Reson.* **1970**, *2*, 286.
(17) Wayland, B. B.; Drago, R. S. *J. Am. Chem. Soc.* **1965**, *87*, 2372.
(18) Fitzgerald, R. J.; Drago, R. S. *J. Am. Chem. Soc.* **1967**, *89*, 2879.
(19) Cramer, R. E.; Drago, R. S. *J. Am. Chem. Soc.* **1970**, *92*, 66.
(20) Levy, D. H. *Mol. Phys.* **1966**, *10*, 233.
(21) Perry, W. D.; Drago, R. S.; Herlocker, D. W.; Pagenkopf, G. K.; Czworniak, K. *Inorg. Chem.* **1971**, *10*, 1087.
(22) Quaegebeur, J. P.; Chachaty, C.; Yasukawa, T. *Mol. Phys.* **1979**, *37*, 409.
(23) Karplus, M.; Fraenkel, G. K. *J. Chem. Phys.* **1961**, *35*, 1312.
(24) Eaton, D. R.; Josey, A. D.; Phillips, W. D.; Benson, R. E. *Mol. Phys.* **1962**, *5*, 407.
(25) Fermi, E. *Z. Phys.* **1930**, *60*, 320.
(26) Golding, R. M. *Applied Wave Mechanics*; D. Van Nostrand: London, 1969.
(27) McConnell, H. M.; Chestnut, D. B. *J. Chem. Phys.* **1958**, *28*, 107.
(28) McConnell, H. M. *J. Chem. Phys.* **1956**, *24*, 764.
(29) Kluiber, R. W.; Horrocks, W. D. J. *J. Am. Chem. Soc.* **1965**, *87*, 5350.
(30) Horrocks, W. D., Jr.; Hall, D. D. *Inorg. Chem.* **1971**, *10*, 2368.
(31) Horrocks, W. D., Jr.; *Inorg. Chem.* **1970**, *9*, 670.
(32) Benelli, C.; Bertini, I.; Gatteschi, D. *J. Chem. Soc., Dalton Trans.* **1971**, 661.
(33) Bleaney, B.; Dobson, C. M.; Levine, B. A.; Martin, R. B.; Williams, R. J. P.; Xavier, A. V. *J. Chem. Soc., Chem. Commun.* **1972**, 791.
(34) Doddrell, D. M.; Roberts, J. D. *J. Am. Chem. Soc.* **1970**, *92*, 6839.
(35) Banci, L.; Bertini, I.; Luchinat, C. *Magn. Reson. Rev.* **1986**, *11*, 1.
(36) Muus, L. T.; Atkins, P. W. *Electronic Spin Relaxation in Liquids*; Plenum Press: New York, 1972.
(37) Bertini, I.; Luchinat, C.; Martini, G. In *Electron spin resonance handbook*; Poole, C. P., Ed.; American Association of Physics, CRC: Boca Raton, Part I, in press.
(38) Bertini, I.; Luchinat, C.; Martini, G. In *Electron spin resonance handbook*; Poole, C. P., Ed.; American Association of Physics, CRC: Boca Raton, Part II, in press.
(39) Gueron, M. *J. Magn. Reson.* **1975**, *19*, 58.
(40) Vega, A. J.; Fiat, D. *Mol. Phys.* **1976**, *31*, 347.
(41) Kowalewski, J.; Nordenskiöld, L.; Benetis, N.; Westlund, P.-O. *Progr. Nucl. Magn. Reson. Spectrosc.* **1985**, *17*, 141.
(42) Bloembergen, N.; Purcell, E. M.; Pound, R. V. *Phys. Rev.* **1948**, *73*, 679.
(43) Solomon, I. *Phys. Rev.* **1955**, *99*, 559.
(44) Bloembergen, N. *J. Chem. Phys.* **1957**, *27*, 572.
(45) Bloembergen, N.; Morgan, L. O. *J. Chem. Phys.* **1961**, *34*, 842.
(46) Redfield, A. G. *Phys. Rev.* **1955**, *98*, 1787.
(47) Koenig, S. H. *J. Magn. Reson.* **1982**, *47*, 441.
(48) Bloembergen, N. *J. Chem. Phys.* **1957**, *27*, 575.
(49) Everett, G. W., Jr.; Johnson, A. *J. Am. Chem. Soc.* **1972**, *94*, 6397.
(50) Maekawa, M.; Kitagawa, S.; Munakata, M.; Matsuda, H. *Inorg. Chem.* **1989**, *28*, 1904.
(51) La Mar, G. N.; Thanabal, V.; Johnson, R. D.; Smith, K. M.; Parish, D. W. *J. Biol. Chem.* **1989**, *264*, 5428.
(52) Morishima, I.; Shiro, Y.; Wakino, T. *J. Am. Chem. Soc.* **1985**, *107*, 1063.
(53) Banci, L.; Bertini, I.; Luchinat, C. *Struct. Bonding* **1990**, *72*, 113.
(54) Banci, L.; Bertini, I.; Briganti, F.; Luchinat, C. *New J. Chem.* **1991**, *15*, 467.
(55) Luchinat, C.; Ciurli, S. *Biol. Magn. Reson.*, in press.
(56) Bertini, I.; Lanini, G.; Luchinat, C.; Messori, L.; Monnanni, R.; Scozzafava, A. *J. Am. Chem. Soc.* **1985**, *107*, 4391.
(57) Ming, L. J.; Banci, L.; Luchinat, C.; Bertini, I.; Valentine, J. S. *Inorg. Chem.* **1988**, *27*, 4458.
(58) Banci, L.; Bertini, I.; Luchinat, C.; Viezzoli, M. S.; Wang, Y. *J. Biol. Chem.* **1988**, *263*, 11263.
(59) Vincent, J. B.; Olivier-Lilley, G. L.; Averill, B. A. *Chem. Rev.* **1990**, *90*, 1447.
(60) Que, L., Jr.; True, A. E. *Progr. Inorg. Chem.* **1990**, *38*, 97.
(61) Bertini, I.; Banci, L.; Brown, R. D., III; Koenig, S. H.; Luchinat, C. *Inorg. Chem.* **1988**, *27*, 951.
(62) Dunham, W. R.; Palmer, G.; Sands, R. H.; Bearden, A. J. *Biochim. Biophys. Acta* **1971**, *253*, 373.
(63) Bencini, A.; Gatteschi, D. *Electron Paramagnetic Resonance of Exchange-Coupled Systems*; Springer-Verlag: Berlin, 1990.
(64) Owens, C.; Drago, R. S.; Bertini, I.; Luchinat, C.; Banci, L. *J. Am. Chem. Soc.* **1986**, *108*, 3298.
(65) Bertini, I.; Lanini, G.; Luchinat, C.; Mancini, M.; Spina, G. *J. Magn. Reson.* **1985**, *63*, 56.
(66) Noodleman, L. *Inorg. Chem.* **1991**, *30*, 246.
(67) Noodleman, L. *Inorg. Chem.* **1991**, *30*, 256.
(68) Barbaro, P.; Bencini, A.; Bertini, I.; Briganti, F.; Midollini, S. *J. Am. Chem. Soc.* **1990**, *112*, 7238.
(69) Bertini, I.; Briganti, F.; Luchinat, C.; Scozzafava, A. *Inorg. Chem.* **1990**, *29*, 1874.
(70) Pople, J. A.; Schneider, W. G.; Bernstein, H. J. *High resolution nuclear magnetic resonance*; McGraw-Hill: New York, 1959.
(71) Wilson, L. J.; Bertini, I. *J. Coord. Chem.* **1971**, *1*, 237.
(72) La Mar, G. N.; Walker, F. A. *J. Am. Chem. Soc.* **1973**, *95*, 6950.
(73) Bertini, I.; Johnston, D. L.; Horrocks, W. D. W. *Inorg. Chem.* **1970**, *9*, 693.
(74) Eaton, D. R. *J. Am. Chem. Soc.* **1965**, *87*, 3097.
(75) La Mar, G. N.; Sacconi, L. *J. Am. Chem. Soc.* **1968**, *90*, 7216.
(76) Bertini, I.; Sacconi, L.; Speroni, G. P. *Inorg. Chem.* **1972**, *11*, 1323.
(77) Bertini, I.; Sacconi, L. *J. Mol. Struct.* **1973**, *19*, 371.
(78) La Mar, G. N.; Eaton, G. R.; Holm, R. H.; Walker, F. A. *J. Am. Chem. Soc.* **1973**, *95*, 63.
(79) Eaton, D. R.; Josey, A. D.; Phillips, W. D.; Benson, R. E. *J. Chem. Phys.* **1962**, *37*, 347.
(80) Ernst, R. R.; O'Connor, M. J.; Holm, R. H. *J. Am. Chem. Soc.* **1968**, *90*, 5735.
(81) La Mar, G. N. *J. Am. Chem. Soc.* **1965**, *87*, 3567.
(82) La Mar, G. N.; Horrocks, W. D. J.; Allen, L. C. *J. Chem. Phys.* **1964**, *41*, 2126.
(83) Happe, J. A.; Ward, R. L. *J. Chem. Phys.* **1963**, *39*, 1211.
(84) Satterlee, J. D.; Erman, J. E.; La Mar, G. N.; Smith, K. M.; Langry, K. C. *J. Am. Chem. Soc.* **1983**, *105*, 2099.
(85) La Mar, G. N.; de Ropp, J. S.; Smith, K. M.; Langry, K. C. *J. Biol. Chem.* **1980**, *255*, 6646.
(86) La Mar, G. N.; Anderson, R. R.; Budd, D. L.; Smith, K. M.; Langry, K. C.; Gersonde, K.; Sick, H. *Biochemistry* **1981**, *20*, 4429.
(87) La Mar, G. N.; Budd, D. L.; Smith, K. M.; Langry, K. C. *J. Am. Chem. Soc.* **1980**, *102*, 1822.
(88) Vold, R. L.; Waugh, J. S.; Klein, M. P.; Phelps, D. E. *J. Chem. Phys.* **1968**, *48*, 3831.
(89) Unger, S. W.; Lecomte, J. T. J.; La Mar, G. N. *J. Magn. Reson.* **1985**, *64*, 521.
(90) Unger, S. W.; Jue, T.; La Mar, G. N. *J. Magn. Reson.* **1985**, *61*, 448.
(91) Banci, L.; Bertini, I.; Luchinat, C.; Scozzafava, A. *J. Am. Chem. Soc.* **1987**, *109*, 2328.

(92) Banci, L.; Bertini, I.; Luchinat, C.; Piccioli, M.; Scozzafava, A.; Turano, P. *Inorg. Chem.* **1989**, *28*, 4650.
(93) Johnson, R. D.; Ramaprasad, S.; La Mar, G. N. *J. Am. Chem. Soc.* **1983**, *105*, 7205.
(94) Granot, J. *J. Magn. Reson.* **1982**, *49*, 257.
(95) Duben, A. J.; Hutton, W. C. *J. Magn. Reson.* **1990**, *88*, 60.
(96) Thanabal, V.; de Ropp, J. S.; La Mar, G. N. *J. Am. Chem. Soc.* **1987**, *109*, 265.
(97) Banci, L.; Bertini, I.; Luchinat, C.; Piccioli, M. *FEBS Lett.* **1990**, *272*, 175.
(98) Wagner, G.; Wüthrich, K. *J. Magn. Reson.* **1979**, *33*, 675.
(99) Gordon, S. L.; Wüthrich, K. *J. Am. Chem. Soc.* **1978**, *100*, 7094.
(100) Paci, M.; Desideri, A.; Sette, M.; Falconi, M.; Rotilio, G. *FEBS Lett.* **1990**, *261*, 231.
(101) Kalk, A.; Berendsen, H. J. C. *J. Magn. Reson.* **1976**, *24*, 343.
(102) Bertini, I.; Luchinat, C.; Messori, L.; Vasak, M. *Eur. J. Biochem.* **1993**, *211*, 235.
(103) Dugad, L. B.; La Mar, G. N.; Unger, S. W. *J. Am. Chem. Soc.* **1990**, *112*, 1386.
(104) Lecomte, J. T. J.; Unger, S. W.; La Mar, G. N. *J. Magn. Reson.* **1991**, *94*, 112.
(105) Inubushi, T.; Becker, E. D. *J. Magn. Reson.* **1983**, *51*, 128.
(106) Hochmann, J.; Kellerhalls, H. *J. Magn. Reson.* **1980**, *38*, 23.
(107) Gueron, M.; Plateau, P.; Decorps, M. *Progr. Nucl. Magn. Reson. Spectrosc.* **1991**, *23*, 135.
(108) Mc Lachan, S. J.; La Mar, G. N.; Lee, K.-B. *Biochim. Biophys. Acta* **1988**, *957*, 430.
(109) Emerson, S. D.; La Mar, G. N. *Biochemistry* **1990**, *29*, 1545.
(110) Bax, A. *Two dimensional nuclear magnetic resonance in liquids*; Reidel: Dordrecht, 1982.
(111) Ernst, R. R.; Bodenhausen, G.; Wokaun, A. *Principles of Nuclear Magnetic Resonance in one and two dimensions*; Oxford University Press: London, 1987.
(112) Wüthrich, K. J. *NMR of protein and nucleic acids*; Wiley: New York, 1986.
(113) Kessler, H.; Gehrke, M.; Griesinger, C. *Angew. Chem. Int. Ed. Engl.* **1988**, 490.
(114) Bax, A. *Annu. Rev. Biochem.* **1989**, *58*, 223.
(115) Croasmun, W. R.; Carlson, R. M. *Two Dimensional NMR Spectroscopy*; VCH Publishers: New York, 1987.
(116) Aue, W. P.; Bachmann, P.; Wokaun, A.; Ernst, R. R. *J. Magn. Reson.* **1978**, *29*, 523.
(117) Macura, S.; Ernst, R. R. *Mol. Phys.* **1980**, *41*, 95.
(118) Banci, L.; Bertini, I.; Luchinat, C. *Methods Enzymol.*, in press.
(119) Bertini, I.; Dikiy, A.; Luchinat, C.; Piccioli, M.; Tarchi, D. *J. Magn. Reson.*, in press.
(120) Jeener, J.; Meier, B. H.; Bachmann, P.; Ernst, R. R. *J. Chem. Phys.* **1979**, *71*, 4546.
(121) Davis, D. G.; Bax, A. *J. Magn. Reson.* **1985**, *64*, 533.
(122) Santos, H.; Turner, D. L.; Xavier, A. V.; LeGall, J. *J. Magn. Reson.* **1984**, *59*, 177.
(123) Feng, Y.; Roder, H.; Englander, S. W. *Biophys. J.* **1990**, *57*, 15.
(124) Feng, Y.; Roder, H.; Englander, S. W.; Wand, A. J.; DiStefano, D. L. *Biochemistry* **1989**, *28*, 195.
(125) Jenkins, B. G.; Lauffer, R. B. *Inorg. Chem.* **1988**, *27*, 4730.
(126) Luchinat, C.; Steuernagel, S.; Turano, P. *Inorg. Chem.* **1990**, *29*, 4351.
(127) Bertini, I.; Briganti, F.; Luchinat, C.; Messori, L.; Monnanni, R.; Scozzafava, A.; Vallini, G. *Eur. J. Biochem.* **1992**, *204*, 831.
(128) Gupta, G. P.; Koenig, S. H.; Redfield, A. G. *J. Magn. Reson.* **1972**, *7*, 66.
(129) Concar, D. W.; Hill, H. A. O.; Moore, G. R.; Whitford, D.; Williams, R. J. P. *FEBS Lett.* **1986**, *206*, 15.
(130) Bertini, I.; Gaudemer, A.; Luchinat, C.; Piccioli, M. *Biochemistry*, in press.
(131) Bax, A.; Freeman, R.; Morris, G. *J. Magn. Reson.* **1981**, *42*, 164.
(132) Bax, A.; Freeman, R. *J. Magn. Reson.* **1981**, *44*, 542.
(133) Yu, L. P.; La Mar, G. N.; Rajarathnam, K. *J. Am. Chem. Soc.* **1990**, *112*, 9527.
(134) Bertini, I.; Capozzi, F.; Luchinat, C.; Turano, P. *J. Magn. Reson.* **1991**, *95*, 244.
(135) Xavier, A. V.; Turner, D. L.; Santos, H. *Methods Enzymol.*, in press.
(136) Talluri, S.; Scheraga, H. A. *J. Magn. Reson.* **1990**, *86*, 1.
(137) Bertini, I.; Luchinat, C.; Tarchi, D. *Chem. Phys. Lett.* **1993**, *203*, 445.
(138) Bax, A.; Griffey, R. H.; Hawkins, B. L. *J. Am. Chem. Soc.* **1983**, *105*, 7188.
(139) Bax, A.; Griffey, R. H.; Hawkins, B. L. *J. Magn. Reson.* **1983**, *55*, 301.
(140) Müller, L. *J. Am. Chem. Soc.* **1979**, *101*, 4481.
(141) Bax, A.; Davis, D. G. *J. Magn. Reson.* **1985**, *65*, 355.
(142) Braunschweiler, L.; Ernst, R. R. *J. Magn. Reson.* **1983**, *53*, 521.
(143) Bothner-By, A. A.; Stephans, R. L.; Lee, J.; Warren, C. D.; Jeanloz, R. W. *J. Am. Chem. Soc.* **1984**, *106*, 811.
(144) Salguerio, C. A.; Turner, D. L.; Santos, H.; LeGall, J.; Xavier, A. V. *FEBS Lett.* **1992**, *314*, 155.
(145) LeMaster, D. M. *Methods Enzymol.* **1989**, *177*, 23.
(146) Meadows, D. H.; Jardetzky, O.; Epand, R. M.; Ruterjans, H. H.; Scheraga, H. A. *Proc. Natl. Acad. Sci. U.S.A.* **1968**, *60*, 766.
(147) Banci, L.; Bertini, I.; Luchinat, C.; Viezzoli, M. S. *Inorg. Chem.* **1990**, *29*, 1438.
(148) Muchmore, D. C.; McIntosh, L. P.; Russell, C. B.; Anderson, D. E.; Dahlquist, F. W. *Methods Enzymol.* **1989**, *177*, 44.
(149) McIntosh, L. P.; Griffey, R. H.; Muchmore, D. C.; Nielson, C. P.; Redfield, A. G.; Dahlquist, F. W. *Proc. Natl. Acad. Sci. U.S.A.* **1987**, *84*, 1244.
(150) Oh, B.-H.; Mooberry, E. S.; Markley, J. L. *Biochemistry* **1990**, *29*, 4004.
(151) Cammack, R. *Adv. Inorg. Chem.* **1992**, *38*, 281.
(152) Howard, J. B.; Rees, D. C. *Adv. Protein Chem.* **1991**, *42*, 99199.
(153) Thompson, A. J. In *Metalloproteins*; Harrison, P., Ed.; Verlag Chemie: Weinheim, FRG, 1985; p 79.
(154) Beinert, H. *FASEB J.* **1990**, *4*, 2483.
(155) Kennedy, M. C.; Stout, C. D. *Adv. Inorg. Chem.* **1992**, *38*, 323.
(156) Berg, J. M.; Holm, R. H. Iron Sulfur Proteins. In *Iron Sulfur Proteins*; Spiro, T. G., Ed.; Wiley-Interscience: New York, 1982; p 1.
(157) Holm, R. H. *Adv. Inorg. Chem.* **1992**, *38*, 1.
(158) Holm, R. H.; Ciurli, S.; Weigel, J. A. In *Progress in Inorganic Chemistry: Bioinorganic Chemistry*; Lippard, S. J., Ed.; John Wiley & Sons, Inc.: New York, 1990; Vol. 38, p 1.
(159) Stack, T. D. P.; Holm, R. H. *J. Am. Chem. Soc.* **1988**, *110*, 2484.
(160) Reynolds, J. G.; Laskowski, E. J.; Holm, R. H. *J. Am. Chem. Soc.* **1978**, *100*, 5315.
(161) Holm, R. H.; Phillips, W. D.; Averill, B. A.; Mayerle, J. J.; Herskovitz, T. *J. Am. Chem. Soc.* **1974**, *96*, 2109.
(162) Rypniewski, W. R.; Breiter, D. R.; Benning, M. M.; Wesenberg, G.; Oh, B.-H.; Markley, J. L.; Rayment, I.; Holden, H. M. *Biochemistry* **1991**, *30*, 4126.
(163) Fukuyama, K.; Hase, T.; Matsumoto, S.; Tsukihara, T.; Katsube, Y.; Tanaka, N.; Kakudo, M.; Wada, K.; Matsubara, H. *Nature* **1980**, *286*, 522.
(164) Tsukihara, T.; Fukuyama, K.; Nakamura, M.; Katsube, Y.; Tanaka, N.; Kakudo, M.; Wasa, K.; Hase, T.; Matsubara, H. *J. Biochem.* **1981**, *90*, 1763.
(165) Carter, C. W. J.; Kraut, J.; Freer, S. T.; Alden, R. A. *J. Biol. Chem.* **1974**, *249*, 6339.
(166) Carter, C. W. J. In *Iron Sulfur Protein*; Lovenberg, W., Ed.; Academic Press: New York, 1977; p 157.
(167) Breiter, D. R.; Meyer, T. E.; Rayment, I.; Holden, H. M. *J. Biol. Chem.* **1977**, *252*, 18660.
(168) Kissinger, C. R.; Adman, E. T.; Sieker, L. C.; Jensen, L. H.; LeGall, J. *FEBS Lett.* **1989**, *244*, 447.
(169) Kissinger, C. R.; Adman, E. T.; Sieker, L. C.; Jensen, L. H. *J. Am. Chem. Soc.* **1988**, *110*, 8721.
(170) Matsubara, H.; Saeki, K. *Adv. Inorg. Chem.* **1992**, *38*, 223.
(171) Backes, G.; Mino, Y.; Loehr, T. M.; Meyer, T. E.; Cusanovich, M. A.; Sweeney, W. V.; Adman, E. T.; Sanders-Loehr, J. *J. Am. Chem. Soc.* **1991**, *113*, 2055.
(172) Fukuyama, K.; Nagahara, Y.; Tsukihara, T.; Katsube, Y. *J. Mol. Biol.* **1988**, *199*, 183.
(173) Fukuyama, K.; Nagahara, Y.; Tsukihara, T.; Katsube, Y. *J. Mol. Biol.* **1989**, *210*, 383.
(174) Kissinger, C. R.; Sieker, L. C.; Adman, E. T.; Jensen, L. H. *J. Mol. Biol.* **1991**, *219*, 693.
(175) Krishnamoorthy, H. M.; Hendrickson, W. A.; Orme-Johnson, W. H.; Merritt, E. A.; Phizackerley, R. P. *J. Biol. Chem.* **1988**, *263*, 18430.
(176) Stout, G. H.; Turley, S.; Sieker, L. C.; Jensen, L. H. *Proc. Natl. Acad. Sci. U.S.A.* **1988**, *85*, 1020.
(177) Jacobson, B. L.; Chae, Y. K.; Markley, J. L.; Rayment, I.; Holden, H. M. *Biochemistry* **1993**, *32*, 6788.
(178) Stout, C. D. *J. Mol. Biol.* **1989**, *205*, 545.
(179) Adman, E. T.; Sieker, L. C.; Jensen, L. H. *J. Biol. Chem.* **1976**, *251*, 3801.
(180) Adman, E. T.; Sieker, L. C.; Jensen, L. H. *J. Biol. Chem.* **1973**, *248*, 3987.
(181) Hagen, W. R.; Pierik, A. J.; Veeger, C. *J. Chem. Soc., Faraday Trans.* **1989**, *85*, 4083.
(182) Pierik, A. J.; Wolbert, R. B. G.; Mutsaers, P. H. A.; Hagen, W. R.; Veeger, C. *Eur. J. Biochem.* **1992**, *206*, 697.
(183) Gurbiel, R. J.; Ohnishi, T.; Robertson, D. E.; Daldal, F.; Hoffman, B. M. *Biochemistry* **1991**, *30*, 11579.
(184) Gurbiel, R. J.; Batie, C. J.; Sivaraja, M.; True, A. E.; Fee, J. A.; Hoffman, B. M.; Ballou, D. P. *Biochemistry* **1989**, *28*, 4861.
(185) Werst, M. M.; Kennedy, M. C.; Beinert, H.; Hoffman, B. M. *Biochemistry* **1990**, *29*, 10526.
(186) George, S. J.; Armstrong, F. A.; Hatchikian, E. C.; Thompson, A. J. *Biochem. J.* **1989**, *264*, 275.
(187) Conover, R. C.; Kowal, A. T.; Fu, W.; Park, J.-B.; Aono, S.; Adams, M. W. W.; Johnson, M. K. *J. Biol. Chem.* **1990**, *265*, 8533.
(188) Phillips, W. D.; Poe, M.; Weiher, J. F.; McDonald, C. C.; Lovenberg, W. *Nature* **1970**, *227*, 574.
(189) Poe, M.; Phillips, W. D.; McDonald, C. C.; Lovenberg, W. *Proc. Natl. Acad. Sci. U.S.A.* **1970**, *65*, 797.
(190) Poe, M.; Phillips, W. D.; Glickson, J. D.; McDonald, C. C.; San Pietro, A. *Proc. Natl. Acad. Sci. U.S.A.* **1971**, *68*, 68.
(191) Phillips, W. D.; Poe, M.; McDonald, C. C.; Bartsch, R. G. *Proc. Natl. Acad. Sci. U.S.A.* **1970**, *67*, 682.

(192) Nagayama, K.; Ozaki, Y.; Kyogoku, Y.; Hase, T.; Matsubara, H. *J. Biochem.* **1983**, *94*, 893.
(193) Takahashi, Y.; Hase, T.; Wada, K.; Matsubara, H. *J. Biochem.* **1981**, *90*, 1825.
(194) Chan, T.-M.; Markley, J. L. *Biochemistry* **1983**, *22*, 6008.
(195) Krishnamoorthi, R.; Cusanovich, M. A.; Meyer, T. E.; Przysiecki, C. T. *Eur. J. Biochem.* **1989**, *181*, 81.
(196) Moura, J. J. G.; Xavier, A. V.; Bruschi, M.; LeGall, J. *Biochim. Biophys. Acta* **1977**, *459*, 306.
(197) Nagayama, K.; Ohmori, D.; Imai, Y.; Oshima, T. In *Iron-Sulfur Protein Research*; Matsubara, H., Ed.; Springer-Verlag: Berlin, 1986; p 125.
(198) Watenpaugh, K. D.; Sieker, L. C.; Jensen, L. H. *J. Mol. Biol.* **1979**, *131*, 509.
(199) Stenkamp, R. E.; Sieker, L. C.; Jensen, L. H. *Proteins* **1990**, *8*, 352.
(200) Bruschi, M.; Moura, I.; LeGall, J.; Xavier, A. V.; Sieker, L. C. *Biochem. Biophys. Res. Commun.* **1979**, *90*, 596.
(201) Moura, I.; Tavares, P.; Moura, J. J. G.; Ravi, N.; Huynh, B. H.; Liu, M.-Y.; LeGall, J. *J. Biol. Chem.* **1990**, *265*, 21596.
(202) LeGall, J.; Prickril, B. C.; Moura, I.; Xavier, A. V.; Moura, J. J. G.; Huynh, B. H. *Biochemistry* **1988**, *27*, 1636.
(203) Krishnamoorthi, R.; Markley, J. L.; Cusanovich, M. A.; Przysiecki, C. T. *Biochemistry* **1986**, *25*, 50.
(204) Werth, M. T.; Kurtz, D. M., Jr.; Moura, I.; LeGall, J. *J. Am. Chem. Soc.* **1987**, *109*, 273.
(205) Hagen, K. S.; Watson, A. D.; Holm, R. H. *J. Am. Chem. Soc.* **1983**, *105*, 3905.
(206) Hagen, K. S.; Holm, R. H. *Inorg. Chem.* **1984**, *23*, 418.
(207) Blake, P. R.; Park, J.-B.; Bryant, F. O.; Aono, S.; Magnuson, J. K.; Eccleston, E.; Howard, J. B.; Summers, M. F.; Adams, M. W. W. *Biochemistry* **1991**, *30*, 10885.
(208) Moura, I.; Teixeira, M.; LeGall, J.; Moura, J. J. G. *J. Inorg. Biochem.* **1991**, *44*, 127.
(209) Bruschi, M.; Guerlesquin, F. *FEMS Microbiol. Rev.* **1988**, *54*, 155.
(210) Palmer, G.; Dunham, W. R.; Fee, J. A.; Sands, R. H.; Izuka, T.; Yonetani, T. *Biochim. Biophys. Acta* **1971**, *245*, 201.
(211) Petersson, L.; Cammack, R.; Krishna Rao, K. *Biochim. Biophys. Acta* **1980**, *622*, 18.
(212) Abragam, A. *The Principles of Nuclear Magnetism*; Oxford University Press: Oxford, 1961.
(213) Glickson, J. D.; Phillips, W. D.; McDonald, C. C.; Poe, M. *Biochem. Biophys. Res. Commun.* **1992**,
(214) Skjeldal, L.; Westler, W. M.; Oh, B.-H.; Krezel, A. M.; Holden, H. M.; Jacobson, B. L.; Rayment, I.; Markley, J. L. *Biochemistry* **1991**, *30*, 7363.
(215) Skjeldal, L.; Westler, W. M.; Markley, J. L. *Arch. Biochem. Biophys.* **1990**, *278*, 482.
(216) Dugad, L. B.; La Mar, G. N.; Banci, L.; Bertini, I. *Biochemistry* **1990**, *29*, 2263.
(217) Salmeen, I.; Palmer, G. *Arch. Biochem. Biophys.* **1972**, *150*, 767.
(218) Glickson, J. D.; Phillips, W. D.; McDonald, C. C.; Poe, M. *Biochem. Biophys. Res. Commun.* **1971**, *42*, 271.
(219) Phillips, W. D.; McDonald, C. C.; Stombaugh, N. A.; Orme-Johnson, W. H. *Proc. Natl. Acad. Sci. U.S.A.* **1974**, *71*, 140.
(220) Skjeldal, L.; Markley, J. L.; Coghlan, V. M.; Vickery, L. E. *Biochemistry* **1991**, *30*, 9078.
(221) Miura, R.; Ichikawa, Y. *J. Biol. Chem.* **1991**, *266*, 6252.
(222) Anderson, R. E.; Dunham, W. R.; Sands, R. H.; Bearden, A. J.; Crespi, H. L. *Biochem. Biophys. Acta* **1975**, *408*, 306.
(223) Bertini, I.; Lanini, G.; Luchinat, C. *Inorg. Chem.* **1984**, *23*, 2729.
(224) Oh, B.-H.; Markley, J. L. *Biochemistry* **1990**, *29*, 3993.
(225) Oh, B.-H.; Markley, J. L. *Biochemistry* **1990**, *29*, 4012.
(226) Carloni, P.; Corongiu, G. *Model*, submitted for publication.
(227) Bertini, I.; Briganti, F.; Luchinat, C.; Scozzafava, A.; Sola, M. *J. Am. Chem. Soc.* **1991**, *113*, 1237.
(228) Xavier, A. V.; Moura, J. J. G.; Moura, I. *Struct. Bonding* **1981**, *43*, 187.
(229) Emptage, M. H.; Kent, T. A.; Huynh, B. H.; Rawlings, J.; Orme-Johnson, W. H.; Munck, E. *J. Biol. Chem.* **1980**, *255*, 1793.
(230) Robbins, A. H.; Stout, C. D. *Proc. Natl. Acad. Sci. U.S.A.* **1989**, *86*, 3639.
(231) Kent, T. A.; Huynh, B. H.; Munck, E. *Proc. Natl. Acad. Sci. U.S.A.* **1980**, *77*, 6574.
(232) Huynh, B. H.; Moura, J. J. G.; Moura, I.; Kent, T. A.; LeGall, J.; Xavier, A. V.; Munck, E. *J. Biol. Chem.* **1980**, *255*, 3242.
(233) Gayda, J. P.; Bertrand, P.; Theodule, F. X.; Moura, J. J. G. *J. Chem. Phys.* **1982**, *77*, 3387.
(234) Macedo, A. L.; Moura, I.; Moura, J. J. G.; LeGall, J.; Huynh, B. H. *Inorg. Chem.* **1993**, *32*, 1101.
(235) Busse, S. C.; La Mar, G. N.; Yu, L. P.; Howard, J. B.; Smith, E. T.; Zhou, Z. H.; Adams, M. W. W. *Biochemistry* **1992**, *31*, 11952.
(236) Papaefthymiou, V.; Girerd, J.-J.; Moura, I.; Moura, J. J. G.; Munck, E. *J. Am. Chem. Soc.* **1987**, *109*, 4703.
(237) Blondin, G.; Girerd, J.-J. *Chem. Rev.* **1990**, *90*, 1359.
(238) Munck, E.; Papaefthymiou, V.; Surerus, K. K.; Girerd, J.-J. In *Metal Clusters in Proteins*; Que, L., Jr., Ed.; American Chemical Society: Washington, DC, 1988; p 302.
(239) Moura, I.; Moura, J. J. G.; Munck, E.; Papaefthymiou, V.; LeGall, J. *J. Am. Chem. Soc.* **1986**, *108*, 349.
(240) Conover, R. C.; Park, J.-B.; Adman, E. T.; Adams, M. W. W.; Johnson, M. K. *J. Am. Chem. Soc.* **1990**, *112*, 4562.
(241) Surerus, K. K.; Munck, E.; Moura, I.; Moura, J. J. G.; LeGall, J. *J. Am. Chem. Soc.* **1987**, *109*, 3805.
(242) Ciurli, S.; Ross, P. K.; Scott, M. J.; Yu, S.-B.; Holm, R. H. *J. Am. Chem. Soc.* **1992**, *114*, 5415.
(243) Gaillard, J.; Albrand, J.-P.; Moulis, J.-M.; Wemmer, D. E. *Biochemistry* **1992**, *31*, 5632.
(244) Carter, C. W. J.; Kraut, J.; Freer, S. T.; Alden, R. A. *J. Biol. Chem.* **1974**, *49*, 6339.
(245) Middleton, P.; Dickson, D. P. E.; Johnson, C. E.; Rush, J. D. *Eur. J. Biochem.* **1980**, *104*, 289.
(246) Bertini, I.; Campos, A. P.; Luchinat, C.; Teixeira, M. *J. Inorg. Biochem.*, in press.
(247) Antanaitis, B. C.; Moss, T. H. *Biochim. Biophys. Acta* **1975**, *405*, 262.
(248) Dunham, W. R.; Hagen, W. R.; Fee, J. A.; Sands, R. H.; Dunbar, J. B.; Humblet, C. *Biochim. Biophys. Acta* **1991**, *1079*, 253.
(249) Noodleman, L. *Inorg. Chem.* **1988**, *27*, 3677.
(250) Bertini, I.; Briganti, F.; Luchinat, C. *Inorg. Chim. Acta* **1990**, *175*, 9.
(251) Krishnamoorthi, R.; Markley, J. L.; Cusanovich, M. A.; Przysiecki, C. T.; Meyer, T. E. *Biochemistry* **1986**, *25*, 60.
(252) Banci, L.; Bertini, I.; Briganti, F.; Luchinat, C.; Scozzafava, A.; Vicens Oliver, M. *Inorg. Chim. Acta* **1991**, *180*, 171.
(253) Banci, L.; Bertini, I.; Briganti, F.; Luchinat, C.; Scozzafava, A.; Vicens Oliver, M. *Inorg. Chem.* **1991**, *30*, 4517.
(254) Banci, L.; Bertini, I.; Capozzi, F.; Carloni, P.; Ciurli, S.; Luchinat, C.; Piccioli, M. *J. Am. Chem. Soc.* **1993**, *115*, 3431.
(255) Cowan, J. A.; Sola, M. *Biochemistry* **1990**, *29*, 5633.
(256) Bertini, I.; Capozzi, F.; Ciurli, S.; Luchinat, C.; Messori, L.; Piccioli, M. *J. Am. Chem. Soc.* **1992**, *114*, 3332.
(257) Nettesheim, D. G.; Harder, S. R.; Feinberg, B. A.; Otvos, J. D. *Biochemistry* **1992**, *31*, 1234.
(258) Bertini, I.; Capozzi, F.; Luchinat, C.; Piccioli, M.; Vicens Oliver, M. *Inorg. Chim. Acta* **1992**, *483*, 198.
(259) Banci, L.; Bertini, I.; Ciurli, S.; Ferretti, S.; Luchinat, C.; Piccioli, M. *Biochemistry*, in press.
(260) Bertini, I.; Capozzi, F.; Luchinat, C.; Piccioli, M. *Eur. J. Biochem.* **1993**, *212*, 69.
(261) Sola, M.; Cowan, J. A.; Gray, H. B. *Biochemistry* **1989**, *28*, 5261.
(262) Thompson, C. L.; Johnson, C. E.; Dickson, D. P. E.; Cammack, R.; Hall, D. O.; Weser, U.; Rao, K. K. *Biochem. J.* **1974**, *139*, 97.
(263) Ho, F. F.-L.; Reilley, C. N. *Anal. Chem.* **1969**, *41*, 1835.
(264) Fitzgerald, R. J.; Drago, R. S. *J. Am. Chem. Soc.* **1968**, *90*, 2523.
(265) Bertini, I.; Capozzi, F.; Luchinat, C.; Piccioli, M.; Vila, A. J. *J. Am. Chem. Soc.*, in press.
(266) Jardetzky, O.; Robert, G. C. K. In *NMR in Molecular Biology*; Academic Press: New York, 1981.
(267) Packer, E. L.; Sweeney, W. V.; Rabinowitz, J. C.; Sternlicht, H.; Shaw, E. N. *J. Biol. Chem.* **1977**, *252*, 2245.
(268) Jordanov, J.; Roth, E. K. H.; Fries, P. H.; Noodleman, L. *Inorg. Chem.* **1990**, *29*, 4288.
(269) Bertini, I.; Briganti, F.; Luchinat, C.; Messori, L.; Monnanni, R.; Scozzafava, A.; Vallini, G. *FEBS Lett.* **1991**, *289*, 253.
(270) Busse, S. C.; La Mar, G. N.; Howard, J. B. *J. Biol. Chem.* **1991**, *266*, 23714.
(271) Moulis, J.-M.; Auric, P.; Gaillard, J.; Meyer, J. *J. Biol. Chem.* **1984**, *259*, 11396.
(272) Gersonde, K.; Schlaak, H.-E.; Breitenbach, M.; Parak, F.; Eicher, H.; Zgorzalla, W.; Kalvius, M. G.; Mayer, A. *Eur. J. Biochem.* **1974**, *43*, 307.
(273) Auric, P.; Gaillard, J.; Meyer, J.; Moulis, J.-M. *Biochem. J.* **1987**, *242*, 525.
(274) Middleton, P.; Dickson, D. P. E.; Johnson, C. E.; Rush, J. D. *Eur. J. Biochem.* **1978**, *88*, 135.
(275) Packer, E. L.; Sternlicht, H.; Lode, E. T.; Rabinowitz, J. C. *J. Biol. Chem.* **1975**, *250*, 2062.
(276) Sweeney, W. V. *J. Biol. Chem.* **1981**, *256*, 12222.
(277) Cheng, H.; Grohmann, K.; Sweeney, W. V. *J. Biol. Chem.* **1990**, *265*, 12388.
(278) Cheng, H.; Grohmann, K.; Sweeney, W. V. *J. Biol. Chem.* **1992**, *267*, 8073.
(279) Nagayama, K.; Ohmori, D. *FEBS Lett.* **1984**, *173*, 15.
(280) Nagayama, K.; Imai, Y.; Ohmori, D.; Oshima, T. *FEBS Lett.* **1984**, *169*, 79.
(281) Nagayama, K.; Ohmori, D.; Imai, Y.; Oshima, T. *FEBS Lett.* **1983**, *158*, 208.
(282) Meyer, J.; Moulis, J.-M.; Gaillard, J.; Lutz, M. *Adv. Inorg. Chem.* **1992**, *38*, 73.
(283) Gaillard, J.; Moulis, J.-M.; Meyer, J. *Inorg. Chem.* **1987**, *26*, 320.
(284) Sola, M.; Cowan, J. A.; Gray, H. B. *J. Am. Chem. Soc.* **1989**, *111*, 6627.
(285) Reynolds, J. G.; Coyle, C. L.; Holm, R. H. *J. Am. Chem. Soc.* **1980**, *102*, 4350.
(286) Reynolds, J. G.; Holm, R. H. *Inorg. Chem.* **1981**, *20*, 1873.
(287) Carney, M. J.; Papaefthymiou, G. C.; Whitener, M. A.; Spartalian, K.; Frankel, R. B.; Holm, R. H. *Inorg. Chem.* **1988**, *27*, 346.
(288) Hay, P. J.; Thibeault, J. C.; Hoffmann, R. *J. Am. Chem. Soc.* **1975**, *97*, 4884.

(289) Gaillard, J.; Moulis, J.-M.; Auric, P.; Meyer, J. *Biochemistry* **1986**, *25*, 464.
(290) Moulis, J.-M.; Meyer, J. *Biochemistry* **1982**, *21*, 4762.
(291) Moulis, J.-M.; Meyer, J. *Biochemistry* **1984**, *23*, 6605.
(292) Meyer, J.; Gaillard, J.; Moulis, J.-M. *Biochemistry* **1988**, *27*, 6150.
(293) Timkovich, R.; Bondoc, L. L. *Adv. Biol. Chem.* **1990**, *1*, 203.
(294) Nichol, A. W.; Angel, L. A.; Moon, T.; Clezy, P. S. *Biochem. J.* **1987**, *247*, 147.
(295) Sievers, G. *FEBS Lett.* **1981**, *127*, 253.
(296) Van Gelder, B. F.; Beinert, H. *Biochim. Biophys. Acta* **1969**, *189*, 1.
(297) Thomson, A. J.; Greenwood, C.; Gadsby, P. M. A.; Peterson, J.; Eglington, D. G.; Hill, B. C.; Nicholls, P. *J. Inorg. Biochem.* **1985**, *23*, 187.
(298) Murphy, M. J.; Siegel, L. M. *J. Biol. Chem.* **1973**, *248*, 6911.
(299) Ortiz de Montellano, P. R. In *Cytochrome P450: Structure, Mechanism, and Biochemistry*; Ortiz de Montellano, P. R., Ed.; Plenum Press: New York, 1986; p 217.
(300) Dunford, H. B. In *Peroxidases in Chemistry and Biology*; Everse, J., Everse, K. E., Grisham, M. B., Eds.; CRC Press: Boca Raton, FL, 1991; p 51.
(301) Bosshard, H. R.; Anni, H.; Yonetani, T. In *Peroxidases in Chemistry and Biology*; Everse, J., Everse, K. E., Grisham, M. B., Eds.; CRC Press: Boca Raton, FL, 1991; p 84.
(302) Dawson, J. H. *Science* **1988**, *240*, 433.
(303) Miller, V. P.; dePillis, G. D.; Ferrer, J. C.; Mauk, A. G.; Ortiz de Montellano, P. R. *J. Biol. Chem.* **1992**, *267*, 8936.
(304) La Mar, G. N. In *Biological Applications of Magnetic Resonance*; Shulman, R. G., Ed.; Academic: New York, 1979; p 305.
(305) Satterlee, J. D. In *Metal ions in biological systems*; Sigel, H., Ed.; Marcell Dekker: New York, 1987; p 121.
(306) Goff, H. M. In *Iron Porphyrins*; Lever, A. B. P., Gray, H. B., Eds.; Addison-Wesley: Reading, MA, 1983; p 237.
(307) Satterlee, J. D. *Annu. Rep. NMR Spectrosc.* **1986**, *17*, 79.
(308) La Mar, G. N.; Walker, F. A. In *The Porphyrins*; Dolphin, D., Ed.; Academic Press: New York, 1979; Vol. IV, p 61.
(309) Budd, D. L.; La Mar, G. N.; Langry, K. C.; Smith, K. M.; Nayyir-Mazhir, R. *J. Am. Chem. Soc.* **1979**, *101*, 6091.
(310) Morishima, I.; Shiro, Y.; Wakino, T. *J. Am. Chem. Soc.* **1985**, *107*, 1063.
(311) Bertrand, P.; Theodule, F. X.; Gayda, J. P.; Mispelter, J.; Momenteau, M. *Chem. Phys. Lett.* **1983**, *102*, 442.
(312) Scheidt, W. R.; Osvath, S. R.; Lee, Y. J.; Christopher, A. R.; Shaevitz, B.; Gupta, G. P. *Inorg. Chem.* **1989**, *28*, 1591.
(313) Maltempo, M. M.; Moss, T. H. *Q. Rev. Biophys.* **1976**, *9*, 181.
(314) Goff, H. M.; Shimomura, E. *J. Am. Chem. Soc.* **1980**, *102*, 31.
(315) Boersma, A. D.; Goff, H. M. *Inorg. Chem.* **1982**, *21*, 581.
(316) Unger, S. W.; Lecomte, J. T. J.; La Mar, G. N. *J. Magn. Reson.* **1985**, *64*, 521.
(317) Pande, U.; La Mar, G. N.; Lecomte, J. T. J.; Ascoli, F.; Brunori, M.; Smith, K. M.; Pandey, R. K.; Parish, D. W.; Thanabal, V. *Biochemistry* **1986**, *25*, 5638.
(318) Bolognesi, M.; Coda, A.; Batti, G.; Ascenzi, P.; Brunori, M. *J. Mol. Biol.* **1985**, *183*, 113.
(319) Suzuki, T. *Biochim. Biophys. Acta* **1987**, *914*, 170.
(320) Yamamoto, Y.; Osawa, A.; Inoue, Y.; Chujo, R.; Suzuki, T. *Eur. J. Biochem.* **1990**, *192*, 225.
(321) La Mar, G. N.; Chatfield, M. J.; Peyton, D. H.; de Ropp, J. S.; Smith, W. S.; Krishnamoorthi, R.; Satterlee, J. D.; Erman, J. E. *Biochim. Biophys. Acta* **1988**, *956*, 267.
(322) Springer, B. A.; Sligar, S. G. *Proc. Natl. Acad. Sci. U.S.A.* **1987**, *84*, 8961.
(323) Rajarathnam, K.; La Mar, G. N.; Chiu, M. L.; Sligar, S. G.; Singh, J. P.; Smith, K. M. *J. Am. Chem. Soc.* **1991**, *113*, 7886.
(324) Pease, E. A.; Andrawis, A.; Tien, M. *J. Biol. Chem.* **1989**, *264*, 13531.
(325) Welinder, K. G. *FEBS Lett.* **1976**, *72*, 19.
(326) Satterlee, J. D.; Russell, D. J.; Erman, J. E. *Biochemistry* **1991**, *30*, 9072.
(327) Wang, J.; Mauro, J. M.; Edwards, S. L.; Oatley, S. J.; Fishel, L. A.; Ashford, V. A.; Xuong, N.; Kraut, J. *Biochemistry* **1990**, *29*, 7160.
(328) Edwards, S. L.; Raag, R.; Wariishi, H.; Gold, M. H.; Poulos, T. L. *Proc. Natl. Acad. Sci. U.S.A.* **1993**, *90*, 750.
(329) Piontek, K.; Glumoff, T.; Winterhalter, K. *FEBS Lett.* **1993**, *315*, 119.
(330) Poulos, T. L.; Edwards, S. L.; Wariishi, H.; Gold, M. H. *J. Biol. Chem.* **1993**, *268*, 4429.
(331) Satterlee, J. D.; Erman, J. E.; La Mar, G. N.; Smith, K. M.; Langry, K. C. *Biochim. Biophys. Acta* **1983**, *743*, 246.
(332) Lukat, G. S.; Rodgers, K. R.; Jabro, M. N.; Goff, H. M. *Biochemistry* **1989**, *28*, 3338.
(333) Dugad, L. B.; Goff, H. M.; Abeles, F. B. *Biochim. Biophys. Acta* **1991**, *1118*, 36.
(334) de Ropp, J. S.; La Mar, G. N.; Wariishi, H.; Gold, M. H. *J. Biol. Chem.* **1991**, *266*, 15001.
(335) Banci, L.; Bertini, I.; Turano, P.; Tien, M.; Kirk, T. K. *Proc. Natl. Acad. Sci. U.S.A.* **1991**, *88*, 6956.
(336) Banci, L.; Bertini, I.; Pease, E.; Tien, M.; Turano, P. *Biochemistry* **1992**, *31*, 10009.
(337) Dugad, L. B.; Goff, H. M. *Biochim. Biophys. Acta* **1992**, *1122*, 63.
(338) Satterlee, J. D.; Erman, J. E.; Mauro, J. M.; Kraut, J. *Biochemistry* **1990**, *29*, 8797.
(339) Ferrer, J. C.; Turano, P.; Banci, L.; Bertini, I.; Morris, I. K.; Smith, K. M.; Smith, M.; Mauk, A. G. Submitted for publication.
(340) La Mar, G. N.; de Ropp, J. S. *Biochem. Biophys. Res. Commun.* **1979**, *90*, 36.
(341) Neya, S.; Morishima, I. *J. Biol. Chem.* **1981**, *256*, 793.
(342) La Mar, G. N.; Nagai, K.; Jue, T.; Budd, D. L.; Gersonde, K.; Sick, H.; Kajimoto, T.; Hayashi, A.; Taketa, F. *Biochem. Biophys. Res. Commun.* **1980**, *96*, 1172.
(343) Thanabal, V.; La Mar, G. N.; de Ropp, J. S. *Biochemistry* **1988**, *27*, 5400.
(344) Thanabal, V.; de Ropp, J. S.; La Mar, G. N. *J. Am. Chem. Soc.* **1986**, *108*, 4244.
(345) de Ropp, J. S.; La Mar, G. N. *J. Am. Chem. Soc.* **1991**, *113*, 4348.
(346) Ellfolk, N.; Ronnberg, M.; Aasa, R.; Vanngard, T.; Angstrom, J. *Biochim. Biophys. Acta* **1984**, *791*, 9.
(347) Villalain, J.; Moura, I.; Liu, M. C.; Payne, W. J.; LeGall, J.; Xavier, A. V.; Moura, J. J. G. *Eur. J. Biochem.* **1984**, *141*, 305.
(348) Morishima, I.; Ogawa, S.; Inubushi, T.; Yonezawa, T.; Iiuzuka, T. *Biochemistry* **1977**, *16*, 5109.
(349) Iizuka, T.; Ogawa, S.; Inubushi, T.; Yonezawa, T.; Morishima, I. *FEBS Lett.* **1976**, *64*, 156.
(350) Gonzales-Vergara, E.; Meyer, M.; Goff, H. M. *Biochemistry* **1985**, *24*, 6561.
(351) Krishnamoorthi, R.; La Mar, G. N.; Mizukami, H.; Romero, A. *J. Biol. Chem.* **1984**, *259*, 265.
(352) Yamamoto, Y.; Suzuki, T.; Hori, H. *Biochim. Biophys. Acta* **1993**, in press.
(353) Morishima, I. In *Current perspectives in high pressure biology*; Academic Press: London, 1987; p 315.
(354) Satterlee, J. D.; Erman, J. E. *Arch. Biochem. Biophys.* **1980**, *202*, 608.
(355) Morishima, I.; Ogawa, S.; Yamada, H. *Biochemistry* **1980**, *19*, 1569.
(356) Sakurada, J.; Takahashi, S.; Hosoya, T. *J. Biol. Chem.* **1987**, *262*, 4007.
(357) Modi, S.; Behere, D. V.; Mitra, S. *J. Biol. Chem.* **1989**, *264*, 19677.
(358) Moench, S.; Satterlee, J. D.; Erman, J. E. *Biochemistry* **1987**, *26*, 3821.
(359) Satterlee, J. D.; Moench, S.; Erman, J. E. *Biochim. Biophys. Acta* **1987**, *912*, 87.
(360) Moench, S.; Shi, T.-M.; Satterlee, J. D. *Eur. J. Biochem.* **1991**, *197*, 631.
(361) Morishima, I.; Ogawa, S. *J. Biol. Chem.* **1979**, *254*, 2814.
(362) Casella, L.; Gullotti, M.; Poli, S.; Bonfa', M.; Ferrari, R. P.; Marchesini, A. *Biochem. J.* **1991**, *279*, 245.
(363) Thanabal, V.; de Ropp, J. S.; La Mar, G. N. *J. Am. Chem. Soc.* **1987**, *109*, 7516.
(364) Veitch, N. C.; Williams, R. J. P. *Eur. J. Biochem.* **1990**, *189*, 351.
(365) Veitch, N. C.; Williams, R. J. P. In *Biochemical and Physiological Aspects of Plant Peroxidases*; Lobarzewski, J., Greppin, H. L., Penel, C., Gaspar, T. H., Eds.; University of Geneva: Geneva, 1991; p 99.
(366) Veitch, N. C.; Williams, R. J. P.; Bray, R. C.; Burke, J. F.; Sanders, S. A.; Thornley, R. N. F.; Smith, A. T. *Eur. J. Biochem.* **1992**, *207*, 521.
(367) Morishima, I.; Kurono, M.; Shiro, Y. *J. Biol. Chem.* **1986**, *261*, 9391.
(368) Ogawa, S.; Shiro, Y.; Morishima, I. *Biochem. Biophys. Res. Commun.* **1979**, *90*, 674.
(369) Harris, R. Z.; Wariishi, H.; Gold, M. H.; Ortiz de Montellano, P. R. *J. Biol. Chem.* **1991**, *266*, 8751.
(370) Banci, L.; Bertini, I.; Bini, T.; Tien, M.; Turano, P. *Biochemistry* **1993**, *32*, 5825.
(371) Goff, H. M.; Gonzalez-Vergara, E.; Ales, D. C. *Biochem. Biophys. Res. Commun.* **1985**, *133*, 794.
(372) Shiro, Y.; Morishima, I. *Biochemistry* **1986**, *25*, 5844.
(373) Sakurada, J.; Takahashi, S.; Shimizu, T.; Hatano, M.; Nakamura, S.; Hosoya, T. *Biochemistry* **1987**, *26*, 6478.
(374) Modi, S.; Behere, D. V.; Mitra, S. *Biochemistry* **1989**, *28*, 4689.
(375) Ikeda-Saito, M.; Inubushi, T. *FEBS Lett.* **1987**, *214*, 111.
(376) Poulos, T. L.; Finzel, B. C.; Howard, A. J. *J. Mol. Biol.* **1987**, *195*, 687.
(377) Poulos, T. L.; Finzel, B. C.; Howard, A. J. *Biochemistry* **1986**, *25*, 5314.
(378) Poulos, T. L.; Finzel, B. C.; Gunsalus, I. C.; Wagner, G.; Kraut, J. *J. Biol. Chem.* **1985**, *260*, 16122.
(379) Keller, R. M.; Wüthrich, K. J.; Debrunner, P. G. *Proc. Natl. Acad. Sci. U.S.A.* **1972**, *69*, 2073.
(380) Lukat, G. S.; Goff, H. M. *Biochim. Biophys. Acta* **1990**, *1037*, 351.
(381) Banci, L.; Bertini, I.; Eltis, L. D.; Pierattelli, R. *Biophys. J.*, in press.
(382) Morris, D. R.; Hager, L. P. *J. Biol. Chem.* **1966**, *241*, 1763.
(383) Hewson, W. D.; Hager, L. P. In *The Porphyrins*; Dolphin, D., Ed.; Academic Press: New York, 1979; p 295.
(384) Dawson, J. H.; Sono, M. *Chem. Rev.* **1987**, *87*, 1255.
(385) Dawson, J. H. *Science* **1988**, *240*, 433.
(386) Hager, L. P.; Morris, D. R.; Brown, F. S.; Eberwein, H. *J. Biol. Chem.* **1966**, *241*, 1769.

(387) Goff, H. M.; Gonzales-Vergara, E.; Bird, M. R. *Biochemistry* **1985**, *24*, 1007.
(388) Lukat, G. S.; Goff, H. M. *J. Biol. Chem.* **1986**, *261*, 165285.
(389) Bartsch, R. G. In *The Photosynthetic Bacteria*; Clayton, R. K., Sistrom, W. R., Eds.; Plenum Press: New York, 1978; p 249.
(390) Weber, P. C.; Bartsch, R. G.; Cusanovich, M. A.; Hamlin, R. C.; Howard, A.; Jordan, S. R.; Kamen, M. D.; Meyer, T. E.; Westherford, D. W.; Xuong, N. H.; Salemme, F. R. *Nature* **1980**, *286*, 302.
(391) McRee, D. E.; Redford, S. M.; Meyer, T. E.; Cusanovich, M. A. *J. Biol. Chem.* **1990**, *265*, 5364.
(392) Emptage, M. H.; Xavier, A. V.; Wood, J. M.; Alsaadi, B. M.; Moore, G. M.; Pitt, R. C.; Williams, R. J. P.; Ambler, R. P.; Bartsch, R. G. *Biochemistry* **1981**, *20*, 58.
(393) La Mar, G. N.; Jackson, J. T.; Bartsch, R. G. *J. Am. Chem. Soc.* **1981**, *103*, 4405.
(394) La Mar, G. N.; Jackson, J. T.; Dugad, L. B.; Cusanovich, M. A.; Bartsch, R. G. *J. Biol. Chem.* **1990**, *265*, 16173.
(395) Bertini, I.; Briganti, F.; Monnanni, R.; Scozzafava, A.; Carlozzi, P.; Materassi, R. *Arch. Biochem. Biophys.* **1990**, *282*, 84.
(396) Banci, L.; Bertini, I.; Turano, P.; Vicens Oliver, M. *Eur. J. Biochem.* **1992**, *204*, 107.
(397) Bertini, I.; Gori, G.; Luchinat, C.; Vila, A. J. *Biochemistry* **1993**, *32*, 776.
(398) Weber, P. C. *Biochemistry* **1982**, *21*, 5116.
(399) Chatfield, M. J.; La Mar, G. N.; Lecomte, J. T. J.; Balch, A. L.; Smith, K. M.; Langry, K. C. *J. Am. Chem. Soc.* **1986**, *108*, 7108.
(400) Chatfield, M. J.; La Mar, G. N.; Smith, K. M.; Leung, H. K.; Pandey, R. K. *Biochemistry* **1988**, *27*, 1500.
(401) Kaufman, J.; Spicer, L. D.; Siegel, L. M. *Biochemistry* **1993**, *32*, 2853.
(402) Williams, G.; Clayden, N. J.; Moore, G. R.; Williams, R. J. P. *J. Mol. Biol.* **1985**, *183*, 447.
(403) Feng, Y.; Roder, H.; Englander, S. W. *Biochemistry* **1990**, *29*, 3494.
(404) Emerson, S. D.; La Mar, G. N. *Biochemistry* **1990**, *29*, 1556.
(405) Yamamoto, Y.; Iwafune, K.; Nanai, N.; Osawa, A.; Chujo, R.; Suzuki, T. *Eur. J. Biochem.* **1991**, *198*, 299.
(406) La Mar, G. N.; Budd, D. L.; Goff, H. M. *Biochem. Biophys. Res. Commun.* **1977**, *77*, 104.
(407) Chacko, V. P.; La Mar, G. N. *J. Am. Chem. Soc.* **1982**, *104*, 7002.
(408) La Mar, G. N.; de Ropp, J. S.; Chacko, V. P.; Satterlee, J. D. *Biochim. Biophys. Acta* **1982**, *708*, 317.
(409) Mayer, A.; Ogawa, S.; Shulman, R. G.; Yamane, T.; Cavaleiro, J. A. S.; Rocha Gonsalves, A. M. d'A.; Kenner, G. W.; Smith, K. M. *J. Mol. Biol.* **1974**, *86*, 749.
(410) Cutnell, J. D.; La Mar, G. N.; Kong, S. B. *J. Am. Chem. Soc.* **1981**, *103*, 3567.
(411) La Mar, G. N.; Davis, N. L.; Parish, D. W.; Smith, K. M. *J. Mol. Biol.* **1983**, *168*, 887.
(412) Ramaprasad, S.; Johnson, R. D.; La Mar, G. N. *J. Am. Chem. Soc.* **1984**, *106*, 3632.
(413) Ramaprasad, S.; Johnson, R. D.; La Mar, G. N. *J. Am. Chem. Soc.* **1984**, *106*, 5330.
(414) Kuriyan, J.; Wilz, S.; Karplus, M.; Petsko, G. A. *J. Mol. Biol.* **1986**, *192*, 133.
(415) Horrocks, W. D., Jr.; Greenberg, E. S. *Biochim. Biophys. Acta* **1973**, *322*, 382.
(416) Hori, H. *Biochim. Biophys. Acta* **1971**, *251*, 227.
(417) Peisach, J.; Blumberg, W.; Wyluda, B. J. *Eur. Biophys. Congr.* **1971**, *1*, 109.
(418) Rajarathnam, K.; La Mar, G. N.; Chiu, M. L.; Sligar, S. G. *J. Am. Chem. Soc.* **1992**, *114*, 9048.
(419) Adachi, S.; Sunohara, N.; Ishimori, K.; Morishima, I. *J. Biol. Chem.* **1992**, *267*, 12614.
(420) Yamamoto, Y.; Osawa, A.; Inoue, Y.; Chujo, R.; Suzuki, T. *FEBS. Lett.* **1989**, *247*, 263.
(421) Lecomte, J. T. J.; La Mar, G. N. *Eur. Biophys. J.* **1986**, *13*, 373.
(422) Emerson, S. D.; Lecomte, J. T. J.; La Mar, G. N. *J. Am. Chem. Soc.* **1988**, *110*, 4176.
(423) Yamamoto, Y. *FEBS Lett.* **1987**, *222*, 115.
(424) Yamamoto, Y.; Nanai, N.; Chujo, R.; Suzuki, T. *FEBS Lett.* **1990**, *264*, 113.
(425) Yamamoto, Y.; Nanai, N.; Inoue, Y.; Chujo, R. *Bull. Chem. Soc. Jpn.* **1988**, *110*, 4176.
(426) Yamamoto, Y.; Nanai, N.; Chujo, R. *J. Chem. Soc., Chem. Commun.* **1990**, *22*, 1556.
(427) Yamamoto, Y.; Komori, K.; Nanai, N.; Chujo, R.; Inoue, Y. *J. Chem. Soc., Dalton Trans.* **1992**, 1813.
(428) McConnell, H. M. *Proc. Natl. Acad. Sci. U.S.A.* **1957**, *43*, 721.
(429) Eich, G.; Bodenhausen, G.; Ernst, R. R. *J. Am. Chem. Soc.* **1982**, *104*, 3731.
(430) Wagner, G. *J. Magn. Reson.* **1983**, *55*, 151.
(431) Banci, L.; Bermel, W.; Luchinat, C.; Pierattelli, R.; Tarchi, D. *Magn. Reson. Chem.*, in press.
(432) Raag, R.; Swanson, B. A.; Poulos, T. L.; Ortiz de Montellano, P. R. *Biochemistry* **1990**, *29*, 8119.
(433) Hauksson, J. B.; La Mar, G. N.; Pandey, R. K.; Rezzano, I. N.; Smith, K. M. *J. Am. Chem. Soc.* **1990**, *112*, 6198.
(434) Hauksson, J. B.; La Mar, G. N.; Pandey, R. K.; Rezzano, I. N.; Smith, K. M. *J. Am. Chem. Soc.* **1990**, *112*, 8315.
(435) Morishima, I.; Neya, S.; Inubushi, T.; Yonezawa, T.; Iizuka, T. *Biochim. Biophys. Acta* **1978**, *534*, 307.
(436) Yamamoto, Y.; Chujo, R.; Suzuki, T. *Eur. J. Biochem.* **1991**, *198*, 285.
(437) Yamamoto, Y.; Inoue, Y.; Chujo, R.; Suzuki, T. *Eur. J. Biochem.* **1990**, *189*, 567.
(438) Simonneaux, G.; Bondon, A.; Sodano, P. *Biochim. Biophys. Acta* **1990**, *1038*, 199.
(439) Yamamoto, Y.; Inoue, Y.; Suzuki, T. *Magn. Reson. Chem.*, in press.
(440) Morishima, I.; Hara, M. *Biochemistry* **1983**, *22*, 4102.
(441) Satterlee, J. D.; Erman, J. E.; de Ropp, J. S. *J. Biol. Chem.* **1987**, *262*, 11578.
(442) Satterlee, J. D.; Erman, J. E. *Biochemistry* **1991**, *30*, 4398.
(443) Banci, L.; Bertini, I.; Turano, P.; Ferrer, J. C.; Mauk, A. G. *Inorg. Chem.* **1991**, *30*, 4510.
(444) Thanabal, V.; de Ropp, J. S.; La Mar, G. N. *J. Am. Chem. Soc.* **1988**, *110*, 3027.
(445) de Ropp, J. S.; Yu, L. P.; La Mar, G. N. *J. Biomol. NMR* **1991**, *1*, 175.
(446) Sette, M.; de Ropp, J. S.; Hernandez, G.; La Mar, G. N. *J. Am. Chem. Soc.* **1993**, *115*, 5237.
(447) Banci, L.; Bertini, I.; Kuan, I-C.; Tien, M.; Turano, P.; Vila, A. J. *Biochemistry*, in press.
(448) Veitch, N. C.; Williams, R. J. P.; Smith, A. T.; Sanders, R. N. F.; Thornley, R. N. F.; Bray, R. C.; Burke, J. F. *Biochem. Soc. Trans.* **1992**, *20*, 114S.
(449) Williams, R. J. P.; Wright, P. E.; Mazza, G.; Ricard, J. R. *Biochim. Biophys. Acta* **1975**, *412*, 127.
(450) Siegel, L. M.; Rueger, D. C.; Barber, M. J.; Krueger, R. J.; Orme-Johnson, N. R.; Orme-Johnson, W. H. *J. Biol. Chem.* **1982**, *257*, 6343.
(451) La Mar, G. N.; Hernàndez, G.; de Ropp, J. S. *Biochemistry* **1992**, *31*, 9158.
(452) Yi, Q.; Erman, J. E.; Satterlee, J. D. *J. Am. Chem. Soc.* **1992**, *114*, 7907.
(453) Thanabal, V.; La Mar, G. N. *Biochemistry* **1989**, *28*, 7038.
(454) Dugad, L. B.; La Mar, G. N.; Lee, H. C.; Ikeda-Saito, M.; Booth, K. S.; Caughey, W. S. *J. Biol. Chem.* **1990**, *265*, 7173.
(455) Shulman, R. G.; Glamur, S. H.; Karplus, M. *J. Mol. Biol.* **1971**, *57*, 93.
(456) Traylor, T. G.; Berzinis, A. P. *J. Am. Chem. Soc.* **1980**, *102*, 2844.
(457) Shimizu, T.; Sotokawa, H.; Hatano, M. *Inorg. Chim. Acta* **1985**, *108*, 195.
(458) Dugad, L. B.; Wang, X.; Wang, C.-C.; Lukat, G. S.; Goff, H. M. *Biochemistry* **1992**, *31*, 1651.
(459) Mathews, M.; Levine, M.; Argos, P. *Nature* **1971**, *233*, 15.
(460) Mathews, M.; Levine, M.; Argos, P. *J. Mol. Biol.* **1972**, *64*, 449.
(461) Takano, T.; Dickerson, R. E. *J. Mol. Biol.* **1981**, *153*, 79.
(462) Louie, G. V.; Hutcheon, W. L. B.; Brayer, G. D. *J. Mol. Biol.* **1988**, *102*, 563.
(463) Wüthrich, K. *Proc. Natl. Acad. Sci. U.S.A.* **1969**, *63*, 1071.
(464) Redfield, A. G.; Gupta, G. P. *Cold Spring Harbor Symp. Quant. Biol.* **1971**, *36*, 405.
(465) Wüthrich, K.; Keller, R. M. *Biochim. Biophys. Acta* **1978**, *533*, 195.
(466) Williams, G.; Moore, G. R.; Porteous, R.; Robinson, M. N.; Soffe, N.; Williams, R. J. P. *J. Mol. Biol.* **1985**, *183*, 409.
(467) Moore, G. R.; Williams, R. J. P. *Eur. J. Biochem.* **1980**, *103*, 493.
(468) Moore, G. R.; Williams, R. J. P. *Eur. J. Biochem.* **1980**, *103*, 503.
(469) Satterlee, J. D.; Moench, S. *Biophys. J.* **1987**, *52*, 101.
(470) Santos, H.; Turner, D. L. *FEBS Lett.* **1987**, *226*, 179.
(471) Wand, A. J.; Englander, S. W. *Biochemistry* **1985**, *24*, 5290.
(472) Wand, A. J.; Englander, S. W. *Biochemistry* **1986**, *25*, 1100.
(473) Wand, A. J.; Di Stefano, D. L.; Feng, Y.; Roder, H.; Englander, S. W. *Biochemistry* **1989**, *28*, 186.
(474) Feng, Y.; Roder, H.; Englander, S. W.; Wand, A. J.; Di Stefano, D. L. *Biochemistry* **1989**, *28*, 195.
(475) Feng, Y.; Roder, H.; Englander, S. W. *Biophys. J.* **1990**, *57*, 15.
(476) Gao, Y.; Lee, A. J. D.; Williams, R. J. P.; Williams, G. *Eur. J. Biochem.* **1989**, *182*, 57.
(477) Pielak, G. J.; Atkinson, R. A.; Boyd, J.; Williams, R. J. P. *Eur. J. Biochem.* **1988**, *177*, 179.
(478) Moore, G. R.; Williams, R. J. P. *Biochim. Biophys. Acta* **1984**, *788*, 147.
(479) Pielak, G. J.; Boyd, J.; Moore, G. R.; Williams, R. J. P. *Eur. J. Biochem.* **1988**, *177*, 167.
(480) Gao, Y.; Boyd, J.; Pielak, G. J.; Williams, R. J. P. *Biochemistry* **1991**, *30*, 1928.
(481) Gao, Y.; Boyd, J.; Williams, R. J. P.; Pielak, G. J. *Biochemistry* **1990**, *29*, 6994.
(482) Thurgood, A. G. P.; Davies, A. M.; Greenwood, C.; Mauk, A. G.; Smith, M.; Guillemette, J. G.; Moore, G. R. *Eur. J. Biochem.* **1991**, *202*, 339.
(483) Gao, Y.; Boyd, J.; Pielak, G. J.; Williams, R. J. P. *Biochemistry* **1991**, *30*, 7033.
(484) Gao, Y.; McLendon, G.; Pielak, G. J.; Williams, R. J. P. *Eur. J. Biochem.* **1992**, *204*, 337.
(485) Moore, G. M.; Robinson, M. N.; Williams, G.; Williams, R. J. P. *J. Mol. Biol.* **1985**, *183*, 429.
(486) Eley, C. G. S.; Moore, G. R.; Williams, G.; Williams, R. J. P. *Eur. J. Biochem.* **1982**, *124*, 295.

(487) Rush, J. D.; Koppenol, W. H.; Garber, E. A. E.; Margoliash, E. *J. Biol. Chem.* **1988**, *263*, 7514.
(488) Boswell, A. P.; Eley, C. G. S.; Moore, G. R.; Robinson, M. N.; Williams, G.; Williams, R. J. P.; Neupert, W. J.; Henning, B. *Eur. J. Biochem.* **1982**, *124*, 289.
(489) Eley, C. G. S.; Moore, G. R.; Williams, G.; Williams, R. J. P. *Eur. J. Biochem.* **1982**, *124*, 295.
(490) Whitford, D.; Concar, D. W.; Williams, R. J. P. *Eur. J. Biochem.* **1991**, *199*, 561.
(491) Concar, D. W.; Whitford, D.; Williams, R. J. P. *Eur. J. Biochem.* **1991**, *199*, 569.
(492) Hazzard, J. T.; Tollin, G. *Biochem. Biophys. Res. Commun.* **1985**, *130*, 1281.
(493) Eley, C. G. S.; Moore, G. R. *Biochem. J.* **1983**, *215*, 11.
(494) Moench, S.; Chroni, S.; Lou, B. S.; Erman, J. E.; Satterlee, J. D. *Biochemistry* **1992**, *31*, 3661.
(495) Pelletier, H.; Kraut, J. *Science* **1992**, *258*, 1748.
(496) Gupta, G. P. *Biochim. Biophys. Acta* **1973**, *292*, 291.
(497) Dixon, D. W.; Hong, X.; Woehler, S. E. *Biophys. J.* **1989**, *56*, 339.
(498) Concar, D. W.; Whitford, D.; Williams, R. J. P. *Eur. J. Biochem.* **1991**, *199*, 553.
(499) Timkovich, R.; Cai, M. L. *Biochem. Biophys. Res. Commun.* **1988**, *150*, 1044.
(500) Gupta, R. K.; Koenig, S. H.; Redfield, A. G. *J. Magn. Reson.* **1972**, *7*, 66.
(501) Gupta, R. K. *Biochim. Biophys. Acta* **1973**, *292*, 291.
(502) Senn, H.; Eugster, A.; Wüthrich, K. *Biochim. Biophys. Acta* **1983**, *743*, 58.
(503) Timkovich, R.; Cork, M. S.; Taylor, P. V. *Biochemistry* **1984**, *23*, 3526.
(504) Keller, R. M.; Wüthrich, K.; Schejter, A. *Biochim. Biophys. Acta* **1977**, *491*, 409.
(505) Timkovich, R.; Cork, M. S. *Biochemistry* **1984**, *23*, 851.
(506) Senn, H.; Wüthrich, K. *Biochim. Biophys. Acta* **1983**, *743*, 69.
(507) Keller, R. M.; Wüthrich, K.; Pecht, I. *FEBS Lett.* **1976**, *70*, 180.
(508) Senn, H.; Wüthrich, K. *Biochim. Biophys. Acta* **1983**, *746*, 48.
(509) Feng, Y.; Englander, S. W. *Biochemistry* **1990**, *29*, 3505.
(510) Jeng, M-F.; Englander, S. W.; Elove, G. A.; Wand, A. J.; Roder, H. *Biochemistry* **1990**, *29*, 10433.
(511) Ozols, J. *J. Biol. Chem.* **1972**, *247*, 2242.
(512) Mauk, M. R.; Reid, L. S.; Mauk, A. G. *Biochemistry* **1982**, *21*, 1843.
(513) Whitford, D.; Concar, D. W.; Veitch, N. C.; Williams, R. J. P. *Eur. J. Biochem.* **1990**, *192*, 715.
(514) Livingstone, D. J.; McLachlan, S. J.; La Mar, G. N.; Brown, W. D. *J. Biol. Chem.* **1985**, *260*, 15699.
(515) Mauk, M. R.; Mauk, A. G. *Biochemistry* **1982**, *21*, 4730.
(516) Keller, R. M.; Wüthrich, K. *Biochim. Biophys. Acta* **1980**, *621*, 204.
(517) Keller, R. M.; Groudinsky, O.; Wüthrich, K. *Biochim. Biophys. Acta* **1976**, *427*, 497.
(518) La Mar, G. N.; Burns, P. D.; Jackson, J. T.; Smith, K. M.; Langry, K. C. *J. Biol. Chem.* **1981**, *256*, 6075.
(519) La Mar, G. N.; de Ropp, J. S.; Smith, K. M.; Langry, K. C. *J. Am. Chem. Soc.* **1980**, *102*, 4833.
(520) Satterlee, J. D.; Erman, J. E. *J. Am. Chem. Soc.* **1981**, *103*, 199.
(521) La Mar, G. N.; Budd, D. L.; Viscio, D. B.; Smith, K. M.; Langry, K. C. *Proc. Natl. Acad. Sci. U.S.A.* **1978**, *75*, 5755.
(522) La Mar, G. N.; Overkamp, M.; Sick, H.; Gersonde, K. *Biochemistry* **1978**, *17*, 352.
(523) La Mar, G. N.; Viscio, D. B.; Gersonde, K.; Sick, H. *Biochemistry* **1978**, *17*, 361.
(524) McLachlan, S. J.; La Mar, G. N.; Sletten, E. *J. Am. Chem. Soc.* **1986**, *108*, 1285.
(525) Mathews, M. *Biochim. Biophys. Acta* **1980**, *622*, 375.
(526) Whitford, D. *Eur. J. Biochem.* **1992**, *203*, 211.
(527) Lee, K.-B.; La Mar, G. N.; Kehres, L. A.; Fujinari, E. M.; Smith, K. M.; Pochapsky, T. C.; Sligar, S. S. *Biochemistry* **1990**, *29*, 9623.
(528) Lee, K.-B.; La Mar, G. N.; Pandey, R. K.; Rezzano, I. N.; Mansfield, K. E.; Smith, K. M.; Pochapsky, T. C.; Sligar, S. S. *Biochemistry* **1991**, *30*, 1878.
(529) Moura, J. J. G.; Santos, H.; Moura, I.; LeGall, J.; Moore, G. M.; Williams, R. J. P.; Xavier, A. V. *Eur. J. Biochem.* **1982**, *127*, 151.
(530) Santos, H.; Moura, J. J. G.; LeGall, J.; Xavier, A. V. *Eur. J. Biochem.* **1984**, *141*, 283.
(531) Santos, H; Turner, D. L.; Xavier, A. V. *J. Magn. Reson.* **1984**, *59*, 177.
(532) Fan, K.; Akutsu, H.; Kyogoku, Y.; Niki, K. *Biochemistry* **1990**, *29*, 2257.
(533) Park, J.-S.; Kano, K.; Niki, K.; Akutsu, H. *FEBS Lett.* **1991**, *285*, 149.
(534) Sola, M.; Cowan, J. A. *Inorg. Chim. Acta* **1992**, *202*, 261.
(535) Keller, R. M.; Wüthrich, K. *Biochim. Biophys. Acta* **1972**, *285*, 326.
(536) Takano, T.; Dickerson, R. E. *J. Mol. Biol.* **1981**, *153*, 95.
(537) Mailer, C.; Taylor, C. P. S. *Can. J. Biochem.* **1972**, *85*, 1048.
(538) Arean, C. O.; Moore, G. R.; Williams, G.; Williams, R. J. P. *Eur. J. Biochem.* **1988**, *173*, 607.
(539) Veitch, N. C.; Whitford, D.; Williams, R. J. P. *FEBS Lett.* **1990**, *269*, 297.
(540) Veitch, N. C.; Whitford, D.; Williams, R. J. P. *FEBS Lett.* **1990**, *269*, 79.
(541) Turner, D. L.; Williams, R. J. P. *Eur. J. Biochem.* **1993**, *211*, 555.
(542) Keller, R. M.; Wüthrich, K. *Biochem. Biophys. Res. Commun.* **1978**, *83*, 1132.
(543) La Mar, G. N.; Viscio, D. B.; Smith, K. M.; Caughey, W. S.; Smith, M. L. *J. Am. Chem. Soc.* **1978**, *100*, 8085.
(544) Moore, G. R. *Biochim. Biophys. Acta* **1985**, *829*, 425.
(545) Turner, D. L. *Eur. J. Biochem.* **1993**, *211*, 563.
(546) McDonald, C. C.; Phillips, W. D. *Biochemistry* **1973**, *12*, 3170.
(547) Chao, Y. H.; Bersohn, R.; Aisen, P. *Biochemistry* **1979**, *18*, 774.
(548) Smith, G. M. *Biochemistry* **1979**, *18*, 1628.
(549) Senn, H.; Wüthrich, K. *Biochim. Biophys. Acta* **1983**, *743*, 69.
(550) Mathews, F. S.; Czerwinski, E. W.; Argos, P. In *The Porphyrins*; Dolphin, D., Ed.; Academic Press: New York, 1979; p 108.
(551) Safo, M. K.; Gupta, G. P.; Walker, F. A.; Scheidt, W. R. *J. Am. Chem. Soc.* **1991**, *113*, 5497.
(552) Rigby, S. E. J.; Alleyne, T. A.; Wilson, M. T.; Moore, G. R. *FEBS Lett.* **1989**, *257*, 155.
(553) Cowan, J. A.; Sola, M. *Inorg. Chem.* **1990**, *29*, 2176.
(554) Scheidt, W. R. In *The porphyrins*; Dolphin, D., Ed.; Academic Press: New York, 1978; p 463.
(555) Collmann, J. P.; Gagne', R. R.; Reed, C. A.; Robinson, W. T.; Rodley, G. A. *Proc. Natl. Acad. Sci. U.S.A.* **1974**, *71*, 1326.
(556) Goff, H. M.; La Mar, G. N. *J. Am. Chem. Soc.* **1977**, *99*, 6599.
(557) Goff, H. M. *J. Am. Chem. Soc.* **1981**, *103*, 3714.
(558) Takahashi, S.; Lin, A. K.-L.; Ho, C. *Biochemistry* **1980**, *19*, 5196.
(559) Nagai, K.; La Mar, G. N.; Jue, T.; Bunn, H. F. *Biochemistry* **1982**, *21*, 842.
(560) Ishimori, K.; Morishima, I. *Biochemistry* **1988**, *27*, 4060.
(561) Ishimori, K.; Morishima, I.; Imai, K.; Fushitani, K.; Miyazaki, G.; Shih, D.; Tame, J.; Pegnier, J.; Nigay, K. *J. Biol. Chem.* **1989**, *264*, 14624.
(562) La Mar, G. N.; Davis, N. L.; Johnson, R. D.; Smith, W. S.; Hauksson, J. B.; Budd, D. L.; Dalichow, F.; Langry, K. C.; Morris, I. K.; Smith, K. M. *J. Am. Chem. Soc.* **1993**, *115*, 3869.
(563) Banci, L.; Bertini, I.; Marconi, S.; Pierattelli, R. *Eur. J. Biochem.*, in press.
(564) Yamamoto, Y.; Iwafune, K.; Chujo, R.; Inoue, Y.; Imai, K.; Suzuki, T. *J. Biochem.* **1992**, *112*, 414.
(565) Sankar, S. S.; La Mar, G. N.; Smith, K. M.; Fujinari, E. M. *Biochim. Biophys. Acta* **1987**, *912*, 220.
(566) Wüthrich, K.; Hochmann, J.; Keller, R. M.; Wagner, G.; Brunori, M.; Giacometti, C. *J. Magn. Reson.* **1975**, *19*, 111.
(567) La Mar, G. N.; Budd, D. L.; Sick, H.; Gersonde, K. *Biochim. Biophys. Acta* **1978**, *537*, 270.
(568) Adachi, S.; Morishima, I. *Biochemistry* **1992**, *31*, 8613.
(569) Johnson, M. E.; Fung, L. W.-M.; Ho, C. *J. Am. Chem. Soc.* **1977**, *99*, 1245.
(570) Hochmann, J.; Kellerhalls, H. *J. Magn. Reson.* **1980**, *38*, 23.
(571) La Mar, G. N.; de Ropp, J. S. *J. Am. Chem. Soc.* **1982**, *104*, 5203.
(572) Inubushi, T.; Yonetani, T. *FEBS Lett.* **1983**, *160*, 287.
(573) Berry, M. J.; George, S. J.; Thomson, A. J.; Santos, H.; Turner, D. L. *Biochem. J.* **1990**, *270*, 413.
(574) Santos, H.; Turner, D. L. *Biochim. Biophys. Acta* **1988**, *954*, 277.
(575) Costa, H. S.; Santos, H.; Turner, D. L.; Xavier, A. V. *Eur. J. Biochem.* **1992**, *208*, 427.
(576) Johnson, M. E.; Fung, L. W.-M.; Ho, C. *J. Am. Chem. Soc.* **1977**, *99*, 1245.
(577) Dolphin, D.; Forman, A.; Borg, D. C.; Fajer, J.; Felton, R. H. *Proc. Natl. Acad. Sci. U.S.A.* **1971**, *68*, 614.
(578) Theorell, H.; Ehrenberg, A. *Arch. Biochem. Biophys.* **1952**, *41*, 442.
(579) Maeda, Y.; Morita, Y. *Biochem. Biophys. Res. Commun.* **1967**, *29*, 680.
(580) Moss, T. H.; Ehrenberg, A.; Bearden, A. J. *Biochemistry* **1969**, *8*, 4159.
(581) Schulz, C. E.; Devaney, P. W.; Winkler, H.; Debrunner, P. G.; Doan, N.; Chaing, R.; Rutter, R.; Hager, L. P. *FEBS Lett.* **1979**, *103*, 102.
(582) Felton, R. H.; Romans, A. Y.; Nai-Teng, Y.; Schonbaum, G. R. *Biochim. Biophys. Acta* **1967**, *434*, 82.
(583) Rakhit, G.; Spiro, T. G.; Ueda, M. *Biochem. Biophys. Res. Commun.* **1976**, *71*, 803.
(584) Aasa, R.; Vanngard, T.; Dunford, H. B. *Biochim. Biophys. Acta* **1975**, *391*, 259.
(585) Groves, J. T.; Haushalter, R. C.; Nakamura, M.; Nemo, T. E.; Evans, B. J. *J. Am. Chem. Soc.* **1981**, *103*, 2884.
(586) Balch, A. L.; Latos-Grazynski, L.; Renner, M. W. *J. Am. Chem. Soc.* **1985**, *107*, 2983.
(587) Chin, D. H.; Balch, A. L.; La Mar, G. N. *J. Am. Chem. Soc.* **1980**, *102*, 1446.
(588) Chin, D. H.; La Mar, G. N.; Balch, A. L. *J. Am. Chem. Soc.* **1980**, *102*, 4344.
(589) Mandon, D.; Weiss, R.; Jayaraj, K.; Gold, A.; Terner, J.; Bill, E.; Trautwein, A. X. *Inorg. Chem.* **1992**, *31*, 4404.
(590) La Mar, G. N.; de Ropp, J. S.; Smith, K. M.; Langry, K. C. *J. Biol. Chem.* **1981**, *256*, 237.
(591) Morishima, I.; Ogawa, S. *Biochem. Biophys. Res. Commun.* **1978**, *83*, 946.
(592) Morishima, I.; Ogawa, S. *Biochemistry* **1978**, *17*, 4384.
(593) Morishima, I.; Ogawa, S. *J. Am. Chem. Soc.* **1978**, *100*, 7125.
(594) La Mar, G. N.; de Ropp, J. S.; Latos-Grazynski, L.; Balch, A. L. *J. Am. Chem. Soc.* **1983**, *105*, 782.

(595) Balch, A. L.; La Mar, G. N.; Latos-Grazynski, L.; Renner, M. W.; Thanabal, V. *J. Am. Chem. Soc.* **1985**, *107*, 3003.
(596) La Mar, G. N.; de Ropp, J. S. *J. Am. Chem. Soc.* **1980**, *102*, 395.
(597) Swift, T. J. In *NMR of Paramagnetic Molecules*; La Mar, G. N., Horrocks, W. D., Jr., Holm, R. H., Eds.; Academic Press: New York, 1973; p 53.
(598) Morishima, I.; Shiro, Y.; Takamuki, Y. *J. Am. Chem. Soc.* **1983**, *105*, 6168.
(599) Morishima, I.; Shiro, Y.; Nakajima, K. *Biochemistry* **1986**, *25*, 3576.
(600) Morishima, I.; Takamuki, Y.; Shiro, Y. *J. Am. Chem. Soc.* **1984**, *106*, 7666.
(601) Satterlee, J. D.; Erman, J. E. *J. Biol. Chem.* **1981**, *256*, 1091.
(602) Erman, J. E.; Satterlee, J. D. In *Proceedings of the symposium on the interaction between iron and proteins in oxygen and electron transport*; Chien, H., Ed.; Elsevier: New York, 1980.
(603) Sivraja, M.; Goodin, D. B.; Smith, M.; Hoffman, B. M. *Science* **1989**, *245*, 738.
(604) Sanders-Loehr, J. Binuclear iron. Proteins. In *Iron carriers and iron proteins*; Loehr, T. M., Ed.; VCH: New York, 1989; p 373.
(605) Que, L., Jr. The catechol dioxygenases. In *Iron carriers and iron proteins*; Loehr, T. M., Ed.; VCH: New York, 1989; p 467.
(606) Wilkins, R. G. *Chem. Soc. Rev.* **1992**, *21*, 171.
(607) Kurtz, D. M., Jr. *Chem. Rev.* **1990**, *90*, 585.
(608) Heistand, R. H.; Lauffer, R. B.; Fikrig, E.; Que, L., Jr. *J. Am. Chem. Soc.* **1982**, *104*, 2789.
(609) Lauffer, R. B.; Antanaitis, B. C.; Aisen, P.; Que, L., Jr. *J. Biol. Chem.* **1983**, *258*, 14212.
(610) Armstrong, W. H.; Spool, A.; Papaefthymiou, G. C.; Frankel, R. B.; Lippard, S. J. *J. Am. Chem. Soc.* **1984**, *106*, 3653.
(611) Pyrz, J. W.; Roe, A. L.; Stern, L. J.; Que, L., Jr. *J. Am. Chem. Soc.* **1985**, *107*, 614.
(612) Que, L., Jr.; Kolanczyk, R. C.; White, L. S. *J. Am. Chem. Soc.* **1987**, *109*, 5373.
(613) Borovik, A. S.; Murch, B. P.; Que, L., Jr. *J. Am. Chem. Soc.* **1987**, *109*, 7190.
(614) Ming, L. J.; Que, L., Jr. *Inorg. Chem.* **1992**, *31*, 359.
(615) Ohlendorf, D. H.; Lipscomb, J. D.; Weber, P. C. *Nature* **1988**, *336*, 403.
(616) Que, L., Jr.; Lauffer, R. B.; Lynch, J. B.; Murch, B. P.; Pyrz, J. W. *J. Am. Chem. Soc.* **1987**, *109*, 5381.
(617) Lauffer, R. B.; Que, L., Jr. *J. Am. Chem. Soc.* **1982**, *104*, 7324.
(618) Ming, L. J.; Que, L., Jr.; Kriauciunas, A.; Frolik, C. A.; Chen, V. J. *Inorg. Chem.* **1990**, *26*, 111.
(619) Ming, L. J.; Que, L., Jr.; Kriauciunas, A.; Frolik, C. A.; Chen, V. J. *Biochemistry* **1991**, *30*, 11653.
(620) Wilkins, R. G.; Harrington, P. C. *Adv. Inorg. Biochem.* **1983**, *5*, 51.
(621) Harrington, P. C.; Wilkins, R. G. *Coord. Chem. Rev.* **1987**, *79*, 195.
(622) Sheriff, S.; Hendrickson, W. A.; Smith, J. L. *J. Mol. Biol.* **1987**, *197*, 273.
(623) Holmes, M. A.; Trong, I. L.; Turley, S.; Sieker, L. C.; Stenkamp, R. E. *J. Mol. Biol.* **1991**, *218*, 583.
(624) Maroney, M. J.; Lauffer, R. B.; Que, L., Jr. *J. Am. Chem. Soc.* **1984**, *106*, 6445.
(625) Maroney, M. J.; Kurtz, D. M., Jr.; Nocek, J. M.; Pearce, L. L.; Que, L., Jr. *J. Am. Chem. Soc.* **1986**, *108*, 6871.
(626) Reem, R. C.; Solomon, E. I. *J. Am. Chem. Soc.* **1984**, *106*, 8323.
(627) Muhoberac, B. B.; Wharton, D. C.; Babcock, L. M.; Harrington, P. C.; Wilkins, R. G. *Biochim. Biophys. Acta* **1980**, *626*, 337.
(628) Sjöberg, B.-M.; Graslund, A. *Adv. Inorg. Biochem.* **1983**, *5*, 87.
(629) Sahlin, M.; Ehrenberg, A.; Graslund, A.; Sjöberg, B.-M. *J. Biol. Chem.* **1986**, *261*, 2778.
(630) Sahlin, M.; Gräslund, A.; Petersson, L.; Ehrenberg, A.; Sjöberg, B.-M. *Biochemistry* **1989**, *28*, 2618.
(631) Nordlund, P.; Sjöberg, B.-M.; Ecklund, H. *Nature* **1990**, *345*, 593.
(632) Antanaitis, B. C.; Aisen, P. *Adv. Inorg. Biochem.* **1983**, *5*, 111.
(633) Doi, K.; Antanaitis, B. C.; Aisen, P. *Struct. Bonding* **1988**, *70*, 1.
(634) Debrunner, P. G.; Hendrich, M. P.; De Jersey, J.; Keough, D. T.; Sage, J. T.; Zerner, B. *Biochim. Biophys. Acta* **1983**, *745*, 103.
(635) Day, E. P.; David, S. S.; Peterson, J.; Dunham, W. R.; Bonvoisin, J. J.; Sands, R. H.; Que, L., Jr. *J. Biol. Chem.* **1988**, *263*, 15561.
(636) Scarrow, R. C.; Pyrz, J. W.; Que, L., Jr. *J. Am. Chem. Soc.* **1990**, *112*, 657.
(637) Holz, R. C.; Que, L., Jr.; Ming, L. J. *J. Am. Chem. Soc.* **1992**, *114*, 4434.
(638) Wang, Z.; Ming, L. J.; Que, L., Jr.; Vincent, J. B.; Crowder, M. W.; Averill, B. A. *Biochemistry* **1992**, *31*, 5263.
(639) Bertini, I.; Luchinat, C. *Adv. Inorg. Biochem.* **1985**, *6*, 71.
(640) Bertini, I.; Luchinat, C. In *Metal ions in biological systems*; Sigel, H., Ed.; Marcel Dekker, Inc.: New York, 1983; p 101.
(641) Bertini, I.; Luchinat, C.; Viezzoli, M. S. In *Zinc Enzymes*; Bertini, I., Luchinat, C., Maret, W., Zeppezauer, M., Eds.; Birkhauser: Boston, 1986; p 27.
(642) Chapman, S. K. In *Perspectives on bioinorganic chemistry*; Hay, R. W., Dilworth, J. R., Nolan, K. B., Eds.; Jai Press: London, 1991; p 95.
(643) Kodaka, M.; Shimizu, T.; Hatano, M. *Inorg. Chim. Acta* **1983**, *78*, L55.
(644) Shimizu, T.; Hatano, M. *Inorg. Chim. Acta* **1983**, *76*, L177.
(645) Bertini, I.; Luchinat, C. In *Biological and Inorganic Copper Chemistry*; Karlin, K. D., Zubieta, J., Eds.; Adenine Press: New York, 1986; p 23.
(646) Shirazi, A.; Goff, H. M. *Inorg. Chem.* **1982**, *21*, 3420.
(647) Inubushi, T.; Ikeda-Saito, M.; Yonetani, T. *Biochemistry* **1983**, *22*, 2904.
(648) Haffner, P. H.; Coleman, J. E. *J. Biol. Chem.* **1973**, *248*, 6630.
(649) Bertini, I. *J. Mol. Struct.* **1978**, *45*, 173.
(650) Bertini, I.; Lanini, G.; Luchinat, C. *Inorg. Chim. Acta* **1983**, *80*, 123.
(651) Makinen, M. W.; Kuo, L. C.; Yim, M. B.; Wells, G. B.; Fukuyama, J. M.; Kim, J. E. *J. Am. Chem. Soc.* **1985**, *107*, 5245.
(652) Silverman, D. N.; Lindskog, S. *Acc. Chem. Res.* **1988**, *21*, 30.
(653) Bertini, I.; Luchinat, C.; Monnanni, R. In *Carbon dioxide as a source of carbon*; Aresta, M., Forti, G., Eds.; D. Reidel: Dordrecht, 1987; p 139.
(654) Eriksson, A. E.; Liljas, A. In *The carbonic anhydrases*; Dodgson, S., Tashian, R., Gros, G., Carter, N., Eds.; Plenum Publishing Corporation: New York, 1991; p 33.
(655) Bertini, I.; Luchinat, C. *Acc. Chem. Res.* **1983**, *16*, 272.
(656) Banci, L.; Bertini, I.; Luchinat, C.; Donaire, A.; Martinez, M.-J.; Moratal Mascarell, J. M. *Comments Inorg. Chem.* **1990**, *9*, 245.
(657) Bertini, I.; Dei, A.; Luchinat, C.; Monnanni, R. In *Zinc enzymes*; Bertini, I., Luchinat, C., Maret, W., Zeppezauer, M., Eds.; Birkhauser: Boston, 1986; p 371.
(658) Liljas, A.; Kannan, K. K.; Bergsten, P. C.; Waara, I.; Fridborg, K.; Strandberg, B.; Carlbom, U.; Jarup, L.; Lovgren, S.; Petefel, M. *Nature New Biol.* **1972**, *235*, 131.
(659) Eriksson, A. E.; Jones, T. A.; Liljas, A. *Proteins* **1989**, *4*, 274.
(660) Vidgren, J.; Liljas, A.; Walker, N. P. C. *Int. J. Biol. Macromol.* **1990**, *12*, 342.
(661) Eriksson, A. E.; Kylsten, P. M.; Jones, T. A.; Liljas, A. *Proteins* **1989**, *4*, 283.
(662) Hakannson, K.; Carlsson, M.; Svensson, A.; Liljas, A. *J. Mol. Biol.* **1992**, *227*, 1192.
(663) Lindahl, M.; Habash, J.; Harrop, S.; Helliwell, J. R.; Liljas, A. *Acta Crystallogr.* **1992**, *B48*, 281.
(664) Mangani, S.; Hakannson, K. *Eur. J. Biochem.* **1992**, *210*, 867.
(665) Farmer, B. T., II; Venters, R. A.; Spicer, L. D.; Wittekind, M. G.; Müller, L. *J. Biomol. NMR* **1992**, *2*, 195.
(666) Bertini, I.; Luchinat, C.; Scozzafava, A. *Struct. Bonding* **1982**, *48*, 45.
(667) Bertini, I.; Canti, G.; Luchinat, C.; Mani, F. *J. Am. Chem. Soc.* **1981**, *103*, 7784.
(668) Bertini, I.; Lanini, G.; Luchinat, C. *J. Am. Chem. Soc.* **1983**, *105*, 5116.
(669) Banci, L.; Dugad, L. B.; La Mar, G. N.; Keating, K. A.; Luchinat, C.; Pierattelli, R. *Biophys. J.* **1992**, *63*, 530.
(670) Bertini, I.; Luchinat, C.; Pierattelli, R.; Vila, A. J. *Eur. J. Biochem.* **1992**, *208*, 607.
(671) Bertini, I.; Jonsson, B.-H.; Luchinat, C.; Pierattelli, R.; Vila, A. J. Submitted for publication.
(672) Banci, L.; Bertini, I.; Luchinat, C.; Monnanni, R.; Moratal Mascarell, J. M. *Gazz. Chim. Ital.* **1989**, *119*, 23.
(673) Lipscomb, J. D.; Harstuck, J. A.; Reeke, G. N.; Quiocho, F. A.; Bethge, P. H.; Ludwig, M. L.; Steitz, T. A.; Miurhead, H.; Coppola, J. C. *Brookhaven Symp. Biol.* **1968**, *21*, 24.
(674) Christianson, D. W.; Lipscomb, J. D. *Acc. Chem. Res.* **1989**, *22*, 62.
(675) Bertini, I.; Canti, G.; Luchinat, C. *J. Am. Chem. Soc.* **1982**, *104*, 4943.
(676) Bertini, I.; Luchinat, C.; Messori, L.; Monnanni, R.; Auld, D. S.; Riordan, J. F. *Biochemistry* **1988**, *27*, 8318.
(677) Auld, D. S.; Bertini, I.; Donaire, A.; Messori, L.; Moratal Mascarell, J. M. *Biochemistry* **1992**, *31*, 3840.
(678) Bicknell, R.; Schaeffer, A.; Bertini, I.; Luchinat, C.; Auld, D. S.; Vallee, B. L. *Biochemistry* **1988**, *27*, 1050.
(679) Cedergren-Zeppezauer, E. S.; Andersson, I.; Ottonello, S.; Bignetti, E. *Biochemistry* **1985**, *24*, 4000.
(680) Bertini, I.; Gerber, M.; Lanini, G.; Luchinat, C.; Maret, W.; Rawer, S.; Zeppezauer, M. *J. Am. Chem. Soc.* **1984**, *106*, 1826.
(681) Bertini, I.; Banci, L.; Luchinat, C.; Piccioli, M. *Coord. Chem. Rev.* **1990**, *100*, 67.
(682) Parge, H. E.; Hallewell, R. A.; Tainer, J. *Proc. Natl. Acad. Sci. U.S.A.* **1992**, *89*, 6109.
(683) Rotilio, G.; Finazzi Agro', A.; Calabrese, L.; Bossa, F.; Guerrieri, P.; Mondovì, B. *Biochemistry* **1971**, *10*, 616.
(684) Fee, J. A.; Gaber, B. P. *J. Biol. Chem.* **1972**, *247*, 60.
(685) Fee, J. A. *J. Biol. Chem.* **1973**, *248*, 4229.
(686) Tainer, J. A.; Getzoff, E. D.; Beem, K. M.; Richardson, J. S.; Richardson, D. C. *J. Mol. Biol.* **1982**, *160*, 181.
(687) Valentine, J. S.; Pantoliano, M. W. In *Copper Proteins*; Spiro, T. G., Eds.; Wiley: New York, 1981; p 291.
(688) Bertini, I.; Luchinat, C.; Monnanni, R. *J. Am. Chem. Soc.* **1985**, *107*, 2178.
(689) Moss, T. H.; Fee, J. A. *Biochem. Biophys. Res. Commun.* **1975**, *66*, 799.
(690) Blackburn, N. J.; Hasnain, S. S.; Binsted, N.; Diakun, G. P.; Garner, C. D.; Knowles, P. F. *Biochem. J.* **1984**, *219*, 985.
(691) Bertini, I.; Luchinat, C.; Piccioli, M.; Vicens Oliver, M.; Viezzoli, M. S. *Eur. J. Biophys.* **1991**, *20*, 269.

(692) Morgenstern-Badarau, I.; Cocco, D.; Desideri, A.; Rotilio, G.; Jordanov, J.; Dupre', N. *J. Am. Chem. Soc.* **1986**, *108*, 300.
(693) Banci, L.; Bertini, I.; Luchinat, C.; Piccioli, M.; Scozzafava, A. *Gazz. Chim. Ital.* **1993**, *123*, 95.
(694) Ming, L. J.; Banci, L.; Luchinat, C.; Bertini, I.; Valentine, J. S. *Inorg. Chem.* **1988**, *27*, 728.
(695) Banci, L.; Bertini, I.; Luchinat, C.; Scozzafava, A. *J. Biol. Chem.* **1989**, *264*, 9742.
(696) Banci, L.; Bencini, A.; Bertini, I.; Luchinat, C.; Piccioli, M. *Inorg. Chem.* **1990**, *29*, 4867.
(697) Banci, L.; Bertini, I.; Luchinat, C.; Scozzafava, A.; Turano, P. *Inorg. Chem.* **1989**, *28*, 2377.
(698) Bertini, I.; Banci, L.; Luchinat, C.; Bielski, B. H. J.; Cabelli, D.; Mullenbach, G. T.; Hallewell, R. A. *J. Am. Chem. Soc.* **1989**, *111*, 714.
(699) Banci, L.; Bertini, I.; Turano, P. *Eur. Biophys. J.* **1991**, *19*, 141.
(700) Banci, L.; Bertini, I.; Luchinat, C.; Hallewell, R. A. *J. Am. Chem. Soc.* **1988**, *110*, 3629.
(701) Bertini, I.; Lepori, A.; Luchinat, C.; Turano, P. *Inorg. Chem.* **1991**, *30*, 3363.
(702) Desideri, A.; Cocco, D.; Calabrese, L.; Rotilio, G. *Biochim. Biophys. Acta* **1984**, *784*, 111.
(703) Banci, L.; Bertini, I.; Luchinat, C.; Monnanni, R.; Scozzafava, A.; Salvato, B. *Gazz. Chim. Ital.* **1986**, *116*, 51.
(704) Banci, L.; Bertini, I.; Luchinat, C.; Monnanni, R.; Scozzafava, A. *Inorg. Chem.* **1987**, *26*, 153.
(705) Ming, L. J.; Valentine, J. S. *J. Am. Chem. Soc.* **1990**, *112*, 4256.
(706) Kim, E. E.; Wyckoff, H. W. *J. Mol. Biol.* **1991**, *218*, 449.
(707) Banci, L.; Bertini, I.; Luchinat, C.; Viezzoli, M. S.; Wang, Y. *Inorg. Chem.* **1988**, *27*, 1442.
(708) Harper, L. V.; Amann, B. T.; Vinson, V. K.; Berg, J. M. *J. Am. Chem. Soc.* **1993**, *115*, 2577.
(709) Hill, H. A. O.; Storm, C. B.; Ambler, R. P. *Biochem. Biophys. Res. Commun.* **1976**, *70*, 783.
(710) Nar, H.; Messerschimdt, A.; Huber, R.; van de Kamp, M.; Canters, G. W. *J. Mol. Biol.* **1991**, *221*, 765.
(711) Moratal Mascarell, J. M.; Salgado, J.; Donaire, A.; Jimenez, H. R.; Castells, J. Submitted for publication.
(712) Hill, H. A. O.; Lee, W. B. *Biochem. Soc. Trans.* **1979**, *7*, 733.
(713) Dahlin, S.; Reinhammar, B.; Angstrom, J. *Biochemistry* **1989**, *28*, 7224.
(714) Hill, H. A. O.; Lee, W. B. *J. Inorg. Biochem.* **1979**, *11*, 101.
(715) Braun, W.; Wagner, G.; Worgotter, E.; Vasak, M.; Kagi, J. H.; Wüthrich, K. J. *J. Mol. Biol.* **1986**, *187*, 125.
(716) Bailey, S.; Evans, R.; Garratt, R. C.; Gorinsky, B.; Hasnain, S.; Horsburgh, C.; Jhoti, H.; Lindley, P. F.; Mydin, A.; Sarra, R.; Watson, J. L. *Biochemistry* **1988**, *27*, 5804.
(717) Smith, C. A.; Baker, H. M.; Baker, E. N. *J. Mol. Biol.* **1991**, *219*, 155.
(718) Bertini, I.; Luchinat, C.; Messori, L.; Scozzafava, A. *Eur. J. Biochem.* **1984**, *141*, 375.
(719) Bertini, I.; Luchinat, C.; Messori, L.; Monnanni, R.; Scozzafava, A. *J. Biol. Chem.* **1986**, *261*, 1139.
(720) Bertini, I.; Viezzoli, M. S.; Luchinat, C.; Stafford, E.; Cardin, A. D.; Behnke, W. D.; Bhattacharrya, L.; Brewer, C. *J. Biol. Chem.* **1987**, *262*, 16984.
(721) Vasak, M. In *Zinc Enzymes*; Bertini, I., Luchinat, C., Maret, W., Zeppenhauer, M., Eds.; Birkhauser: Boston, MA, 1986; p 565.
(722) Arseniev, A.; Schultze, P.; Worgotter, E.; Braun, W.; Wagner, G.; Vasak, M.; Kagi, J. H.; Wüthrich, K. *J. Mol. Biol.* **1988**, *201*, 637.
(723) Schultze, P.; Worgotter, E.; Braun, W.; Wagner, G.; Vasak, M.; Kagi, J. H.; Wüthrich, K. *J. Mol. Biol.* **1988**, *203*, 251.
(724) Bertini, I.; Luchinat, C.; Messori, L.; Vasak, M. *J. Am. Chem. Soc.* **1989**, *111*, 7296.
(725) Bertini, I.; Luchinat, C.; Messori, L.; Vasak, M. *J. Am. Chem. Soc.* **1989**, *111*, 7300.
(726) Bertini, I.; Borghi, E.; Luchinat, C. *Bioinorg. Chem.* **1978**, *9*, 495.
(727) Bertini, I.; Borghi, E.; Luchinat, C.; Monnanni, R. *Inorg. Chim. Acta* **1982**, *67*, 99.
(728) Moratal Mascarell, J. M.; Martinez Ferrer, M.-J.; Donaire, A.; Castells, J.; Salgado, J.; Jimenez, H. R. *J. Chem. Soc., Dalton Trans.* **1991**, 3393.
(729) Moratal Mascarell, J. M.; Martinez Ferrer, M.-J.; Jimenez, H. R.; Donaire, A.; Castells, J.; Salgado, J. *J. Inorg. Biochem.* **1992**, *45*, 231.
(730) Bertini, I.; Donaire, A.; Monnanni, R.; Moratal Mascarell, J. M.; Salgado, J. *J. Chem. Soc., Dalton Trans.* **1992**, 1443.
(731) Ming, L. J.; Valentine, J. S. *Inorg. Chem.* **1987**, *109*, 4426.
(732) Bertini, I.; Luchinat, C.; Ming, L. J.; Piccioli, M.; Sola, M.; Valentine, J. S. *Inorg. Chem.* **1992**, *31*, 4433.
(733) Ming, L. J.; Valentine, J. S. *J. Am. Chem. Soc.* **1990**, *112*, 6374.
(734) Blaszak, J. A.; Ulrich, E. L.; Markley, J. L.; McMillin, D. R. *Biochemistry* **1982**, *21*, 6253.
(735) Moratal Mascarell, J. M.; Salgado, J.; Donaire, A.; Jimenez, H. R.; Castells, J. *J. Chem. Soc., Chem. Commun.*, in press.
(736) Krizek, B. A.; Berg, J. M. *Inorg. Chem.* **1992**, *31*, 2984.
(737) Yocom, K. M.; Shelton, J. B.; Shelton, J. R.; Schroeder, W. A.; Worosila, G.; Isied, S. S.; Bordignon, E.; Gray, H. B. *Proc. Natl. Acad. Sci. U.S.A.* **1982**, *79*, 7052.
(738) Toi, H.; La Mar, G. N.; Margalit, R.; Che, C.-M.; Gray, H. B. *J. Am. Chem. Soc.* **1984**, *106*, 6213.
(739) Ascenso, J. R.; Xavier, A. V. In *Systematic properties of lanthanides*; Sinha, S., Ed.; Reidel: Dordrecht, 1983; p 501.
(740) Lee, L.; Sykes, B. D. In *Advances in Inorganic Biochemistry*; Darnall, D. W., Wilkins, R. G., Eds.; Elsevier: New York, 1980; Vol. 2, p 183.
(741) Williams, R. J. P. *Struct. Bonding* **1982**, *50*, 79.
(742) Dobson, C. M.; Williams, R. J. P.; Xavier, A. V. *J. Chem. Soc., Dalton Trans.* **1973**, 2662.
(743) Reuben, J. *J. Magn. Reson.* **1973**, *11*, 103.
(744) Shelling, J. G.; Bjorson, M. E.; Hodges, R. S.; Taneja, A. K.; Sykes, B. D. *J. Magn. Reson.* **1984**, *57*, 99.
(745) Bleaney, B. *J. Magn. Reson.* **1972**, *8*, 91.
(746) Campbell, I. D.; Dobson, C. M.; Williams, R. J. P.; Xavier, A. V. *Ann. N.Y. Acad. Sci.* **1973**, *222*, 163.
(747) Campbell, I. D.; Dobson, C. M.; Williams, R. J. P. *Proc. R. Soc. London* **1975**, *A345*, 41.
(748) Lee, L.; Sykes, B. D. *Biochemistry* **1980**, *19*, 3208.
(749) Lee, L.; Sykes, B. D. *Biochemistry* **1981**, *20*, 1156.
(750) Lee, L.; Sykes, B. D. *Biochemistry* **1983**, *22*, 4366.
(751) Jenkins, B. G.; Lauffer, R. B. *J. Magn. Reson.* **1988**, *80*, 328.
(752) Capozzi, F.; Cremonini, M. A.; Luchinat, C.; Sola, M. *Magn. Reson. Chem.*, in press.
(753) Messori, L.; Piccioli, M. *J. Inorg. Biochem.* **1991**, *42*, 185.
(754) Oh, B.-H.; Westler, W. M.; Markley, J. L. *J. Am. Chem. Soc.* **1989**, *111*, 3083.
(755) Oh, B.-H.; Westler, W. M.; Darba, P.; Markley, J. L. *Science* **1988**, *240*, 908.
(756) Packer, E. L.; Rabinowitz, J. C.; Sternlicht, H. *J. Biol. Chem.* **1978**, *253*, 7722.
(757) Santos, H.; Turner, D. L. *Eur. J. Biochem.* **1992**, *206*, 721.
(758) Wüthrich, K.; Baumann, R. *Helv. Chim. Acta* **1973**, *56*, 585.
(759) Santos, H.; Turner, D. L. *FEBS Lett.* **1986**, *194*, 73.
(760) Timkovich, R. *Inorg. Chem.* **1991**, *30*, 37.
(761) Yamamato, Y.; Nanai, N.; Inoue, Y.; Chujo, R. *Biochem. Biophys. Res. Commun.* **1988**, *151*, 262.
(762) Banci, L.; Bertini, I.; Pierattelli, R.; Vila, A. J. Unpublished results.
(763) Bertini, I.; Piccioli, M.; Viezzoli, M. S.; Vila, A. J. Unpublished results.
(764) Moratal Mascarell, J. M.; Salgado, J.; Donaire, A.; Jimenez, H. R.; Castells, J. *J. Chem. Soc., Chem. Commun.* **1993**, 110.